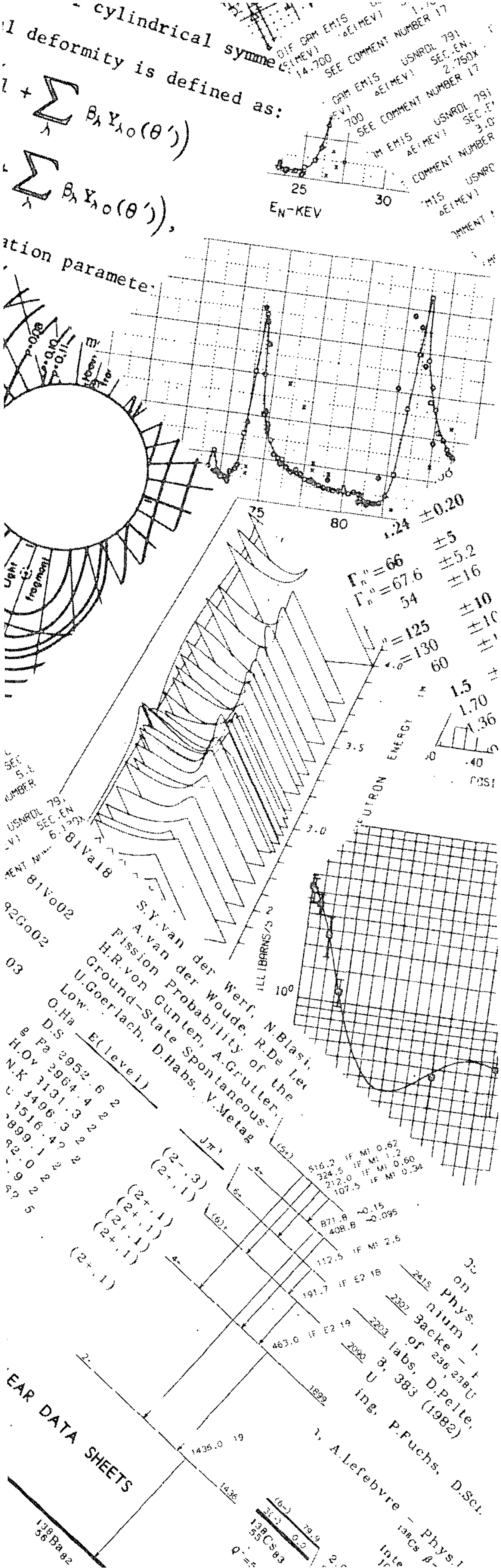

BNL-NCS-37699
DOE/NDC-38/U
NEANDC(US)-222/U
INDC(USA)-97L
INFORMAL REPORT
LIMITED DISTRIBUTION

REPORTS TO THE DOE NUCLEAR DATA COMMITTEE

Compiled by
NATIONAL NUCLEAR DATA CENTER
for the
U.S. Department of Energy
Nuclear Data Committee

May 1986

BROOKHAVEN NATIONAL LABORATORY
ASSOCIATED UNIVERSITIES, INC.
UPTON, LONG ISLAND, NEW YORK 11973

national
nuclear
data
Center

BNL-NCS-37699
DOE/NDC-38/U
NEANDC(US)-222/U
INDC(USA)-97/L
Informal Report
Limited Distribution

REPORTS TO

THE DOE NUCLEAR DATA COMMITTEE

MAY 1986

National
Nuclear
Data
Center

Compiled by the

NATIONAL NUCLEAR DATA CENTER
BROOKHAVEN NATIONAL LABORATORY
ASSOCIATED UNIVERSITIES, INC.

UNDER CONTRACT NO. DE-AC02-76CH00016 WITH THE
UNITED STATES DEPARTMENT OF ENERGY

Printed in the United States of America
Available from
National Technical Information Service
U.S. Department of Commerce
5285 Port Royal Road
Springfield, VA 22161

NTIS price codes:
Printed Copy: A09; Microfiche Copy: A01

PREFACE

The reports in this document were submitted to the Department of Energy, Nuclear Data Committee (DOE-NDC) in April, 1986. The reporting laboratories are those with a substantial program for the measurement of neutron and nuclear cross sections of relevance to the U.S. applied nuclear energy program.

The authors of the Status Report contributions are responsible for collecting and editing individual contributions from their laboratory and are not necessarily the sole authors of the contributions. The scientists responsible for the work described in each individual contribution are listed at the beginning of the contribution.

The material contained in these reports is to be regarded as comprised of informal statements of recent developments and preliminary data. Persons wishing to make use of these data should contact the individual experimenter for further details. The data which appear in this document should be quoted only by permission of the contributor and should be referenced as private communication, and not by this document number. Appropriate subjects are listed as follows:

1. Microscopic neutron cross sections relevant to the nuclear energy program, including shielding. Inverse reactions where pertinent are included.

2. Charged-particle cross sections, where they are relevant to (1.) above, and where relevant to developing and testing nuclear models.

3. Gamma ray production, radioactive decay, and theoretical developments in nuclear structure which are applicable to nuclear energy programs.

4. Proton and alpha-particle cross sections, at energies of up to 1 GeV, which are of interest to the space program.

These reports cannot be regarded as a complete summary of the nuclear research efforts in the U.S. A number of laboratories whose research is less programmatically oriented do not submit reports; neither do the submitted reports reflect all the work related to nuclear data in progress at the submitting laboratory.

This compilation has been produced almost completely from master copies prepared by the individual contributors listed in the Table of Contents, and reports are reproduced without change from these master copies.

The CINDA-type index which follows the Table of Contents was prepared by Norman E. Holden and Alyce Daly of the National Nuclear Data Center, Brookhaven National Laboratory, Upton, Long Island, New York.

TABLE OF CONTENTS

TABLE OF CONTENTS (cont.)

NEUTRON DATA REFERENCES

Element	Quantity	Energy (eV) Min	Max	Type	Documentation Ref	Page	Date	Lab	Comments
^{1}H	$\sigma_{el}(\theta)$	5.0+7	6.5+7	Expt	DOE-NDC-38	32	May86	DAV	Drummond+ 2ENS.CS(180/90 DEGS).
^{1}H	$\sigma_{n,\gamma}$	2.5-2		Expt	DOE-NDC-38	133	May86	NMX	Arbildo+ CS RATIO WITH S, B, MN.
^{6}Li	σ_{pol}	NDG		Expt	DOE-NDC-38	168	May86	TNL	Gould+ NDG.
^{6}Li	$\sigma_{n,t}$	+0	2.0+1	Expt	DOE-NDC-38	123	May86	NBS	Carlson. RATIO TO 10B(N,A).
^{7}Be	$\sigma_{n,p}$	3.0-2	3.0+2	Expt	DOE-NDC-38	90	May86	LAS	Koehler+ GRPH. PRELIMINARY SIG.
^{9}Be	σ_{tot}	1.8+6	1.0+7	Expt	DOE-NDC-38	12	May86	ANL	Smith+ NDG. TBD.
^{9}Be	$\sigma_{el}(\theta)$	1.8+6	1.0+7	Expt	DOE-NDC-38	12	May86	ANL	Smith+ NDG. TBD.
^{9}Be	$\sigma_{el}(\theta)$	1.1+7	1.7+7	Expt	DOE-NDC-38	166	May86	TNL	Gould+ NDG. TBP. NSE.
^{9}Be	σ_{pol}	9.0+6	1.7+7	Expt	DOE-NDC-38	167	May86	TNL	Gould+ SEE NP/A 427, 36.
^{9}Be	$\sigma_{dif.inl}$	1.1+7	1.7+7	Expt	DOE-NDC-38	166	May86	TNL	Gould+ NDG. TBP. NSE.
B	σ_{abs}	2.5-2		Expt	DOE-NDC-38	133	May86	NMX	Arbildo+ CS=770.MB REL H=332.55MB.
^{10}B	$\sigma_{el}(\theta)$	5.0+6	5.8+6	Expt	DOE-NDC-38	149	May86	OHO	Sadowski+ NDG.99.6 PCT ENRICHED TGT.
^{10}B	σ_{pol}	1.5+7	1.7+7	Expt	DOE-NDC-38	167	May86	TNL	Gould+ NDG. SEE TUNL-24 REPORT.
^{10}B	$\sigma_{dif.inl}$	5.0+6	5.8+6	Expt	DOE-NDC-38	149	May86	OHO	Sadowski+ NDG.99.6 PCT ENRICHED TGT.
^{10}B	$\sigma_{n,\alpha}$	+0	2.0+1	Expt	DOE-NDC-38	123	May86	NBS	Carlson. RATIO TO 6LI(N,T).
^{11}B	σ_{pol}	1.5+7	1.7+7	Expt	DOE-NDC-38	167	May86	TNL	Gould+ NDG. SEE TUNL-24 REPORT.
^{12}C	$\sigma_{el}(\theta)$	2.0+7	2.6+7	Expt	DOE-NDC-38	149	May86	OHO	Finlay+ NDG. MEAS + ANALYSIS.
^{12}C	$\sigma_{el}(\theta)$	1.8+7	2.6+7	Expt	DOE-NDC-38	154	May86	OHO	Petler+ NDG. USED IN OM ANALYSIS.
^{12}C	$\sigma_{el}(\theta)$	1.1+7	1.4+7	Expt	DOE-NDC-38	167	May86	TNL	Gould+ NDG. TO BE ANALYZED.
^{12}C	σ_{pol}	1.7+7		Theo	DOE-NDC-38	168	May86	TNL	Gould+ NDG. SEE TUNL-24.
^{12}C	σ_{pol}	8.9+6	1.2+7	Theo	DOE-NDC-38	168	May86	TNL	Gould+ SEE JP/G 11, 379.
^{12}C	$\sigma_{dif.inl}$	2.0+7	2.6+7	Expt	DOE-NDC-38	149	May86	OHO	Finlay+ NDG. MEAS + ANALYSIS.
^{12}C	$\sigma_{dif.inl}$	1.1+7	1.4+7	Expt	DOE-NDC-38	167	May86	TNL	Gould+ NDG. TO BE ANALYZED.
^{12}C	$\sigma_{n,p}$	6.5+7		Expt	DOE-NDC-38	32	May86	DAV	Sorenson+ GRPH CFD CALC,OTHER EXPT.
^{12}C	$\sigma_{n,p}$	1.4+7		Expt	DOE-NDC-38	133	May86	NMX	Rowland+ CS=2+-1 MB.
^{13}C	$\sigma_{p,emis}$	6.5+7		Expt	DOE-NDC-38	32	May86	DAV	Drummond+ NDG.SPECTRA(0-50 DEGS)TBC.
^{14}C	$\sigma_{p,emis}$	6.5+7		Expt	DOE-NDC-38	32	May86	DAV	Drummond+ NDG.SPECTRA(0-50 DEGS)TBC.
^{14}N	$\sigma_{el}(\theta)$	1.8+7	2.6+7	Expt	DOE-NDC-38	154	May86	OHO	Petler+ NDG. USED IN OM ANALYSIS.
^{14}N	$\sigma_{el}(\theta)$	1.1+7	1.7+7	Expt	DOE-NDC-38	166	May86	TNL	Gould+ NDG. TBP. NSE.
^{14}N	$\sigma_{n,2n}$	1.4+7	1.5+7	Expt	DOE-NDC-38	132	May86	NMX	Robertson+ DISAGREES BNL-325. TBP.
^{14}N	$\sigma_{n,p}$	2.7+7	6.1+7	Expt	DOE-NDC-38	34	May86	DAV	Subramanian+ NDG. DOUBLE DIFF. CS.
^{14}N	$\sigma_{n,d}$	2.7+7	6.1+7	Expt	DOE-NDC-38	34	May86	DAV	Subramanian+ NDG. DOUBLE DIFF. CS.
^{14}N	$\sigma_{n,t}$	2.7+7	6.1+7	Expt	DOE-NDC-38	34	May86	DAV	Subramanian+ NDG. DOUBLE DIFF. CS.

NEUTRON DATA REFERENCES

Element	Quantity	Energy (eV) Min	Max	Type	Documentation Ref	Page	Date	Lab	Comments
^{14}N	$\sigma_{n,^3He}$	2.7+7	6.1+7	Expt	DOE-NDC-38	34	May86	DAV	Subramanian+ NDG. DOUBLE DIFF. CS.
^{14}N	$\sigma_{n,\alpha}$	2.7+7	6.1+7	Expt	DOE-NDC-38	34	May86	DAV	Subramanian+ NDG. DOUBLE DIFF. CS.
^{16}O	$\sigma_{el}(\theta)$	1.8+7	2.6+7	Expt	DOE-NDC-38	154	May86	OHO	Petler+ NDG. USED IN OM ANALYSIS.
^{16}O	$\sigma_{n,p}$	2.7+7	6.1+7	Expt	DOE-NDC-38	34	May86	DAV	Subramanian+ NDG. DOUBLE DIFF. CS.
^{16}O	$\sigma_{n,d}$	2.7+7	6.1+7	Expt	DOE-NDC-38	34	May86	DAV	Subramanian+ NDG. DOUBLE DIFF. CS.
^{16}O	$\sigma_{n,t}$	2.7+7	6.1+7	Expt	DOE-NDC-38	34	May86	DAV	Subramanian+ NDG. DOUBLE DIFF. CS.
^{16}O	$\sigma_{n,^3He}$	2.7+7	6.1+7	Expt	DOE-NDC-38	34	May86	DAV	Subramanian+ NDG. DOUBLE DIFF. CS.
^{16}O	$\sigma_{n,\alpha}$	2.7+7	6.1+7	Expt	DOE-NDC-38	34	May86	DAV	Subramanian+ NDG. DOUBLE DIFF. CS.
^{18}O	$\sigma_{el}(\theta)$	5.0+6	7.5+6	Expt	DOE-NDC-38	150	May86	OHO	Koehler+ NDG. MEAS. + ANALYSIS.
^{18}O	$\sigma_{dif.inl}$	5.0+6	7.5+6	Expt	DOE-NDC-38	150	May86	OHO	Koehler+ NDG. MEAS. + ANALYSIS.
^{19}F	$\sigma_{n,2n}$	1.4+7	1.5+7	Expt	DOE-NDC-38	132	May86	NMX	Robertson+ AGREES BNL-325. TBP.
^{27}Al	$\sigma_{el}(\theta)$	1.8+7	2.6+7	Expt	DOE-NDC-38	154	May86	OHO	Petler+ NDG. USED IN OM ANALYSIS.
^{27}Al	σ_{pol}	1.1+7	1.7+7	Expt	DOE-NDC-38	168	May86	TNL	Gould+ NDG. SEE PR/C 30, 1435.
^{27}Al	$\sigma_{n,X\gamma}$	+6	5.0+7	Theo	DOE-NDC-38	97	May86	LAS	Arthur+ EXTEND ENDF/B GT 20 MEV.
^{27}Al	$\sigma_{n,emis}$	+6	5.0+7	Theo	DOE-NDC-38	97	May86	LAS	Arthur+ EXTEND ENDF/B GT 20 MEV.
^{27}Al	$\sigma_{n,p}$	1.5+7		Expt	DOE-NDC-38	5	May86	ANL	Meadows. GRPH MEAS CFD EVAL.
^{27}Al	$\sigma_{n,\alpha}$	1.5+7		Expt	DOE-NDC-38	5	May86	ANL	Meadows. GRPH MEAS CFD EVAL.
^{27}Al	$\sigma_{n,\alpha}$	1.5+7		Expt	DOE-NDC-38	120	May86	MHG	Lai+ NDG. TBC.
^{27}Al	$\sigma_{\alpha,emis}$	+6	5.0+7	Theo	DOE-NDC-38	97	May86	LAS	Arthur+ EXTEND ENDF/B GT 20 MEV.
^{27}Al	$\sigma_{d,emis}$	+6	5.0+7	Theo	DOE-NDC-38	97	May86	LAS	Arthur+ EXTEND ENDF/B GT 20 MEV.
^{27}Al	$\sigma_{p,emis}$	+6	5.0+7	Theo	DOE-NDC-38	97	May86	LAS	Arthur+ EXTEND ENDF/B GT 20 MEV.
^{28}Si	$\sigma_{el}(\theta)$	8.0+6	4.0+7	Theo	DOE-NDC-38	168	May86	TNL	Gould+ GRPH CC CALC CFD EXPT.
^{28}Si	σ_{pol}	8.0+6	1.7+7	Expt	DOE-NDC-38	168	May86	TNL	Gould+ NDG.
^{28}Si	$\sigma_{dif.inl}$	1.0+7	2.6+7	Theo	DOE-NDC-38	168	May86	TNL	Gould+ GRPH CC CALC CFD EXPT.
^{31}P	$\sigma_{n,\gamma}$	2.6+3	5.0+5	Expt	DOE-NDC-38	137	May86	ORL	Macklin+ CS(30KEV)=1.74+-0.09MB.
^{31}P	Res.Params.	NDG		Expt	DOE-NDC-38	137	May86	ORL	Macklin+ NDG.
S	σ_{abs}	2.5-2		Expt	DOE-NDC-38	133	May86	NMX	Arbildo+ CS(S/H)=1.621. TBP ANE.
^{32}S	σ_{pol}	8.0+6	1.7+7	Expt	DOE-NDC-38	168	May86	TNL	Gould+ NDG.
^{32}S	γ Spectra	2.5-2		Expt	DOE-NDC-38	139	May86	LAS	Raman+ NDG SEE PR/C 32, 18.
^{33}S	σ_{tot}	1.0+4	2.0+6	Expt	DOE-NDC-38	135	May86	ORL	Coddens+ NDG.
^{33}S	γ Spectra	2.5-2		Expt	DOE-NDC-38	139	May86	LAS	Raman+ NDG SEE PR/C 32, 18.
^{33}S	$\langle\Gamma\rangle/D$	NDG		Expt	DOE-NDC-38	135	May86	ORL	Coddens+ NDG. S, P-WAVE.
^{34}S	γ Spectra	2.5-2		Expt	DOE-NDC-38	139	May86	LAS	Raman+ NDG SEE PR/C 32, 18.

NEUTRON DATA REFERENCES

Element	Quantity	Energy (eV) Min	Max	Type	Documentation Ref	Page	Date	Lab	Comments
^{36}S	γ Spectra	2.5-2		Expt	DOE-NDC-38	139	May86	LAS	Raman+ NDG SEE PR/C 32, 18.
^{39}K	$\sigma_{n,p}$	1.4+7	1.5+7	Expt	DOE-NDC-38	66	May86	LRL	Borg+ TBL. SIG CFD OTHER MEAS.
^{39}K	$\sigma_{n,np}$	1.4+7	1.5+7	Expt	DOE-NDC-38	66	May86	LRL	Borg+ TBL. SIG CFD OTHER MEAS.
^{40}Ca	$\sigma_{el}(\theta)$	9.9+6	4.0+7	Theo	DOE-NDC-38	169	May86	TNL	Gould+ GRPH MDL CALC CRD EXPT.
^{40}Ca	σ_{pol}	9.9+6	1.7+7	Theo	DOE-NDC-38	169	May86	TNL	Gould+ GRPH MDL CALC CFD EXPT.
^{40}Ca	$\sigma_{dif.inl}$	NDG		Theo	DOE-NDC-38	169	May86	TNL	Gould+ NDG.
^{48}Ca	σ_{tot}		1.0+7	Expt	DOE-NDC-38	135	May86	ORL	Carlton+ NDG. 96PCT ENRICHED.
^{48}Ca	σ_{tot}		1.0+7	Expt	DOE-NDC-38	137	May86	ORL	Harvey+ CS(E LT.15MEV)=0.5+-0.2B.
^{48}Ca	$\sigma_{n,\gamma}$		1.0+7	Expt	DOE-NDC-38	135	May86	ORL	Carlton+ NDG. 96PCT ENRICHED.
^{48}Ca	Res.Params.	NDG		Expt	DOE-NDC-38	137	May86	ORL	Harvey+ NDG.
^{48}Ca	$<\Gamma>/D$	NDG		Expt	DOE-NDC-38	135	May86	ORL	Carlton+ S0 LT 0.07 $X(10)^{-4}$.
^{47}Ti	$\sigma_{n,p}$	1.2+6	8.0+6	Expt	DOE-NDC-38	7	May86	ANL	Mannhart+ NDG.
^{47}Ti	$\sigma_{n,p}$	FISS		Expt	DOE-NDC-38	7	May86	ANL	Mannhart+ 252CF, 235U SPECTRA, NDG.
^{51}V	Evaluation	NDG		Eval	DOE-NDC-38	8	May86	ANL	Smith+ TBC. NDG.
^{51}V	$\sigma_{el}(\theta)$	4.0+6	1.0+7	Expt	DOE-NDC-38	1	May86	ANL	Smith+ NDG. TBC.
^{51}V	$\sigma_{n,p}$	1.5+7		Expt	DOE-NDC-38	5	May86	ANL	Meadows. GRPH MEAS CFD EVAL.
^{51}V	$\sigma_{n,\alpha}$	1.5+7		Expt	DOE-NDC-38	5	May86	ANL	Meadows. GRPH MEAS CFD EVAL.
Cr	$\sigma_{el}(\theta)$	4.0+6	1.0+7	Expt	DOE-NDC-38	1	May86	ANL	Smith+ NDG. TBC.
^{52}Cr	$\sigma_{n,p}$	1.5+7		Expt	DOE-NDC-38	118	May86	MHG	Lai+ NAT CR TGT. 52V PROD CS.
^{55}Mn	σ_{abs}	2.5-2		Expt	DOE-NDC-38	133	May86	NMX	Arbildo+ CS=13.32MB REL H=332.55MB.
^{55}Mn	$\sigma_{n,2n}$	1.5+7		Expt	DOE-NDC-38	5	May86	ANL	Meadows. GRPH MEAS CFD EVAL.
Fe	$\sigma_{el}(\theta)$	4.0+6	1.0+7	Expt	DOE-NDC-38	1	May86	ANL	Smith+ NDG. TBC.
Fe	$\sigma_{n,emis}$	6.6+7		Expt	DOE-NDC-38	36	May86	DAV	Hjort+GRPH. DOUBLE DIFF. CS.
^{54}Fe	σ_{tot}	5.0+5	4.0+6	Expt	DOE-NDC-38	4	May86	ANL	Guenther+ NDG. TBP.
^{54}Fe	$\sigma_{el}(\theta)$	5.0+5	4.0+6	Expt	DOE-NDC-38	4	May86	ANL	Guenther+ NDG. TBP.
^{54}Fe	σ_{pol}	NDG		Theo	DOE-NDC-38	171	May86	TNL	Gould+ NDG.
^{54}Fe	$\sigma_{n,n'\gamma}$	5.0+5	4.0+6	Expt	DOE-NDC-38	4	May86	ANL	Guenther+ NDG. TBP.
^{54}Fe	$\sigma_{n,X\gamma}$	+6	5.0+7	Theo	DOE-NDC-38	97	May86	LAS	Arthur+ EXTEND ENDF/B GT 20 MEV.
^{54}Fe	$\sigma_{n,emis}$	+6	5.0+7	Theo	DOE-NDC-38	97	May86	LAS	Arthur+ EXTEND ENDF/B GT 20 MEV.
^{54}Fe	$\sigma_{n,\alpha}$	1.5+7		Expt	DOE-NDC-38	5	May86	ANL	Meadows. GRPH MEAS CFD EVAL.
^{54}Fe	$\sigma_{\alpha,emis}$	+6	5.0+7	Theo	DOE-NDC-38	97	May86	LAS	Arthur+ EXTEND ENDF/B GT 20 MEV.
^{54}Fe	$\sigma_{d,emis}$	+6	5.0+7	Theo	DOE-NDC-38	97	May86	LAS	Arthur+ EXTEND ENDF/B GT 20 MEV.
^{54}Fe	$\sigma_{p,emis}$	+6	5.0+7	Theo	DOE-NDC-38	97	May86	LAS	Arthur+ EXTEND ENDF/B GT 20 MEV.

NEUTRON DATA REFERENCES

Element	Quantity	Energy (eV) Min	Max	Type	Documentation Ref	Page	Date	Lab	Comments
^{56}Fe	$\sigma_{n,X\gamma}$	+6	5.0+7	Theo	DOE-NDC-38	97	May86	LAS	Arthur+ EXTEND ENDF/B GT 20 MEV.
^{56}Fe	$\sigma_{n,emis}$	+6	5.0+7	Theo	DOE-NDC-38	97	May86	LAS	Arthur+ EXTEND ENDF/B GT 20 MEV.
^{56}Fe	$\sigma_{n,p}$	1.5+7		Expt	DOE-NDC-38	5	May86	ANL	Meadows. GRPH MEAS CFD EVAL.
^{56}Fe	$\sigma_{n,p}$	1.5+7		Expt	DOE-NDC-38	120	May86	MHG	Lai+ NDG. TBC.
^{56}Fe	Res.Params.	1.2+3		Expt	DOE-NDC-38	138	May86	ORL	Macklin. WN=60.7MV.WN(WG/WT)=54.9MV.
^{56}Fe	$\sigma_{\alpha,emis}$	+6	5.0+7	Theo	DOE-NDC-38	97	May86	LAS	Arthur+ EXTEND ENDF/B GT 20 MEV.
^{56}Fe	$\sigma_{d,emis}$	+6	5.0+7	Theo	DOE-NDC-38	97	May86	LAS	Arthur+ EXTEND ENDF/B GT 20 MEV.
^{56}Fe	$\sigma_{p,emis}$	+6	5.0+7	Theo	DOE-NDC-38	97	May86	LAS	Arthur+ EXTEND ENDF/B GT 20 MEV.
^{cmp}Fe	$\sigma_{\alpha,emis}$	9.4+6	1.1+7	Expt	DOE-NDC-38	153	May86	OHO	Ahmad+ NDG. STAINLESS STEEL.
^{cmp}Fe	$\sigma_{p,emis}$	9.4+6	1.1+7	Expt	DOE-NDC-38	153	May86	OHO	Ahmad+ NDG. STAINLESS STEEL.
^{59}Co	Evaluation	NDG		Eval	DOE-NDC-38	8	May86	ANL	Smith+ TBC. NDG.
^{59}Co	σ_{tot}	NDG		Eval	DOE-NDC-38	8	May86	ANL	Smith+ TBC. NDG.
^{59}Co	$\sigma_{el}(\theta)$	3.6+5	1.0+7	Expt	DOE-NDC-38	1	May86	ANL	Smith+ GRPH. MEAS, CALC CFD. TBC.
^{59}Co	$\sigma_{el}(\theta)$	NDG		Eval	DOE-NDC-38	8	May86	ANL	Smith+ TBC. NDG.
^{59}Co	$\sigma_{dif.inl}$	1.6+6	1.0+7	Expt	DOE-NDC-38	1	May86	ANL	Smith+ GRPH. MEAS, CALC CFD. TBC.
^{59}Co	$\sigma_{dif.inl}$	5.0+6	1.0+7	Expt	DOE-NDC-38	4	May86	ANL	Guenther+ NDG. TBC.
^{59}Co	$\sigma_{n,2n}$	1.5+7		Expt	DOE-NDC-38	5	May86	ANL	Meadows. GRPH MEAS CFD EVAL.
^{59}Co	$\sigma_{n,2n}$	1.4+7	1.5+7	Expt	DOE-NDC-38	132	May86	NMX	Robertson+ M,G ST.CS. TB ANALYZED.
^{59}Co	$\sigma_{n,p}$	1.5+7		Expt	DOE-NDC-38	5	May86	ANL	Meadows. GRPH MEAS CFD EVAL.
^{59}Co	$\sigma_{n,\alpha}$	1.5+7		Expt	DOE-NDC-38	5	May86	ANL	Meadows. GRPH MEAS CFD EVAL.
Ni	$\sigma_{el}(\theta)$	4.0+6	1.0+7	Expt	DOE-NDC-38	1	May86	ANL	Smith+ NDG. TBC.
^{58}Ni	σ_{tot}		8.0+7	Theo	DOE-NDC-38	171	May86	TNL	Gould+ GRPH CC CALC CFD EXPT.
^{58}Ni	$\sigma_{el}(\theta)$	1.4+6	1.0+7	Expt	DOE-NDC-38	1	May86	ANL	Smith+ GRPH. MEAS, CALC CFD. TBC.
^{58}Ni	σ_{pol}	NDG		Theo	DOE-NDC-38	171	May86	TNL	Gould+ NDG.
^{58}Ni	$\sigma_{n,X\gamma}$	+6	5.0+7	Theo	DOE-NDC-38	97	May86	LAS	Arthur+ EXTEND ENDF/B GT 20 MEV.
^{58}Ni	$\sigma_{n,2n}$	1.5+7		Expt	DOE-NDC-38	5	May86	ANL	Meadows. GRPH MEAS CFD EVAL.
^{58}Ni	$\sigma_{n,2n}$	1.4+7	1.5+7	Expt	DOE-NDC-38	132	May86	NMX	Robertson+ NDG. TBD.
^{58}Ni	$\sigma_{n,emis}$	+6	5.0+7	Theo	DOE-NDC-38	97	May86	LAS	Arthur+ EXTEND ENDF/B GT 20 MEV.
^{58}Ni	$\sigma_{\alpha,emis}$	+6	5.0+7	Theo	DOE-NDC-38	97	May86	LAS	Arthur+ EXTEND ENDF/B GT 20 MEV.
^{58}Ni	$\sigma_{\alpha,emis}$	8.0+6	1.1+7	Expt	DOE-NDC-38	151	May86	OHO	Graham+ NDG. CS, SPECTRA MEAS.
^{58}Ni	$\sigma_{d,emis}$	+6	5.0+7	Theo	DOE-NDC-38	97	May86	LAS	Arthur+ EXTEND ENDF/B GT 20 MEV.
^{58}Ni	$\sigma_{p,emis}$	+6	5.0+7	Theo	DOE-NDC-38	97	May86	LAS	Arthur+ EXTEND ENDF/B GT 20 MEV.
^{58}Ni	$\sigma_{p,emis}$	8.0+6	1.1+7	Expt	DOE-NDC-38	151	May86	OHO	Graham+ NDG. CS, SPECTRA MEAS.

Element	Quantity	Energy (eV) Min	Max	Type	Documentation Ref	Page	Date	Lab	Comments
^{60}Ni	$\sigma_{n,X\gamma}$	+6	5.0+7	Theo	DOE-NDC-38	97	May86	LAS	Arthur+ EXTEND ENDF/B GT 20 MEV.
^{60}Ni	$\sigma_{n,emis}$	+6	5.0+7	Theo	DOE-NDC-38	97	May86	LAS	Arthur+ EXTEND ENDF/B GT 20 MEV.
^{60}Ni	$\sigma_{\alpha,emis}$	+6	5.0+7	Theo	DOE-NDC-38	97	May86	LAS	Arthur+ EXTEND ENDF/B GT 20 MEV.
^{60}Ni	$\sigma_{\alpha,emis}$	9.4+6	1.1+7	Expt	DOE-NDC-38	151	May86	OHO	Graham+ NDG. CS, SPECTRA MEAS.
^{60}Ni	$\sigma_{d,emis}$	+6	5.0+7	Theo	DOE-NDC-38	97	May86	LAS	Arthur+ EXTEND ENDF/B GT 20 MEV.
^{60}Ni	$\sigma_{p,emis}$	+6	5.0+7	Theo	DOE-NDC-38	97	May86	LAS	Arthur+ EXTEND ENDF/B GT 20 MEV.
^{60}Ni	$\sigma_{p,emis}$	9.4+6	1.1+7	Expt	DOE-NDC-38	151	May86	OHO	Graham+ NDG. CS, SPECTRA MEAS.
^{62}Ni	$\sigma_{n,X\gamma}$	+6	5.0+7	Theo	DOE-NDC-38	97	May86	LAS	Arthur+ EXTEND ENDF/B GT 20 MEV.
^{62}Ni	$\sigma_{n,emis}$	+6	5.0+7	Theo	DOE-NDC-38	97	May86	LAS	Arthur+ EXTEND ENDF/B GT 20 MEV.
^{62}Ni	$\sigma_{\alpha,emis}$	+6	5.0+7	Theo	DOE-NDC-38	97	May86	LAS	Arthur+ EXTEND ENDF/B GT 20 MEV.
^{62}Ni	$\sigma_{d,emis}$	+6	5.0+7	Theo	DOE-NDC-38	97	May86	LAS	Arthur+ EXTEND ENDF/B GT 20 MEV.
^{62}Ni	$\sigma_{p,emis}$	+6	5.0+7	Theo	DOE-NDC-38	97	May86	LAS	Arthur+ EXTEND ENDF/B GT 20 MEV.
^{63}Cu	$\sigma_{n,X\gamma}$	+6	5.0+7	Theo	DOE-NDC-38	97	May86	LAS	Arthur+ EXTEND ENDF/B GT 20 MEV.
^{63}Cu	$\sigma_{n,2n}$	1.5+7		Expt	DOE-NDC-38	132	May86	NMX	Robertson+ CS=549+-11MB.TBP ANE.
^{63}Cu	$\sigma_{n,emis}$	+6	5.0+7	Theo	DOE-NDC-38	97	May86	LAS	Arthur+ EXTEND ENDF/B GT 20 MEV.
^{63}Cu	$\sigma_{\alpha,emis}$	+6	5.0+7	Theo	DOE-NDC-38	97	May86	LAS	Arthur+ EXTEND ENDF/B GT 20 MEV.
^{63}Cu	$\sigma_{d,emis}$	+6	5.0+7	Theo	DOE-NDC-38	97	May86	LAS	Arthur+ EXTEND ENDF/B GT 20 MEV.
^{63}Cu	$\sigma_{p,emis}$	+6	5.0+7	Theo	DOE-NDC-38	97	May86	LAS	Arthur+ EXTEND ENDF/B GT 20 MEV.
^{64}Cu	$\sigma_{n,\gamma}$	PILE		Expt	DOE-NDC-38	163	May86	AI	Kneff+ CS=270+-170B (HFIR REACT.)
^{64}Cu	$\sigma_{n,\gamma}$	2.5-2		Expt	DOE-NDC-38	7	May86	ANL	Greenwood. SIG=270+-170B.
^{65}Cu	$\sigma_{n,X\gamma}$	+6	5.0+7	Theo	DOE-NDC-38	97	May86	LAS	Arthur+ EXTEND ENDF/B GT 20 MEV.
^{65}Cu	$\sigma_{n,2n}$	1.5+7		Expt	DOE-NDC-38	5	May86	ANL	Meadows. GRPH MEAS CFD EVAL.
^{65}Cu	$\sigma_{n,2n}$	1.5+7		Expt	DOE-NDC-38	120	May86	MHG	Lai+ NDG. TBD.
^{65}Cu	$\sigma_{n,2n}$	1.5+7		Expt	DOE-NDC-38	132	May86	NMX	Robertson+ CS=968+-20MB.TBP ANE.
^{65}Cu	$\sigma_{n,emis}$	+6	5.0+7	Theo	DOE-NDC-38	97	May86	LAS	Arthur+ EXTEND ENDF/B GT 20 MEV.
^{65}Cu	$\sigma_{n,p}$	1.5+7		Expt	DOE-NDC-38	5	May86	ANL	Meadows. GRPH MEAS CFD EVAL.
^{65}Cu	$\sigma_{\alpha,emis}$	+6	5.0+7	Theo	DOE-NDC-38	97	May86	LAS	Arthur+ EXTEND ENDF/B GT 20 MEV.
^{65}Cu	$\sigma_{d,emis}$	+6	5.0+7	Theo	DOE-NDC-38	97	May86	LAS	Arthur+ EXTEND ENDF/B GT 20 MEV.
^{65}Cu	$\sigma_{p,emis}$	+6	5.0+7	Theo	DOE-NDC-38	97	May86	LAS	Arthur+ EXTEND ENDF/B GT 20 MEV.
^{64}Zn	$\sigma_{n,2n}$	1.5+7		Expt	DOE-NDC-38	5	May86	ANL	Meadows. GRPH MEAS CFD EVAL.
^{64}Zn	$\sigma_{n,2n}$	1.4+7	1.5+7	Expt	DOE-NDC-38	132	May86	NMX	Robertson+ NDG. TBC.
^{64}Zn	$\sigma_{n,p}$	1.5+7		Expt	DOE-NDC-38	5	May86	ANL	Meadows. GRPH MEAS CFD EVAL.
^{64}Zn	$\sigma_{n,p}$	1.5+7		Expt	DOE-NDC-38	120	May86	MHG	Lai+ NDG. TBD.

Element	Quantity	Energy (eV) Min	Max	Type	Documentation Ref	Page	Date	Lab	Comments
^{64}Zn	$\sigma_{n,p}$	1.4+7	1.5+7	Expt	DOE-NDC-38	132	May86	NMX	Robertson+ NDG. TBC.
^{65}Zn	σ_{abs}	PILE		Expt	DOE-NDC-38	163	May86	AI	Kneff+ CS=66+-8B (HFIR REACTOR)
^{65}Zn	σ_{abs}	2.5-2		Expt	DOE-NDC-38	7	May86	ANL	Greenwood. SIG=66+-8 B.
^{65}Zn	$\sigma_{n,\alpha}$	PILE		Expt	DOE-NDC-38	163	May86	AI	Kneff+ CS=4.7+-0.5B (HFIR REACT.)
^{65}Zn	$\sigma_{n,\alpha}$	2.5-2		Expt	DOE-NDC-38	7	May86	ANL	Greenwood. SIG=4.7+-0.5 B.
^{66}Zn	$\sigma_{n,2n}$	1.4+7	1.5+7	Expt	DOE-NDC-38	132	May86	NMX	Robertson+ NDG. TBC.
^{86}Sr	$\sigma_{n,\gamma}$	1.0+2	1.0+6	Expt	DOE-NDC-38	69	May86	LRL	Bauer+ TBL. MAXW CS.
^{87}Sr	$\sigma_{n,\gamma}$	1.0+2	1.0+6	Expt	DOE-NDC-38	69	May86	LRL	Bauer+ TBL. MAXW CS.
^{88}Y	$\sigma_{dif.inl}$	1.6+6	1.5+7	Theo	DOE-NDC-38	83	May86	LRL	Gardner+ GRPH. (M/G)88Y CFD.
^{88}Y	$\sigma_{n,2n}$	1.0+7	1.5+7	Theo	DOE-NDC-38	83	May86	LRL	Gardner+ GRPH. (M/G)87Y CFD EXPT.
^{89}Y	Evaluation	2.5-2	2.0+7	Eval	DOE-NDC-38	8	May86	ANL	Smith+ NDG.
^{89}Y	$\sigma_{el}(\theta)$	1.5+6	1.0+7	Expt	DOE-NDC-38	1	May86	ANL	Smith+ NDG. TBC.
^{89}Y	$\sigma_{el}(\theta)$	7.9+6	1.7+7	Expt	DOE-NDC-38	172	May86	TNL	Gould+ GRPH CFD SPHERICAL OM.CALC.
^{89}Y	σ_{pol}	7.9+6	1.7+7	Expt	DOE-NDC-38	172	May86	TNL	Gould+ GRPH CFD SPHERICAL OM.CALC.
^{89}Y	$\sigma_{dif.inl}$	5.0+6	1.0+7	Expt	DOE-NDC-38	4	May86	ANL	Guenther+ NDG. TBC.
Zr	$\sigma_{el}(\theta)$	1.5+6	1.0+7	Expt	DOE-NDC-38	1	May86	ANL	Smith+ NDG. TBC.
^{90}Zr	$\sigma_{n,p}$	6.5+7		Expt	DOE-NDC-38	33	May86	DAV	Ford+ GRPH. ANG. DIST. CFD. CALC.
^{90}Zr	$\sigma_{p,emis}$	6.5+7		Expt	DOE-NDC-38	33	May86	DAV	Ford+ NDG. SPECTRA (0-40 DEGS).
^{93}Zr	σ_{tot}	6.0+1	6.0+3	Expt	DOE-NDC-38	138	May86	ORL	Macklin+ NDG.
^{93}Zr	Res.Params.	NDG		Expt	DOE-NDC-38	138	May86	ORL	Macklin+ EN=110.43EV, WN=348MV.
^{93}Nb	$\sigma_{el}(\theta)$	1.5+6	1.0+7	Expt	DOE-NDC-38	1	May86	ANL	Smith+ NDG.
^{93}Nb	$\sigma_{el}(\theta)$	8.0+6	1.7+7	Expt	DOE-NDC-38	172	May86	TNL	Gould+ GRPH CFD SPHERICAL OM.CALC.
^{93}Nb	σ_{pol}	8.0+6	1.7+7	Expt	DOE-NDC-38	172	May86	TNL	Gould+ NDG.
^{93}Nb	$\sigma_{dif.inl}$	5.0+6	1.0+7	Expt	DOE-NDC-38	4	May86	ANL	Guenther+ NDG. TBC.
^{93}Nb	$\sigma_{dif.inl}$	FISS		Expt	DOE-NDC-38	38	May86	INL	Rogers+ 252CF,235U,SPEC.FISS AVG CS.
^{92}Mo	$\sigma_{n,2n}$	1.4+7	1.5+7	Expt	DOE-NDC-38	132	May86	NMX	Robertson+ NDG. TBD.
^{94}Mo	$\sigma_{n,p}$	1.5+7		Expt	DOE-NDC-38	5	May86	ANL	Greenwood. PRELIM. SIG=56MB.
^{95}Mo	$\sigma_{n,\gamma}$	5.0+3	1.0+5	Expt	DOE-NDC-38	140	May86	ORL	Winters+ CS(30KEV)=292+-2MB.
^{95}Mo	$\sigma_{n,np}$	1.5+7		Expt	DOE-NDC-38	5	May86	ANL	Greenwood. (N,NP)+(N,D)=16 MB.
^{95}Mo	$\sigma_{n,d}$	1.5+7		Expt	DOE-NDC-38	5	May86	ANL	Greenwood. (N,NP)+(N,D)=16 MB.
^{96}Mo	$\sigma_{n,\gamma}$	5.0+3	1.0+5	Expt	DOE-NDC-38	140	May86	ORL	Winters+ CS(30KEV)=112+-6MB.
^{97}Mo	$\sigma_{n,\gamma}$	5.0+3	1.0+5	Expt	DOE-NDC-38	140	May86	ORL	Winters+ CS(30KEV)=339+-2MB.
^{98}Mo	$\sigma_{n,\gamma}$	5.0+3	1.0+5	Expt	DOE-NDC-38	140	May86	ORL	Winters+ CS(30KEV)=99+-5MB.

NEUTRON DATA REFERENCES

Element	Quantity	Energy (eV) Min	Max	Type	Documentation Ref	Page	Date	Lab	Comments
^{99}Tc	$\sigma_{n,\gamma}$	5.0+3	1.0+5	Expt	DOE-NDC-38	140	May86	ORL	Winters+ CS(30KEV)=782+-39MB.
^{116}Sn	σ_{tot}	3.0+5	5.0+6	Expt	DOE-NDC-38	55	May86	KTY	Zhou+ NDG. SELF-SHIELDING CORR.
^{116}Sn	$\sigma_{el}(\theta)$	1.0+4	5.0+6	Expt	DOE-NDC-38	55	May86	KTY	Harper+ NDG.
^{116}Sn	$\sigma_{el}(\theta)$	8.0+6	1.4+7	Theo	DOE-NDC-38	173	May86	TNL	Gould+ NDG. CC ANALYSIS.
^{116}Sn	$\sigma_{dif.inl}$	1.0+4	5.0+6	Expt	DOE-NDC-38	55	May86	KTY	Harper+ NDG.
^{116}Sn	$\sigma_{n,n'\gamma}$	3.8+6	4.5+6	Expt	DOE-NDC-38	60	May86	KTY	Gasci+ NDG. ANG. DIST.
^{118}Sn	σ_{tot}	3.0+5	5.0+6	Expt	DOE-NDC-38	55	May86	KTY	Zhou+ NDG. SELF-SHIELDING CORR.
^{118}Sn	$\sigma_{el}(\theta)$	1.0+4	5.0+6	Expt	DOE-NDC-38	55	May86	KTY	Harper+ NDG.
^{118}Sn	$\sigma_{dif.inl}$	1.0+4	5.0+6	Expt	DOE-NDC-38	55	May86	KTY	Harper+ NDG.
^{120}Sn	σ_{tot}	3.0+5	5.0+6	Expt	DOE-NDC-38	55	May86	KTY	Zhou+ NDG. SELF-SHIELDING CORR.
^{120}Sn	$\sigma_{el}(\theta)$	1.0+4	5.0+6	Expt	DOE-NDC-38	55	May86	KTY	Harper+ NDG.
^{120}Sn	$\sigma_{el}(\theta)$	8.0+6	1.4+7	Theo	DOE-NDC-38	173	May86	TNL	Gould+ NDG. CC ANALYSIS.
^{120}Sn	$\sigma_{dif.inl}$	1.0+4	5.0+6	Expt	DOE-NDC-38	55	May86	KTY	Harper+ NDG.
^{120}Sn	$\sigma_{n,n'\gamma}$	3.2+6	4.5+6	Expt	DOE-NDC-38	61	May86	KTY	Shi+ NDG. ANG. DIST.
^{122}Sn	σ_{tot}	3.0+5	5.0+6	Expt	DOE-NDC-38	55	May86	KTY	Zhou+ NDG. SELF-SHIELDING CORR.
^{122}Sn	$\sigma_{el}(\theta)$	1.0+4	5.0+6	Expt	DOE-NDC-38	55	May86	KTY	Harper+ NDG.
^{122}Sn	$\sigma_{dif.inl}$	1.0+4	5.0+6	Expt	DOE-NDC-38	55	May86	KTY	Harper+ NDG.
^{124}Sn	σ_{tot}	3.0+5	5.0+6	Expt	DOE-NDC-38	55	May86	KTY	Zhou+ NDG. SELF-SHIELDING CORR.
^{124}Sn	$\sigma_{el}(\theta)$	1.0+4	5.0+6	Expt	DOE-NDC-38	55	May86	KTY	Harper+ NDG.
^{124}Sn	$\sigma_{dif.inl}$	1.0+4	5.0+6	Expt	DOE-NDC-38	55	May86	KTY	Harper+ NDG.
^{145}Pm	$\sigma_{n,\gamma}$	FISS		Theo	DOE-NDC-38	79	May86	LRL	Gardner+ CS GT 144SM(N,G).
^{145}Pm	$\sigma_{n,\gamma}$	2.5-2		Theo	DOE-NDC-38	79	May86	LRL	Gardner+ NDG.
^{144}Sm	$\sigma_{n,\gamma}$	2.5-2		Theo	DOE-NDC-38	79	May86	LRL	Gardner+ NDG.
^{144}Sm	$\sigma_{n,\gamma}$	FISS		Theo	DOE-NDC-38	79	May86	LRL	Gardner+ CS LT 145SM,145PM.
^{145}Sm	$\sigma_{n,\gamma}$	FISS		Theo	DOE-NDC-38	79	May86	LRL	Gardner+ CS GT 144SM(N,G).
^{145}Sm	$\sigma_{n,\gamma}$	2.5-2		Theo	DOE-NDC-38	79	May86	LRL	Gardner+ NDG.
Gd	σ_{tot}	1.0+4	2.0+7	Theo	DOE-NDC-38	101	May86	LAS	Young. GRPH CALC.CFD EXPTS.
^{152}Gd	$\sigma_{n,\gamma}$	NDG		Eval	DOE-NDC-38	37	May86	HED	Schenter+ NDG. EPITHERMAL ENERGIES.
^{153}Gd	$\sigma_{n,\gamma}$	NDG		Eval	DOE-NDC-38	37	May86	HED	Schenter+ NDG. EPITHERMAL ENERGIES.
^{165}Ho	σ_{tot}	1.0+6	1.0+8	Theo	DOE-NDC-38	99	May86	LAS	Arthur+ GRPH. CC CALC CFD EXPT.
^{165}Ho	$\sigma_{n,\gamma}$	1.0+4	4.0+6	Theo	DOE-NDC-38	101	May86	LAS	Young. GRPH CALC.CFD EXPTS.
^{165}Ho	$\sigma_{n,X\gamma}$	4.0+2	3.0+6	Expt	DOE-NDC-38	91	May86	LAS	Wender+ GRPH. GAMMA PROD.
^{175}Lu	γ Spectra	2.0+3		Theo	DOE-NDC-38	75	May86	LRL	Gardner+ GRPH,PRIMARY G-SPECTRA.

Element	Quantity	Energy (eV) Min	Max	Type	Documentation Ref	Page	Date	Lab	Comments
^{182}W	$\sigma_{el}(\theta)$	4.9+6	6.0+6	Expt	DOE-NDC-38	151	May86	OHO	Annand+ NDG.
^{182}W	$\sigma_{dif.inl}$	4.9+6	6.0+6	Expt	DOE-NDC-38	151	May86	OHO	Annand+ NDG.
^{182}W	$\sigma_{n,X\gamma}$	+6	5.0+7	Theo	DOE-NDC-38	97	May86	LAS	Arthur+ EXTEND ENDF/B GT 20 MEV.
^{182}W	$\sigma_{n,emis}$	+6	5.0+7	Theo	DOE-NDC-38	97	May86	LAS	Arthur+ EXTEND ENDF/B GT 20 MEV.
^{182}W	$\sigma_{p,emis}$	+6	5.0+7	Theo	DOE-NDC-38	97	May86	LAS	Arthur+ EXTEND ENDF/B GT 20 MEV.
^{184}W	$\sigma_{el}(\theta)$	4.9+6	6.0+6	Expt	DOE-NDC-38	151	May86	OHO	Annand+ NDG.
^{184}W	$\sigma_{dif.inl}$	4.9+6	6.0+6	Expt	DOE-NDC-38	151	May86	OHO	Annand+ NDG.
^{184}W	$\sigma_{n,X\gamma}$	+6	5.0+7	Theo	DOE-NDC-38	97	May86	LAS	Arthur+ EXTEND ENDF/B GT 20 MEV.
^{184}W	$\sigma_{n,emis}$	+6	5.0+7	Theo	DOE-NDC-38	97	May86	LAS	Arthur+ EXTEND ENDF/B GT 20 MEV.
^{184}W	$\sigma_{p,emis}$	+6	5.0+7	Theo	DOE-NDC-38	97	May86	LAS	Arthur+ EXTEND ENDF/B GT 20 MEV.
^{186}Os	σ_{tot}	2.7+1	1.0+3	Expt	DOE-NDC-38	140	May86	ORL	Winters. NDG.TBP PR/C.
^{186}Os	Res.Params.	NDG		Expt	DOE-NDC-38	140	May86	ORL	Winters. NDG.TBP PR/C.
^{187}Os	σ_{tot}	2.7+1	1.4+2	Expt	DOE-NDC-38	140	May86	ORL	Winters. NDG.TBP PR/C.
^{187}Os	$\sigma_{dif.inl}$	6.0+4		Expt	DOE-NDC-38	58	May86	KTY	Hershberger+ CS(9.75 KEV LVL) LARGE.
^{187}Os	Res.Params.	NDG		Expt	DOE-NDC-38	140	May86	ORL	Winters. NDG.TBP PR/C.
^{188}Os	σ_{tot}	2.7+1	1.0+3	Expt	DOE-NDC-38	140	May86	ORL	Winters. NDG.TBP PR/C.
^{188}Os	Res.Params.	NDG		Expt	DOE-NDC-38	140	May86	ORL	Winters. NDG.TBP PR/C.
^{189}Os	$\sigma_{el}(\theta)$	6.0+4	9.7+4	Expt	DOE-NDC-38	58	May86	KTY	Hershberger+ NDG.
^{189}Os	$\sigma_{dif.inl}$	6.0+4	9.7+4	Expt	DOE-NDC-38	58	May86	KTY	Hershberger+ NDG.
^{189}Os	$\sigma_{n,\gamma}$	2.0+2	5.0+5	Expt	DOE-NDC-38	140	May86	ORL	Winters+ CS(30KEV)=1168+-47MB.
^{189}Os	Res.Params.	NDG		Expt	DOE-NDC-38	140	May86	ORL	Winters+ AVG.WG=83+-5MV.
^{189}Os	$\langle\Gamma\rangle/D$	NDG		Expt	DOE-NDC-38	140	May86	ORL	Winters+ S0=(2.9+-0.5)X(10)$^{-4}$.
^{190}Os	σ_{tot}	NDG		Expt	DOE-NDC-38	53	May86	KTY	Hicks+ NDG.
^{192}Os	σ_{tot}	NDG		Expt	DOE-NDC-38	53	May86	KTY	Hicks+ NDG.
^{192}Os	$\sigma_{el}(\theta)$	1.6+6	4.5+6	Expt	DOE-NDC-38	53	May86	KTY	Hicks+ NDG.
^{192}Os	$\sigma_{dif.inl}$	1.6+6	4.5+6	Expt	DOE-NDC-38	53	May86	KTY	Hicks+ NDG.
^{194}Pt	σ_{tot}	NDG		Expt	DOE-NDC-38	53	May86	KTY	Hicks+ NDG.
^{194}Pt	$\sigma_{el}(\theta)$	1.6+6	4.5+6	Expt	DOE-NDC-38	53	May86	KTY	Hicks+ NDG.
^{194}Pt	$\sigma_{dif.inl}$	1.6+6	4.5+6	Expt	DOE-NDC-38	53	May86	KTY	Hicks+ NDG.
^{204}Pb	σ_{tot}	3.0+5	4.0+6	Expt	DOE-NDC-38	54	May86	KTY	Hanly+ NDG.
^{204}Pb	$\sigma_{el}(\theta)$	2.5+6	4.5+6	Expt	DOE-NDC-38	54	May86	KTY	Hanly+ NDG.
^{206}Pb	σ_{tot}	3.0+5	4.0+6	Expt	DOE-NDC-38	54	May86	KTY	Hanly+ NDG.
^{206}Pb	$\sigma_{el}(\theta)$	2.5+6	4.5+6	Expt	DOE-NDC-38	54	May86	KTY	Hanly+ NDG.

Element	Quantity	Energy (eV) Min	Max	Type	Documentation Ref	Page	Date	Lab	Comments
^{208}Pb	$\sigma_{el}(\theta)$	4.0+6	7.0+6	Expt	DOE-NDC-38	152	May86	OHO	Annand+ NDG.
^{208}Pb	$\sigma_{el}(\theta)$	8.0+6	1.4+7	Theo	DOE-NDC-38	173	May86	TNL	Gould+ NDG. CC ANALYSIS.
^{208}Pb	$\sigma_{dif.inl}$	4.0+6	7.0+6	Expt	DOE-NDC-38	152	May86	OHO	Annand+ NDG.
^{209}Bi	$\sigma_{el}(\theta)$	4.0+6	1.0+7	Expt	DOE-NDC-38	3	May86	ANL	Smith+ NDG. TBC.
^{209}Bi	$\sigma_{el}(\theta)$	4.0+6	7.0+6	Expt	DOE-NDC-38	152	May86	OHO	Annand+ NDG.
^{209}Bi	$\sigma_{dif.inl}$	4.0+6	1.0+7	Expt	DOE-NDC-38	3	May86	ANL	Smith+ NDG. TBC.
^{209}Bi	$\sigma_{dif.inl}$	4.0+6	7.0+6	Expt	DOE-NDC-38	152	May86	OHO	Annand+ NDG.
^{230}Th	$\sigma_{n,f}$	1.5+7		Expt	DOE-NDC-38	4	May86	ANL	Meadows. NDG. RATIO TO 235U. TBD.
^{230}Th	Fiss.Yield	FAST		Expt	DOE-NDC-38	141	May86	ORL	Dickens+ NDG.
^{232}Th	$\sigma_{el}(\theta)$	1.9+5		Expt	DOE-NDC-38	107	May86	LTI	Beghian+ ANG.DIST.
^{232}Th	$\sigma_{dif.inl}$	1.9+5		Expt	DOE-NDC-38	107	May86	LTI	Beghian+ ANG.DIST.
^{232}Th	$\sigma_{dif.inl}$	2.0+6		Expt	DOE-NDC-38	110	May86	LTI	Beghian+ NDG. TBD.
^{232}Th	$\sigma_{n,\gamma}$	2.7+5	9.6+5	Expt	DOE-NDC-38	117	May86	MHG	Melton+ NDG.
^{232}Th	$\sigma_{n,f}$	1.5+7		Expt	DOE-NDC-38	4	May86	ANL	Meadows. NDG. RATIO TO 235U. TBD.
^{232}Th	Fiss.Yield	FAST		Expt	DOE-NDC-38	141	May86	ORL	Dickens+ NDG.
^{231}Pa	Fiss.Yield	FAST		Expt	DOE-NDC-38	141	May86	ORL	Dickens+ NDG.
^{233}U	$\sigma_{n,f}$	1.5+7		Expt	DOE-NDC-38	4	May86	ANL	Meadows. RATIO TO 235U. NDG.
^{233}U	ν_p	5.0+2	1.0+7	Expt	DOE-NDC-38	142	May86	ORL	Gwin+ REL NU(252CF).NDG.
^{233}U	ν_d	2.5-2	5.0+6	Expt	DOE-NDC-38	112	May86	LTI	Couchell+ NDG. TBD.
^{233}U	ν_d	2.0+6	5.0+6	Expt	DOE-NDC-38	112	May86	LTI	Couchell+ NDG. TBD.
^{233}U	Fiss.Yield	FAST		Expt	DOE-NDC-38	141	May86	ORL	Dickens+ NDG.
^{234}U	$\sigma_{n,f}$	1.5+7		Expt	DOE-NDC-38	4	May86	ANL	Meadows. RATIO TO 235U. NDG.
^{234}U	Fiss.Yield	FAST		Expt	DOE-NDC-38	141	May86	ORL	Dickens+ NDG.
^{235}U	$\sigma_{el}(\theta)$	1.9+5		Expt	DOE-NDC-38	107	May86	LTI	Beghian+ ANG.DIST.
^{235}U	$\sigma_{dif.inl}$	1.9+5		Expt	DOE-NDC-38	107	May86	LTI	Beghian+ ANG.DIST.
^{235}U	$\sigma_{dif.inl}$	9.5+4		Expt	DOE-NDC-38	109	May86	LTI	Beghian+ NDG. CS(13KEV LVL).TBD.
^{235}U	$\sigma_{n,n'\gamma}$		5.0+5	Expt	DOE-NDC-38	109	May86	LTI	Beghian+ NDG. SEE 85SANTA FE.
^{235}U	$\sigma_{n,f}$	2.5-2	1.0+3	Expt	DOE-NDC-38	121	May86	NBS	Schrack+ NDG.TBC.
^{235}U	$\sigma_{n,f}$	3.0+5	3.0+6	Expt	DOE-NDC-38	123	May86	NBS	Carlson+ NDG.ENDF/B VI INPUT.
^{235}U	$\sigma_{n,f}$	FISS		Expt	DOE-NDC-38	124	May86	NBS	Schroeder+ 252CF.SPECT. CS=1234MB.
^{235}U	ν_p	5.0+2	1.0+7	Expt	DOE-NDC-38	142	May86	ORL	Gwin+ REL NU(252CF).NDG.
^{235}U	ν_d	2.5-2		Expt	DOE-NDC-38	112	May86	LTI	Couchell+ TBL. TBP. NSE.
^{235}U	Fiss.Yield	2.5-2		Expt	DOE-NDC-38	159	May86	BNW	Reeder+ ISOMER YLD RATIO,90RB,138CS.

NEUTRON DATA REFERENCES

Element	Quantity	Energy (eV) Min	Max	Type	Documentation Ref	Page	Date	Lab	Comments
^{235}U	Fiss.Yield	FAST		Expt	DOE-NDC-38	141	May86	ORL	Dickens+ NDG.
^{236}U	$\sigma_{n,f}$	1.5+7		Expt	DOE-NDC-38	4	May86	ANL	Meadows. RATIO TO 235U. NDG.
^{236}U	Fiss.Yield	FAST		Expt	DOE-NDC-38	141	May86	ORL	Dickens+ NDG.
^{238}U	$\sigma_{el}(\theta)$	1.9+5		Expt	DOE-NDC-38	107	May86	LTI	Beghian+ ANG.DIST.
^{238}U	$\sigma_{dif.inl}$	1.9+5		Expt	DOE-NDC-38	107	May86	LTI	Beghian+ ANG.DIST.
^{238}U	$\sigma_{dif.inl}$	2.0+6		Expt	DOE-NDC-38	110	May86	LTI	Beghian+ NDG. TBD.
^{238}U	$\sigma_{n,\gamma}$	2.3+4	9.6+5	Expt	DOE-NDC-38	117	May86	MHG	Melton+ NDG.
^{238}U	$\sigma_{n,f}$	1.5+7		Expt	DOE-NDC-38	4	May86	ANL	Meadows. RATIO TO 235U=0.574+-0.005.
^{238}U	$\sigma_{n,f}$	FISS		Expt	DOE-NDC-38	124	May86	NBS	Schroeder+ 252CF.SPECT. CS=332MB.
^{238}U	Fiss.Yield	FAST		Expt	DOE-NDC-38	141	May86	ORL	Dickens+ NDG.
^{238}U	Res.Params.	9.0+2	1.0+4	Expt	DOE-NDC-38	143	May86	ORL	Olsen. NDG.WN FOR 676 RES.
^{238}U	$\langle\Gamma\rangle/D$		1.0+4	Expt	DOE-NDC-38	143	May86	ORL	Olsen. $S0=0.94X(10)^{-4}$.
^{237}Np	$\sigma_{n,f}$	1.5+7		Expt	DOE-NDC-38	4	May86	ANL	Meadows. RATIO TO 235U. NDG.
^{242}Np	$\sigma_{n,f}$	1.5+7		Expt	DOE-NDC-38	4	May86	ANL	Meadows. RATIO TO 235U. NDG.
^{238}Pu	$\sigma_{n,f}$	1.0-1	1.0+5	Expt	DOE-NDC-38	161	May86	RPI	Alam+ GRPH PRELIM.CS.
^{238}Pu	Fiss.Yield	FAST		Expt	DOE-NDC-38	141	May86	ORL	Dickens+ NDG.
^{239}Pu	Evaluation		6.0+2	Eval	DOE-NDC-38	147	May86	ORL	Derrien+ R-MATRIX ANALYSIS.
^{239}Pu	$\sigma_{n,f}$	1.5+7		Expt	DOE-NDC-38	4	May86	ANL	Meadows. RATIO TO 235U. NDG.
^{239}Pu	$\sigma_{n,f}$	FISS		Expt	DOE-NDC-38	124	May86	NBS	Schroeder+ 252CF.SPECT. CS=1844MB.
^{239}Pu	ν_p	5.0+2	1.0+7	Expt	DOE-NDC-38	142	May86	ORL	Gwin+ REL NU(252CF).NDG.
^{239}Pu	ν_d	2.5-2		Expt	DOE-NDC-38	112	May86	LTI	Couchell+ GRPH SPECTRA. TBC.
^{239}Pu	ν_d	5.0+6		Expt	DOE-NDC-38	112	May86	LTI	Couchell+ NDG. TBD.
^{239}Pu	Fiss.Yield	FAST		Expt	DOE-NDC-38	141	May86	ORL	Dickens+ NDG.
^{240}Pu	Fiss.Yield	FAST		Expt	DOE-NDC-38	141	May86	ORL	Dickens+ NDG.
^{241}Pu	ν_p	5.0+2	1.0+7	Expt	DOE-NDC-38	142	May86	ORL	Gwin+ REL NU(252CF).NDG.
^{241}Pu	Fiss.Yield	FAST		Expt	DOE-NDC-38	141	May86	ORL	Dickens+ NDG.
^{244}Pu	Fiss.Yield	FAST		Expt	DOE-NDC-38	141	May86	ORL	Dickens+ NDG.
^{241}Am	Fiss.Yield	FAST		Expt	DOE-NDC-38	141	May86	ORL	Dickens+ NDG.
^{243}Am	Fiss.Yield	FAST		Expt	DOE-NDC-38	141	May86	ORL	Dickens+ NDG.
^{243}Cm	Fiss.Yield	FAST		Expt	DOE-NDC-38	141	May86	ORL	Dickens+ NDG.
^{244}Cm	Fiss.Yield	FAST		Expt	DOE-NDC-38	141	May86	ORL	Dickens+ NDG.
^{246}Cm	Fiss.Yield	FAST		Expt	DOE-NDC-38	141	May86	ORL	Dickens+ NDG.
^{248}Cm	Fiss.Yield	FAST		Expt	DOE-NDC-38	141	May86	ORL	Dickens+ NDG.

NEUTRON DATA REFERENCES

Element	Quantity	Energy (eV) Min	Energy (eV) Max	Type	Documentation Ref	Page	Date	Lab	Comments
^{252}Cf	ν_p	SPON		Expt	DOE-NDC-38	142	May86	ORL	Gwin+ RATIO 235U,233U,239PU,241PU.
^{252}Cf	Spect.fiss n	SPON		Theo	DOE-NDC-38	104	May86	LAS	Madland+ GRPHS CALC. EXPTS.

A. CROSS-SECTION MEASUREMENTS

1. The Energy Dependence of The Optical Model of Neutron Scattering from Niobium
(A. Smith, P. Guenther and R. Lawson)

A paper reporting the elastic-scattering cross sections of niobium over the incident-neutron-energy range 1.5-10.0 MeV, has been accepted for publication in Nuclear Physics. Differential cross sections were determined in energy increments of 200 keV below 4.0 MeV and of approximately 500 keV over the range 4.0-10.0 MeV. Scattering angles were distributed between 20 and 160 degrees. The observed values were interpreted in terms of the spherical optical-statistical model. It was found that the volume integral of the real (imaginary) potential decreases (increases) with energy in an essentially linear manner. Using the dispersion relationship between real and imaginary potentials, it was possible to correlate the two energy dependencies to a good degree of accuracy. The real potential strengths necessary to predict the binding energies of bound particle states are reasonably consistent with the linear formulation of the real potential indicated above, but the correlation with the bound hole states is ambiguous since the results obtained for high- and low-spin values are not consistent. There was no evidence of the "Fermi-surface anomaly" in the unbound-energy region accessible in the above-mentioned-scattering measurements.

2. Neutron Scattering from Structural Materials in the A=60 Region
(A. Smith, P. Guenther and R. Lawson)

An earlier program of measurements below 4.0 MeV in this region has been extended to the range 4.0-10.0 MeV, with emphasis on V, Cr, Fe, Co and Ni targets. Work on the latter two is the nearest to completion. The composite results (combining data above and below 4.0 MeV) provide a very comprehensive data base, as indicated by the elastic distributions of Fig. A-1. All of the data show a substantial direct-inelastic component, as illustrated by the Co results of Fig. A-2. Spherical optical-statistical and coupled-channels interpretations are in progress, with the intent of providing a unified description of the observables throughout the energy range. Careful attention is being paid to the long-known contradiction between high-energy based models and observables from the 1.0-3.0 MeV range.

3. Energy Dependence of the Optical Potential in the A=90 Region
(A. Smith, P. Guenther and R. Lawson)

On-going neutron-scattering studies (see Item A.1) are being extended to other targets (e.g., Y and Zr), and the scope of the physical interpretation is being broadened. In particular, the previously-conventional assumption of energy-independent geometric parameterization has been relaxed and the interrelation of the real and imaginary potentials implied by the dispersion relation has been incorporated in the interpretation. As indicated in Item A.1, preliminary results indicate that there is no evidence for the Fermi-surface anomaly in this mass region, over the 0-10 MeV energy range accessible to these neutron-scattering measurements. The real- and imaginary-potential strengths follow conventional linear-energy dependencies. The interpretations are consistent with a surface-peaked component of the real potential, as implied by the dispersion relation. The strength of this component generally decreases with energy. The imaginary-potential geometric parameters are energy-dependent, as is necessary to interpolate from well-established low-energy values to generally-global optical potentials describing neutron processes at incident energies well above 10 MeV.

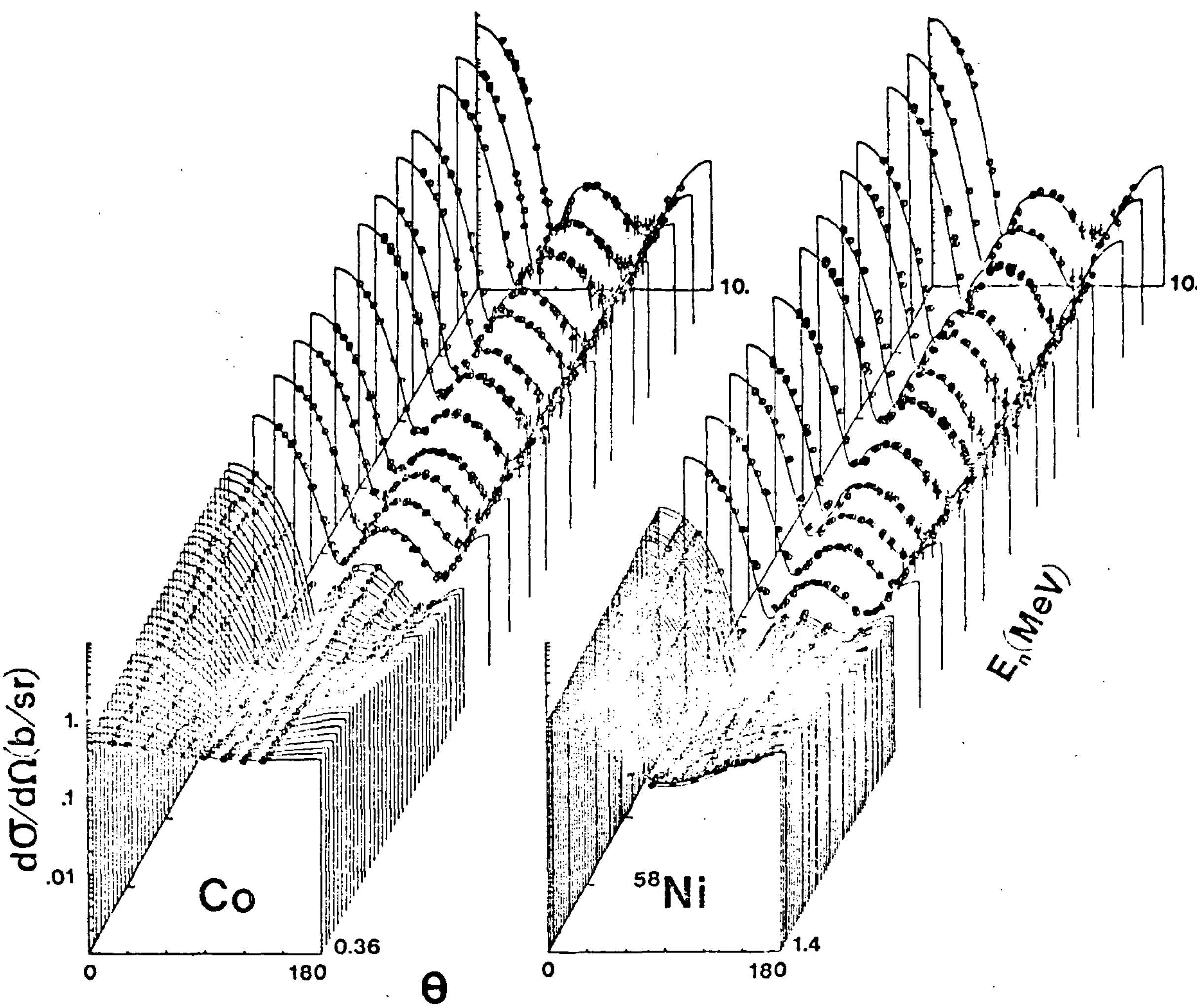

Fig. A-1. Measured (symbols) and calculated (curves) elastic-scattering cross sections from Co and ^{58}Ni.

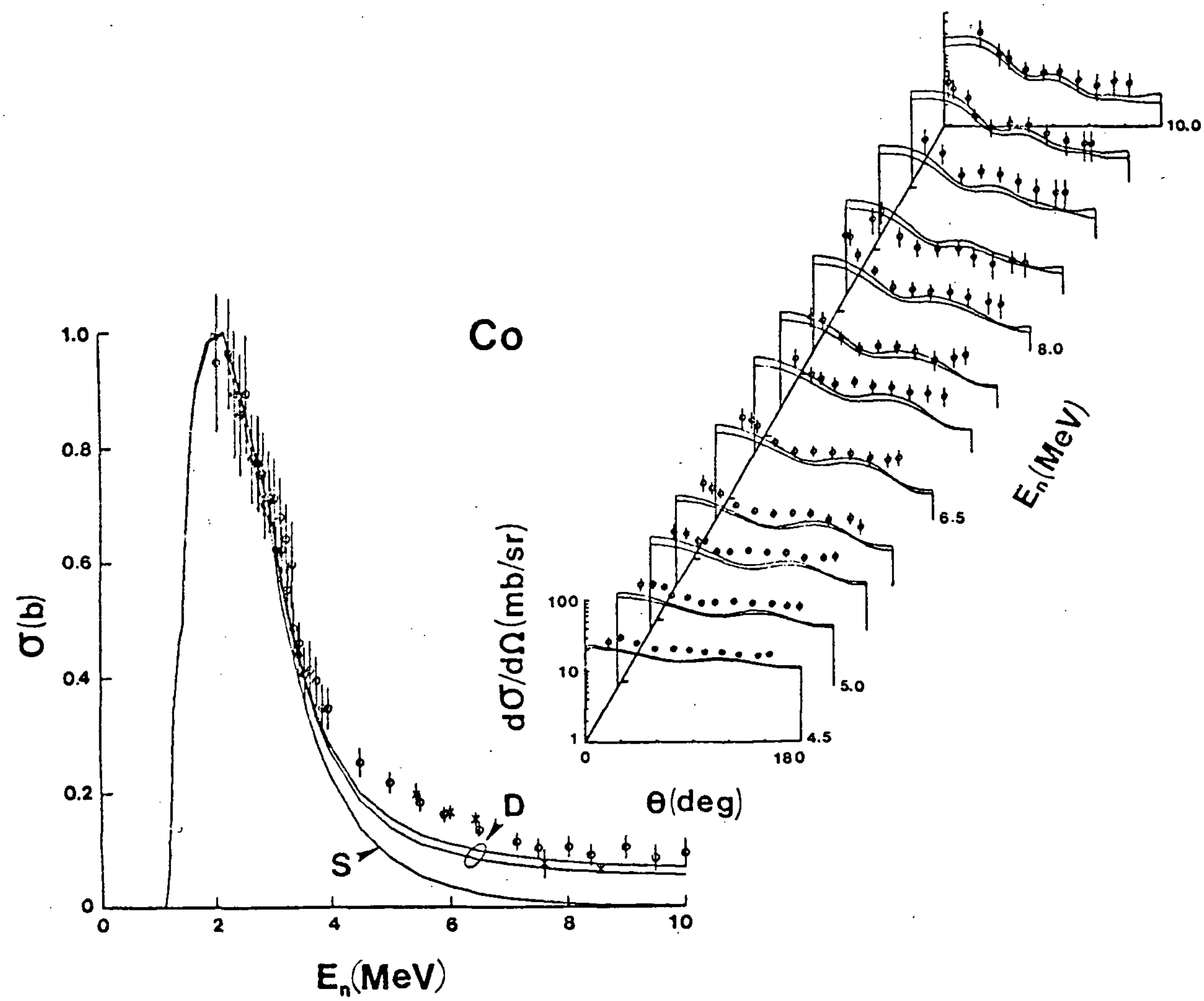

Fig. A-2. Measured (symbols) and calculated (curves) inelastic-scattering excitation of the Co hole states near E_x=1.3 MeV. S=spherical, D=deformed.

4. Neutron Scattering in the A=110-120 Region
(A. Smith, P. Guenther and R. Lawson)

Earlier lower-energy (below 4.0 MeV) studies of elastic and inelastic neutron scattering from targets in this mass region are being extended to 10 MeV.

5. Neutron Scattering in the A=208 Region
(A. Smith, P. Guenther and R. Lawson)

Careful measurements of elastic and inelastic scattering from Bi are in progress, from the 4.0-MeV upper-energy limit of previously-reported work from this laboratory to 10 MeV. Measurements are being made at incident-energy intervals of 500 keV, and at 40 or more scattering angles distributed between 17-158 degrees. Particular attention is being given to detail at the lower energies, to assure that fluctuations are not a concern in subsequent energy-average interpretations. It is hoped that the results will provide further definition of the optical potential. They will also be used eventually to revise the ENDF evaluated file for bismuth.

6. Continuum-inelastic-neutron Scattering
(P. Guenther and A. Smith)

Double-differential inelastic-neutron-scattering measurements are in progress over the incident-energy range 5.0-10.0 MeV. The measurements are being made at incident-energy intervals of approximately 1.0 MeV, and at ten scattering angles distributed between 25 and 160 deg. The neutron-energy distributions are determined relative to the concurrently-measured standard Cf-252 prompt-fission-neutron spectrum. This technique gives good accuracy while avoiding an independent calibration of the detector energy responses. The results are being used to determine energy dependencies of the parameters which describe the statistical-emission process and, at higher energies, to estimate the small precompound-emission contributions. Primary attention is being given to the A=60 region (e.g., Co) and the A=90 region (e.g., Y and Nb). Some preliminary results were presented at the recent Santa Fe conference.

7. Total, Scattering and Gamma-Ray-Production Cross Sections of ^{54}Fe
(P. Guenther, D. Smith, A. Smith and J. Whalen)

This investigation has been completed. Measurements and their interpretation address the incident-energy range 0.5-4 MeV. A paper describing the work is in preparation.

8. Fission Cross-section Ratios at 14.7 MeV
(J. W. Meadows)

Measurements of the fission cross sections of several isotopes relative to ^{235}U, at an average neutron energy of 14.7 MeV, are in progress using many of the samples from earlier work in the 0.1-10 MeV energy range. Measurements have been completed, and the data partially processed, for ^{233}U, ^{234}U, ^{236}U and ^{238}U. Preliminary results are available for the ^{238}U/^{235}U ratio. The simple average of the results from five pairs of samples is 0.574 ± 0.005. This may be compared with an ENDF/B-V value of 0.569.

Additional measurements are planned for ^{230}Th, ^{232}Th, ^{237}Np,

^{239}Pu and ^{242}Pu.

9. Neutron-activation Cross-section Measurements at 14.7 MeV
(J. W. Meadows, D. L. Smith and S. A. Cox)

Cross-sections at 14.7-MeV have been obtained for twenty neutron-activation reactions. Comparison has been made between these data and corresponding values from recent evaluations, including several performed at our laboratory (see Fig. A-3).[a] This work was reported at the Santa Fe conference.[b]

[a]Bernard P. Evain, Donald L. Smith and Paul Lucchese, ANL/NDM-89, Argonne National Laboratory (1985).

[b]J. W. Meadows, D. L. Smith and S. A. Cox, "Measurement and Evaluation of Selected 14-MeV Neutron Cross Sections for Fusion," International Conference on Nuclear Data for Basic and Applied Science, Santa Fe, NM, May 1985.

10. The Production of ^{94}Nb from ^{94}Mo and ^{Nat}Mo near 14.7 MeV
(L. R. Greenwood)

The production cross sections for ^{94}Nb from ^{94}Mo and ^{Nat}Mo have been measured near 14 MeV. This long-lived isotope (20,300 y) is of interest in the activation and disposal of fusion materials. Samples of natural Mo and isotopically-enriched ^{94}Mo were irradiated at the Rotating Target Neutron Source II at Lawrence Livermore National Laboratory. The samples were included with other irradiations for a total exposure time of 81 days. Following irradiation the samples were gamma counted to determine the activation of ^{94}Nb. Preliminary results of two measurements of each material gives production cross sections of 56 mb for the $^{94}Mo(n,p)$ reaction and 7.7 mb for natural Mo. The difference between these two values implies a cross section of about 16 mb for the $^{95}Mo(n,np + d)$ reactions. The average neutron energy was 14.7 MeV, although the RTNSII neutron spectrum has a spread of a few hundred keV. The cross sections are normalized to previous measurements on the $^{92}Nb(n,2n)$ reactions (463 mb) and the values have an estimated uncertainty of 10%. Measurements are in progress on several other long-lived isotopes of interest to the fusion program. Activation cross sections to 22 other radioisotopes measured at the RTNSII in the energy range from 14.5-14.9 MeV have recently been published.[a]

[a]L. R. Greenwood, M. W. Guinan, and D. W. Kneff, "Activation Cross Section Measurements at RTNSII", Damage Analysis and Fundamental Studies Quarterly Progress Report, DOE/ER-0046/21, pp. 15-18, May 1985.

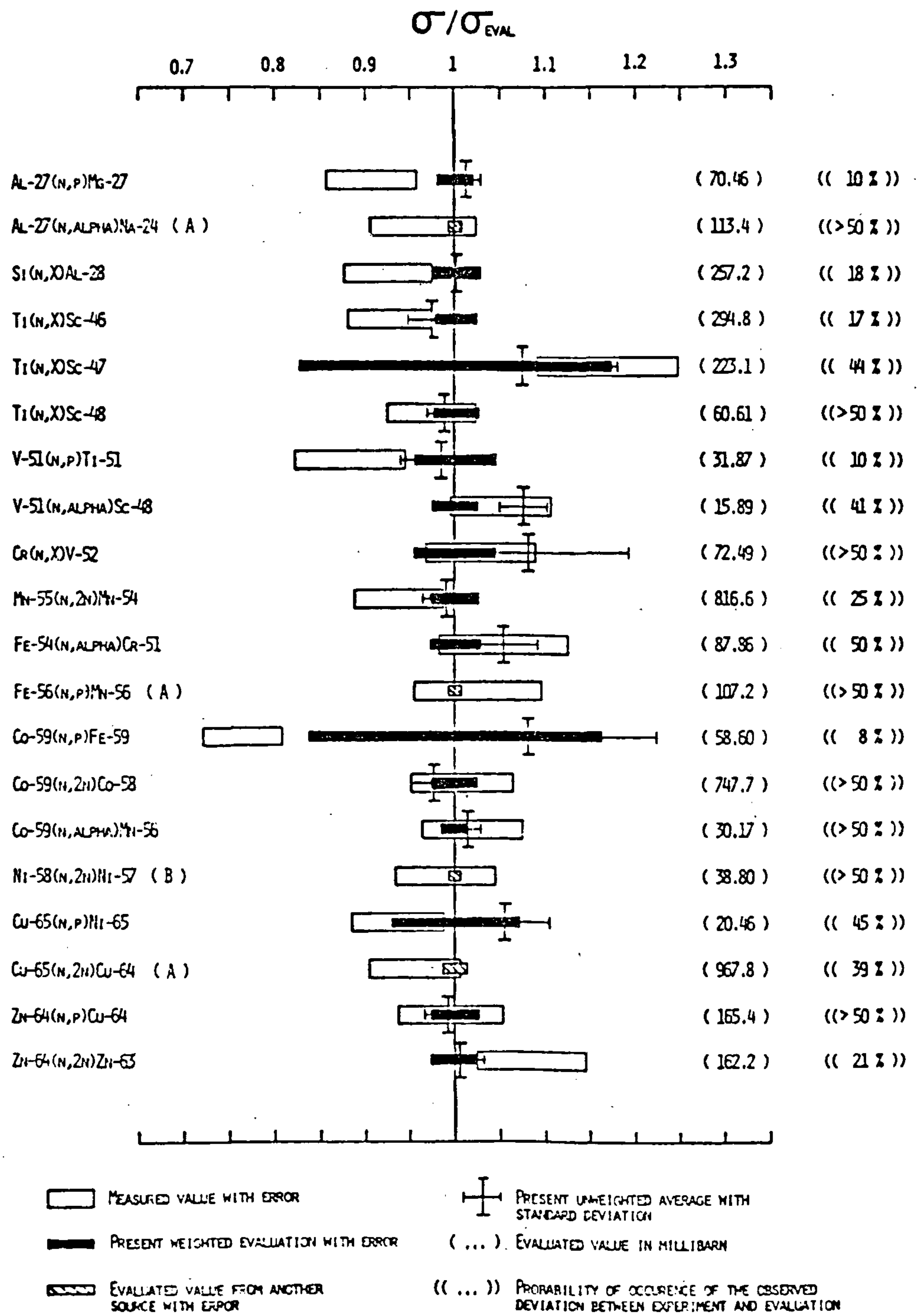

Fig. A-3. Comparison of measured and evaluated 14.7-MeV cross sections.

11. Discovery of Thermal Helium Production from Copper
(L. R. Greenwood)

A new effect has been discovered in copper irradiated in thermal or mixed-spectrum reactors.[a] During lengthy materials irradiations there is a build-up of ^{65}Zn from successive neutron captures starting with $^{63}Cu(n,\gamma)^{64}Cu$ which decays to ^{64}Zn, followed by $^{64}Zn(n,\gamma)^{65}Zn$. The ^{65}Zn has been shown to have a large thermal (n,He) cross section. Helium gas measurements and gamma spectroscopy have been used to determine several new thermal cross sections, as follows:

$^{64}Cu(n,\gamma)^{65}Cu$	270 ± 170 b
$^{65}Zn(n,abs)$	66 ± 8 b
$^{65}Zn(n,He)$	4.7 ± 0.5 b.

This reaction mechanism is especially interesting to fusion material studies since it can be used to enhance the helium production in materials irradiations at mixed-spectrum reactors, similar to the well-known process in nickel and stainless steel. This work was done in collaboration with Rockwell International.

[a]D. W. Kneff, L. R. Greenwood, B. M. Oliver, R. P. Skowronski, and E. L. Callis, "Helium Production in Copper by a Thermal Three-Stage Reaction", Proceedings of the International Conference on Nuclear Data for Basic and Applied Science, Santa Fe, NM, May 1985.

12. Elimination of the Discrepancy Between Differential and Integral Data for $^{47}Ti(n,p)^{47}Sc$
(W. Mannhart[a], D. L. Smith and J. W. Meadows)

The excitation function of $^{47}Ti(n,p)^{47}Sc$ was measured between 1.2 and 8 MeV neutron energy. In parallel, the integral response of this reaction in a ^{252}Cf and ^{235}U neutron spectrum was experimentally determined. All experiments were related to a common radioactivity counting detector. The present results eliminate a previous 25% discrepancy between the differential and integral data. A more detailed discussion of this work is available in the proceedings of the Santa Fe conference.[b]

[a]PTB-Braunschweig, Federal Republic of Germany.

[b]Wolf Mannhart, Donald L. Smith and James W. Meadows, "The Discrepancy Between Differential and Integral Data on $^{47}Ti(n,p)$", Proceedings of the International Conference on Nuclear Data for Basic and Applied Science, Santa Fe, NM, May 1985.

13. Integral-cross-section Measurements in the Thick-target $^{9}Be(d,n)^{10}B$ Spectrum at E_d=7 MeV
(D. L. Smith, J. W. Meadows and M. M. Bretscher)

Neutron-activation cross-section measurements have been performed for $^{7}Li(n,n't)^{4}He$, $^{27}Al(n,p)^{27}Mg$, $^{27}Al(n,\alpha)^{24}Na$, $^{58}Ni(n,p)^{58}Co$ and $^{60}Ni(n,p)^{60}Co$, and final results are available. Comparisons have been made to the most-recent versions of corresponding ENDF/B-V differential cross sections, and the results seem to be very consistent. However, this work has uncovered a discrepancy in contemporary knowledge of the E_d=7 MeV $^{9}Be(d,n)^{10}B$ thick-target neutron spectrum below ~ 3 MeV. Until this matter is resolved by new neutron-spectrum measurements in this energy region, the usefulness of such integral measurements for low threshold reactions will remain somewhat limited. A report on this experiment is in preparation (ANL/NDM-93).

B. CROSS-SECTION EVALUATIONS

1. Evaluated Neutronic-data File for Yttrium
(A. Smith, D. Smith, P. Rousset, R. Lawson and R. Howerton[a])

A comprehensive evaluated neutronic-data file for the fission-product yttrium has been completed and is now undergoing testing. The file extends from thermal energies to 20 MeV, and includes all reactions necessary for comprehensive neutronic calculations. Attention is given to quantitative uncertainty specification. There are very major differences between this file and the comparable ENDF/B-V evaluation, and the latter appears to be highly deficient in a number of contexts. This new file will be submitted for consideration as a part of ENDF/B-VI. The evaluation will be fully documented in a report which is in preparation (ANL/NDM-94).

[a]Lawrence Livermore National Laboratory.

2. An Evaluated Neutronic-data File for Cobalt
(A. Smith, D. Smith and R. Howerton[a])

Work has started on this file. The evaluation of neutron total and scattering cross sections is partially complete.

[a]Lawrence Livermore National Laboratory.

3. An Evaluated Neutronic-data File for Vanadium
(A. Smith, D. Smith, B. Micklich[a] and R. Howerton[b])

The data base for this evaluation is being assembled and the requisite measurements pursued (see Item A.2).

---

[a]University of Illinois.
[b]Lawrence Livermore National Laboratory.

C. THEORY AND MODEL-CODE DEVELOPMENT

1. Fast-Neutrons and the Optical Model: Some Observations
(A. Smith, R. Lawson and P. Guenther)

An invited paper with this title was presented at the NEANDC Specialist's Meeting on the Optical Model for Applications, November 1985. It summarizes many contemporary aspects of the measurement and interpretation program discussed in Items A.1-A.6. The abstract reads as follows: "The optical model of fast-neutron-induced phenomena is considered from the observational viewpoint. Experimental characteristics governing the reliability of the modeling are outlined, with attention to implications on model parameters and their uncertainties. The physical characteristics of experimentally-deduced 'regional'-and 'specific'-model parameters are examined including: parameter trends with mass and energy, implications of collective effects, and fundamental relations between real and imaginary potentials. These physical properties are illustrated by studies in the A=60 and 90 regions. General trends are identified and outstanding issues are cited. Throughout, the approach is that of observational interpretation for basic and applied purposes."

2. The Role of Probability Theory in Nuclear-data Research
(D. L. Smith)

Work is nearly complete on an elementary guide to the basic concepts of probability, with emphasis on its role in nuclear-data research. This guide, intended for students and active investigators, will be made available in report form (ANL/NDM-92).

3. ABAREX
(R. Lawson and A. Smith)

This spherical-optical-model code has been further refined and checked. Agreement with reference codes is excellent, and the fitting algorithms have been extended to improve the interpretation of experimental data. In particular, experimental uncertainties (random and systematic) and their correlations can strongly influence the data interpretations. The code has been modified so as to handle a surface-peaked real potential. This potential is predicted by the dispersion relationship which relates the real and imaginary optical-model potentials.

4. ANLECIS
(R. Lawson)

An improved version of the code ECIS has been successfully implemented. It includes the correlation and fluctuation corrections of Moldauer. Attention is now being focused on enhanced performance in the fitting of experimental data. We are very grateful for the continuing help of J. Raynal, the original author of ECIS.

D. FACILITIES, TECHNIQUES AND DEVELOPING RESEARCH PROGRAMS

1. Redesign of a Gamma-ray Counting Facility
(D. L. Smith and J. W. Meadows)

The apparatus used in the FNG laboratory for gamma counting of neutron-irradiated samples has been redesigned. This apparatus provides more flexibility in the choice of counting geometries while improving reproducibility. It is now possible to accommodate a wide range of activity levels and a variety of sample configurations.

2. Thick-target Neutron-emission Angular-distribution Measurements for $^{9}Be(d,n)^{10}B$ at E_d=7 MeV
(D. L. Smith, J. W. Meadows and P. T. Guenther)

This experiment was completed and the results are available in report.[a] Fig. D-1 shows the main features of the neutron spectrum. Based on these results, it has been determined that neutron-anisotropy corrections to measured integral neutron-activation cross sections can be quite sizable for reactions with thresholds in the few-MeV range (see Item D.3).

---

[a]D. L. Smith, J. W. Meadows and P. T. Guenther, ANL/NDM-90, Argonne National Laboratory (1985). Emission-neutron energy ranges are indicated.

3. Development of Integral Cross-section Data-processing Methods for Thick-target Neutron-activation Measurements
(D. L. Smith and J. W. Meadows)

Procedures for analyzing thick-target neutron-activation cross-section data have been worked out, including corrections for neutron emission anisotropy and multiple-scattering. A report on the details of this work is in preparation (ANL/NDM-93).

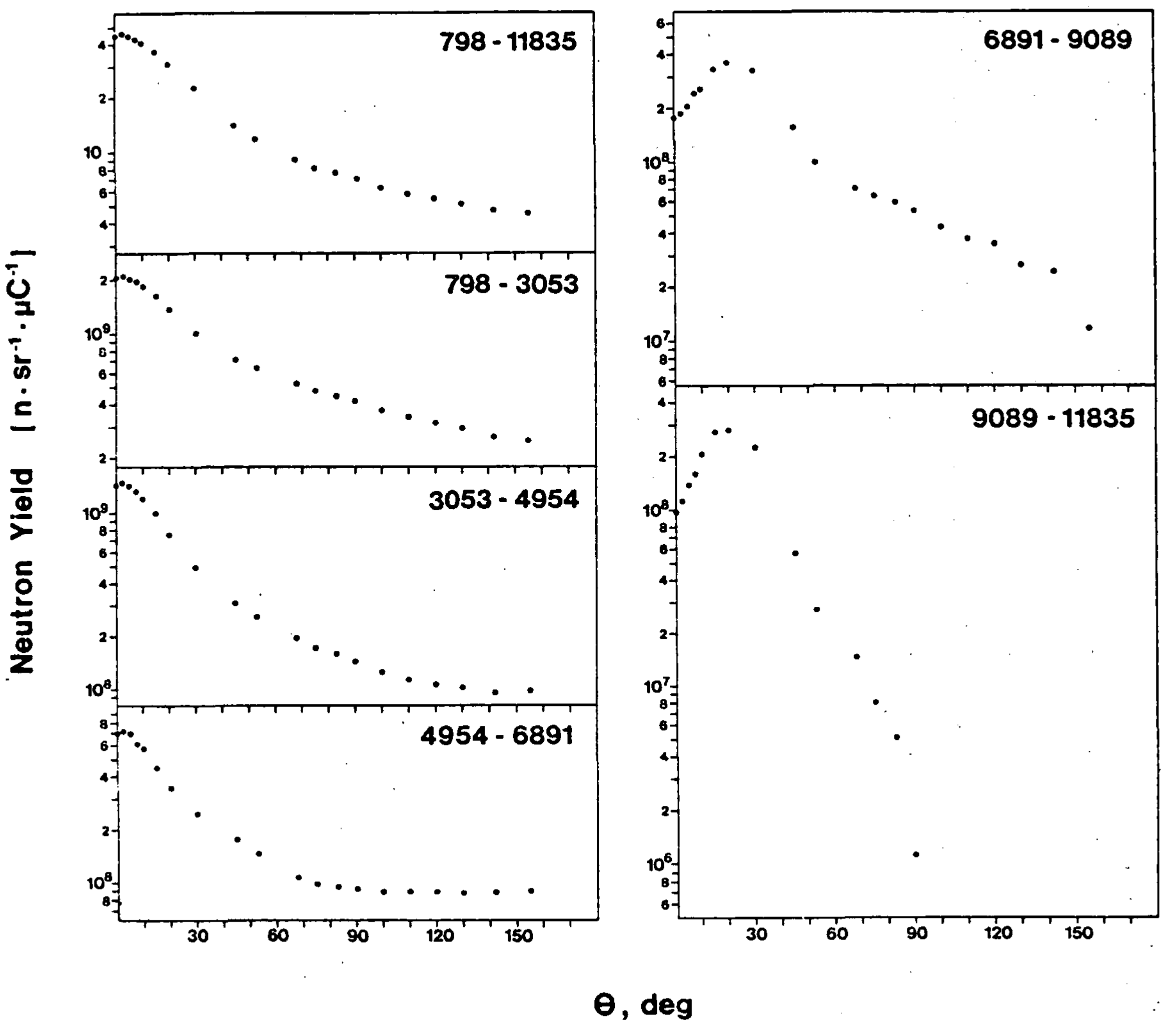

Fig. D-1. Neutron-emission distribution for the $^{9}Be(d,n)^{10}B$ thick-target reaction at E_d=7 MeV. Emission-neutron energy ranges are indicated.

4. Construction of a Shielded Irradiation Cavity for Thick-target Experiments

(D. L. Smith, J. W. Meadows and A. Engfer)

A blockhouse facility was constructed in order to limit the neutron radiation levels elsewhere in the FNG laboratory for biological safety purposes, and to provide a means for generating a collimated external beam for spectrum measurements. The cavity itself is roughly cubical with linear dimensions ~ 2m on each edge. The external dimensions of the facility are $\gtrsim$ 4m for each edge, corresponding to walls and a ceiling $\gtrsim$ 1m thick. The shielding material is hydrogenous, except for a thin cadmium lining inside the cavity. The shielding consists mainly of concrete, though polyethelene blocks are also used. A baffle-wall access to the cavity is employed to permit rapid entry and exit. This facility has been tested with 7-MeV deuterons on a thick beryllium-metal target. It has been found that the neutron radiation escaping the cavity is considerably less than that produced by stray deuterons interacting with beam-tube components outside the cavity. Work is in progress on fitting the cavity with neutron-fluence monitors and a collimator arrangement to permit the definition of an external neutron beam.

5. Neutron Multiplication in Beryllium
(A. Smith, B. Micklich[a] and R. Howerton[b])

Results of recent microscopic measurements have caused concern for fast-neutron multiplication in beryllium, particularly as applicable to fusion- and high-temperature fission-energy systems. A program of measurements and calculations of neutron emission from relatively-thick spheres of beryllium is being set up to test the validity of current microscopic data. The influence of thick beryllium spheres upon continuum neutron spectra emitted at their center will be investigated. The initial neutron source will be the Be(d,n) reaction, supported by the monoenergetic D(d,n) reaction. The energy distributions of interest will extend from the (n,2n) threshold to 10+ MeV. The corresponding calculations will use monte-carlo techniques. This integral study is to be complemented by microscopic scattering and total-cross-section studies of beryllium extending from the (n,2n) threshold to 10 MeV. The ultimate goal is an improved and rigorously-tested beryllium evaluation for ENDF/B.

---

[a]University of Illinois.

[b]Lawrence Livermore National Laboratory.

1. BROOKHAVEN NATIONAL LABORATORY

The reactor-based neutron-nuclear physics research at BNL is composed of three categories: the study of nuclear structure with the (n,γ) reaction, the (n,γ) reaction mechanism and its application to pure and applied physics, and the spectroscopy of neutron-rich, fission product nuclides. These programs use the H-1 and H-2 beam ports of the HFBR. The tailored beam facility produces beams of thermal, 2- and 24-keV neutrons. A monochromator is used for resonance neutron studies. The TRISTAN on-line mass separator is used with a U-235 target to produce fission product nuclei. These facilities are operated in collaboration with a wide variety of collaborators from national laboratories and universities. In the following sections the complete program is outlined, and those sections of relevance to nuclear energy and other applications are described in detail.

A. NUCLEAR STRUCTURE WITH THE (n,γ) REACTION

The H-1 beam tube at the HFBR provides two beams used almost entirely for neutron capture γ-ray studies. These include the tailored beam facility, which provides beams of thermal, 2 and 24 keV neutrons, and the neutron monochromator, which provides thermal and energy-selected beams up to about 25 eV. These wide ranging beams provide a unique method of nuclear structure investigation due to the primarily nonselective character of the (n,γ) reaction. Indeed, in appropriate cases, all levels of a given spin-parity range in the final nucleus may be about equally populated without regard to the structure of the final state wave functions. This is primarily achieved with the use of the tailored beams, which provide resonance averaging of the primary transitions, and which are absolutely indispensable in the construction of level schemes. The primary transitions unambiguously disclose level positions, which can only be done indirectly from secondary transitions by the inferential application of the Ritz Combination Principle. The secondary transitions, however, are themselves of crucial importance for the information they provide on the electromagnetic matrix elements connecting low lying levels and, thereby, on the applicability of different nuclear models.

1. The N_pN_n Scheme and Related Studies

During this year a proposal was made for a new parameterization of nuclear data. Called the N_pN_n scheme, it appears to be highly successful both in correlating the data within a given mass region and in relating different regions. Moreover, it has a simple microscopic basis. The idea has developed numerous offshoots and ramifications including such concepts as N_pN_n multiplets, radically simplified IBA calculations, a new approach to the study of evolving subshell structure, the relation of intruder states to deformation, and so on. The basic N_pN_n scheme and these related ideas are sketched in the paragraphs below.

1.1 The N_pN_n Scheme

The proton-neutron interaction is the principal non-pairing residual interaction in nuclei that determines the evolution and development of collectivity. This has been known for decades and, indeed, is the basis behind the pioneering work of Talmi and of Federman and Pittel in explaining the origin of configuration mixing and nuclear deformation. Despite this well-recognized situation, there has been little systematic effort to exploit this idea to understand and interpret the evolution of nuclear structure as a function of A, N, and Z. Early in FY 1985, a new parameterization of nuclear data was proposed that is explicitly based on the proton-neutron interaction and which has come to be known as the N_pN_n scheme. In it, nuclear observables are plotted, not against A, N, or Z, in terms of which they are complicated multi-dimensional functions, but rather against the product N_pN_n of the number of valence protons times the number of valence neutrons. (These are counted to the nearest closed shells--that is, as holes past midshell.) This product approximates the total integrated proton-neutron interaction strength (while neglecting its orbit dependence). It was shown that this scheme led to an enormous simplification of the systematics--each observable now follows a single smooth universal curve for a given region.

Results so far show that the idea works for various observables, $E_{2^+_1}$, $E_{4^+_1}/E_{2^+_1}$ (and, therefore, presumably for other ground band levels at least up to the first backbend), $E_{2^+_2}$ (that is, the first intrinsic vibrational excitation), $B(E2:2^+_1 \rightarrow 0^+_1)$ and isotope shifts. It may work for other B(E2) values and perhaps for such properties as separation energies and lifetimes.

It has long been thought that different transition regions in nuclei were very diverse in character. For example, the A=100 region is considered to be the most rapid in heavy nuclei, while the Os-Pt nuclei are considered to display a more gradual change in structure: the A=130 region is still more gradual. This situation, of course, impedes a unified interpretation. The N_pN_n scheme removes this difficulty since, in this parameterization, all those transition regions appear nearly identical. They display nearly the same rate of evolution when measured in units of N_pN_n. This offers the hope, for the first time, of a truly unified understanding of the structure and evolution of heavy nuclei. In turn, of course, this greatly enhances the possibilities for predicting and studying the structure of unknown nuclei far off stability.

It is possible to interpret the N_pN_n curves very simply in terms of the proton-neutron interaction, especially in highly overlapping orbits where the interaction is strongest. Thus, this unified approach to nuclear structure has an essential microscopic underpinning as well.

In constructing N_pN_n plots, care must be taken to account for significant subshell closures (and their evolution) which affect the counting of N_p and N_n. Thus, it was necessary to incorporate the dissolution of proton gaps at Z=38 near N=60 and at Z=64 near N=90 in order to obtain the smooth systematics. These changes in proton subshell structure as a function of neutron number were previously known. Applying similar ideas, the presence of a new gap, at N≈114 for Z≥78 was suggested in order to obtain smooth curves for the A=190 region.

Of course, a few exceptions to the smooth N_pN_n systematics are seen to occur. These are not unwelcome. The N_pN_n scheme accounts for the smooth evolution of nuclear structure. Deviations disclose deviant behavior and therefore highlight interesting physics. At N=60 in the A=100 region and N=90 in the A=150 region, several nuclei split off from the smooth curves. These have been interpreted as due to an oversimplification in the assumption that proton gaps dissolve suddenly at these neutron numbers. It was possible, in fact, to utilize the deviations in a reverse procedure to deduce effective valence proton numbers. These turn out to be remarkably similar to ones deduced completely independently from an IBA analysis of nuclear 2^+_1 g factors. In the A≈190 region, a deviant ^{184}Hg point can be ascribed to effects of an intruder configuration which, as an orbit descending into the valence space from the shell above, effectively alters the N_p counting.

The publication of the N_pN_n scheme proposal, though only a few months old, has already attracted widespread interest. The suggestion of a gap in the neutron single particle spectrum at N=114 implies that, near ^{196}Pt, neutrons are particles rather than holes. This conclusion has been adopted in a recent paper by Balantekin and Paar in a rather successful extension of supersymmetry (SUSY) ideas to odd-odd nuclei, in particular, to ^{198}Au. (See a subsequent paragraph on current ARC measurements of this nucleus.) Other researchers have now studied the actinides and the A≈80 region in this scheme. Initial studies of odd mass nuclei have been discussed, with the possibility of using techniques analogous to odd particle blocking to study the orbit dependence of the p-n interaction. A potentially very powerful application has been to exploit the N_pN_n scheme to simplify collective model calculations by at least an order of magnitude. The trick is to parameterize the collective Hamiltonian in terms of N_pN_n instead of N, Z, or A. In a recent IBA calculation (described below) we were able to demonstrate this improvement by obtaining rather good results for 100 nuclei, in three different mass regions in terms of a total of only six constants. Though the fits are not perfect, they achieve a global reproduction of trends that is excellent. These calculations have recently been used, by an Italian group studying the decay of giant resonances, to provide the basis for the description of low lying final states in the decay process. The N_pN_n concept has led us to propose the idea of N_pN_n multiplets, analogous to isospin or F-spin multiplets that link widely diverse nuclei and that can serve as a predictor for unknown nuclei. Finally, Otten and Neugart of Mainz have been compiling a set of isotope shifts in the A=150 region. A preliminary N_pN_n plot of these looks very encouraging. It even appears possible to distinguish changes in radius due simply to increasing mass from those due to deformation effects.

To summarize: In an optimistic but perhaps not unrealistic scenario, the N_pN_n scheme may become the standard approach to the construction of nuclear systematics, for the interpretation of nuclear phase transitions, for the parameterization of collective model calculations, for the prediction of properties of nuclei far off stability and, more generally, for a unified approach to nuclear structure and its evolution throughout medium and heavy nuclei. It clearly points to nuclei far off stability as a testing ground for its validity and, at the same time, offers an umbrella scheme for interpreting the data that will emerge concerning these nuclei. Some specific extensions or exploitations of the N_pN_n scheme and related ideas are discussed in the following paragraphs. (BNL/Koln)

a. The Extrapolation-Interpretation Inversion in N_pN_n: Nuclei Far Off Stability

The N_pN_n scheme has numerous ramifications. One of particular importance relates to nuclei far off stability and therefore to the TRISTAN research program. The smoothness of the systematics for an observable in N_pN_n obviously aids in extrapolating to unknown nuclei. Secondly, the similarity of curves for different regions allows one region to serve as a paradigm for another, a procedure totally unusable in normal plots. Thirdly, and most importantly, the N_pN_n scheme frequently converts the process of extrapolation into one of interpolation with its attendent greater reliability. A nucleus far off stability but with a very unequal number of valence nucleons of each type will have a lower N_pN_n product than other nuclei, closer to stability (compare the unknown nucleus ^{148}Ba (Z=56, N=92), N_pN_n = 60 with the known nucleus ^{154}Sm (Z=62, N=92), N_pN_n = 120). This fact allows much greater and widespread reliability in predicting the properties of nuclei far off stability and should, therefore, have applications in testing nuclear models, in choosing certain nuclei for study, in astrophysics, and even in nuclear reactor applications. (BNL/Koln)

b. F-spin Multiplets

The concept of F spin was proposed a few years ago to describe the symmetry of IBA-2 wave functions in the context of their neutron and proton boson degrees of freedom. It is the boson analogue of isospin and carries a very similar formal mathematical structure. A given nucleus has a fixed Z component of F spin given by $F_0 = 1/2\ (N_p-N_n)$: different states can have any F spin values up to $F_{max} = 1/2\ (N_p+N_n)$. A given state may be pure or mixed in F spin. Generally, the low lying states are thought to be rather pure F_{max} levels. The lowest mixed symmetry state is usually expected to be a collective 1^+ state with $F = F_{max}-1$. This new collective mode has recently been discovered in electron and photon scattering experiments in Germany, and has attracted widespread theoretical and experimental interest throughout the world. Another outcome of this burgeoning of interest in F-spin (proton-neutron) symmetry was a proposal, made jointly with the Koln group, of the concept of F-spin multiplets analogous to isospin multiplets. These are sets of nuclei, with the same F_{max} (i.e., the same number of valence nucleons) but different F_0 (i.e., different distributions of the number of valence protons and neutrons).

The idea is that if the nuclear Hamiltonian is F-spin invariant, with parameters independent of F_0, then the low lying states with $F = F_{max}$ should have constant energies and structure across the multiplet. Several F-spin multiplets were studied, and it was shown that this concept could explain the similarity of widely disparate nuclei such as ^{158}Dy and ^{182}Pt, although deviations from constant energies were also noted. This idea has attracted theoretical interest and has been interpreted in terms of generalized group theoretical approaches to the IBA. (Koln/BNL)

c. N_pN_n Multiplets

Two ideas have just been discussed, one that structure depends on F-spin (i.e., total valence nucleon number), the other that it is a function of N_pN_n. The first led to the concept of F-spin multiplets and is appealing because it can be discussed elegantly in terms of a new quantum number and with simple group theoretical techniques. The other lacks this but has a more microscopic formulation in the p-n interaction: it also leads to the concept of multiplets, that is, sets of nuclei with constant (or nearly constant in a slightly relaxed deformation) values of N_pN_n. These multiplets also link diverse nuclei and, in fact, are better reflected in the data than F-spin multiplets: indeed, the small non-constancies of energies within F-spin multiplets can be attributed to somewhat changing N_pN_n values. Both multiplet concepts, but particularly that of N_pN_n (because it works better) allow one to predict the properties of nuclei far off stability better than before. (BNL/Koln)

The question arises as to the relation between these two approaches. Nuclear data clearly shows that the N_pN_n parameterization is a better measure of structure than the total valence nucleon number (F-spin), especially in transition regions. The issue, then, is whether F-spin is a fundamental symmetry that is partially reflected in the data or whether it is an approximation to N_pN_n. The motivation for the latter possibility is that $N_pN_n = 1/2\ (N^2_p - N^2_n - N^2_t)$ and, for typical values of N_p and N_n, the first term on the right (i.e., the F-spin term) dominates. This question is not yet settled and is of high current interest. (BNL/Koln)

d. IBA-1 Calculations in the N_pN_n Scheme

The simplicity of N_pN_n plots suggests a new approach to nuclear collective calculations. In a typical traditional phenomenological calculation the nuclear Hamiltonian has several terms with coefficients treated as parameters. One might typically have 4-5 parameters/nucleus. For a sequence of isotopes this would imply either 10-20 parameters or the need to make a model relating the parameters. For an entire region the structure becomes rapidly worse. However, since an entire region can be simply described by universal curves depending only on N_pN_n, the N_pN_n scheme suggests that if the Hamiltonian parameters were also written as functions of N_pN_n, then a great economy might be achieved. This has recently been demonstrated in IBA-1 calculations in two regions. The A≈130 region is a complex U(5)→O(6)→SU(3) double-transition region of about 30 nuclei. It has been successfully calculated in terms of seven constants. Even more striking, the structure, levels, and B(E2) values of 100 nuclei in three separate regions (A=100, 150, 170) were reproduced in IBA-1 calculations involving a total of only six constants. These three regions, all representing U(5)→SU(3) transitions, have N_pN_n curves that are essentially parallel. Therefore, the same Hamiltonian, with the same parameters, was used for each with the exception of one parameter for each region which specifies a displacement of the N_pN_n curves. As noted, the net effect is a 6 constant calculation for 100 nuclei, representing at least an order of magnitude simplification over previous approaches, and providing the basis for a global interpretation of large tracts of nuclei heretofore considered diverse and as reflecting very different physics. (BNL/Koln)

e. IBA-2 Calculations with Constant Parameters

One can relate IBA-2 parameters to those of the IBA-1. For many cases the relationship has the schematic form

$$P(\text{IBA-1}) = P(\text{IBA-2})\ f(N_pN_n/N_B(N_B-1)\ \ldots$$

Since it is known (see an earlier paragraph) that IBA-1 calculations with parameters only dependent on N_pN_n can be very successful even for complex transition regions, the possibility occurs that one might exploit the above equation and do equivalent IBA-2 calculations with constant parameters. The N_p and N_n dependence of IBA properties would account for changing structure. Unfortunately, this is not verified since it must be recalled that as N_p and N_n change, so does N_B and the quotient $N_pN_n/N_B(N_B-1)$ actually changes rather little. One cannot, it seems, reproduce the rapid structural changes in transition regions with constant IBA-2 parameters. Nevertheless, a set of calculations within the deformed rare-earth nuclei has shown excellent agreement with the data with constant IBA-2 parameters, as long as the phase transition is not crossed. This is a less ambitious achievement than the IBA-1 results discussed above, but is of complementary interest in that it has a closer relationship and impact on the derivation of these parameter values in a microscopic basis. (Koln/BNL/Maryland)

f. Intruder States and Deformation in Nuclei

A very simple model was proposed that links in a simple scheme the presence and excitation energies of intruder states in some mass regions and of deformation in others. The idea is that the excitation of nuclear pairs (usually protons) above a shell gap leads to an effectively larger number of valence nucleons, hence greater collectivity in these configurations. These proton pair configurations interact (attractively) with the valence neutrons with a strength dependent on N'_pN_n where $N'_p>N_p$ (normal) because of the extra pair excitation. Thus this excitation descends in energy more rapidly than the "normal" one and is more collective. Therefore, depending on the scale of the p-n interaction (the proton-neutron overlap) compared to the size of the energy gap to be overcome, this collective/deformed configuration may descend to become an intruder excited state (e.g., in Cd and Pb) or may actually cross the ground (normal) state (A=100, 150 regions) to become a new deformed ground state. This simple model, based on the single quantity $\langle\phi_n/\phi_p\rangle/E_{gap}$, can simultaneously account, then, for both intruder states and deformation and their appearance in different regions of the periodic table. In calculating the p-n interaction, it is crucial to take into account both monopole and quadrupole components. (BNL/Koln/Gent)

g. Valence Nucleon Number Effects in Nuclei

With the recognition of the importance of the valence nucleon product N_pN_n it is interesting to look once again at some of the existing data on nuclear systematics to see if this new approach provides a simpler theoretical framework. If one assumes that much of the evolution in structure is due to changing proton and neutron valence nucleon numbers, it turns out to be extremely simple to understand many effects that have heretofore been puzzling and thought to have required complex detailed calculations. Examples are the behavior of even the first 2^+ energy in the rare earth region vis a vis the Z=64 shell gap and the question of where, in a given shell, the nuclei of maximum deformation occur. An analysis of several diverse phenomena such as these is underway. (BNL/Koln/Sussex)

2. Studies of Even-even Nuclei

2.1 Tests and Refinements of the Interacting Boson Approximation (IBA)

In the last several years a major advance in nuclear structure studies has been the development and testing of the IBA. Briefly, the basic problem of nuclear structure in heavy nuclei is the practical intractability of the shell model in the face of large numbers of valence nucleons. The familiar geometrical models attempt to overcome this difficulty by the macroscopic strategem of assuming an overall nuclear shape. The IBA offers an alternate scheme, at once more abstract and more general: it assumes an enormous truncation of the possible shell model configurations such that low lying excitations can be treated, in effect, in terms of bosons which represent pairs of fermions that are coupled to angular momentum 0 (s bosons) or 2 (d bosons). The complex Hamiltonian of the shell model is replaced by an extraordinarily simple one consisting of elementary interactions between bosons. A particularly attractive feature is that three natural limiting symmetries, denoted group theoretically as U(5), SU(3), and 0(6), arise when one or another term in this Hamiltonian dominates. These symmetries correspond crudely to the familiar vibrator, rotor, and asymmetric rotor of the geometrical models but contain features unique to the IBA which have been empirically verified. Since intermediate situations are easily handled by adjusting the relative sizes of the various terms in the Hamiltonian, the IBA offers the very attractive possibility of treating vastly different nuclei within a single scheme. Many of the most crucial and detailed tests to date have been carried out at BNL using data from the (n,γ) reaction which, due to its inherent nonselectivity and general applicability, is ideally suited to testing a model that itself attempts to generate complete sets of low lying, collective excitations over broad regions of nuclei. Thus the experimental program has generated a symbiotic theoretical effort to better understand the IBA itself, and its relationship to other models.

a. An Extension of the Consistent Q Formalism (CQF)

The CQF has proved to be a particularly simple and attractive starting point in the IBA description of a broad range of even-even nuclei. However as originally proposed, the approach was only applied to the region of SU(3) to 0(6) nuclei, since the term involving the boson energy, which generates vibrational structure, was not included in the Hamiltonian. This term has now been included and the predictions have been compared with the data in the spherical-deformed transition region around A=150. The results indicate that the most important characteristics of that transition, such as the lowering of the 0^+_β energy and the concomitant increase in the $B(E2{:}0^+_g \rightarrow 2^+_\beta)$ value, are well reproduced. One feature of particular interest which emerges is that the structure of the boson quadrupole operator tends towards its SU(3) form as the spherical limit is approached. In fact, this can be easily understood in terms of the relationship between this approach and that of the IBA-2 (neutron-proton) formalism, where the equivalent behavior is expected on the basis of the underlying shell structure. (Jyvaskala/BNL)

b. Study of ^{102}Ru

Analysis of (n,γ) and (n,e) experiments on ^{102}Ru have been completed. A level scheme has been completed. The principal interest centers on the excited 0^+ states which have previously been interpreted in terms of intruder levels. The present data implies that the earlier interpretations need re-examination, both as regards this nucleus and the systematics of intruder levels and the onset of deformation in the A=100 region. (BNL/Peking/Stony Brook/ILL)

2.2 Studies of Odd-A Nuclei

a. The IBFA, Boson-Fermion Symmetries and Supersymmetries

The concept of symmetry in the IBA description of even-even nuclei has proved to be one of the model's crucial ingredients, both because of the recognition of the existence of the symmetries themselves, and because they provide benchmarks in the formulation of a unified description of a broad range of nuclei. The importance of the recently proposed symmetries in odd-even systems can thus be viewed in the same light, and their role in pointing to a simple prescription for the changing collective structure in odd A nuclei throughout a major shell is likely to prove even more essential, given the much greater complexity of the general IBFA Hamiltonian. The group structure of a boson-fermion system is described by $U^B(6)$ x $U^F(m)$ where m specifies the number of states available to the odd fermion, and thus depends on the single particle space assumed. Of the structures studied in detail to date, the case of m=12 is the one with the broadest potential. The fermion is allowed to occupy orbits with j = 1/2, 3/2, and 5/2, so that the assumed single particle space corresponds to the negative parity states available to an odd neutron at the end of the N = 82-126 shell, namely, $p_{1/2}$, $p_{3/2}$, and $f_{5/2}$. The region of interest thus spans the W-Pt nuclei, and since one prerequisite for an odd-A symmetry is the existence of that same symmetry in the neighboring even-even core nucleus, the odd Pt nuclei around A = 196 offer the obvious testing ground for the 0(6) limit of $U^B(6)xU^F(12)$. The heavier even-even W nuclei, on the other hand, have the characteristics of an axial rotor, and hence the neighboring odd W isotopes offer the possibility to study the validity of the SU(3) limit. Finally, given a definition and understanding of these two limits, the construction of a simple description of the transitional odd A Os nuclei can be considered.

An extensive program, both experimental and theoretical, has therefore been underway during FY 1985, to explore and develop these possibilities. In addition, if a particular symmetry exists in neighboring even-even and odd-even nuclei, it is possible to ask whether the two schemes stem from a common parent supersymmetric group structure of the type U(6/m). The concept of supersymmetry is currently of high interest in high energy physics, gravity theories, astrophysics, and condensed matter physics. However, it is only in nuclear physics that actual empirical evidence for the validity of this type of idea has so far been obtained. During FY 1985, a number of possible extensions to this concept have been proposed, and are currently under investigation. These include a search for dynamical supersymmetries in regions of transitional structure, and also the prediction of "supersymmetric quartets" of nuclei, which stems from an extension of the algebra to encompass neutron and proton degrees of freedom separately. Such quartets contain, in addition to the even-even, odd-neutron and odd-proton nuclei, an odd-odd nucleus, for which the residual n-p interaction is uniquely specified by the formalism.

b. Dynamical Supersymmetry in Transitional Nuclei

Until now the concept of dynamical supersymmetry has only been considered in conjunction with the assumption of dynamical symmetry. That is, the idea that both even-even and odd-even systems should be describable by the same Hamiltonian has only been applied in cases where the Hamiltonian is constructed from the Casimir operators of one of the three limiting symmetries of the IBA. However, it has recently become apparent that there is no *a priori* requirement for this constraint.In general, if an even-even nucleus is fitted by a Hamiltonian consisting of Casimir operators of more than one group chain, then it is still possible to ask whether its odd-even supersymmetric partner can be described by the same Hamiltonian. This idea has been investigated for two different transitional regions, namely, the Ru-Rh nuclei and the Os nuclei. In both cases, the agreement between the predicted and empirical odd-even spectra is unsatisfactory. In particular, in the Os case, the calculations were performed in the CQF framework, and it was apparent that the structure of the quadrupole operator required in the odd-A nucleus was considerably more SU(3)-like than that in the even-even fit. Given our physical understanding of this framework, this would indicate that in this transitional region, the odd particle has the effect of reducing the extent of the fluctuations in the γ direction, and hence of stiffening the nucleus against this type of deformation. (UNAM/Sussex/BNL)

c. B(E2) Values in ^{189}Os and ^{195}Pt

Coulomb excitation studies on ^{195}Pt have been undertaken in order to ascertain whether characteristic E2 selection rules predicted by the O(6) symmetry scheme are indeed observed. Measurements were made at the Manchester Van de Graaff with 5.6 MeV α particles to determine the strengths for direct excitation from the ground state. Additional angular distribution data were obtained using 6 MeV α particles, and conversion electron measurements were made at the ILL β spectrometer. The comparison between the deduced B(E2) values and the symmetry scheme reveals a number of discrepancies, some of which can be explained by considering the semi-microscopic form of the E2 operator. The observed decay of one level, however, remains inconsistent with the predictions of the symmetry scheme. A similar set of measurements is currently in progress for ^{189}Os, and in this case, the data will be combined with the new information gained from (n,γ) studies, to provide a stringent test of the CQF approach in this region. (BNL/Manchester/ILL/Koln)

d. Odd-odd Nuclei and Supersymmetry; ^{76}As and ^{198}Au

As mentioned earlier, recent theoretical work has postulated the existence of "supersymmetric quartets" of nuclei, consisting of an even-even, odd-neutron, odd-proton, and an odd-odd nucleus, in which all boson members are described by the same Hamiltonian. The crucial extension to earlier work centers on the odd-odd nucleus, since the claim is that, having fit the Hamiltonian to the appropriate even-even nucleus, the structure of the odd-odd nucleus can then be predicted without further parameterization. Two experimental investigations are therefore underway to test these predictions. ARC data at 2 and 24 keV neutron energies have been taken and analyzed for ^{76}As, and at 2 keV for ^{198}Au. The 24 keV measurement in this case is planned for FY 1986. In addition, curved crystal spectrometer measurements have been completed for ^{76}As and are currently being analyzed. In the case of ^{198}Au there already exist two competing supersymmetry predictions which involve different assumptions concerning the underlying shell structure. The ARC data should resolve the question of which prediction is more apt. (BNL/UNAM/ILL)

2.3 Other Studies

a. An Unusual M1 Transition Linking Octupole and Quadrupole Vibrations in ^{179}Hf

In an extensive (n,γ) and (d,p) study of ^{179}Hf, an M1 transition linking an octupole vibration built on one Nilsson state and a quadrupole vibration built on another orbit was observed and found to be the strongest decay matrix element of the former state. Clearly, such a transition is normally forbidden--both because of a change of two vibrational quanta and an additional change in quasiparticle orbit. It was shown, however, that a microscopic interpretation of the vibrational wave functions in an RPA context resolves this puzzle. The principal three quasiparticle amplitudes of each excitation turn out to contain two quasiparticles in common (the base state of one is involved in the vibration of the other) and therefore a single quasiparticle changing transition can connect the states. Qualitative implications of this idea were consistent with other (E1) decay properties as well. (Koln/BNL/Munich/ILL)

B. NUCLEAR SPECTROSCOPY OF FISSION PRODUCT NUCLEI

The on-line isotope separator, TRISTAN, at the HFBR is a facility, unique in this country, for the study of neutron-rich nuclei far off stability, produced by thermal neutron induced fission of uranium. The reactor provides an intense external neutron beam, making excellent shielding possible. This combination of high beam intensity, long running time, low background, and the world's most powerful array of ion sources makes TRISTAN an unrivaled facility which can do experiments which are impossible elsewhere. As a user facility, most experiments to date have been of a collaborative BNL/USER nature. The fruitful collaboration with a large group of outside users (including an expanding group of foreign scientists) permits a wide variety of approaches to nuclear structure studies. TRISTAN is also proving to be an excellent resource for training the next generation of nuclear chemists and physicists. During FY 1985-1986 fifteen graduate students were performing their experimental doctoral studies at TRISTAN.

A high interest is associated with the study of nuclei far off stability for a number of reasons. The neutron-proton force is sensitive to the spatial overlaps of neutron and proton orbits, and, therefore, its effects vary with both neutron and proton number. By providing combinations of these not available elsewhere, neutron-rich nuclei provide the opportunity to study not just an extension of familiar phenomena but the possibility of observing entirely new effects. Particularly important areas of study center on the investigation of a wide variety of collective phenomena, of phase transitions, of deformation regions, of symmetries and, possibly, of supersymmetries. The latter two phenomena are especially relevant for odd nuclei where the predicted symmetries require specific combinations of single particle and core structure, some of which may not be available near stability. Besides the work on collective phenomena, TRISTAN provides access to nuclear regions that are expected to be magic in nature such as those near the doubly closed shell nuclei ^{132}Sn and ^{78}Ni. Nuclei far off stability also have a crucial importance in astrophysics since their lifetimes and β-decay energies affect the production of the heavier elements and can be used to distinguish different r-process models. Finally, the access to unstable nuclei with sufficiently large decay energies leads to the possibility of observing radioactivity in the form of β-delayed neutron emission and, in a few cases, of double delayed neutron radioactivity. Such studies are of both applied and structure importance, since they give information on the emission of decay heat from fission products and because they represent the inverse of neutron capture experiments on unstable targets, so that they can provide information on cross sections of neutron-rich nuclides, which is of particular interest for astrophysics and nuclear theory.

1. Studies in the A=150 Region

a. g Factors in Transitional Nuclei near N=90

At TRISTAN, g factors are measured using the perturbed angular correlation technique, wherein a sample of the nuclide of interest is placed in a superconducting magnet and the effect of the field on γ-ray cascades is observed. In previous studies the g factors have been shown to be sensitive to the presence and structure of proton subshell closures. Furthermore, it was shown that for 2^+_1 states the g factors can be described for a wide range of nuclei by using empirically-determined constant values for g_π and g_ν, the proton and neutron g factors, respectively. By noting deviations from the predicted g factors, the effective number of valence protons can be deduced.

During FY 1985, the g factors of the 2^+_1 states in ^{148}Ce and ^{142}Ba were carefully measured. The result for ^{148}Ce was compared to ^{146}Ce (measured in FY 1984) and was found to quantitatively support the concept of a truncated proton valence space due to a subshell closure at Z=64 which vanishes for N$\approx$88-90. This concept was originally developed, following the discovery of the Z=64 gap, as an alternate explanation of the onset of deformation near A=150. It is patterned after the Federman-Pittel model for the A=100 nuclei. The basic ideas have received substantial support from earlier TRISTAN g factor measurements as well as from energy level and B(E2) data. The idea is also supported by N_pN_n plots and, in fact, on the basis of such plots has now been proposed as applying in analogous fashion to the dissolution of a neutron gap at N=114 as well. Thus the "p-n interaction gap dissolution" picture of the onset of deformation has become, not a curiosity pertaining only to the A=100 region, but a notion of widespread applicability. Our understanding both of the mechanism for deformation in nuclei and of the crucial role of the p-n interaction has been substantially altered in this process.

The ^{142}Ba measurement was difficult due to the short lifetime (79 ps) of the 2^+_1 state by using the constant values for g_π and g_ν determined by a fit to many nuclei in the A$\approx$150 region, a $g(2^+_1)$ value of 0.4 is predicted. A value of 0.48 ± 0.14 was measured. In general, the IBA-2 model, on which these predictions are based, yields a more rapidly decreasing g factor as N increases for a given Z, than Z/A predictions. The IBA-2 uses a "modified" Z/A dependence, where Z is replaced by N_π (the number of valence proton bosons) and A is replaced by N_t (the total number of valence neutron and proton bosons). g_π becomes the effective strength of a valence proton-boson interacting with the other valence bosons. Since N_π and N_t are always less than Z and A, going to heavier isotopes will result in the prediction of a more rapidly decreasing g factor than Z/A due to the relative magnitudes of the numbers involved. In general, the IBA-2 predictions give a better description of $g(2^+_1)$ than Z/A estimates. (BNL/Negev)

b. Levels in ^{148}Ba: A Test of N_pN_n Predictions Far from Stability

Improvements in ion sources and targets made it possible to measure levels in ^{148}Ba from the decay of ^{148}Cs for the first time. ^{148}Ba is the heaviest Z=56 and the lightest N=92 nucleus known, thus its levels are extensions of both Z and N systematics. If the usual technique of extrapolating Z and N systematics is used, no firm prediction of even the first excited state energy can be made. In contrast, if a plot of N_pN_n for all nuclei in the A≈150 region is used, a definite prediction can be made since such a plot involves an <u>interpolation</u> between well known data rather than an <u>extrapolation</u> into a region of unknown structure. The N_pN_n interpolations were found to be in excellent agreement with $E_{2^+_1}$ and $E_{4^+_1}$ states and to give a good estimate for $E_{2^+_2}$. Further tests of the interpolative power of the N_pN_n scheme are desirable to obtain confidence in the apparently general applicability of the technique. It may prove especially useful for astrophysical calculations, where crucial nuclei often are impossible to produce or study. (BNL/ISU/Oklahoma).

c. Decay of ^{145}Cs to Levels in ^{145}Ba

The decay of ^{145}Cs has been extensively studied by using γ-γ angular correlations and conversion electron spectroscopy in the Si(Li) detector facility. Gamma ray-electron coincidences have also been measured. Over 90 new γ rays have been assigned to levels in ^{145}Ba and proposed spin and parity assignments are based on transition multipolarities and γ-γ angular correlation measurements. A 5/2-1/2-5/2 cascade to the ground state has been observed, showing that, in contrast to previous studies, the low lying level structure for odd Ba isotopes remains very stable. (Maryland/Oklahoma/BNL)

d. Identification of Four New Neutron-rich Rare-earth Isotopes

Isotopic anomalies in the rare earth region, especially for Nd and Sm, have been attributed to various origins such as unknown nuclear effects and unusual mixtures of s- and r-process materials in stellar environments. This uncertainty makes studies of nuclear properties in this region potentially important for understanding these anomalies. A modification to the thermal ion source at TRISTAN enabled the observation of a series of new short-lived rare-earth isotopes from ^{235}U fission. These isotopes are difficult to study by on-line mass separation techniques due to low fission yield and relatively long diffusion times from the target. The new isotopes were identified as ^{156}Pm ($t_{1/2}$ = 28.2 ± 1.4s), ^{159}Sm ($t_{1/2}$ = 15 ± 2s), ^{160}Sm ($t_{1/2}$ = 8.7 ± 1.4s), and ^{161}Eu ($t_{1/2}$ = 27 ± 3s). In addition, the half lives of other isotopes were also measured: ^{157}Sm ($t_{1/2}$ = 6.7 ± 0.4m), ^{158}Sm ($t_{1/2}$ = 5.2 ± 0.2m), and ^{160}Eu ($t_{1/2}$ = 31 ± 4s). When these half lives are compared to recent predictions by the model of Klapdor, it is found that the model, upon which many astrophysical calculations are based, consistently and significantly predicts shorter half lives than have been measured at TRISTAN. In addition, since the model was first presented, about 50 new neutron-rich nuclides have been discovered. In most all cases the model is less successful for the new nuclei than for previously-known nuclides. In FY 1986, further examination of the rare-earth region will be made to see if additional information can be obtained. Other studies, such as g-factor measurements, will be performed if sufficient activity and time is available. (BNL)

2. Studies in the Cd Region: First Evidence for True Vibrational Nuclei

a. ^{118}Cd: The First Example of a Good Vibrational (or U(5)) Nucleus

Even-even nuclei near closed shells have traditionally been depicted in terms of vibrational models which predict the well-known set of equally-spaced phonon multiplets. Yet, well-behaved examples of the 2- and 3-phonon multiplets have never been observed. The systematic structure of Cd nuclei with two proton holes in the Z=50 shell has been successfully described in terms of the coexistence of vibrational and intruder rotational degrees of freedom. The results obtained at TRISTAN for ^{118}Cd show that the intruding configuration bandhead occurs well separated from the normal states which display a closely spaced 2-phonon triplet. Thus, the interaction of the two configurations is weak and ^{118}Cd represents an unusual case where the vibrational structure could be left relatively undisturbed. Complete analysis of the data has indeed now revealed an isolated set of close-lying states that decay preferentially by E2 transitions to the 2-phonon triplet. These states have been identified as <u>all five members of the three-phonon quintuplet</u>. This represents the first observation of all five members, even though the vibrational model has been known for 30 years. In addition, evidence has been found for higher collective states. (Clark/BNL)

b. Q Values of Neutron-rich Ag Isotopes

Q values of $^{118-122}$Ag isotopes have been measured using the superconducting magnet fitted with an internal Ge detector in place of the lower pole tip. This configuration decreases the effective solid angle for γ rays (due to source to detector distance) while increasing the electron solid angle by magnetic focusing of the β rays emitted from the source. Thus, the system gives an enhanced efficiency for measuring endpoint energies. Data were taken for ^{118,120,121,122}Ag and are being analyzed. Preliminary results are available which give $Q_\beta(^{118}\mathrm{Ag}) \approx 7492$ keV and $Q_\beta(^{120}\mathrm{Ag}) \approx 8450$ keV. Additional level scheme information may be necessary to ascertain whether the endpoint is due to ground state or excited state feeding in $^{121-122}$Ag. (Lafayette/Clark/BNL)

3. Nuclear Structure near A=100

a. Decay of the New Isotope ^{102}Sr

The new isotope ^{102}Sr was produced for the first time at TRISTAN using a thermal ion source. The ^{102}Sr half life was determined to be 68 ± 8 ms. Observation of the 128-keV γ ray which depopulates the first excited state in ^{101}Y indicated that ^{102}Sr is a delayed neutron emitter. By use of singles and coincidence information, a level scheme with 7 excited states up to 1689 keV was established with 21 placed γ rays. A spin and parity of 1^+ was established for a level at 244 keV, which appears to be the bandhead of a nearly rigid $K^\pi = 1^+$ rotational band. (ISU/Oklahoma/BNL).

b. Shape Coexistence in ^{100}Zr

The level structure of the N=60 isotone ^{100}Zr has been studied via the β decay of the low-spin isomer of ^{100}Y. A half life of 735 ± 7 ns was determined from γ-ray multiscaling measurements. γ singles, conversion electron spectra, and γ-γ coincidence measurements have resulted in the placement of 64 γ transitions in a decay scheme with 20 levels up to 4288 keV. Angular correlation measurements were used to deduce a J^π of 0^+ for the 829 keV level. This level is the $0^+{}_3$ state and appears to correspond in energy to the usual β vibrational bandhead of a symmetric rotor. An asymmetric shape description of ^{100}Zr predicts that the $0^+{}_3$ state should be much higher in energy, thus giving support to the interpretation of shape coexistence in this nucleus. In addition, band mixing calculations which make the assumption of a spherical band mixing with a deformed band give an excellent reproduction of the observed reduced transition rates. (ISU/Julich/Oklahoma/BNL)

c. Decay of ^{82}Ga to Levels in ^{82}Ge

A study of excited states in even-even ^{82}Ge was begun in FY 1985. After the first series of experiments, it was found necessary to also acquire data on the daughters, especially ^{82}As, in order to fully identify interfering γ rays. ^{82}Ge has N=50, so it is expected to have the traits of a closed shell nucleus. In addition, ^{82}Ge is the lightest known N=50 isotone and the heaviest known isotope of Ge. Thus, it offers another possibility to test the N_pN_n scheme. In this case the testing is not as clear cut since for a closed shell nucleus, $N_pN_n = 0$ since there are no valence particles of the type whose shell is closed. However, such nuclei often exhibit particle-hole excitation over the shell gap, and a test may be found in examining excited bands. In FY 1986, other nuclei in this region will be examined, with a particular interest in testing the N_pN_n scheme near the doubly-magic nucleus ^{78}Ni. (ISU/BNL).

4. Other Studies

a. The β Decay of ^{139}I

A preliminary investigation of the decay of ^{139}I to ^{139}Xe was made at TRISTAN, using the negative surface ionization ion source. Over 100 new γ rays were assigned to levels in ^{139}Xe. In this study, as well as a previous TRISTAN study of the decay of ^{139}Xe, the data are consistent with a ground state of $3/2^-$ for ^{139}Xe rather than the value of $7/2^-$ reported in the literature. The lowering of the $3/2^-$ state to become the ground state in ^{141}Ba and ^{143}Ce has been attributed to the mixing of the $(\nu f_{7/2})^3 3/2$ cluster state in the $p_{3/2}$ level. The level structure below 1 MeV of ^{139}Xe is very similar to the isotones mentioned above. Thus, the structure of these N=85 nuclides seems to be only weakly affected by the addition of protons to the core. (Maryland/BNL)

C. RESEARCH AND DEVELOPMENT IN SUPPORT OF FACILITIES

1. TRISTAN Ion Source Development

Following several years of research and development, successful and reliable designs have been arrived at for the positive surface ionization and FEBIAD (Forced Electron Beam Induced Arc Discharge) sources. These can now be constructed on a regular basis, as the need arises, and in each case they exhibit typical lifetimes of 1500 hours or more. Further development will therefore be concentrated on improving the lifetimes and efficiencies of the thermal, high temperature plasma, and negative surface ionization sources.

During 1984, the lifetime of the thermal ion source was extended to about fourteen days. One important improvement to this source consists of supporting the Ta filament by thin W wires, instead of Ta. This prevents the filament from fusing to the support wire, which causes bending, and ultimately short circuits, during thermal expansion. The source also used a W target container to withstand higher temperatures. However, W vapor tended to collect on the filament, forming a Ta-W alloy which is extremely brittle. The filament easily broke during thermal expansion while the current was being changed. An additional modification was the use of Ta for the ionizer rather than Re. This gave enhanced yields, about 2-5 times greater, even at lower temperatures. During 1985, other combinations of target container/filament materials will be tested in hopes of extending the lifetime and reliability of this ion source. Improvements to the filament support design as described for the thermal ion source have also extended the reliability and lifetime of the high temperature plasma source to about ten days. Further tests will be performed to investigate the operating mechanism of the source. In the case of the negative surface ionization source, much higher efficiency operation with a yield as high as 10^8 atoms/sec was obtained by using LaB_6, an electron deflection magnet/

collector system and efficient heat shields. Initial tests suffered from long holdup times due to too large a target. A smaller graphite cloth target gave much improved yields for shorter lived fission products. However, the source exhibited long-term beam instabilities and further tests are necessary to fully understand their origins.

2. Ion Source Handling and Containment Facilities

The considerable increase in the number of ion sources in use at TRISTAN, and in their lifetimes and efficiencies, has created a need to develop improved facilities for handling and storing these sources once they have been irradiated. Consequently, a considerable effort has been expended to develop remote handling tools for the removal and repair of sources, and also to improve and expand existing storage facilities. A long manipulator to remove the clamps that hold the source to the housing and also the ion source itself has been designed and tested off line. All of the ion sources are being modified to provide a fixture to allow the use of this tool. Similarly, the ion source housing is being modified to allow remote removal of the Faraday cage and electrical connectors. The electrical connectors have been standardized and can now be rapidly inserted and removed. Several surplus lead storage pigs have been obtained and are being modified to accommodate TRISTAN ion sources. In 1985 a lead storage vault will be built to serve as an additional holding area for ion sources.

3. TRISTAN Beam Line Modifications

A general purpose electrostatic quadrupole triplet lens was designed and fabricated and will now be tested. If the design proves satisfactory, several more lenses will be constructed, as it is expected that for ideal operation two will be required on the 0° line and another on each of the 45° lines to provide additional flexibility in designing and installing equipment. The designs for electrostatic switch yards used at two other on-line isotope separators (ISOLDE and GSI) have been obtained and studied in preparation for the design of a second mass line facility at TRISTAN. The GSI design is more usable at TRISTAN than the ISOLDE type. As time is available, modifications necessary to implement the switch yard will be considered.

D. National Nuclear Data Center

1. Cross Section Evaluation Working Group (CSEWG) Activities

The annual CSEWG meeting was held at BNL in May 1985. A major thrust of the discussions at the meeting was the expected impact of the funding decrease and the assumption of responsibility for CSEWG within DOE by Basic Energy Sciences. Plans for production of ENDF/B-VI have been stretched out to FY89 and appropriate evaluations produced outside the U. S. will be considered for inclusion.

Progress on completion of the "standards" continues to be behind schedule. Present projections are for completion in the summer of 1986.

2. BNL-325, Volume 2

The computer programs for producing a neutron data atlas for $\sigma(E)$ from the experimental data file CSISRS have been completed and thoroughly tested. Overlay curves can be generated directly from the ENDF/B-V evaluated data base. Curve fitting procedures using interactive spline fits for data where no evaluation exists in ENDF/B have been implemented.

Work has started on the data reviews with emphasis on (1) including all significant data sets, (2) the accuracy of the reaction specification, and (3) the correctness of the data. A review of $Z \leqslant 40$ has been completed. Photoready copy should be sent to the publisher before the end of 1986.

3. Nuclear Data Sheets

The NNDC has been producing the Nuclear Data Sheets at the rate of about an issue a month. Of these, nine issues a year are devoted to the nuclear structure evaluation and the remaining three to the publication of Recent References. The publication of the Nuclear Data Sheets is back on schedule as of the August 1985 issue, i.e. Vol. 45, No. 4.

The NNDC evaluated A=143, 49, 145, 46 and 165 and submitted them for publication.

The U. S. is part of an international network of evaluators contributing recommended values of nuclear structure information to the Evaluated Nuclear Structure Data File (ENSDF). Publication of the Nuclear Data Sheets proceeds directly from this computerized file. In addition to the U. S., evaluations have been received or are anticipated from Germany, USSR, France, Japan, Belgium, Kuwait, Sweden, the People's Republic of China and Canada. Italy and India have shown interest in joining the network and are expected to start evaluation in the near future.

The NNDC organized and participated in a general clean-up of the ENSDF along with other members of the network.

The NNDC organized and hosted an evaluator training session attended by new evaluators from Kuwait, West Germany, the People's Republic of China and Taiwan.

4. On-line Data Services

During the past year, NNDC has made available for on-line user access some data bases on a trial basis. The data bases involved are the neutron bibliography CINDA, the nuclear structure bibliography NSR, and nuclear structure, radioactivity, and ground and metastable state properties. Access is to the NNDC VAX 11/780 via telephone lines.

CROCKER NUCLEAR LABORATORY AND DEPARTMENT OF PHYSICS
UNIVERSITY OF CALIFORNIA, DAVIS

A. MEASUREMENTS

1. n-p Cross Sections at 65 and 50 MeV Over the Angular Range 90° - 180°*. (J.R. Drummond, F.P. Brady, J.L. Romero, T.D. Ford,** C.M. Castaneda, and B.C. McEachern**)

Scattered protons produced by bombarding CH-2 with monoenergetic neutrons were detected using position sensitive detectors to measure the cross sections for angles between 0° and 45° (scattered protons in lab frame). By measuring all angles at the same time most systematic errors could be canceled out. A ratio of 1.8 ± 0.1 was obtained for $\sigma(\sim 180)/\sigma(90)$ at 65 MeV. This result is consistent with earlier results from CNL but smaller than results recently obtained at Louvain le Neuve. Ratios for the entire angular range are being analyzed.

2. The $^{12}C(n,p)$ Reaction at 65 MeV from 0° to 40°†. (D.S. Sorenson, T.D Ford,** J.L. Romero, F.P. Brady, C.M. Castaneda, J.R. Drummond, B.C. McEachern**)

Spectra from the new Crocker Nuclear Laboratory zero degree dual target facility (see B1) for the (n,p) reaction on ^{12}C have been obtained at 65 MeV. Cross sections have been extracted from 0° to 40° for the ground state (fig. A-1), the 4.4 MeV excited state(s) and the region between 6 and 10 MeV. Cross sections are compared to previous data as well as to theoretically predicted cross sections. From the 0° cross section for the Gamow-Teller transition (ground state) we extract $v^{c}_{\sigma\tau}(0)$ (the isovector part of the effective spin-flip nucleon-nucleon interaction) and compared it with values obtained previously from (n,p) cross sections extrapolated to 0°[1]. The data was normalized (at each angle) using the n-p parameterization of Binstock.

3. The ^{14}C and $^{13}C(n,p)$ Reactions at 65 MeV from 0° to 50°. (J.R. Drummond, F.P. Brady, C.M. Castaneda, T.D. Ford,**, B.C. McEachern,** J.L. Romero, D.S. Sorenson, K. Wang,***, D. Pocanica,***, J. Martoff,***, and S.S. Hanna***)

The zero degree dual target facility (see B1) was used for (n,px) spectrum measurements on isotopically enriched ^{14}C and ^{13}C targets. The ^{14}C spectra are consistent with states observed using the (π^-,γ) are LAMPF. Data analysis on both targets is in progress.

---

* Work supported by NSF grant #84-19380
** Associated Western Universities Graduate Fellow
*** Department of Physics, Stanford University, Stanford, CA 94305
† Supported by NSF grants PHY81-21003 and 84-19380
(1) F.P. Brady et al., Phys. Rev. Lett. 48:860 (1982).

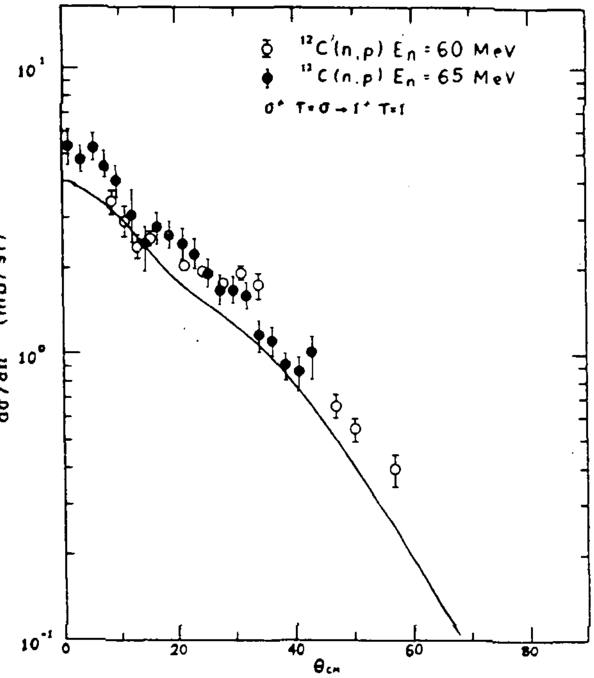

Figure A-1. Angular distribution in center of mass frame, for ground and first excited state in ^{12}B. Open points are previous data from Davis at 60 MeV. Solid points are present data. Curve is a distorted wave calculation.

4. The (n,px) Reaction on ^{90}Zr at 65 MeV*. (T.D. Ford,** J.L. Romero, F.P. Brady, C.M. Castaneda, J.R. Drummond, B.C. McEachern,** M.L. Webb**)

Zero degree scattering should provide a tool to help separate excitation of the giant isovector monopole resonance (IVMR), expected to peak at forward angles.[1] The (n,p) reaction has the feature than only T_o+1 components of transitions are excited. Recent (π^-,π^o) data from LANL give evidence of the IVMR.[2] We have used our improved zero degree dual target facility at Crocker Nuclear Laboratory (which allows measurements from two targets simultaneously, see B1) to obtain energy spectra for the $^{90}Zr(n,px)$ reaction from 0 to 40 degrees. A bump over the proton continuum at about 22 MeV excitation energy is seen, consistent with the expected location of the IVMR and IVQR. Figure A-2 shows the differential cross sections for that region (after subtracting the continuum) and compares it with predictions by Love[3].

---

* Supported by NSF grants PHY81-21003 and 84-19380
** Associated Western Universities Graduate Fellow
(1) N. Auerbach et al, Phys. Rev. C28:280 (1983).
(2) J.D. Bowman et al., Phys. Rev. Lett. 50:1195 (1983); A. Erell et al., Phys. Rev. Lett. 52:2134 (1984).

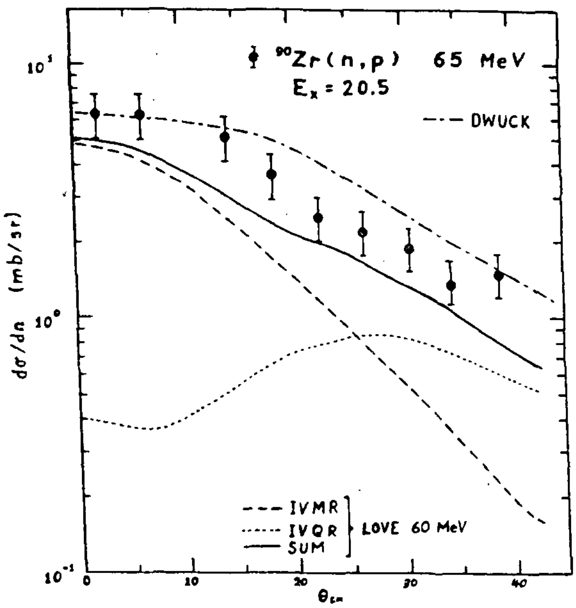

Figure A-2. Angular distribution in center of mass frame for unresolved IVMR and IVQR seen at 20.5 MeV in ^{90}Y. Shown are the predicted distributions from RPA calculations at 60 MeV, and DWUCK prediction at 65 MeV, for IVMR only.

5. Double-Differential Inclusive Hydrogen and Helium Spetra from Neutron-Induced Reactions at 27.4, 39.7, and 60.7 MeV. II. Oxygen and Nitrogen$. (T.S. Subramanian,* J.L. Romero, F.P. Brady, D.H. Fitzgerald,** R. Garrett,*** G.A. Needham,# J.L. Ullmann,## J.W. Watson,† and C.I. Zanelli, D.J. Brenner, and R.E. Prael)

Double-differential cross sections for the neutron-induced production of p,d,t,He-3 and alpha particles from oxygen and nitrogen have been measured using the unpolarized neutron facility at the Crocker Nuclear Laboratory. Neutron beam energies of 27.4, 39.7, and 60.7 MeV were used.

---

(3) Love W.G., RCNP-Kikuchi Summer School on Nuclear Physics, Kyoto, Japan, May 23-27 (1983).

$ We acknowledge the support of NCI (Grants CA-16261 and CA-15307), the NSF (Grants PHY71-03400 and PHY77-05301) and DOE (Contract DE-AC02-83ER-60142).

* Memorial Hospital Radiation Center, Hollywood, FL 33021.
** Department of Physics, UCLA, Los Angeles, CA.
*** Department of Physics, University of Auckland, Auckland, New Zealand.
# Rocketdyne Dvision, Rockwell, Canoga Park, CA 91304.
Nuclear Physics Laboratory, University of Colorado, Boulder, CO 80309.
† Department of Physics, KSU, Kent, OH.

Previously, a similar set of data was published for carbon[1]. The charged particle energy spectra, at six forward laboratory angles, 15, 20, 35, 40, 45, and 65, and, where feasible, at three backward angles, 90, 130, and 150 degrees, range up to the kinematic maximum, from a typical low-energy cut-off of 4 MeV for p,d,t and alpha and 8 MeV for He-3. Intranuclear cascade plus de-excitation calculations were carried out. The data are compared with the available proton-induced (charge-symmetric) reaction spectra for oxygen measured at Oak Ridge yielding good agreement. Comparisons between measurements and calculations yield similar conclusions to those obtained for carbon[1]: namely that, in general, the agreement is surprisingly good, since the assumptions of cascade models are usually thought to be breaking down at energies much below 100 MeV.

B. FACILITIES AND DETECTORS

1. A Detection System for 65 MeV (n,p) Measurements from 0° to 60°*.

(B.C. McEachern,**, T.D. Ford,**, F.P. Brady, J.L. Romero, C.M. Castaneda, J.R. Drummond, and D.S. Sorenson)

A detection system to study (n,p) reactions at medium energies and over a wide angular range down to zero degrees has been developed. A two-target system is used (fig. B-1). Target 1 is placed ahead of the magnetic field and protons emitted at small angles pass through the field into a large area Multiwire Chamber, ΔE-E scintillator telescope. Protons from target 2 which is downstream from the magnet are hardly deflected and

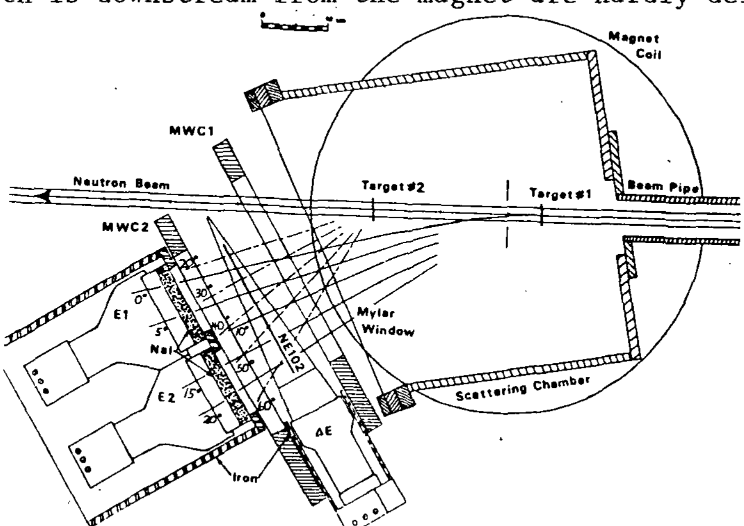

Figure B-1. Set-up to measure 0° - 60° (n,p).

---

(1) T.S. Subramanian, J.L. Romero, F.P. Brady, J.W. Watson, D.H. Fitzgerald, R. Garrett, G.A. Needham, J.L. Ullmann, C.I. Zanelli, D.J. Brenner, and R.E. Prael; Phys. Rev. C28:521 (1983).

* Supported by NSF Grants PHY81-21003 and 84-19380

** Associated Western Universties Graduate Fellow provide larger angle data (up to 60°). Trajectory analysis separates the images of the two targets as well as that due to vacuum chamber window over a wide angle and energy range. Results using this system are presented in A2-4.

2. A Detection System for and $^{nat}Fe(n,n'x)$ Measurement at 65.5 MeV*. (E.L. Hjort, M.A. Hamilton, T.D. Ford,** F.P. Brady, J.L. Romero, C.M. Castaneda, and J.L. Drummond)

A detection system for measurements of (n,n'x) continuum spectra has been developed. This system uses a CH_2 proton convertor in front of a large area multiwire chamber scintillator counter telescope which includes an NE102 ΔE detector and NE102 and NaI Energy detectors to measure the angle and energy of the recoil proton. The first spectra from this facility are presented for a ^{nat}Fe target. Analysis has been conducted from 14 to 24 degrees and cross section comparisons are made between the (n,n'x) and 62 MeV (p,p'x) spectra (see Fig. B-2). Evidence for (n,n'x) excitation of giant resonances has been found and the ratio of a neutron to proton matrix elements is being extracted.

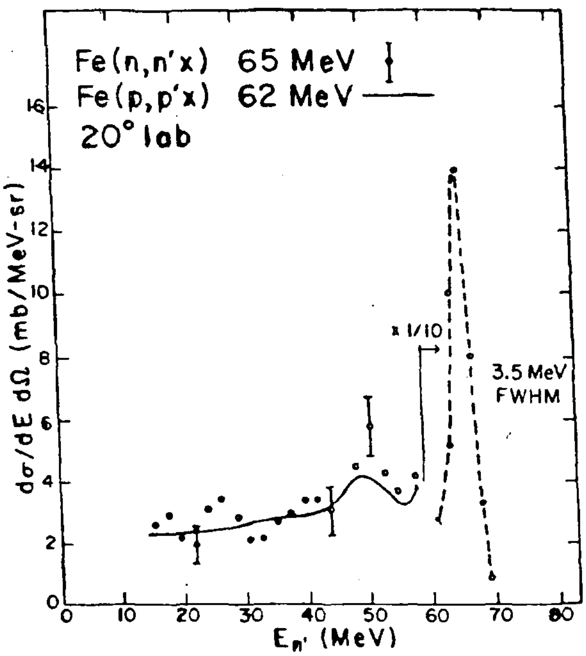

Figure B-2. $^{nat}Fe(n,n'x)$ at 65 MeV compared to $^{56}Fe(p,p'x)$ data at 62 MeV from Oak Ridge.

---

* Supported by NSF Grants PHY81-21003 and 84-19380
** Associated Western Universities Graduate Fellow

DOE NUCLEAR DATA COMMITTEE REPORT

FEBRUARY 1986

R. E. Schenter

HANFORD ENGINEERING DEVELOPMENT LABORATORY

A. NUCLEAR DATA EVALUATIONS

1. Pn Evaluation (F. M. Mann)

Experimental data giving the probability of the emission of a neutron following beta decay (Pn) have been compiled. Using this data, Pn values for 83 isotopes have been evaluated using a generalized least squares technique which allows for laboratory bias. Data up to April, 1985 were reported at the Santa Fe conference.

2. Spectrum Integrated (n,α) Cross Section Comparisons and Least Squares Analyses for ^{6}Li and ^{10}B in Benchmark Fields* (R. E. Schenter, B. M. Oliver** and H. Farrar IV**)

Spectrum integrated cross sections for ^{6}Li and ^{10}B from five benchmark fast reactor neutron fields are compared with calculated values obtained using the ENDF/B-V Cross Section Files. The benchmark fields include the Coupled Fast Reactivity Measurements Facility (CFRMF) at the Idaho National Engineering Laboratory, the 10% Enriched U-235 Critical Assembly (BIG-10) at Los Alamos National Laboratory, the Sigma-Sigma and Fission Cavity fields of the BR-1 Reactor at CEN/SCK, and the Intermediate Energy Standard Neutron Fields (ISNF) at the National Bureau of Standards.

Results from least square analyses using the FERRET computer code to obtain adjusted cross section values and their uncertainties are presented. Input to these calculations include the above five benchmark data sets. These analyses indicate a need for revision in the ENDF/B-V files for the ^{10}B and ^{6}Li cross sections for energies above 50 keV.

3. Cross Section Evaluations for Radioisotope Production in FFTF (Gd-152, Gd-153) (R. E. Schenter)

Capture cross section evaluations for Gd-152 and Gd-153 are being made with emphasis on accuracy in the epithermal energy region. Results of these evaluations will be used in calculations to predict Gd-153 production for various positions in the Fast Flux Test Facility (FFTF). Gd-153 is an important isotope used for medical diagnostic application (bone disease diagnostics).

---

* To be presented at Symposium on the Effects of Radiation on Materials, Seattle, Washington, June 23-25, 1986.

** Rockwell International.

A. NUCLEAR DATA MEASUREMENTS

1. Precise Gamma-ray Emission-Probability Measurements for Selected Actinide Nuclides (R. G. Helmer, C. W. Reich)

As a part of our laboratory involvement in the work of an International Atomic Energy Agency Coordinated Research Program to measure and evaluate nuclear decay data for selected transactinium nuclides, we have made precise (overall accuracy $\lesssim$ 1%) measurements of the emission probabilities (absolute intensities) of the prominent gamma-ray transitions from a number of such nuclides of particular importance for fission-reactor technology. Nuclides whose gamma-ray emission probabilities have been measured in this activity include: $^{238,239,240}Pu$, $^{241}Pu(+^{237}U)$, ^{232}U (and members of its decay chain), $^{233,235}U$, ^{233}Pa and ^{229}Th (and members of its decay chain). Papers presenting the results of all of these measurements have appeared in the literature, except ^{229}Th and its daughter nuclides, which has been accepted for publication.

2. Niobium Irradiations in Standardized Neutron Fields (JW Rogers, J. D. Baker, R. J. Gehrke)

Irradiations of niobium will be conducted in well characterized ^{252}Cf spontaneous fission neutron and ^{235}U fission neutron fields. The irradiated niobium material will be used to produce neutron fluence standards and the activity produced by the $^{93}Nb(n,n')^{93m}Nb$ reactions will be used along with the neutron intensities to determine spectrum averaged neutron cross sections for this reaction.

High purity and well characterized niobium material has been obtained for these irradiations. The neutron field intensities of the ^{252}Cf and ^{235}U facilities will be measured by NBS using standardized fission chambers. Perturbations of the irradiations and measurements will be calculated to provide the necessary corrections. The ^{235}U facility at NBS and the ^{252}Cf facility at the University of Arkansas will be used for the irradiations. The irradiated niobium material will be prepared for fluence standards at INEL. The radioactivity of these materials will be measured at these and other laboratories.

The results from these irradiations, measurements and calculations will produce accurately determined fission spectrum cross sections for these neutron fields, which will be used in data reduction and interpretation of neutron dosimetry with this reaction. Results will also be used to compare the measured reaction rates with calculated reaction rates as a test of the differential cross section data for these fission spectra. The results from these experiments will benefit nuclear technology by providing useful nuclear cross section data that will be applicable to light water reactors, breeder reactors, fusion reactors and any other fields which require fast neutron monitoring.

3. Delayed-Neutron Spectral Measurements (R. C. Greenwood, A. J. Caffrey)

A series of delayed-neutron energy spectral measurements for the fission-product precursors $^{93-97}Rb$ and $^{143-145}Cs$ was successfully completed using the TRISTAN ISOL facility at Brookhaven National Laboratory. The specific goal of these experiments was to improve the spectral definition for each of these isotopes both at the lower energies (below ~20 keV) and at the higher energies (above ~800 keV). To that end, the following series of experiments was conducted: (1) measurements using a H_2 proton-recoil proportional counter (200 cm pressure) with pulse-shape discrimination (between beta/gammas and neutrons) at a gain setting of 0.3 keV/channel (77 keV maximum energy); (2) measurements using a CH_4 proportional counter (400 cm pressure) at a gain setting of 8 keV/channel (2 MeV maximum energy); and (3) measurements using a 2 in. diameter x 0.5 in. thick BC501 liquid scintillation detector with pulse-shape discrimination (between beta/gammas and neutrons) at a neutron gain setting of 40 keV/channel (10 MeV maximum neutron energy). These latter experiments represented our first use of a liquid scintillation detector for delayed-neutron energy spectral measurements, in preparation for delayed neutron-gamma coincidence experiments to be performed in measurements of beta-strength functions.

4. E1 Transition Probabilities within the $K^{\pi} = 1/2^{\pm}$ Parity-Doublet Bands in ^{225}Ra (C. W. Reich, I. Ahmad*, G. A. Leander**)

The $K^{\pi} = 1/2^{\pm}$ bands in ^{225}Ra have previously been interpreted as parity doublet bands based on a single Nilsson orbit in a reflection asymmetric nuclear potential. The accuracy of this description has been tested by using recently measured level lifetimes to deduce the reduced matrix elements for three E1 transitions within these bands. This analysis assumes good K = 1/2 for both bands. The reduced E1 matrix elements with $\Delta K = 0$ and 1, respectively, are found to be 0.0626 ± 0.0033 e·fm and -0.0046 ± 0.0013 e·fm. As expected, the $\Delta K = 0$ E1 strength is considerably larger than that found in heavier actinides, where reflection asymmetric shapes do not occur. The deduced $\Delta K = 1$ E1 strength, which is related to the "electric decoupling factor", is smaller but is nevertheless surprisingly large for a reflection-asymmetric shape and remains to be explained.

A paper describing the methods employed to deduce these matrix elements and discussing some of their implications for the nuclear structure of ^{225}Ra has recently been accepted for publication in Physics Letters B.

---

* Argonne National Laboratory
** UNISOR, Oak Ridge Associated Universities

5. Identification of New Isotopes ^{154}Nd and ^{155}Nd, Produced in ^{252}Cf Fission (R. C. Greenwood, J. D. Cole, R. A. Anderl)

New isotopes ^{154}Nd and ^{155}Nd have been identified, and the decay of ^{153}Nd confirmed, from studies using the Idaho ISOL system. In this system, spontaneous fission of ^{252}Cf is used as the source of fission products with transport to the mass separator via a He-gas-jet arrangement. The observed decay rates of the Pm K x rays in mass separated 153 through 155 fractions, together with the associated γ-ray decay spectra, provided direct identification of the corresponding Nd isotopes. Half-life values of ~26 s and ~10 s were determined for the ^{154}Nd and ^{155}Nd isotopes, respectively. Also, some 36 and 19 γ rays have been associated with the ^{154}Nd and ^{155}Nd decay, respectively.

6. Ion-Source Development at the INEL ^{252}Cf ISOL Facility (R. A. Anderl, J. D. Cole, R. C. Greenwood)

An on-line isotope separator system has been developed at the INEL. The system utilizes the He-gas-jet technique to transport fission products from milligram-size ^{252}Cf spontaneous fission sources to the ion source of an electromagnetic mass separator. Solid aerosols of NaCl are used as activity carriers in the gas-jet system. Recent work has focussed on the development and utilization of a long-lived, high-temperature, gas-jet-coupled ion source for production of rare-earth fission-product ion beams. We have successfully tested such a source that employs electron bombardment heating of the cathode. Temperatures up to 2500°C have been achieved with a tantalum cathode. The lifetime of the source is better than 100 hours of gas-jet-coupled operation. Total separation efficiencies (based on the ratio of radionuclide activity collected at the focal plane of the mass separator to radionuclide activity generated by the ^{252}Cf source) has been estimated to be better than 2% for Cs, 0.1% for Ba, and 1% for Pm. This ion source was used in recent experiments with the ISOL system in which two new isotopes of neodymium, ^{154}Nd and ^{155}Nd, were discovered.

Future improvements will include the use of tungsten ion-source components and better heat shielding and cooling. With these improvements we expect to achieve routine operation of the ion source at temperatures greater than 2700°C with high-efficiency production of rare-earth ion beams.

7. Problems Associated with β- Feeding Information Deduced from Conventional Studies of Complex Decay Schemes: The Specific Example of ^{87}Br Decay (C. W. Reich)

Because of their intimate link with energy production in nuclear reactors, fission products and their nuclear data have long occupied an important position in reactor technology. In recent years, interest in short-lived fission-product decay data has increased markedly, as their relevance to many different areas of research and technology has become more apparent. In addition to their recognized importance for estimation of the fission-product decay-heat source term in operating reactors, the increasing attention being focused on the assessment of the hazards associated with the release, transport and deposition of fission products following reactor accidents has produced a need for additional information on their energy spectra, especially for the isotopes of the more volatile elements.

Over the years, our knowledge of the important decay data for the longer-lived fission products, those amenable to study using conventional methods of nuclear spectroscopy, has steadily improved, so that it is presently adequate (with occasional exceptions) for most applications. Such is unfortunately not the case for the shorter-lived fission products.

In common with all nuclides having complex decay schemes, the study of the short-lived fission-product decay schemes presents special problems. Because of the complexity of the spectrum of the emitted radiation and the large number of energy levels that can be populated, the observation of all the γ-ray transitions and the correct placement of them within the daughter-nucleus level scheme is a difficult and extremely time-consuming process, if it is indeed possible at all. Consequently, in actual practice, it is almost never done. For most purposes in low-energy nuclear physics this is not a serious problem, since it is usually only the level properties in the first MeV or two of excitation that are of interest, and these can be obtained with considerable confidence from even a relatively incomplete decay scheme. In cases where an accurate knowledge of how the emitted energy is distributed, however, the lack of a complete decay scheme can be a fundamental limitation.

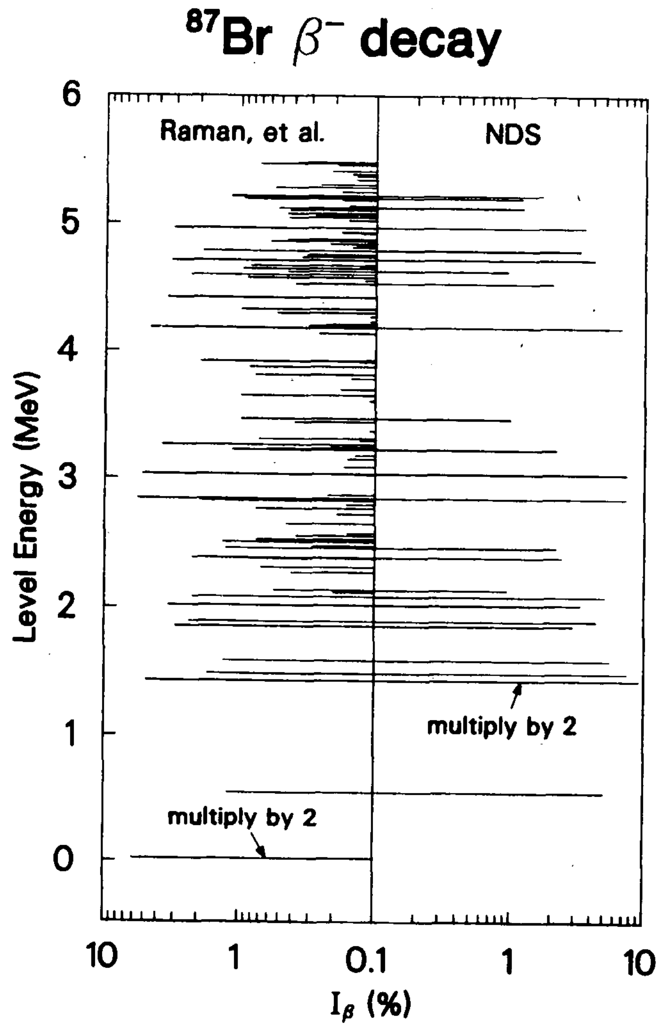

Fig. A-1. β-transition intensities from ^{87}Br decay, from the results of two different studies. Only transitions with intensities >0.1% and feeding levels below the neutron binding energy are shown.

A simple illustration of some of the problems involved in utilizing currently available decay data on short-lived fission products is provided by the ^{87}Br decay ($T_{1/2}$ = 55.7 s). Two different estimates of the distribution of β-intensity feeding the levels in the daughter nucleus, ^{87}Kr, are shown in Fig. A-1. At the right are shown the data from the most recent Nuclear Data Sheets evaluation, published[1] in 1979. At the left the results of a more recent, very detailed study [2] are given.

It is clear that the distribution of β intensity is quite different in these two cases, being generally shifted higher up in the ^{87}Kr level scheme (i.e., to lower β energies) in the more detailed study. This finding is consistent with what would be expected from the so-called "Pandemonium" effect[3], since the higher statistical quality of the data of Ref. 2 leads to the identification of more γ-ray transitions and hence to a reduction of the β intensity deduced to be feeding the lower-lying levels in the daughter nucleus, as previously discussed in a number of places. A more dramatic, and possibly less well appreciated effect, however, is associated with the values of the γ-ray emission probabilities (absolute intensities). In Ref. 2 the γ-ray emission probabilities, P_γ, are reported to be ~30% smaller than those used in Ref. 1 (22.0 ± 1.5% vs. 32.0 ± 2.5% for the prominent 1419-keV γ ray). Use of this smaller value in the evaluation of Ref. 1 leads to a significant change in the deduced average-energy values, as shown in Table A-1. The marked increase in $\langle E_\beta \rangle$ occurs largely because of the need to introduce a 31% β branch to the ^{87}Kr ground state in order to maintain an overall intensity balance within the decay scheme. (With the higher P_γ values used in Ref. 1., the intensity of the ground-state β branch was <4.5%.)

TABLE A-1. Comparison of average decay-energy values (in keV) for ^{87}Br, as deduced from two different experiments.

Quantity	Raman, et al.[2]	Nuclear Data[1] Sheets	NDS as revised
$\langle E_\beta \rangle$	1643.	1861.	2095.
$\langle E_\nu \rangle$	2122.	2358.	2764.
$\langle E_\gamma \rangle$	3204.	4113.	2828.
sum	6969.	8332.	7687.

Note: Q_β (^{87}Br) = 6830 ± 120 keV. For a "perfect" intensity balance, the three average-energy values should sum to this value.

1 P. Luksch and J. W. Tepel, Nuclear Data Sheets 27, 389 (1979).
2 S. Raman et al., Phys. Rev. C 28, 602 (1983).
3 J. C. Hardy et al., Phys. Lett. 71B, 307 (1977).

In assessing the adequacy for many applications of the decay data presently available on the short-lived nuclides, the following points should be noted:

(a) ^{87}Br is exceptional among the short-lived fission products; very few of these nuclides have been studied in the detail that this one has been. This detailed study, which represents several years of work, has led to significant changes in the previously accepted average-energy values for this decay, which values were themselves based on an evaluation of data that were certainly adequate for many purposes in low-energy nuclear physics and were typical, as regards completeness, of data for other high-Q-value nuclides;

(b) ^{87}Br lies in the light-mass peak of the fission-product mass-yield curve; and even at daughter-nucleus excitation energies near the β-decay Q value (ignoring the effects of delayed-neutron emission here) the level spacings are sufficiently large (a few keV), that discrete-line γ spectroscopy might still, at least in principle, identify all the emitted γ-ray transitions. For significantly heavier nuclides, those in the heavy-mass peak, however, the level spacings accessible to β decay are expected to be much smaller (0.1 keV) and discrete-line spectroscopy cannot be expected to identify all the γ transitions and, hence, to accurately determine the distribution of the β intensity in a typical decay scheme; and

(c) ^{87}Br is not very far off the line of β stability, and its relatively long half-life (55.7s) and the ease with which isotope-separated samples of it can be prepared make it a relatively simple case to study.

Since, even for this "simple" case, a detailed study has produced such drastic changes in many of the deduced decay properties, caution should be taken in using for many applications presently available data on such nuclides. It seems likely, for example, that the somewhat poorer prediction of the β- and γ-ray components of the decay-heat source term using the ENDF/B-V decay data than was obtained using ENDF/B-IV resulted from the inclusion in the former of decay data for a number of short-lived fission products that were obtained from just such incompletely determined decay schemes.

B. NUCLEAR DATA EVALUATION

1. <u>Mass-Chain Evaluation for the Nuclear Data Sheets</u> (M. A. Lee, R. G. Helmer, C. W. Reich)

As part of our involvement in the work of the International Nuclear Structure and Decay Data Evaluation Network, which carries out the evaluation of basic nuclear-physics data for publication in the Nuclear Data Sheets, we have the evaluation responsibility for the ten mass chains in the region 153 $\leq$ A $\leq$ 162. The plan for the evaluation of these mass chains has been to undertake those most out of date first.

The status of the evaluation work for our region of responsibility can be summarized as follows:

A chain	Status (according to currency)
154	underway in FY-1986; last published 1979
159	underway in FY-1986; last published 1979
158	NDS 31, 381 (1980)
153	NDS 37, 487 (1982)
157	NDS 39, 103 (1983)
161	NDS 43, 1 (1984)
162	NDS 44, 659 (1985)
160	NDS 46, 187 (1985)
155	completed in FY-1985
156	completed in FY-1985

As is evident from this listing, with the completion of the A=154 and 159 evaluations, our mass chains will, with one exception, satisfy one of the desired objectives of the international evaluation network, namely currency < 5 years.

2. IAEA Coordinated Research Program on Decay Data for Ge Detector Efficiency Calibration (R. G. Helmer)

An advisory group meeting was convened May 30-31, 1985 in Grenoble by Alex Lorenz of the International Atomic Energy Agency (IAEA) to discuss the status of the quality of the decay data for the nuclides commonly used for the efficiency calibration of Ge detectors for gamma- and X-ray spectrometry. The participants in the meeting were from nine laboratories in seven countries, including R. G. Helmer from the INEL.

The goal of this group will be to get subsequent evaluators to use the values it recommends and, thereby, generate one internationally adopted set of values. To achieve this goal will require some promotion after the technical work is done. In order to reach this goal it was agreed that even in cases where the decay data are sufficiently accurate for efficiency calibration, this group should generate an evaluated value on which it agrees. The quantities to be evaluated are the nuclide half-life and the emission probabilities of the gamma- and X-rays that are used for Ge detector efficiency calibrations. It is also the purpose of the group to identify cases for which new measurements are needed, that is, where the data are poor or discrepant.

The group agreed on the preliminary list of 32 nuclides given in Table B-1. A preliminary evaluation of the data for these nuclides is to be carried out by the end of this calendar year. At INEL we have evaluated the gamma-ray emission probabilities for ^{152}Eu and ^{155}Eu. We have also supplied a list of the X- and gamma-ray energies for all 32 nuclides.

TABLE B-1. Nuclides to be Considered in IAEA Review of Decay Data

^{22}Na	^{75}Se	^{137}Cs
^{24}Na	^{85}Sr	^{139}Ce
^{46}Sc	^{88}Y	^{152}Eu
^{51}Cr	^{93m}Nb	^{154}Eu
^{54}Mn	^{94}Nb	^{155}Eu
^{55}Fe	^{95}Nb	^{198}Au
^{56}Co	^{109}Cd	^{203}Hg
^{57}Co	^{111}In	^{228}Th with daughters
^{58}Co	^{125}I	^{241}Am
^{60}Co	^{133}Ba	^{243}Am
^{65}Zn	^{134}Cs	

The Advisory Group also generated a recommendation for the formation of an IAEA Coordinated Research Program (CRP). This CRP is now being formed.

3. Participation in ICRM Working Group (R. G. Helmer)

The six Working Groups and the General Board of the International Committee for Radionuclide Metrologie (ICRM) held their biennial meetings June 3-7, 1985 at CENG, Grenoble. The participants involved about 70 people from about 20 countries including China, Czechoslovakia, Hungary, and Japan.

The various working groups and the chairmen are:

Low-Level Counting Working Group
Chaired by J. M. R. Hutchinson, NBS, USA.
Alpha Spectrometry Working Group
Chaired by G. Bortels, CBNM, Belgium
Techniques for Radionuclide Metrology Working Group
Chaired by T. Radoszewski, IEA, Poland
Beta- and Gamma-Ray Spectrometry Working Group
Chaired by K. Debertin, PTB, FRG
Life Sciences Working Group
Chaired by M. Woods, NPL, U.K.
Non-Neutron Nuclear Data Working Group
Chaired by A. Nichols, Winfrith, U.K.

The general meeting of the ICRM was chaired by W. Bambynek, CBNM, Belgium. The president reviewed the status of business remaining from the previous meetings, especially 1981 in Warsaw and 1983 in Geel. Working group coordinators reported on the activities of their groups.

The following officers were elected:

President: W. Bambynek, CBNM, 1985-87,
Secretary: P. Christmas, NPL, 1985-87,
New coordinators of working groups:
Gamma- and beta-ray spectrometry: R. Helmer, INEL, USA, 1985-88
Life sciences: S. Waters, U.K., 1985-88

With the election of R. G. Helmer to chair one of the working groups of the ICRM, we will continue to be actively involved in the activities of this group. The next ICRM general meeting will be in 1987 in Italy.

4. IUPAP Task Group on Gamma-Ray Energies (R. G. Helmer)

During the 4th International Conference on Atomic Masses and Fundamental Constants, Teddington, U.K., 1971, it was decided that progress in precise gamma-ray spectroscopy, especially the study of (n,γ) and (p,γ) reactions, was hampered by a lack of uniformity and precision in the gamma-ray energy standards used. In response to this need, in 1972 the Commission on Atomic Masses and Fundamental Constants of the International Union of Pure and Applied Physics (IUPAP) established a task group. Its task is the production, recommendation, and publication of a consistent set of calibration standards for use in gamma-ray spectroscopy. The members of the task group were, and still are: Chairman, C. van der Leun, Rijksuniversiteit, Utrecht, The Netherlands; P. H. M. Van Assche, SCK/CEN, Nuclear Energy Center, Mol, Belgium; and R. G. Helmer, INEL, USA.

In 1979 this task group published the first such list of gamma-ray energies in Atomic Data and Nuclear Data Tables 24, 39 (1979). The selection criteria for the data included: energy value of good quality and precision (uncertainties of 10 ppm or less); gamma-rays from radioactive decay, generally with half-life of 30 days or more; and well documented measurements.

This committee met June 10-11, 1985 in Mol and discussed the scope and schedule for the development of a new list of gamma-ray energies. The expansion of the scope of the current list will be in the following areas:

more low-energy (below 60 keV) gamma rays;
add nuclides that are useful for Ge detector efficiency calibration (e.g., ^{125}Sb, ^{152}Eu, ^{154}Eu);

add many more high-energy gamma rays (including some from short-lived nuclides and reactions); and
discussion of wave-length and mass-based energy scales.

The next committee meeting will be in 1986 with the time and place yet to be decided.

DECAY STUDIES OF FISSION PRODUCTS WITH TRISTAN AT THE HFBR AT BNL

The TRISTAN on-line mass separator facility at the High Flux Beam Reactor at Brookhaven National Laboratory is used to study the decays of mass-separated neutron-rich nuclides produced in thermal neutron fission of ^{235}U. A number of different elements can be ionized and separated using a variety of ion sources including the newly developed high-temperature thermal and high-temperature plasma ion sources. Measurements made at TRISTAN are discussed below. Members of the Ames Laboratory group (John C. Hill, F. K. Wohn, J. A. Winger, and M. E. Nieland) have collaborated with other users from BNL, K. Sistemich (KFA Jülich, Germany), R. Moreh, A. Wolf and Z. Berant (Nuclear Research Centre, Beer Sheva, Israel) and R. F. Petry (U. of Oklahoma). Experiments involved decay scheme studies via γ-ray spectroscopy, $\gamma\gamma$ angular correlations, $\beta\gamma$ coincidences and perturbed angular correlations.

1. The Half-life of ^{80}Zn: the First Measurement for an R-Process Waiting-Point Nucleus (Gill *et al.*, Hill *et al.*)

A half-life of 0.55±0.02 s was measured for the neutron-rich fission-product nucleus $^{80}_{30}Zn_{50}$. A Q_β value for the decay of ^{80}Zn of 7.15±0.15 MeV has also been deduced. A preliminary level scheme was obtained for ^{80}Ga containing 14 γ rays and 8 excited states up to 2655 keV. The properties of this N=50 waiting-point nucleus are significant for the evaluation of different models of r-process environments and exposure times.

2. Decay of ^{82}Ga to Levels in the N=50 Isotone ^{82}Ge (Winger *et al.*)

The decay of ^{82}Ga to levels in the N=50 isotone ^{82}Ge was investigated by γ singles, and $\gamma\gamma$ coincidence techniques. The structure of ^{82}Ge is of interest since it can be pictured as 4 protons outside of a doubly-magic ^{78}Ni core. The half-life was measured to be 0.62±0.02 s. A total of 9 γ rays have been placed in a level scheme for ^{82}Ge with 6 excited states up to 3257 keV.

3. Decay of ^{83}Ge to Levels in the N=50 Isotone ^{83}As (Winger *et al.*)

The decay of ^{83}Ge to levels in the N=50 isotone ^{83}As was investigated by γ singles, multispectral scaling, and $\gamma\gamma$ coincidence techniques. The structure of ^{83}As is of interest since it can be pictured as 5 protons outside of a doubly-magic ^{78}Ni core. We have measured the half-life to be 1.85±0.07 s. A total of 47 γ rays have been assigned to ^{83}Ge decay. A preliminary level scheme for ^{83}As includes 27 excited states from 306 to 4840 keV. Using a large space shell-model code which is now running on the Ames Laboratory VAX computer, calculations are in progress on the level structure of various N=50 isotones.

4. g-Factor of the 1264-keV Level in ^{97}Zr (Berant *et al.*, Hill *et al.*)

The g-factor of the $7/2^+$, 1264.4 keV level in ^{97}Zr has been measured using the time-differential perturbed angular correlation method.[1] The resultant g-factor (g=+0.39±0.04) is consistent with the simple shell model prediction for a $g_{7/2}$ neutron assuming g_s=g_s(free). This is in contrast to the measured $\nu g_{7/2}$ g-factors in ^{115}Sn, ^{121}Te, $^{125,127}Xe$ where consistency is obtained with theoretical calculations by assuming $g_s \approx 0.7\ g_s$(free) and is seen as another confirmation of quasi-shell closure at Zr^{96}.

5. Coexistence and Level Structure of ^{100}Zr from Decay of the Low-Spin Isomer of ^{100}Y (Wohn *et al.*)

The level structure of the N=60 isotone ^{100}Zr has been studied[2] via the decay of the low-spin isomer of ^{100}Y. A half-life of 735±7 ms was determined from γ-ray multiscaling measurements. γ singles and γγ coincidence measurements have resulted in the placement of 64 γ transitions in a decay scheme with 20 levels up to 4288 keV. Angular correlation measurements were used to deduce a J^π of 0^+ for the 829-keV level. A simple band-mixing calculation is presented which supports a picture of the structure of the low-lying levels in ^{100}Zr as that of coexistence between an axially symmetric deformed yrast band and a nearly spherical excited band.

6. Identification and Decay of Neutron-Rich ^{102}Sr (Hill *et al.*)

The previously unreported decay of ^{102}Sr to levels in ^{102}Y was studied by γ singles and γγ coincidence techniques. A total of 24 γ rays were placed in a level scheme for ^{102}Y with nine excited states up to 1689 keV. Four excited states were assigned J^π's of 1^+ from logft values. A γ ray observed at 128 keV was attributed to delayed neutron emission from ^{102}Sr. Evidence for a band with moment of inertia close to that of a rigid rotor was obtained. This work has been submitted to Phys. Rev. C.

7. Magnetic Moments of 2^+ States in ^{146}Ce and ^{148}Ce (Gill *et al.*, Wohn *et al.*)

The g-factors of the lowest 2^+ states in ^{146}Ce and ^{148}Ce were measured using the time integral perturbed angular correlation technique. The levels were populated in the decay of ^{146}La and ^{148}La. The measured $g(2^+)$ are 0.24±0.05 and 0.37±0.06 for $^{146}_{58}Ce_{88}$ and $^{148}_{58}Ce_{90}$ respectively. The results provide a probe of the number of valence protons participating

---

[1] Berant, Gill, Rafailovich, Chrien, Hill, Wohn, Petry, Chung, Peaslee, and Mohsen, Phys. Lett. 156B, 159 (1985).

[2] Wohn, Hill, Howard, Sistemich, Petry, Gill, Mach, and Piotrowski, Phys. Rev. C 33, 677 (1986).

in the collective motion. A change in the value of $g(2^+)$ as the neutron number increases from 88 to 90 is attributed to the effects of the strong interaction between the $\pi h_{11/2}$ and $\nu h_{9/2}$ orbits which causes a gradual dissipation of the Z=64 subshell gap. This work has been accepted by Phys. Rev. C.

8. <u>Level Structure of ^{148}Ba: A Test of the Valence Nucleon Product Scheme Far Off Stability</u> (Hill *et al.*)

The decay of ^{148}Cs to levels in the even-even nucleus ^{148}Ba was studied by γ singles and $\gamma\gamma$ coincidence measurements. The ^{148}Cs half-life was determined to be 171 ms. Preliminary inspection of the data revealed 8 γ rays attributable to ^{148}Cs decay which were placed in a level scheme with 5 excited states up to 1.05 MeV. The 2_1^+ and 4_1^+ levels have been tentatively identified at 142 and 423 keV. The corresponding ratio $E(4_1^+)/E(2_1^+)$ of 2.98 is greater than that of 2.84 for ^{146}Ba but is short of the rigid limit of 3.33, thus indicating a slower development of deformation than observed for the Sm and Nd nuclei. ^{148}Ba is the heaviest Z=56 and the lightest N=92 nucleus known, thus its levels are extrapolations of both Z and N systematics. Values of $E(2_1^+)$, $E(4_1^+/2_1^+)$, and $E(2_2^+)$ are in excellent agreement with interpolative predictions from systematics of the valence-nucleon product.

A. INTRODUCTION

The Univ. of Kentucky Research Program has continued its special emphases on nuclear structure studies with neutrons, studies of neutron induced reaction mechanisms, and studies of special problems of interest in nuclear astrophysics. A new aspect of the program, that dealing with capture gamma-ray studies, is under development. Considerable progress has been made in the physical and electronic developments required to make the new capture program fully operational. Progress in each of our areas of emphasis will be briefly described in the following pages. First, a brief characterization of activity and progress in each of these areas is presented in this summary.

Studies of low energy neutron scattering from deformable and/or shape transitional nuclei have been continued to determine the extent to which collective excitations other than those of the quasi-ground band strongly affect elastic and inelastic neutron scattering. A special concern now is the possibility that nuclear structure dynamics may affect neutron scattering differently than the scattering of other probes, or that distinct dynamical information may be available from neutron scattering. Collective effects studies so far have examined well only ground-band excitations; these show that the same electric quadrupole (E2) excitation properties of nuclei are measured with neutrons as with other hadrons. Little quantitative is known about collective excitations other than those of the ground-band, for neutron scattering.

During the last couple of years we have concentrated especially on scattering from the shape-transitional Os and Pt isotopes, which show strong and highly variable gamma-band excitations. We are examining the effects of these and E3 excitations on scattering. During this last year we have extended our work to the even-A Pb isotopes. These have been included in our studies near A = 200 partly as spherical reference nuclei, but also because of particular questions in the Pb isotopes to be discussed below.

An extensive study of neutron scattering from the spherical Sn nuclei is virtually complete now. This study explores several questions relating to constraints applied to scattering analyses, particularly systematics of scattering analyses. Earlier attempts to analyze scattering by Sn isotopes had had grave difficulty accommodating the extremely small s-wave strength functions and other scattering data into a single analysis. This has now been successfully done here, without invoking any special or intermediate structures in the neutron scattering. We have also seen directly the importance of the Tepel-Hofman-Herman corrections to the usual statistical models, and confirmed that they do indeed give an excellent distribution of scattered flux into the open channels. Finally, we have seen directly the necessity of using a scattering potential which reflects the projectile kinetic energy <u>in each channel</u>.

The recent postulation that effective mass effects in microscopic models of scattering potentials lead to non-linear energy dependencies could present an interesting way to test the validity of approximations that the currently employed microscopic models use in approximating scattering fields. But to test this we need highly accurate data near closed shells. That has contributed to our interests in the Pb isotopes, and has also inspired us to attempt a scattering comparison between ^{40}Ca and ^{48}Ca targets. The Ca study is just now being planned for initiation in the Spring of 1986. This promises to be one of the most difficult experimental challenges, because only a very small enriched ^{48}Ca sample is available, and it is a $CaCO_3$ sample. The potential rewards of properly treating scattering from these two magic nuclei at low energies is great, however.

A second thrust of our neutron induced reaction program is the study of the collective excitations of deformed and shape transitional nuclei themselves, through the study of the $(n,n'\gamma)$ reactions and other reaction studies pursued with triton beams at the Los Alamos tandem accelerator facility. These studies deal with the symmetries of collective excitations, primarily through application of the Interacting Boson Approximation (IBA) symmetries for even-A nuclei and through boson-fermion mixed models which employ supersymmetry concepts to classify excitations in odd-A nuclei. These studies are important in connecting nuclear structures in different mass ranges to each other, and also extend and complement the scattering studies mentioned in the paragraph above.

A third area in which considerable progress has been made this year is the development of new facilities for neutron and proton capture. A new vacuum beam line has been completed, with the triple angle target chamber which, together with the dipole magnet, will allow gamma-ray detection directly at 0 and 180 degrees. The new tritium target assembly has been completed and its Uranium oven loaded with tritium. At this point we lack only the completion of the dipole magnet coils, and assembly of the magnet itself.

The fourth area in which all experimental work and most interpretative analysis is completed is in the study of very low energy neutron scattering in ^{189}Os. This study confirms our earlier experiment in ^{187}Os and the roles that neutron scattering and capture play in fixing the s-process ^{187}Os in stars, novae and supernovae. Thus our earlier results for the Re/Os nucleochronology, which depended on our interpretation of neutron induced reactions in the Os isotopes, do not seem to need modification.

We have benefited very much from the direct participation of Gabor Molnar of the Institute of Isotopes in Budapest, Hungary in our nuclear structure research studies. Gabor joined our group in April of 1985 and immediately involved himself in the nuclear structure problems under study, as well as initiating new studies. His collaborative work with Steve Yates has led to the establishment of an NSF funded, three institution, long term collaboration involving the University of Kentucky, the Institute of Isotopes in Budapest, and LLNL in Livermore.

B. NEUTRON SCATTERING

1. Shape-transitional Nuclei (S.E. Hicks, G. Shen, M.T. McEllistrem)

At this point, all scattering data needed to complete our efforts to interpret nucleon, and especially neutron, scattering to see the nuclear dynamics of the Os and Pt nuclei have been measured. High precision and accuracy measurements have been completed on total cross sections of ^{194}Pt and for ^{190,192}Os nuclei. As noted below in the description of the Pb isotope study, both comparisons with other measurements and our own check measurements support the claimed accuracy of about 1% for our total cross sections.

The important sample self-shielding corrections have been made using the newly developed code SESHRX, developed from Froehner's code for such corrections at very low neutron energies by J. L. Weil and Z. Zhou during the last year. The development of this code is discussed in the section of this report on scattering from the Sn nuclei. Our tests show that sample self-shielding corrections are not noticeable for the Os and Pt isotopes for $E_n >$ 300 keV, and thus are not needed for our data.

The differential elastic and inelastic scattering cross sections have been measured for all of the above mentioned isotopes at neutron energies of 1.6, 2.5, and 4.5 MeV except for ^{190}Os. Some older data for that isotope had been taken at 4.0 MeV, but some additional measurements may be needed for that isotope. However, the data we have now are complete enough to make a consistent interpretation of the gamma-band excitations and other collective effects on the scattering from shape-transitional Os and Pt nuclei, and that analysis is in progress.

Additional data for the nuclei of interest to the Os and Pt study are those from the Centre d'Etudes de Bruyeres-le-Chatel (BRC) at an energy of 8 MeV. These data are being reduced to differential cross sections, and soon will be ready for analysis and interpretation.

To date we have found that the different collective excitations of these nuclei, particularly those of the gamma-band, noticeably alter the elastic scattering cross sections at 1.6 MeV and 2.5 MeV incident energy. That is, the elastic scattering cross sections themselves are sensitive to the presence of gamma-band excitations,[1] and even differentiate between gamma-soft and gamma-rigid excitations, as documented in the analysis of Ref. 1. At still lower energies than 2.5 MeV, there is a strong indication that the elastic scattering sensitivity increases markedly,[2] but the validity of this conclusion depends on further, detailed analyses. So far detailed analyses have only been completed and published for ^{194}Pt.

---

[1] Mirzaa, Delaroche, Weil, Hanly, McEllistrem, Phys. Rev. C32, 1488 (1985).

[2] M.T. McEllistrem, Proc. Int'l Conf. on Neutron-Nucleus Collisions, A Probe of Nuclear Structure, AIP Conf. Proc. No. 124 (ed. by Rapaport, Finlay, Grimes, and Dietrich, (1985)), p. 208.

2. <u>Pb Isotope Study</u> (J.M. Hanly, M.T. McEllistrem)

As noted above, the study of the Pb isotopes is motivated partly by the need to have some spherical nucleus scattering for nuclei near the shape-transitional nuclei. Since scattering from ^{208}Pb has been recently extensively studied,[3] the most useful data are those for the other Pb isotopes. We had elected to study scattering in some detail and with care for ^{206}Pb and ^{204}Pb. We have completed measurements of total cross sections for energies from 300 keV to 4 MeV with an accuracy and precision of about 1%, and differential scattering cross sections at 2.5 MeV and 4.5 MeV. Some of the ^{206}Pb data can be compared with very recent, unpublished data from ORELA[4] and shows good agreement. These data, together with well known low energy scattering properties,[5] make a fairly complete data set for systematic analyses to test for the character of scattering potentials, and the role of coupling to excited levels.

Recent reports suggest there may be "anomalous" energy dependence for energy-averaged cross sections in nuclei near doubly closed shells. This suggestion is raised because recent analyses of low energy scattering suggest[6] that the absorptive potential (W) is sharply partial wave dependent, with very small strengths in some partial waves. This would give rise to absorption-broadened resonances, but not so broad as to be impossible to see. Such a doorway state has been suggested for years as the explanation of a strong resonance in scattering from ^{208}Pb, and quite recently this was confirmed in a scattering analysis.[7] Such resonances were not expected in other nuclei, because very small W-values, $W < 0.5$ MeV,[6] were completely unexpected for neutron scattering. It is important to see whether such resonance, or doorway states, are visible in scattering from the other even-A Pb isotopes.

Another motive for studying the Pb isotopes comes from the report of Finlay <u>et al.</u>[3] that a non-linear energy dependence is found for the real part of the scattering potential for ^{208}Pb as the neutron energy is lowered toward the

---

[3] Finlay, Annand, Petler, and Dietrich, Proc. Int'l. Conf. on Neutron-Nucleus Collisions, A Probe of Nuclear Structure, AIP Conf. Proc. No. <u>124</u> (ed. by Rapaport, Finlay, Grimes and Dietrich, (1985)), p. 322.

[4] D.J. Horen, ORELA, ORNL, private communication.

[5] S.F. Mughabghab and D.I. Garber, Brookhaven Nat'l Laboratory Report BNL-325, 1973.

[6] A. MacKellar and B. Castel, Phys. Rev. <u>C29</u>, 1988 (1984) and references cited therein; C.H. Johnson, Proc. Int'l Conf. Neutron-Nucleus Collisions, A Probe of Nuclear Structure, AIP Conf. Rep. <u>124</u> (ed. by Rapaport, Finlay, Grimes and Dietrich (1985)), p. 446.

[7] Horen, Johnson and MacKellar, private communication.

Fermi level.[8] This report is disputed by Horen *et al.*,[7] who completed a coupled channels analysis for low energy scattering from ^{208}Pb. It is possible that this apparent non-linearity, which is alleged[8] to be associated with a variable effective mass for neutrons in nuclei, may be an artifact of the doorway resonances. That could explain the anomalies reported by the Ohio University group,[3] without recourse to variable effective mass arguments.

The nucleus ^{204}Pb shows total cross sections at very low energies characteristic of a spherical nucleus with a truly statistical distribution of compound levels,[9] and no apparent candidates for especially strong resonances. Thus energy-averaged cross sections for that nucleus would be those of a normal, spherical nucleus whose scattering is not distorted by the effects of strong coupling to scattering from excited levels. The experiment with that nucleus assumes a very special role in our efforts to explain the scattering from nuclei with A near 200. Our present data sets, including very low energy total cross sections from ORELA, our own total cross sections measured to 4 MeV, and differential scattering cross sections at two energies, should enable a systematic analysis which will test for the requirement of anomalous absorption potentials and for the role of coupling to collective excited levels.

3. Neutron Scattering from Sn Isotopes (R. Harper, J.L. Weil)

A significant part of our program in the past few years has been to study as completely as possible the interaction of neutrons in the energy range of 0.01 to 5.0 MeV with the five even-A isotopes of tin, $^{116,118,120,122,124}Sn$. This study has included measurements of the neutron total cross sections for each of these isotopes, as well as of the elastic and inelastic scattering cross sections at a number of bombarding energies. The inelastic scattering has been studied by detecting both the scattered neutrons and the gamma-rays emitted in de-excitation of excited levels.

a. Total Cross Section Corrections (Z. Zhou, R.R. Winters,† J.L. Weil)

During this past year we have made resonance self-shielding corrections to the total cross sections measured here in the energy range of 0.3 - 5.0 MeV. The corrections were made with the Monte Carlo computer code SESHRX, the original version of which was written by Froehner.[10] In its original form the program used hard sphere phase shifts to describe potential scattering, but this approximation breaks down badly at neutron energies above a few hundred keV. For Froehner's original purpose, measurements in the eV

---

† R.R. Winters, Denison University, Granville, OH 43023,

[8] C. Mahaux and H. Ngo, Nucl. Phys. A378, 1 (1983) ibid., Phys. Lett. 126B, 1 (1983).

[9] Horen, Macklin, Harvey, and Hill, Phys. Rev. C29, 2126, (1984).

[10] F.H. Froehner, AEC Research and Development Report, GA-8380 (1968).

region, that approximation had been adequate. It was therefore necessary to rewrite much of the program to improve the calculation of both the potential scattering and the absorption parts of the total cross section. The basic input to the revised program is optical model S-matrix elements. Using the formalism of R-matrix theory, certain background R-matrix parameters are calculated from this input and then used to calculate a simulated resonant cross section, using Monte-Carlo techniques to select resonance widths and to follow the scattering processes through the scattering samples. The revised program is completely self-consistent up to at least 3 MeV neutron energy. This means that the scattering cross sections obtained from energy-averaging those of the Monte-Carlo generated scattering amplitudes agree with those of the complex optical potential used to fix the input. The self-shielding, or sample-size corrections are very small above 2 MeV. The correction is about 8% for Sn isotopes at E_n = 500 keV, which is quite significant, and has an important effect on the coupled channels model calculations for scattering from Sn isotopes as described below.

b. Coupled Channels Analysis (Z. Zhou, J.L. Weil)

A coupled channels analysis which gives a unified description of the above mentioned total cross sections, differential scattering cross sections at 1.00, 1.63, and 4.02 MeV, low energy neutron scattering lengths, and s-and p-wave strength functions is now essentially complete. All of the data except the scattering lengths and strength functions were measured in this laboratory. Analyses of all of these data were made both with a standard optical model whose parameters were adjusted to fit the data, and a second order vibrational model with a four state model space of 0+ - 2+ - 3^- - 0_2^+. The depth of the real central well has a linear energy dependence while that of the imaginary well (W) has a term proportional to the square-root of the neutron energy. The distribution of the compound nucleus cross section between the elastic and inelastic channels was calculated with the modified statistical model of Tepel, Hofman and Herman (THH).[11]

A major difficulty encountered in the preliminary stages of the analysis was that the calculated inelastic scattering cross sections at an incident energy of 1.63 MeV were always 20 -30% higher than our measured values, when only two levels had open channels. This was all the more remarkable in that the calculated cross sections included the Lane-Dresner (LD) level-width fluctuation corrections,[12] which are known to reduce the cross sections too much. This problem persisted whether a spherical optical model (SOM) or coupled channels (CC) model was being used, the latter either with a first order or second order vibrational model and with both the LD and THH statistical model calculation. This problem was finally resolved by using the

---

[11] Tepel, Hofman, and Herman, Proc. Int'l Conf. Nuclear Cross Sections for Technology, NBS Spec. Pub. 594, 762 (1980).

[12] P.A. Moldauer, Phys. Rev. 135B, 642 (1964), ibid., Rev. Mod. Phys. 36, 1079 (1964).

outgoing neutron energy to determine the energy dependent well depths used to calculate the outgoing wave functions. Using this prescription for the well depths, both SOM and CC models gave a good account of the inelastic scattering cross sections at an incident energy of 1.63 MeV. The CC calculations of the inelastic scattering cross sections of the strongly coupled states at 4.02 MeV also show better agreement with the data than when one set of well depth parameters is used for all neutron channels.

We believe this is the first unambiguous demonstration of the necessity of using channel-dependent scattering potentials when describing neutron scattering. This demonstration was possible because we had unusually accurately measured scattering cross sections in a situation where the number of competing channels was a minimum, and for an entire set of nuclei.

An interesting and unique feature of the Sn isotopes is that they have some of the smallest s-wave strength functions found anywhere in the periodic table, so small that global analyses usually miss them by large amounts. An important result of this CC analysis with the second order vibrational model is that it was possible to fit these extremely small strength functions with a potential that also gives an excellent fit to the total and differential scattering cross sections, for data ranging from 0.01 MeV to 5 MeV. The sensitivity of the model calculations and the need for accurate measurements are both emphasized by the fact that it was not possible to simultaneously fit the total cross sections as a function of energy and the strength functions until the former were carefully corrected for resonance self-shielding, as described above.

Although the same normal, A-dependent geometry was used for all isotopes, the real and imaginary well depths were adjusted for each isotope to give the best fit to all the neutron data for that isotope. One of the goals of this investigation was to look for a systematic variation in well depth as a function of addition of successive pairs of neutrons; i.e., a neutron-excess or isospin dependence. It was found that both the real and the imaginary well depths have a linear dependence on neutron excess. For the CC fits, they can be parameterized as:

$$V = 49.95 - 19.65((N-Z)/A) \text{ MeV}$$

$$W = 4.34 - 19.35((N-Z)/A) \text{ MeV}$$

A SOM analysis of the total cross sections and the elastic scattering differential cross sections at 1.0 and 4.02 MeV gave the same real potential dependence, but the imaginary potential was found to be different both in strength and in its neutron excess dependence, given by:

$$W = 16.95 - 79.18((N-Z)/A) \text{ MeV}$$

The neutron excess dependence found in this study of Sn isotopes for the real central potential is about the same as that found in various global analyses,[13] about -20 to -27 MeV. The need for a larger imaginary well depth in the SOM as compared to the CC model is also a well known result, but the fact that the neutron excess dependence is also so much larger than normal for the SOM analysis is not so well known. It would seem to indicate that the variation in absorption with neutron number is somehow connected mainly to the strongly coupled states of the system, even though the coupling strengths vary little throughout this sequence of isotopes.

4. Scattering in Odd-A Os Isotopes below 100 keV (R.L. Hershberger, Z. Cao, M.T. McEllistrem)

Earlier estimates of the age of our galaxy based on the Re/Os nucleochronology had led to an age less than 16 Gyrs, but this was partly predicated on a rather low absorption probability for neutrons incident on the 9.75 keV excited level of ^{187}Os (in stars). An experiment completed here[14] showed that the inelastic scattering cross section at an incident energy of 60 keV was quite large, which led to a galactic age close to 20 to 22 Gyrs. But observers pointed out that the inelastic scattering cross section depended on absorption properties of both the ground state and the interesting excited level. Thus we initiated a second experiment to study inelastic scattering from 189Os, whose lowest two levels are almost the two of ^{187}Os inverted. A good description of neutron scattering from both nuclei with a common potential model would remove any doubt that the neutron interactions with both Os levels was correctly described by the potential model. In addition, two other excited levels in ^{189}Os can also be observed with neutron energies below 100 keV, making this a nice test of the effectiveness of complex potential and statistical models at very low incident neutron energies, something that had never been done. All data has now been completed for elastic and inelastic scattering for levels of ^{189}Os at incident neutron energies of 60, 75, and 97 keV. Early results of our potential analyses, using the potential developed earlier,[14] show a good description of scattering from all levels of ^{189}Os.

C. NUCLEAR STRUCTURE STUDIES WITH NEUTRONS AND RELATED EXPERIMENTS

1. Shape Transitional Nuclei (E.W. Kleppinger, R. Gatenby, S.W. Yates)

Our work in the region of shape-transitional nuclei just lighter than lead has been continuing for several years, and we have examined more than a dozen nuclei in this region with the $(n,n'\gamma)$ reaction. Our interest was originally motivated by the observation that ^{196}Pt seemed to be the best example of the O(6) symmetry of the IBA. More recently, it was proposed that evidence for supersymmetries in nuclei could be found in the level structures of these nuclei. We are attempting to clarify the roles of nuclear symmetries in this region.

---

[13] M.T. McEllistrem, Prof. Int'l Conf. Interactions with Nuclei, ERDA Pub. CONF-760715-P1, (ed. by Eric Sheldon (1976)), p. 171.

[14] Hershberger, Macklin, Balakrishnan, Hill & McEllistrem, Phys. Rev. C28, 2249 (1983).

We have studied one supersymmetric triplet (^{192}Os, ^{193}Ir, and ^{194}Pt) and two members (^{190}Os and ^{191}Ir) of another multiplet. While a considerable body of new structural information has emerged from these studies, it has also become evident that multipole mixing ratio measurements are critical to a meaningful description. We are currently performing these demanding measurements on the odd-proton Iridium nuclei. In addition, after many years of waiting for an enriched ^{196}Pt sample, we have been able to study the O(6) nucleus with our methods. Here again, much new information has emerged, but the critical role of multipole mixing ratio measurements has resurfaced. Our preliminary data indicate that the O(6) picture is holding up well -- i.e. only those transitions which are predicted to be hindered have significant M1 mixtures. Still more precise measurements to quantify these admixtures are in progress.

2. Studies of Deformed Nuclei (E.W. Kleppinger, S.W. Yates)

Questions about the existence of two-phonon excitations in deformed, rare earth nuclei have motivated us to study the nuclei ^{168}Er and ^{170}Er. As we reported in our most recent paper on this subject,[15] it is difficult to characterize any of the low-lying excitations in ^{168}Er as two-phonon excitations of either the beta-beta or gamma-gamma type. A large amount of new information on ^{170}Er was obtained in these measurements and we are making steady progress in bringing it into order.

3. Spherical Nuclei (G. Molnar, R. Gatenby, E.W. Kleppinger, S.W. Yates)

From our studies of the shape transition just below the lead nuclei, our investigations of the heaviest stable Mercury nuclei have followed quite naturally. The small sizes of the ^{202}Hg and ^{204}Hg scattering samples (less than 2 grams each) have forced us to push our techniques to new limits, but we are able to obtain useful spectroscopic data for these nuclei. For ^{202}Hg in particular, much new information has become available through our studies.

One of the important projects emphasized by Molnar has been one focussed on the even nuclei in the mass-100 region, a longstanding interest in our laboratories and also in Budapest. In particular, we have studied intensively the ^{96}Zr nucleus, probably the heaviest readily accessible nucleus that exhibits a double subshell closure. We have been able to combine the data from our $(n,n'\gamma)$ experiments with previous multi-particle transfer studies to identify a coexisting four particle, four hole band built on the first excited 0^+ state.[16] An alternative explanation of this phenomenon in terms of alpha clustering may also be possible, but this possible description awaits testing in future experiments. We are combining these experiments with parallel beta-decay experiments at the TRISTAN isotope separator and $(t,p\gamma\gamma)$ and (t,pe^-) measurements at LANL in collaboration with members of the LLNL Nuclear Chemistry Division to obtain a fuller description of this spherical nucleus.

---

[15] Yates, Kleppinger and Kleppinger, J. Phys. G: Nucl. Phys. 11, 877 (1985).

[16] Molnar, Yates and Meyer, submitted to Physical Review Letters.

4. Level Schemes in the Sn Isotopes

The very detailed studies of the even Sn nuclei with the $(n,n'\gamma)$ reactions are partly to complement the neutron scattering studies above, particularly at an incident energy of 4.02 MeV, where resolving many excited levels in neutron detection is not feasible. But also the issue of coexisting collective levels amongst a sea of non-collective levels arising from broken pairs in the Sn nuclei is a subject of considerable interest; some progress has been made, in that rather well defined two-phonon and three-phonon vibrational multiplets have been identified in ^{124}Sn. Thus there seems to be a spherical, or nearly spherical, vibrational spectrum mixed into a level scheme with a great many levels which certainly do not belong to that excitation scheme.

a. ^{116}Sn Decay Scheme (Z. Gacsi, X. Shi, J.L. Weil)

The $(n,n'\gamma)$ reaction is a very sensitive and precise way of locating decaying states and often can also be used to determine or limit the spin of the state. Slow neutron capture provides even more precise gamma-ray energies than $(n,n'\gamma)$, but with ambiguous information about the energy of the gamma emitting states. During the past year we have completed the experiment on $^{116}Sn(n,n'\gamma)$ with measurements of the angular distributions at incident neutron energies of 3.75 and 4.5 MeV. The analysis of the data has been finished and the results have been combined with those from (n,γ) capture experiments done elsewhere[17] to determine a level and decay scheme for ^{116}Sn for levels up to an excitation energy of 5.93 MeV.

The decay scheme contains more than 110 levels and 190 gamma rays. In addition to verifying thirteen previously determined J-values, we have been able to make spin assignments or limitations for an additional 68 levels, so that spin information is now available for approximately 70% of the known levels. We believe that we have located all levels with $J < 7$ and excitation energies below 3.5 MeV, and have located an additional 65 levels with $J < 5$ in the region $3.5 < E < 5.93$ MeV.

Having made what we believe to be a fairly complete determination of the level structure up to approximately 3.5 MeV, except for those states with $J > 6$, we are in a position to test the validity of various models. Since the tin isotopes have a closed proton shell, almost all the low-lying excitations are of the valence neutrons. The most recent calculation of such excitations is that of Bonsignori *et al.*[18] for the broken pair or generalized seniority model, with up to two broken Cooper pairs or four quasi-particles. This is a calculation of the levels of ^{116}Sn that is obtained by placing the unpaired neutrons in the several subshells of the g, d, s, and h configurations, which is a rather large model space. Based upon our level energies and J-values or

---

[17] S. Raman, private communication.

[18] Bonsignori, Savoia, Allaart, Von Egmond and Te Velde, Nucl. Phys. A432, 389 (1985)

limitations, we are able to identify or find candidates for all the calculated levels with $J < 7$ (some 40 in all) up to an excitation energy of 3.6 MeV. Another 14 experimentally fixed levels in this energy range are not accounted for by the model. A more stringent test of Bonsignori's model will be a comparison of the experimental and calculated gamma-decay strengths. The calculations have just been received from Bonsignori and Allaart,[19] and the comparison is awaiting the renormalization of experimental gamma-ray intensities.

b. ^{120}Sn Decay Scheme (S. Shi, Z. Gacsi, J.L. Weil)

Angular distributions of the gamma-rays from the $^{120}Sn(n,n'\gamma)$ reaction were measured during the past year at incident energies of 3.2, 3.8, and 4.5 MeV. Earlier measurements of the gamma-ray excitation functions up to a bombarding energy of 4.5 MeV resulted in the observation of some 130 gamma-rays and their placements as decays from 98 excited levels. The analysis of the angular distribution data for incident energies of 3.2 and 3.8 MeV is now complete and from it the spins of many of the newly found levels have been determined, or limited to two or three possibilities. The most interesting results to date concern observation of a number of negative parity levels with spins ranging from $J = 4$ to $J = 7$; more than half of them have been observed for the first time. From the spins and parities and the branching ratios, it appears that these levels can be explained in terms of simple 2-quasiparticle shell model configurations based on the h(11/2), s(1/2), and d(3/2) subshells. A very similar group of negative parity states was observed previously in the ^{124}Sn nucleus in this laboratory. Analysis of the higher energy data is under way, and when finished a more complete interpretation of the level structure will be attempted. It is hoped that broken pair model calculations can be performed for comparison with these results.

D. RADIATIVE CAPTURE STUDIES

The past 8 months have been primarily a period of construction and testing for the radiative capture program. Following our design studies during the first year, several systems have now entered the construction phase, and several new items have been completed.

1. The NaI Spectrometer (B.G. Pugh, S.L. Riley, M.A. Kovash)

The NaI spectrometer with its 13 mounted phototubes and eleven LED's was received from the Bicron Corp. in September, 1985. The instrument is designed to detect gamma rays of moderate energy--up to about 50 MeV--with high resolution in both energy and time. The central element of the spectrometer is an 8" diameter cylinder of NaI with a length of 10". Housed in the same aluminum container, but optically isolated from the central detection element is an annular array of six individually isolated segments of NaI with a radial thickness of 1-3/4". A separate NaI disk of this same

---

[19] G. Bonsignori, private communication.

thickness which is located just in 'front' of the central element completes the spectrometer.

We have completed our initial tests of the detector and have measured the energy resolution at a gamma-ray energy of 10.7 MeV. Without any use of the escape event rejection capabilities of the annular shield, we find an energy resolution of 1.8%. This figure represents the value of AE/E as measured from 10-90% of the peak height on the high energy side of the peak. We attribute this exceptional performance to a very careful testing and grading program of the manufacturer.

2. Data Acquisition System (S.L. Riley, L. Keeney, M.A. Kovash)

Presently, the detector electronics is being expanded to allow individual ADC and TDC readout of each of the 8 segments of the spectrometer. Our short term goal is to investigate the response of the spectrometer to gamma rays of various energies through the software control offered by the CAMAC system. In particular, we will explore the extent to which escape events can be digitally reconstructed from the energies and times measured in various elements of the detector. The goal here is to improve the efficiency for valid events while maintaining adequate discrimination against backgrounds induced by neutrons and cosmic rays. We continue in our development of the software data acquisition program required by the CAMAC system. A scaled down version of the final code has been used to make tests of the newly purchased CAMAC ADCs and TDCs.

3. Beamline Hardware (B.G. Pugh, J. Trice, M.A. Kovash)

Nearly all of the hardware required to support and adequately shield the spectrometer is either finished or nearing completion. A large lead shield to house the detector has been cast and a support trolley has been fabricated. A borated polyethylene shield will soon be constructed.

We have developed a new target cell for containing the tritium gas required to produce the neutron beams for our radiative capture program. The target uses a double-window design with localized vacuum pumping to contain the escape of tritium gas due to both small leaks through the target foils and any potential catastrophic foil failure. Initial beam tests of the double foil system are scheduled for the Winter of 1985-86.

The final magnet required to complete the 180 degree scattering system is under construction. The 180 degree system, with its three sector beam line design and the dipole magnet, is designed to permit detection of gamma rays over the entire range of angles, from 0 to 180 degrees. The magnet iron has been received and machined into final form. Presently the department shop is developing the techniques required for winding the coils for this instrument. The present power supply for the 90 degree Mobley magnet used in the beam-pulse bunching system in the neutron hall is currently being modified for alternate use by the 180 degree scattering system magnet.

1. LAWRENCE BERKELEY LABORATORY

A. NUCLEAR DATA EVALUATION

1. Isotopes Project (E. Browne, R.B. Firestone, and V.S. Shirley)

The Isotopes Project compiles and evaluates nuclear structure and decay data. The group coordinates its efforts with those of the U.S. Nuclear Data Network and the International Nuclear Data Committee of the IAEA. The Isotopes Project authors the Table of Radioactive Isotopes, evaluates the mass chains $167 \leq A \leq 194$, and maintains the LBL/ENSDF database. During the past year the group was fully occupied with the completion of the Table of Radioactive Isotopes and published no new mass chains. The book was sent to the publisher in January, 1986 and the group is presently evaluating
A = 168, 180 and 183.

2. Table of Radioactive Isotopes (E. Browne, R.B. Firestone, and V.S. Shirley)

The Table of Radioactive Isotopes is a comprehensive and critical evaluation of the nuclear and atomic properties of radioactive isotopes. The book is especially tailored to the needs of applied users in industry, biology, medicine, and other fields, but serves also as an indispensable reference for nuclear physicists and chemists. Detailed radiation data for about 2000 of the 2755 known nuclides are presented in this up-to-date and concise single-volume book.

The main section of the book is organized by mass number (A), with entries for a given A derived from and referenced to the most recent corresponding evaluation in Nuclear Data Sheets or Nuclear Physics. These entries include a mass-chain decay scheme, showing the isotopes for that mass number, some of their properties, and the decay relationships between them. Following the scheme are tables for every isotope, the first of which gives the isotope's atomic number, mass number, element symbol, half-life, decay modes and branchings, mass excess, specific activity, means of production, and natural isotopic abundance. Subsequent tables list the isotope's nuclear and atomic radiations, and include total average energies per disintegration wherever possible. Throughout, the experimental radiation data have been analyzed for statistical consistency, and the resulting best energies and intensities are reported in the tables.

Appendices of interest to users of radioactivity data follow the main section of the book. These include graphs and tables pertaining to the following: fundamental constants and conversion factors, standard γ-ray and α-particle energies and intensities for detector calibration, theoretical internal conversion coefficients, electron-capture subshell ratios, electron binding energies, atomic fluorescence and Coster-Kronig yields, x-ray energies and intensities, Auger-electron intensities, absorption of γ-rays in matter, ranges and stopping powers of charged particles in matter, positron annihilation radiation, total positron decay branchings, average radiation energies per disintegration, and physical properties of the elements.

An extensive introductory section explains the nuclear properties shown on the mass-chain decay schemes, and the contents and structures of the various tables. This is followed by a section, titled Methods of Analysis, which gives a detailed description of the statistical and mathematical formulation used in the data analysis.

3. LBL/ENSDF Database (E. Browne and R.B. Firestone)

The LBL/ENSDF database is complete for $1 \leq A \leq 266$. It contains nearly all of the numerical data from the Evaluated Nuclear Structure Data File (ENSDF) and the adopted decay data from the Table of Radioactive Isotopes. It also contains Wapstra's 1983 Atomic Mass Table. The database has been organized using DATATRIEVE, a DEC database management system. DATATRIEVE provides simple, English commands for retrieving, sorting and printing desired data. Cross-referencing linkage has been provided in the database so that levels and transitions that were measured in different experiments can be readily extracted and compared. A menu of utilities for the extraction, analysis, and tabulation of data from the database is available. In addition DATATRIEVE has a straightforward native programming language that can be used to obtain other combinations of data. The database is maintained on a dedicated 456 megabyte disk which is accessed by the LBL VAX-8600 computer cluster. It is accessible by telephone and via DECNET, MILNET, and TYMNET. Interested users should contact the Isotopes Project for further information.

The Isotopes Project is investigating the possibility of producing the decay data for ENDF/B from the LBL/ENSDF database. Currently, the database contains adopted energies and intensities for γ rays, electrons, and prompt or delayed particles from nearly all known isotopes. It also contains total average energies of photons, electrons, and betas, half-lives (primarily from the 1983 Chart of the Nuclides), and the Wapstra Q-values. Cross sections, fission yields, and calculated Q-values are not currently available in this database. However, ample disk space remains for additional data if desired. The preparation of listings or files of data from the LBL/ENSDF database would require minimal local effort and could be handled as a simple request for data. More complicated requests for calculated quantities must be handled on a case-by-case basis.

The radioactivity data in the LBL/ENSDF database is derived primarily from the ENSDF data file. Although ENSDF does not contain adopted decay data, that information can be extracted semi-automatically with a series of existing Fortran computer programs and DATATRIEVE command procedures. The updating of the database to include new ENSDF evaluations is necessary if the LBL/ENSDF database is to remain current. Although the present high quality of ENSDF evaluations will minimize this effort, the limited resources of the Isotopes Project and its primary evaluation responsibility must be carefully considered before updating can proceed.

B. <u>EXPERIMENTS ON OASIS</u> (J.M. Nitschke, P.A. Wilmarth, J. Gilat, and R.B. Firestone

Our on-going study of the decay properties of very neutron- deficient lanthanides continues to result in the identification of new isotopes. These isotopes are produced at the SuperHILAC's on-line isotope separator OASIS and decay studies are carried out in the new spectroscopy laboratory. The isotope of interest is passed through a slit in the focal plane of the mass separator and transported ionoptically to a cycling tape which is periodically positioned between an array of detectors. On an event by event basis, all possible decay modes are measured and the information written on computer tape for subsequent replay and analysis. Two general classes of decay are of interest: (1) direct or β-delayed particle emission along with any coincident γ rays, x-rays, or positrons, and (2) γ rays in coincidence with positrons or x-rays from electron capture and conversion processes. Most recently the isotopes $^{140,142}Tb$ and $^{142,144}Dy$ have been investigated.

This work was supported by the Director, Office of Energy Research, Division of Nuclear Physics of the Office of High Energy and Nuclear Physics of the U.S. Department of Energy under Contract DE-AC03-76SF00098.

A. NUCLEAR DATA APPLICATIONS - MEASUREMENTS

1. The Production of ^{38}Ar and ^{39}Ar by 14 MeV Neutrons on ^{39}K (Borg and Føland)

We have determined the cross sections for the production of ^{38}Ar and ^{39}Ar from the (n,n'p) and (n,p) reactions by neutrons of approximately 14 MeV incident on ^{39}K. Three potassium-bearing specimens were irradited with $\sim 10^{17}$ neutrons produced by the RTNS-II at the Lawrence Livermore National Laboratory, and the Ar isotopes were measured by mass spectrometry.

The values from the three measurements given in Table A-1 are consistent with one another and indicate an increase in the cross sections for both reactions as the neutron energy increases from approximately 14.5 to 14.8 MeV.

Table A-1. Summary of the measured cross sections for the three experiments.

E_n (average) (Mev)	Total Φ	Expt.	$\sigma_{n,p}$ (mb)	$\sigma_{n,n'p}$ (mb)	$\frac{\sigma_{n,n'p}}{\sigma_{n,p}}$
14.48	8.53×10^{16}	KI	114	434	3.81
14.58	1.40×10^{17}	KBr	125	500	4.02
14.82	6.01×10^{16}	K-feldspar	145	606	4.18

There have been two previous experimental measurements[1,2] of these cross sections in this energy range, and our values are in considerable disagreement with these earlier measurements. Values given by Borman[1] for $^{39}K(n,p)^{39}Ar$, $\sigma(n,p) = 354 \pm 54$ mb and for $^{39}K(n,n'p)^{38}Ar$, $\sigma(n,n'p) = 186 \pm 28$ mb. Aleksandrov[2] reports $\sigma(n,p) = 400 \pm 100$ mb

[1] V. M. Borman, H. Jeremie, G. Andersson-Lindstrom, H. Neuert, H. Pollehn, Z. Naturforsh 15A, 199 (1960).

[2] D. V. Aleksandrov, L. I. Klochkova and B. S. Kovrigin, Atmnya. Enrgya. 39, 137 (1975).

and states that the cross section is decreasing with energy in the range $E_n > 14.1$ MeV, contrary to our observation. Borman determined the total emission of charged particles (α, p and d), subtracted the alpha component from the combined spectra, and calculated the relative contribution of the two reactions using classical statistical theory. A likely source of error is in the deconvolution procedures applied to the combined proton spectrum. Support for this supposition is found from the agreement of their combined values of $\sigma[\sigma(n,p) + \sigma(n,n'p)]$, i.e., 540 mb compared to our combined value of 548 mb.

2. Proton and Deutron Excitation Functions of Natural Chromium (Lanier, West and Mustafa)

We bombarded natural chromium with protons of 5 to 27 MeV and with deuterons of 8 to 20 MeV to produce the reactions $^{52}Cr(p,n)^{52m,g}Mn$ and $^{52}Cr(d,2n)^{52m,g}Mn$. These studies[3] presented a special problem because the reaction produces ^{52}Mn in two forms: a 2^+ metastable state with a half-life of 21.01 ± 0.04 min and the 5.96-d 6^+ ground state. Both states decay directly to ^{52}Cr. Their individual production cross sections are determined by measuring gamma-rays and taking into account the differences in the population of the ^{52}Cr levels by the two modes of decay.

We made both short (1- to 2-min) and long (20- to 30-min) irradiations to enhance the population of the metastable and ground states for their respective periods of gamma-ray counting. The results are shown in Fig. A-1.

In Fig. A-2 we compare the isomer ratios determined for both protons and deuterons. Note that for the (p,n) channel, the 2^+ metastable state is most readily populated even at high energies. Near threshold, almost all of the reaction goes through the metastable channel. For deuterons, however, we find that both states are more or less equally populated except near threshold, where the reaction preferentially forms the 6^+ ground state. We speculate that the relatively identical populations of the 2^+ and 6^+ states in ^{52}Mn are caused by complications introduced by competition of a breakup fusion mechanism with the normal compound-nucleus reaction channel.

---

[3] R. G. Lanier, H. I. West, Jr., and M. G. Mustafa, Lawrence Livermore National Laboratory, UCAR-10062/85-1 (1985).

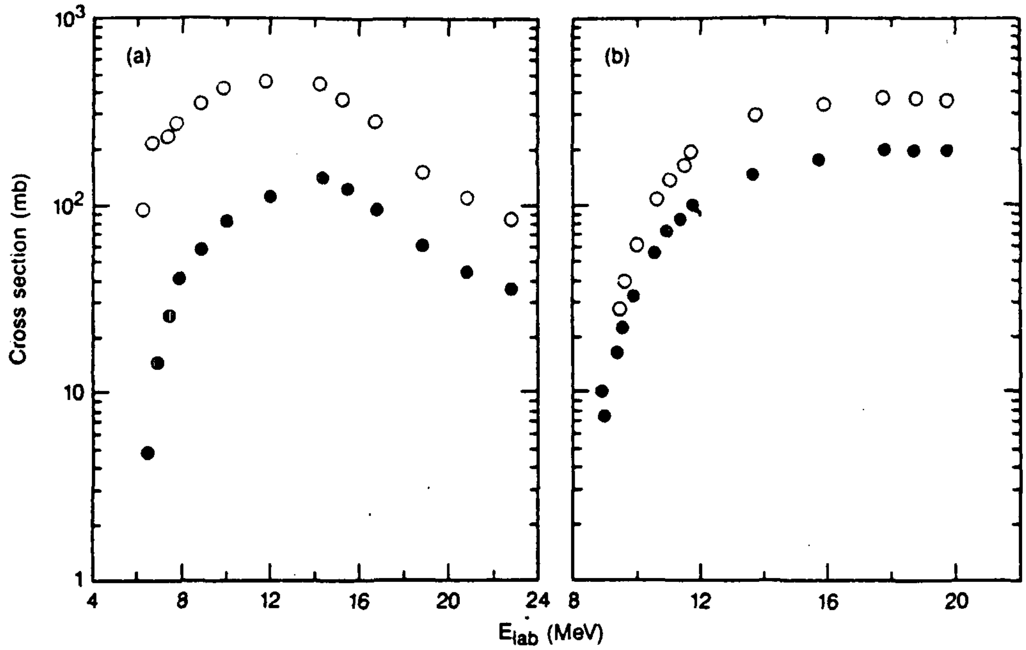

Cross section for $^{52}Cr(p,n)^{52}Mn$

Cross section for $^{52}Cr(d,2n)^{52}Mn$

Fig. A-1. Cross sections derived from measurements of natural chromium. The open data points show the total cross section including the metastable and ground states. The solid data points for the ground state only.

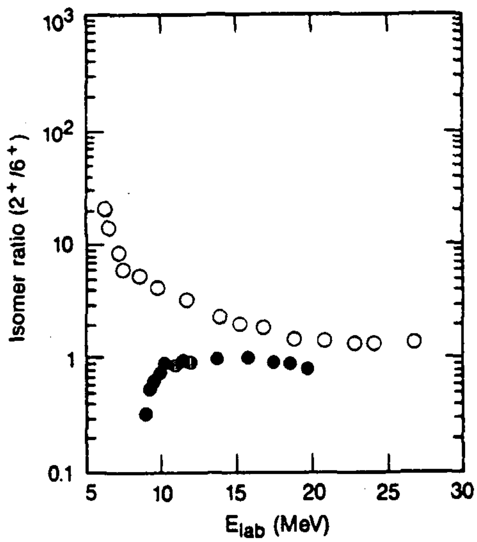

Fig. A-2. Isomer ratios in ^{52}Mn determined experimentally for the reactions $^{52}Cr(p,n)^{52}Mn$ (open data points) and $^{52}Cr(d,2n)^{52}Mn$ (solid data points).

3. Neutron Capture Cross Sections for ^{86,87}Sr at Stellar Temperatures
(Bauer, Mathews, Becker and Howe)

The neutron capture cross sections for ^{86,87}Sr have been measured from 100 eV to 1 MeV by the neutron-time-of-flight technique at the Livermore electron linear accelerator. The capture events were recorded by detecting the prompt gamma-ray cascade with two C_6D_6 scintillators, and were normalized to standard gold cross sections.[4] The Maxwellian-averaged neutron capture cross sections have been calculated for stellar temperatures ranging from kT = 10 to 100 keV. Capture rates for representative temperatures are given in Table A-2.

Combining our results with those reported previously,[5-7] we recommend a Maxwellian-averaged capture cross section at kT = 30 keV of 74 ± 3 mb for ^{86}Sr, and 102 ± 4 mb for ^{87}Sr. The capture cross sections of these two pure shielded s-process nuclei are of importance for stellar nucleosynthesis of nuclei in the mass region near the N = 50 closed shell. Specifically, they are important in the study of the s-process branching through ^{85}Kr as a monitor of the neutron capture time scale, and also in the investigation of the ^{87}Rb-^{87}Sr chronometric pair as an independent measure of the age of the galaxy.

Table A-2. Maxwellian-averaged capture cross sections of the measured isotopes as a function of the thermal energy kT.

Measured isotope	Calculated Maxwellian-averaged capture cross section (mb) at 10 keV	30 keV	100 keV
^{86}Sr	130 ± 6	74 ± 4	40 ± 2
^{87}Sr	198 ± 8	102 ± 5	43 ± 3

[4] P. G. Young and E. D. Arthur, Proc. International Symposium on Capture Gamma-Ray Spectroscopy and Related Topics, Knoxville, TN, AIP Conf. Proc. 125, 530 (1985).
[5] G. Walter and H. Beer, Astron. Astrophys. 142, 268 (1985).
[6] G. C. Hicks, B. J. Allen, A. R. de L. Musgrove and R. L. Macklin, Austral. J. Phys. 35, 267 (1982).
[7] R. L. Macklin and J. H. Gibbons, Rev. Mod. Phys. 37, 166 (1965).

4. Test for the Admixture of Intruder Configurations in the Ground States of Even-Mass Cadmium Nuclei

(Bauer, Becker, Proctor, Decman, Lanier and Cizewski)

The stable even-mass nuclei of cadmium are considered to be good examples of quadrupole vibrational nuclei. However, their level schemes show significant deviations from a simplified description. Extra 0^+ and 2^+ states have been found to occur in cadmium nuclei at the same excitation energy as the two-phonon triplet.[8,9] These additional states are believed to be examples of shape coexistence, which also has been observed in neighboring even-even nuclei near the proton shell closure of Z = 50 and near N = 66 (half-filled neutron shell between N = 50 and 82); they are thought of as particle-hole states resulting from the excitation of a pair of protons across the Z = 50 closed shell.

To further probe the structure of the even-mass nuclei of cadmium, we investigated the (p,t) reaction on $^{106,108,110,112,114,116}Cd$ using the 26-MeV proton beam from the Livermore cyclograaff accelerator and the split-pole spectrograph. Differential cross sections have been measured in the angular range θ_{lab} = 15°-60. The angular distributions have been compared with DWBA calculations. Using one set of optical parameters[8,9] for all six isotopes under investigation, excellent agreement was achieved between calculations and experimental data. Enhancement factors for ground-state to ground-state transitions have been extracted and compared with the predictions for the two-nucleon transfer intensity based on calculations by Arima and Iachello using the SU(6) boson model.[10] If there existed appreciable mixing of the intruder configuration in the ground state, expected especially in ^{112}Cd and ^{114}Cd (where the intruder states are found to be as low as 1.3 MeV above the ground state), significant deviation of the experimentally determined enhancement factors from the calculated two-nucleon transfer strengths is anticipated. No such deviation has been observed within the limits of this experiment.

Thus, though strong mixing of the intruder states in even-mass cadmium nuclei with excited states has been observed, no evidence for an admixture of the intruder states with the ground states has been found in this experiment, not even for the favored cases of ^{112}Cd and ^{114}Cd. Our investigations of the intruder particle-hole configurations near N = 66 is continuing.

---

8 F. G. Perey, Phys. Rev. 131, 745 (1963).
9 E. R. Flynn, D. D. Armstrong, J. G. Berry and A. G. Blair, Phys. Rev. 182, 1113 (1969).
10 A. Arima and F. Iachello, Phys. Rev. C 16, 2085 (1977).

5. Gamma-Ray Emission Spectra from Materials Bombarded with 14 MeV Neutrons
(Goldberg, Hansen and Pohl)

Integral measurements of the gamma emission spectra from materials pulsed with 14 MeV neutrons have been carried out at the ICT Facility for a large number of materials between C and Pb. The gamma spectra have been measured in the 1- to 8-MeV interval using NE213 detectors. The measured spectra show a non-negligible presence of high energy gammas, $E > 3$ MeV.

These measurements would test the accuracy of the gamma cross sections and of the models describing the propagation of neutron-generated gamma-rays through thick assemblies (1 to 3 free paths). Analysis of the data is in progress.

6. Band Structure in ^{81}Y and Its Radioactive Decay
(Becker, Lister, Moscropt, Varley, Price, Warburton and Olness)

Bands of states in ^{81}Y have been identified by using a particle-gamma coincidence technique following the ^{58}Ni(^{28}Si, αp)^{81}Y reaction at beam energies of 80-130 MeV. A probable sequence of spins for the states is presented, and these data are compared with systematic trends in this region. The data indicate that the nucleus has a large prolate deformation. The radioactive decay of ^{81}Y to ^{81}Sr was reinvestigated by interrupting the beam and observing the population of states in ^{81}Sr.

7. Identification of the Yrast Decay Scheme of ^{86}Y
(Becker, Bloom, Lister, Olness and Warburton)

A particle-gamma coincidence experiment following the ^{62}Ni(^{27}Al,xnypz$\alpha\gamma$) fusion-evaporation reaction was performed to decide between two alternative proposals for the ^{86}Y yrast decay scheme. The results verify the scheme found via the ^{76}Ge+^{14}N and ^{73}Ge+^{16}O reactions. It is suggested that the decay scheme seen in ^{85}Rb+α is actually associated with another three-nucleon emission channel. The ^{86}Y decay scheme is compared to a large basis shell model calculation.

8. High-Spin States of ^{86}Zr
(Warburton, Lister, Olness, Haustein, Saha, Alburger, Becker, Dewberry and Naumann)

The level scheme of ^{86}Zr was studied by in-beam measurements on γ transitions in the ^{60}Ni(^{29}Si,2pnγ)^{86}Zr reaction and by helium-jet studies of delayed γ-ray activity from the ^{58}Ni(^{32}S,3pn)^{86}Nb(β^+/EC)^{86}Zr reaction. In the latter study, measurements consisted of γ-γ and β-γ coincidences, excitation functions and a lifetime determination. A ^{86}Nb decay scheme was obtained which suggests $J^{\pi} = 5^{+}$ for the ^{86}Nb ground state. The in-beam study consisted of γ-γ coincidences, excitation functions, angular distributions and lifetime measurements via both Doppler shift attenuation and recoil distance methods. The high-spin decay scheme and level lifetimes obtained from the in-beam studies suggest intrinsic modes of excitation rather than the collective behavior seen in ^{84}Zr.

9. <u>Electromagnetic Transitions in ^{205}Hg</u>
   (Becker, Decman, Henry, Mann, Struble, Maier, Stöffl, Sheline)

Gamma-ray transitions in ^{205}Hg have been observed in the ^{204}Hg(t,d)^{205}Hg reaction. A partial level scheme is obtained. Delayed gamma-rays exhibiting $\tau_m = (1.59 \pm 0.06) \times 10^{-3}$s are observed; the identification with the decay of the $i_{13/2}$ neutron hole state is suggested.

10. <u>Yrast Decays in ^{87,89}Zr, ^{87,88,89,90}Y and ^{86}Sr from ^{74,76}Ge(^{18}O,xn,yp,z$\alpha\gamma$) Reactions</u>

    (Becker, Bloom, Warburton, Olness and Lister)

Gamma-ray data from ^{74,76}Ge + ^{18}O fusion-evaporation reactions have been analyzed to provide data on yrast decay schemes in ^{87,89}Zr, ^{87,88,89,90}Y, and ^{86}Sr. The data include excitation functions, angular distributions, γ-γ coincidences, linear polarization measurements and lifetimes from both Doppler shift attenuation and recoil distance measurements. Shell-model calculations are presented for ^{88,90}Y and ^{86}Sr.

11. <u>The Transport of 14-MeV Neutrons Through Heavy Materials $150 < A < 208$</u>
    (Hansen, Blann, Howerton, Komoto and Pohl)

The emission spectra from ^{165}Ho (0.8 mean free path, mfp), ^{181}Ta (1 and 3 mfp), ^{197}Au (1.9 mfp) and Pb (1.0 mfp) have been measured using the sphere transmission and time-of-flight (TOF) techniques. The 14-MeV incident neutrons are from the Livermore Insulated-Core-Transformer (ICT) accelerator using the ^{3}H(d,n)^{4}He reaction. These materials were chosen to span a wide range of heavy nuclei, including deformed (Ho and Ta), spherical (Au) and closed shell (Pb) nuclei. The neutron emission spectra have been measured in the energy interval of 1 to 5 MeV and the results compared with Monte Carlo calculations performed using the neutron-photon transport code TART and evaluated neutron cross sections files. An alternative representation of the secondary neutron spectra has been carried out by using model calculations for precompound processes and collective effects in the calculations of the pulsed sphere emission spectra. Their importance in the quality of the agreement between measurements and calculations is discussed in a paper written for publication in Nucl. Sci. & Eng. The measurements have been compared with the predictions of two evaluated neutron libraries, the ENDF/B-V and ENDL. In addition, calculations have been carried out using neutron cross sections calculated directly from well accepted nuclear models by the code ALICE/LIVERMORE 82 and by ECIS 79. The quality of the agreements between the measurements and calculations obtained with the latter cross sections and those from the ENDL library are reasonably good for all the targets, and these are systematically better than the results obtained with the ENDF/B-V files. Discrepancies between measurements and calculations as large as 80% are found using the ENDF/B-V files for the emission of neutrons from gold in the 5- to 10-MeV energy range.

In Fig. A-3 are shown the results obtained for the 1 mfp Ta sphere and in Table A-3 are tabulated the ratios of the calculated-to-measured integrals for three energy intervals in the 1- to 15-MeV range.

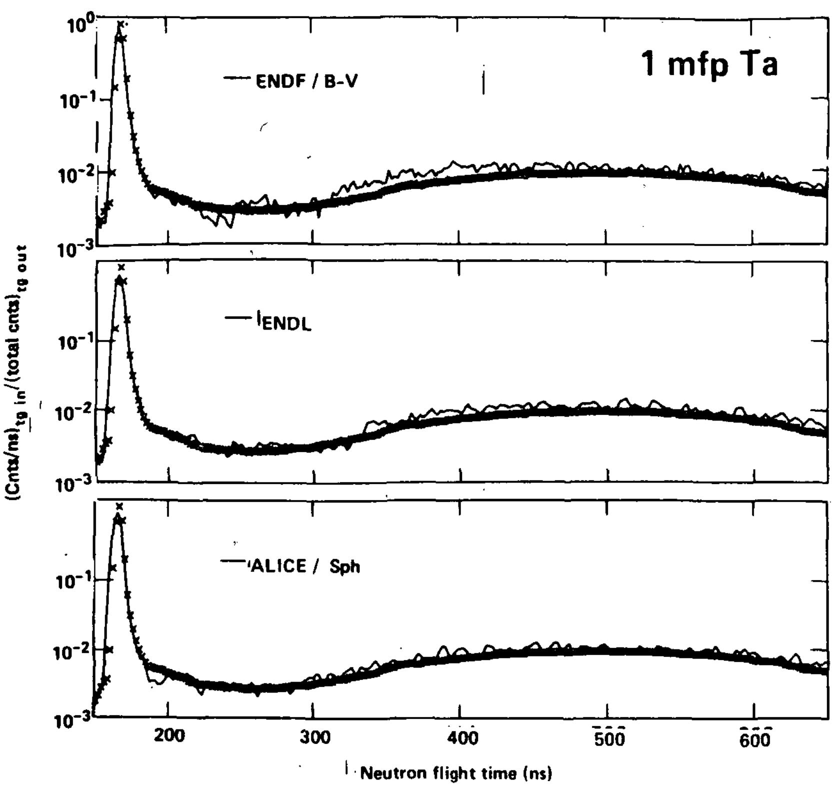

Fig. A-3. Comparison of measured (xxx) and calculated (——) neutron TOF spectra for 1.0-mfp ^{181}Ta. The calculations have been carried out with the ENDF/B-V (upper curve), ENDL (middle curve) and ALICE/Sph (bottom curve) libraries.

Table A-3. Measured Integrals for 1.0- and 3.0-mfp Tantalum and Ratios of Calculated-to-Measured Integrals.*

Mean-Free-Paths	ΔE (MeV)	Experiment* ±5%	R(ENDF/B-V)	R(ENDL)	$R(\text{ALICE})_{Sph}$	$R(\text{ALICE})_{CCh}$
1	1 to 5	0.256	1.281	1.230	1.152	1.148
	5 to 10	0.024	0.975	1.107	1.045	0.984
	10 to 15	0.618	1.047	1.024	1.071	1.083
	1 to 15	0.898	1.115	1.088	1.096	1.102
3	1 to 5	0.316	1.259	1.266	1.196	1.209
	5 to 10	0.027	0.970	1.118	0.908	0.930
	10 to 15	0.278	0.860	0.813	0.950	0.971
	1 to 15	0.621	1.068	1.056	1.074	1.090

*Integrals measured in units of neutron counts (sphere in) divided by the total number of 14-MeV source counts (sphere out).

12. Excitation Functions for $^{89}Y(p,n)$ (O'Brien, West and Lanier)

We have measured cross sections for the $^{89}Y(p,n)$ reaction by using a stacked-foil activation technique. Preliminary results for proton energies in the range of 6-2 MeV are shown in Fig. A-4. The data analysis is continuing and additional measurements are planned.

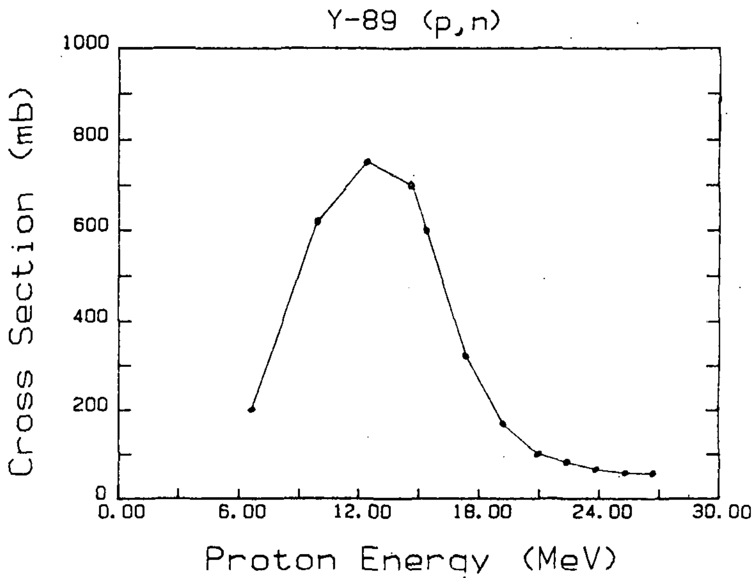

Fig. A-4. Excitation function for the $^{89}Y(p,n)$ reaction. The data points are connected by lines to indicate the trend.

B. NUCLEAR DATA APPLICATIONS - CALCULATIONS

1. An Application of Gamma-Ray Dipole Strength Function Systematics (Gardner, Gardner and Hoff)

As an aid in interpreting primary capture gamma-ray spectra, we have calculated the primary dipole transitions following 2-keV neutron capture by ^{175}Lu to all of the modeled ^{176}Lu discrete levels. A total of 291 discrete energy levels were used between 0 and 1.5 MeV. Figure B-1 presents results for transitions with energies in the range of 0.4 to 0.83 MeV. The positions of the levels accessible with dipole transitions and their spins and parities are indicated. The spectrum was constructed by smearing the calculated transition intensities with a unit gaussian line shape having a resolution of 6 keV.

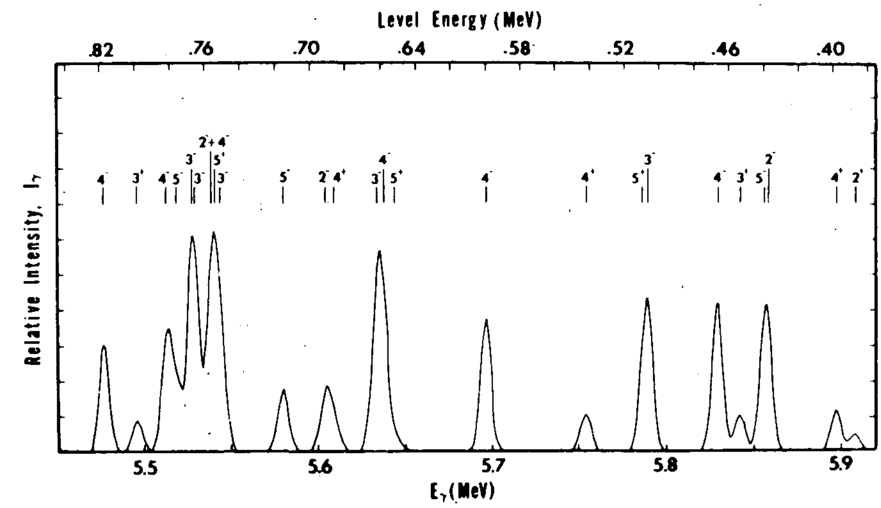

Fig. B-1. A portion of the calculated ^{175}Lu(n,capture) primary gamma-ray spectrum.

Some interesting features of the plot are: 1) for gamma-rays from 5.5 to 5.9 MeV, we see 5 doublets, 1 triplet and 1 quadruplet, all unresolved; 2) the $2^- + 5^-$ doublet just below 0.44 MeV excitation appears to have the same shape and intensity as the singlet 4^- peak at 0.466 MeV, while the triplet, quadruplet and doublet peaks at 0.66, 0.75 and 0.77 MeV, respectively, also show a close resemblance in shape and intensity; and 3) the true singlet E1 peaks, due to transitions to 4^- levels at 0.82, 0.60 and 0.47 MeV, show a pronounced increase in intensity, because of the energy dependence of the E1 strength function itself, in addition to the expected E_γ^3 energy dependence. Such a plot should be quite useful when analyzing experimental data in helping to avoid overlooking levels or misinterpreting their intensities.

2. Absolute Gamma-Ray Strength Function Studies (Gardner, Gardner and Hoff)

We are continuing our studies of absolute gamma-ray strength functions. Previously, we had reported on the deduction of absolute dipole strength-function information for ^{176}Lu using a set of 291 modeled discrete levels and various neutron capture measurements; this led to the modification of our original systematics for E1 and M1 strengths.[1] When we now apply these updated systematics to calculate E1 strength functions in the mass-90 region, we obtain excellent agreement with experiment[2] for ^{89}Y and ^{90}Zr, as shown in Fig. B-2. Our original E1 systematics had predicted strength functions that were about 30% higher.

We have also investigated the importance to modeling of the isoscalar E2 strength in the continuum of ^{176}Lu. From information on the isoscalar giant quadrupole resonance,[3] we chose the peak energy as $E_{RE1} = 63A^{-1/3}$ and the peak width as $\Gamma_{RE2} = 18.9A^{-1/3}$. A formula for the peak cross section, $\sigma_{0E2} = 2.65 \times 10^{-2}(Z^2/A^{2/3})$ mb, was obtained by deriving an E2 sum rule from a prescription of Hayward[4] that related the magnitude of the E2 isoscalar quadrupole strength to the E1 dipole strength. Using these parameters, we calculated the E2 strength function with both a Lorentzian and an energy-dependent Breit-Wigner (EDBW) line shape. The results are shown in Fig. B-3, along with the newly deduced E1 and M1 strength functions. The upper bound of the band results from the Lorentz line shape; the lower bound from that of the EDBW model. In each case, the E2 strength was multiplied by E_γ^2 to provide an equal basis of comparison with the dipole strengths. Over most of the energy range the E2 strength function is about two orders of magnitude lower than the dipole strengths.

---

[1] D. G. Gardner, M. Gardner and R. W. Hoff, Proc. Conf. on Capture Gamma-Ray Spectroscopy and Related Topics, Knoxville, TN, AIP Conf. Proc. 125, 513 (1985).
[2] P. Axel et al., Phys. Rev. C2, 689,(1970); G. Szeflinska et al., Nucl. Phys. A323, 253 (1979).
[3] F. Bertrand, Ann. Rev. Nucl. Sci. 26, 457 (1976).
[4] E. Hayward, Photonuclear Reactions I, 340 (1977).

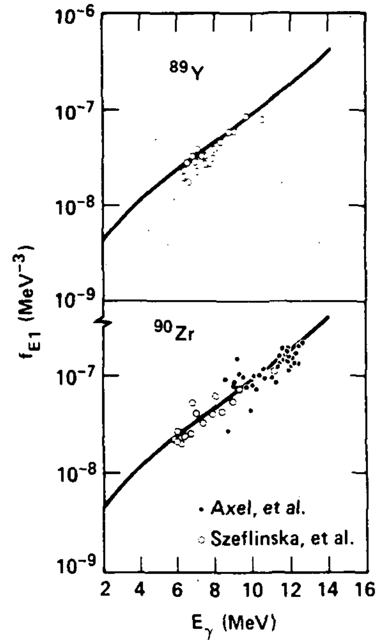

Fig. B-2. Calculated and experimental E1 strength functions for ^{89}Y and ^{90}ZR.

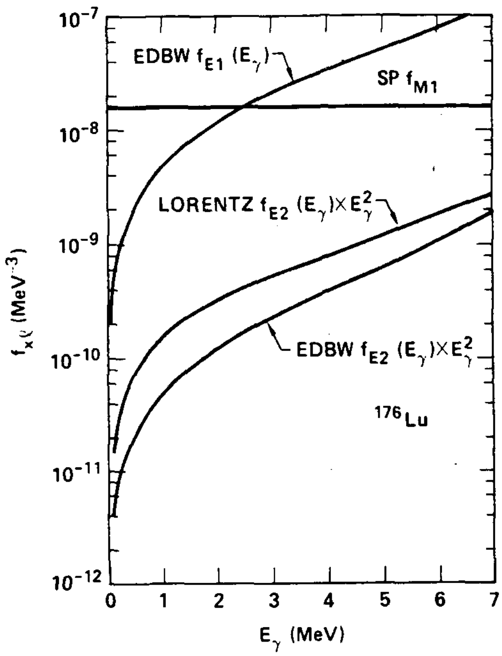

Fig. B-3. Absolute E1, M1 and E2.

3. Production and Destruction of Nuclear Isomers by Photons (Gardner, Gardner and Hoff)

We are modifying one of our nuclear reaction codes to permit photons to be used as incident "particles". We wish to study the photon-induced production and destruction of isomers of various nuclides. Using absolute E1, M1 and E1 gamma-ray strength functions and modeled discrete levels, we have made preliminary calculations for the nuclei ^{176}Lu, ^{235}U and ^{237}Np. In the case of ^{176}Lu, as shown in Fig. B-4, we have confirmed that our absolute E1 strength function

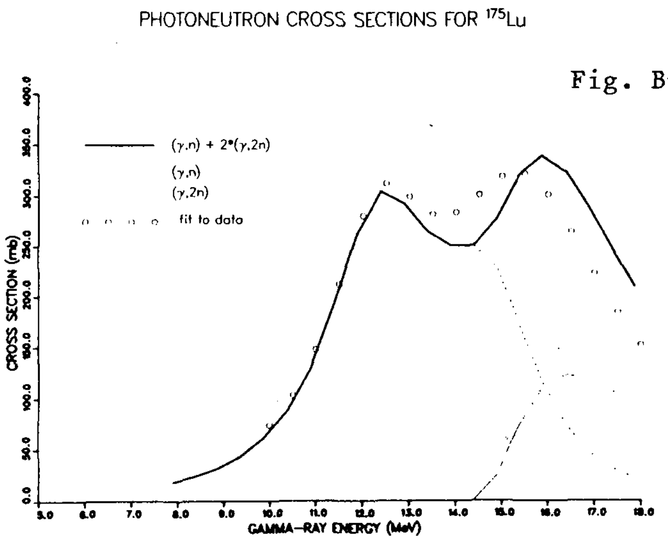

Fig. B-4. Calculated photoneutron cross sections for ^{175}Lu compared with a fit to the data.[5]

reproduces quite well the experimental photoneutron measurements for incident photon energies up to 18 MeV.[5] For photon energies below the neutron separation energy, we find that the production of the isomer from the ground state is significantly more efficient than the reverse process, and relatively insensitive to the incident photon energy. See Fig. B-5. In addition, the photon absorption cross section around 1 MeV appears to be much larger than the laboratory measurements with ^{60}Co

[5] R. Bergere, H. Beil, P. Carlos and A. Veyssceri, Nucl. Phys. A133, 417 (1969).

sources have indicated.[6] With ^{235}U and ^{237}Np, we have used photons only up to 4 MeV in energy. We will make calculations at higher energies when a suitable fission model is working properly in our code.

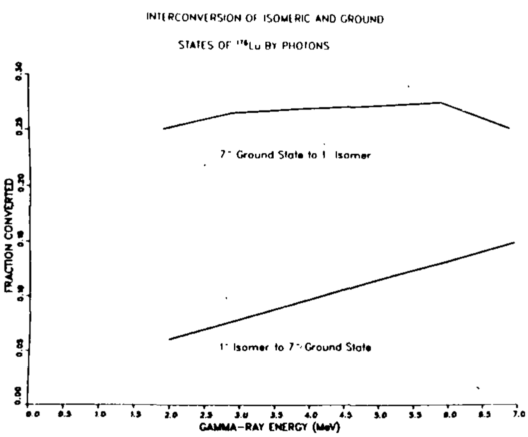

Fig. B-5. Calculated interconversion of the isomeric and ground states of ^{176}Lu by photons.

4. Production of ^{145} Pm from Sm
(Gardner and Gardner)

One method for producing the isotope ^{145}Pm is by producing its short-lived (340 d) β-decay precursor, ^{145}Sm, through the ^{144}Sm (n,γ) reaction. We have estimated the neutron capture cross sections for ^{144}Sm, ^{145}Sm and ^{145}Pm. For production in a nuclear reactor, we conclude that thermal neutrons should be avoided, and that a more desirable neutron energy spectrum should approximate a pure fission spectrum. Even under these conditions, however, the cross section for the production of ^{145}Pm (via ^{144}Sm [n,γ]) is considerably less than those for either of the two possible destruction modes (^{145}Sm and ^{145}Pm [n,γ]).

5. Characterization of Isomers in the Nucleus ^{158}Ho
(Sood, Hoff and Sheline)

We made configuration assignments to the experimentally known isomers in the low-energy spectrum of the N = 91 odd-odd nucleus ^{158}Ho. These characterizations were based on model predictions of two-quasiparticle bandhead energies which used experimental data from neighboring odd-A nuclei and included the n-p interaction contribution.

---

[6] E. Norman and S. Kellogg, Proc. Conf. on Capture Gamma-Ray Spectroscopy and Related Topics, Knoxville, KY, AIP Conf. Proc. 125, 753 (1985).

A 21-m isomer is assigned the configuration $K^{\pi} = 9^{+}$ $\{7/2^{-}[523]_{p} + 11/2^{-}[505]_{n}\}$ and is predicted to lie at 180 keV above the 5^{+} ground state. The antiparallel $K^{\pi} = 2^{+}$ state of this configuration is assigned to an observed level at 316 keV. The 21-m isomer decays by an allowed unhindered transition to a 2528-keV level in ^{158}Dy. For the latter, we assign the two-quasineutron configuration $K^{\pi} = 8^{+}$ $\{5/2^{-}[523]_{n} + 11/2^{-}[505]\}$. A 27-m, 2^{-} isomer at 67.3 keV and a 29-ns, 5^{-} isomer at 156.9 keV are identified with the configuration $\{7/2^{+}[404]_{p} \pm 3/2^{-}[521_{n}])$. A 1.85-ns 1^{-} isomer at 139.2 keV is assigned the configuration $\{5/2^{+}[402]_{p} + 3/2^{-}[521]_{n}\}$ and the $K^{\pi} = 4^{-}$ member of this Gallagher-Moszkowski pair is predicted to occur at 70 keV.

Figure B-6 presents a summary of our results. The calculated two-particle bandheads for the ^{158}Ho are shown in comparison with the available experimental information for isomers and related levels in this nucleus. The labels denote experimental excitation energies (in keV) and configuration assignments $\Omega^{\Pi}[Nn_{z}\Lambda\Sigma]$ deduced for each state. For the calculated bandheads we use the following abbreviated notation. For protrons: A = $7/2^{-}[523\uparrow]$; B = $5/2^{+}[402\uparrow]$; C = $7/2^{+}[404\downarrow]$, and for neutrons: Z = $3/2^{-}[521\uparrow]$; Y = $11/2^{-}[505\uparrow]$; X = $3/2^{+}[402\downarrow]$ and W = $3/2^{+}[651\uparrow]$. The $K^{\pi} = 9^{+}$ and 4^{-} levels are indicated as dashed lines in the experimental scheme at their respective predicted energies.

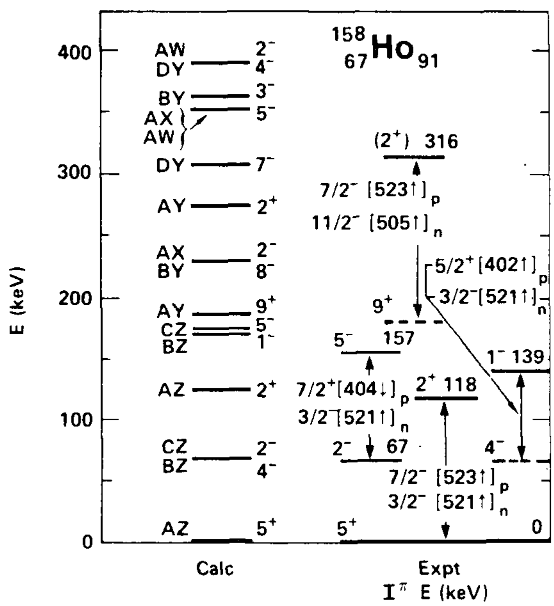

Fig. B-6. Comparison of calculated and experimental two-particle bandhead energies for ^{158}Ho.

6. Predictive Limits of the Statistical Theory of Charged-Particle Reactions in the A = 50 Region[7]

Mustafa, Lanier, West and Meyer

We used accurate measurements of proton and deuteron excitation functions (Fig. B-7) of natural titanium and chromium and the isomer ratio ($2^+/6^+$) in ^{52}Mn to test the predictive limits of the statistical

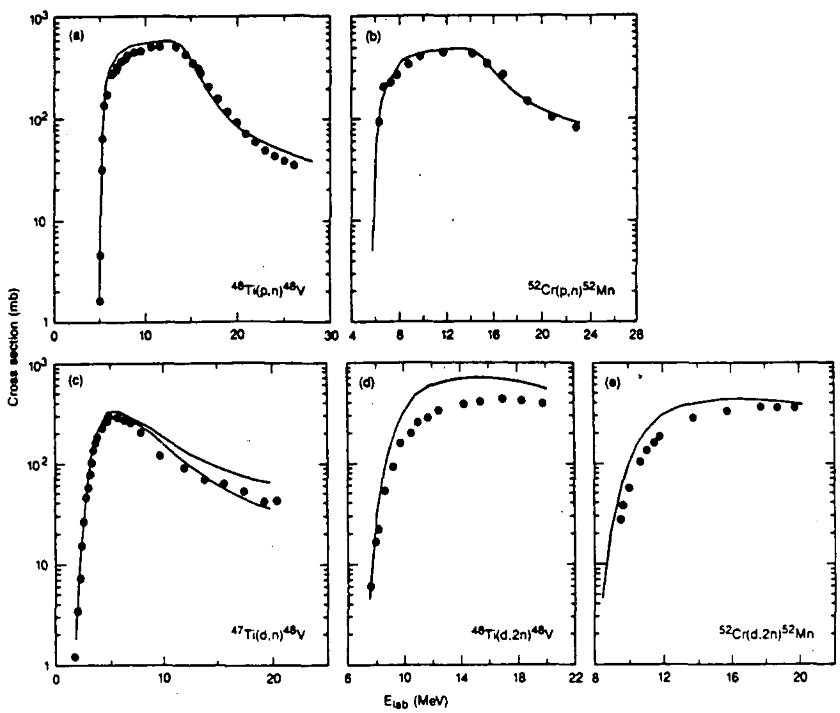

Fig. B-7. Cross sections for (a) ^{48}Ti(p,n)^{48}V, (b) ^{52}Cr(p,n)$^{52m+g}$Cr, (c) ^{47}Ti(d,n)^{48}V, (d) ^{48}Ti(d,2n)^{48}V and (e) ^{52}Cr(d,2n)$^{52m+g}$Mn. The points show the experimental data, and the solid curve shows the results of calculation. In (c), the two curves show the effect of different assumptions about pre-equilibrium initial conditions.

---

[7] M. G. Mustafa, R. G. Lanier, H. I. West and R. A. Meyer, Lawrence Livermore National Laboratory, UCAR-10062/85-1 (1985).

theory of nuclear reactions. We find good agreement between calculation[8] and experiment for proton data; however, the deuteron data differ significantly from statistical model calculations. Our results for the excitation functions are compared in Fig. B-7, and those for the isomer ratio in Fig. B-8.

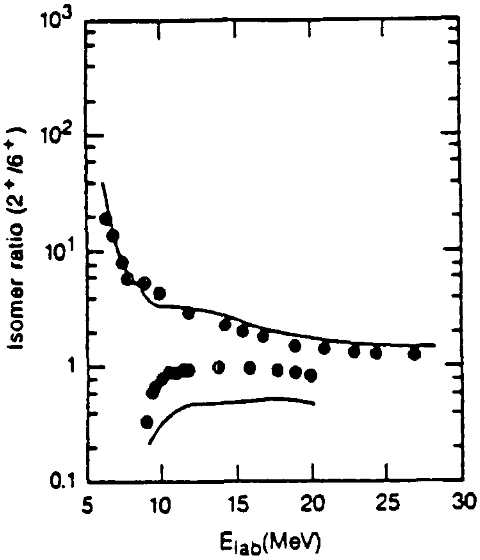

Fig. B-8. Isomer ratio ($2^+/6^+$) in ^{52}Mn. The points are measurements, and the lines are calculations. The upper curve compares the isomer ratios for $^{52}Cr)p,n)^{52}Mn$, and the ratios for $^{52}Cr(d,2n)^{52}Mn$.

We speculate that the discrepancy in the deuteron data results primarily from competition with a semidirect reaction mechanism that involves deuteron break up and is not due to low-energy nuclear structure effects. Experiments and additional calculations are being done to resolve this problem.

7. Shell Model Calculations of $^{90,88}Zr$ and $^{90,88}Y$
(Becker, Bloom and Warburton)

Conventional spherical shell model calculations have been undertaken to describe $^{90,88}Zr$ and $^{90,88}Y$. In these large scale calculations valence orbitals included $1f_{5/2}, 2p_{3/2}, 2p_{1/2}$, and $1g_{9/2}$. The $d_{5/2}$ orbital was included for ^{90}Y and for high-spin calculations in ^{90}Zr. Restrictions were placed on orbital occupancy so that the basis

---

[8] B. Strohmaier and M. Uhl, STAPRE--A Computer Code for Particle Induced Activation Cross Sections and Related Quantities, Institut fur Radiumforschung und Kernphysik, Vienna, Austria, IRK 76/01 with 1976 Addenda (1976).

set amounted to less than 25,000 Slater determinants. Calculations were done with a local, state-independent, two-body interaction with a single Yukawa form factor. Predicted excitation energies and electromagnetic transition rates are compared with recent experimental results.

8. Calculated Excitation Functions for Reactions of Protons with $^{86,87,88}Sr$

(Gardner, Gardner and Henry)[9]

When a monoisotopic element such as ^{89}Y is present in a thermonuclear device, a wide range of Y isotopes is produced after ignition by various neutron-induced nuclear reactions. The understanding of this bulk production process requires a detailed knowledge of (n,γ), (n,n'), (n,2n), (n,p), etc., excitation functions which are associated with the cross sections for the interconversion or destruction of Y material. Many of these cross sections cannot be measured and calculation is the only viable alternate. Assessing the reliability and accuracy of such a cross section "set" remains an outstanding problem in understanding bulk nuclear production/destruction processes in high-flux, variable-energy radiation environments.

One estimate of the reliability of the Y cross section set, which is used in our laboratory, was obtained by calculating a variety of proton-induced reactions on stable isotopes of Sr. This calculation used the same parameter information which formed the basis for the Y set. The results were compared with recent experiments[10] for proton-induced reactions (3 to 17 MeV) on $^{86,87,88}Sr$ which used activation measurements to obtain cross section data for eleven product nuclides: ^{83g}Rb, $^{85m,g}Sr$, ^{87m}Sr, $^{85m,g}Y$, $^{86m,g}Y$, $^{87m,g}Y$ and ^{88}Y. All of the pertinent reactions were calculatd and the effect of isospin, as required with incident protons in this energy range, was included. The comparison with experimental data was quite satisfactory in almost every case, and indicated that no *ad hoc* adjustment of the parameters was required. As an example, Fig. B-9 compares the calculations with the data for the (p,n) and (p,2n) reactions on ^{88}Sr.

---

9 D. G. Gardner, M. A. Gardner and E. A. Henry, Lawrence Livermore National Laboratory, UCAR-10062/85-1 (1985).

10 R. J. Prestwood et al., Phys. Rev. C29, 805 (1984).

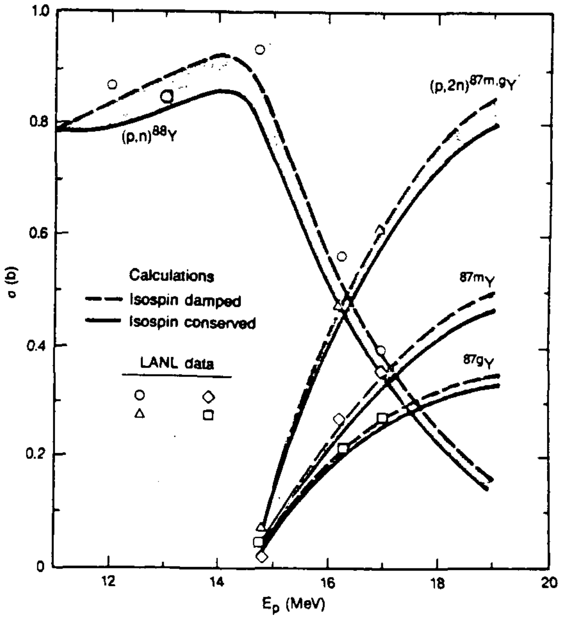

Fig. B-9. Comparison of the calculated and measured excitation functions for the (p,xn) reactions on ^{88}Sr.

The isomer ratios for the ^{88}Sr(p,n)^{88m,g}Y and (p,2n)^{87m,g}Y reactions differ considerably from those produced by the ^{88}Y(n,n')^{88m,g}Y and (n,2n)^{87m,g}Y reactions. This is primarily due to the different target-state spins (0^+ and 4^-). Figure B-10 shows the calculated isomer-ratio values compared with those measured.[10] The only serious discrepancies between our calculations and the data occur with the ^{86}Sr(p,n)^{86m,g}Y and ^{86}Sr(p,pn+np)^{85m,g}Y reactions. This discrepancy and its possible effect on the Y cross section set is being studied.

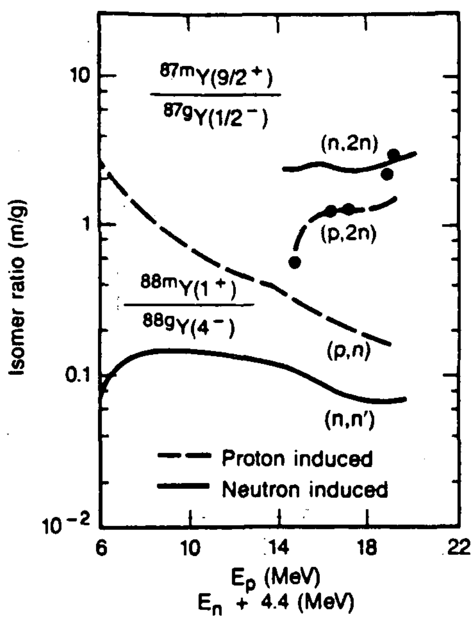

Fig. B-10. Calculated (curves) and measured (points) isomeri-ratio values for proton reactions on ^{88}Sr and neutron reactions on ^{88}Y.

9. A Shell-Model Study of ^{99}Tc Beta-Decay in Astrophysical Environments
(Takahashi, Mathews and Bloom)

Using the shell-model Lanczos method, we calculate the Gamow-Teller matrix elements for beta transitions of astrophysical interest from excited states of ^{99}Tc ($7/2^+$,141 keV; $5/2^+$,181 keV) to the ground and excited states of ^{99}Ru. The level schemes of low-lying positive-parity states in these nuclei and in the analogous isotonic nuclei ^{97}Nb - ^{97}Mo are reproduced fairly well within a model space consisting of low-seniority excitations in the 1g2d shell, which are mixed via the Kallio-Kolltveit effective interaction. The calculations lead to a ^{99}Tc half-life of $\sim$ 20 yr at a stellar temperaure of 3×10^8 K typical for an s-process with a $^{22}Ne(\alpha,n)^{25}Mg$ neutron source. Referring to recent studies of thermal-pulse s-process models, we stress that a substantial amount of ^{99}Tc can survive the s-process in spite of its enormously enhanced decay rate. The factual observation of ^{99}Tc at the surface of certain stars, therefore, does not necessarily contradict the s-process scenario with a ^{22}Ne neutron source.

C. NUCLEAR DATA APPLICATIONS - EVALUATIONS

1. Upgrade of the LLNL Evaluated Charged-Particle Library (ECPL)
(Howerton, MacGregor and Perkins)

The LLNL Evaluated Charged-Particle Library (ECPL) had its beginnings in the early sixties and has existed in its present format since 1974, with occasional extensions of the format to accommodate new reaction properties when the necessity for such extension became clear. During the past year, changes have been made in the data for 11 reactions, and new complete evaluations have been entered for 14 reactions. The current version of ECPL contains complete data for 157 reactions induced by the 5 charged-particles: ^1H, ^2H, ^3He and ^4He. The targets include, in addition to these particles interacting with themselves and each other, ^6Li, ^7Li, ^7Be, ^9Be, ^{10}B, ^{11}B, ^{12}C, ^{14}N and ^{16}O. A sample page of the computer-produced index to the contents of ECPL is shown in Fig. C-1. This will serve to illustrate the reaction properties that are included in the file.

During the coming year, we intend to continue "fleshing-out" the library with the ultimate objective of having complete evaluated data for the 5 incident particles and 14 targets listed above for all reactions of potential interest.

For the past few years, we have had a modest collaborative effort with Leona Stewart and Robert MacFarlane of LANL in the collection of the experimental data that form the basis for these evaluations and in the design and implementation of a storage and retrieval system for the experimental data. We anticipate that this effort will continue.

02/20/86

3-LI-6
ATOMIC MASS = 6.0151E+00
GROUND STATE
STABLE

REACTION	YO	PROPERTY	ENTRIES	DATE	Q-VALUE	E-MIN	E-MAX	QUALIFIER
P,HE3								
	HE3	ENERGY FROM THER. REACT.	11	81/07/18	4.0200E+00	1.0000E-04	1.0000E+00	
	HE3	MAXW.AV.TOT.AV.E OF PART	11	81/07/18	4.0200E+00	1.0000E-04	1.0000E+00	
	A(R)	ANGULAR DIST.	2	81/04/21	4.0200E+00	1.0000E-03	2.0000E+01	
	A(R)	ENERGY DEP. TO YO	2	83/04/05	4.0200E+00	1.0000E-03	2.0000E+01	
	A(R)	ENERGY FROM THER. REACT.	11	81/07/18	4.0200E+00	1.0000E-04	1.0000E+00	
	A(R)	MAXW.AV.TOT.AV.E OF PART	11	81/07/18	4.0200E+00	1.0000E-04	1.0000E+00	
D,A								
		CROSS-SECTION	91	74/09/10	2.2374E+01	1.0000E-03	2.0000E+01	
		MAXW. AV. REACT. RATES	171	78/03/02	2.2374E+01	3.2000E-04	1.0000E+00	
		IN-FLT REACT. X-SECS	20	74/09/10	2.2374E+01	0.	1.0000E+00	
		MAXW.AV.TOT.AV.ENERGY	22	82/05/15	2.2374E+01	2.6000E-04	1.0000E+00	
	A	ANGULAR DIST.	2	81/04/21	2.2374E+01	1.0000E-03	2.0000E+01	
	A	ENERGY DEP. TO YO	2	85/09/11	2.2374E+01	1.0000E-03	2.0000E+01	
	A	ENERGY FROM THER. REACT.	11	81/07/18	2.2374E+01	1.0000E-04	1.0000E+00	
	A	MAXW.AV.TOT.AV.E OF PART	11	81/07/18	2.2374E+01	1.0000E-04	1.0000E+00	
	A(R)	ANGULAR DIST.	2	81/04/21	2.2374E+01	1.0000E-03	2.0000E+01	
	A(R)	ENERGY DEP. TO YO	2	85/09/11	2.2374E+01	1.0000E-03	2.0000E+01	
	A(R)	ENERGY FROM THER. REACT.	11	81/07/18	2.2374E+01	1.0000E-04	1.0000E+00	
	A(R)	MAXW.AV.TOT.AV.E OF PART	11	81/07/18	2.2374E+01	1.0000E-04	1.0000E+00	
A,DA								
		CROSS-SECTION	6	85/04/16	-1.4730E+00	2.6100E+00	2.0000E+01	LEVEL = 0. MEV
		MAXW. AV. REACT. RATES	86	85/04/16	-1.4730E+00	2.0020E-02	1.0000E+00	LEVEL = 0. MEV
		IN-FLT REACT. X-SECS	20	85/04/16	-1.4730E+00	0.	1.0000E+00	LEVEL = 0. MEV
	D	ANGULAR DIST.	5	85/04/16	-1.4730E+00	2.6100E+00	2.0000E+01	LEVEL = 0. MEV
	D	ENERGY DEP. TO YO	9	85/04/16	-1.4730E+00	2.6100E+00	2.0000E+01	LEVEL = 0. MEV
	A	ENERGY-ANGLE DIST.	6	85/04/16	-1.4730E+00	2.6100E+00	2.0000E+01	LEVEL = 0. MEV
	A	ENERGY DEP. TO YO	6	85/04/16	-1.4730E+00	2.6100E+00	2.0000E+01	LEVEL = 0. MEV
	A(R)	ENERGY-ANGLE DIST.	6	85/04/16	-1.4730E+00	2.6100E+00	2.0000E+01	LEVEL = 0. MEV
	A(R)	ENERGY DEP. TO YO	6	85/04/16	-1.4730E+00	2.6100E+00	2.0000E+01	LEVEL = 0. MEV
A,DA								
		CROSS-SECTION	4	85/04/16	-1.4730E+00	7.4400E+00	2.0000E+01	LEVEL = 2.9000E+00 MEV
		MAXW. AV. REACT. RATES	70	85/04/16	-1.4730E+00	5.2020E-02	1.0000E+00	LEVEL = 2.9000E+00 MEV
		IN-FLT REACT. X-SECS	20	85/04/16	-1.4730E+00	0.	1.0000E+00	LEVEL = 2.9000E+00 MEV
	D	ANGULAR DIST.	4	85/04/16	-1.4730E+00	7.4400E+00	2.0000E+01	LEVEL = 2.9000E+00 MEV
	D	ENERGY DEP. TO YO	11	85/04/16	-1.4730E+00	7.4400E+00	2.0000E+01	LEVEL = 2.9000E+00 MEV
	A	ENERGY-ANGLE DIST.	4	85/04/16	-1.4730E+00	7.4400E+00	2.0000E+01	LEVEL = 2.9000E+00 MEV
	A	ENERGY DEP. TO YO	4	85/04/16	-1.4730E+00	7.4400E+00	2.0000E+01	LEVEL = 2.9000E+00 MEV
	A(R)	ENERGY-ANGLE DIST.	4	85/04/16	-1.4730E+00	7.4400E+00	2.0000E+01	LEVEL = 2.9000E+00 MEV
	A(R)	ENERGY DEP. TO YO	4	85/04/16	-1.4730E+00	7.4400E+00	2.0000E+01	LEVEL = 2.9000E+00 MEV
HE3,PA								
		CROSS-SECTION	5	85/08/22	1.6881E+01	1.0000E-03	2.0000E+01	
		MAXW. AV. REACT. RATES	182	80/02/23	1.6881E+01	1.0000E-04	1.0000E+00	
		IN-FLT REACT. X-SECS	20	85/08/22	1.6881E+01	0.	1.0000E+00	
	P	ENERGY-ANGLE DIST.	5	85/08/22	1.6881E+01	1.0000E-03	2.0000E+01	
	P	ENERGY DEP. TO YO	2	85/09/11	1.6881E+01	1.0000E-03	2.0000E+01	
	A	ENERGY-ANGLE DIST.	5	85/08/22	1.6881E+01	1.0000E-03	2.0000E+01	
	A	ENERGY DEP. TO YO	2	85/09/11	1.6881E+01	1.0000E-03	2.0000E+01	
	A(R)	ENERGY-ANGLE DIST.	5	85/08/22	1.6881E+01	1.0000E-03	2.0000E+01	
	A(R)	ENERGY DEP. TO YO	2	85/09/11	1.6881E+01	1.0000E-03	2.0000E+01	

-19- 3-LI-6

Fig. C-1. Computer-produced index to the contents of LLNL Evaluated Charged-Particle Library (ECPL).

A. NUCLEAR DATA MEASUREMENTS

1. <u>Low Energy Fusion Cross Sections</u>: Charged Particle Reactions [N. Jarmie and R. E. Brown]

The goal of this project is to determine cross sections for interactions among the hydrogen isotopes in the bombarding energy range 10-120 keV. Such cross sections are fundamental to the operation of future controlled fusion reactors. We have constructed a system, the low-energy fusion cross-section (LEFCS) facility, in order to make these measurements.

The first phase of our work on the D(t,α)n reaction has been completed and published in Phys. Rev. C29, 2031 (1984). A minor erratum has been published in Phys. Rev. C33, 385 1986. We have now, in addition, extended our measurements: 8 more data points over the lab deuteron energy range 80 to 116 keV (the original set ran from 8.3 to 78 keV). The entire set of data for our D(t,α)n work is shown in Fig. A-1 along with two fitting curves whose significance is discussed in the caption. Neither curve fits accurately. A paper on this extended work has been written and has been submitted for publication (Phys. Rev. C). It contains useful polynomial fits to the astrophysical S function for both the cross section and the reactivity. The S function has the energy dependences of $\lambda\!\!\!^{-}$ and the Coulomb penetrability factored out from the cross section.

Analyses of the completed data sets for D(d,p)T and D(d,^{3}He)n continues and is expected to be finished in the next year. The final T(t,α)nn data set, also now complete, is shown in Fig. A-2 in a preliminary analysis. The final analysis for this reaction will follow completion of a D + D paper. We also did some initial studies on obtaining ^{3}He ions at beam energies below 1 MeV from the Tandem Van de Graff at the IBF. It was clear from these studies that some work must be put into the beam optics if we are to obtain reasonable beam intensities for a study of the D(^{3}He, α)P reaction.

2. <u>Low Energy Fusion Cross Sections</u>: Capture Reactions [R. E. Brown, N. Jarmie, G. C. Morgan, P. W. Lisowski, S. A. Wender, J. F. Wilkerson, and D. M. Drake (Los Alamos); and F. E. Cecil, D. M. Cole, and R. Philbin (Colorado School of Mines)]

This past year saw the completion of the analysis of our ^{3}He(d,γ)^{5}Li experiment performed in collaboration with the Colorado School of Mines, Phys. Rev. C 32, 690 (1985). We have had a paper accepted for publication by Phys. Rev. C on a measurement of the γ-ray to neutron branching ratio. T(d,γ)/T(d,n), measured with a thick tritium gas target and using the vertical Van de Graaff accelerator at the Los Alamos Ion Beam Facility (IBF). Both of these studies are of interest for diagnostic work in the fusion-energy program. In addition, we successfully detected the 20-MeV

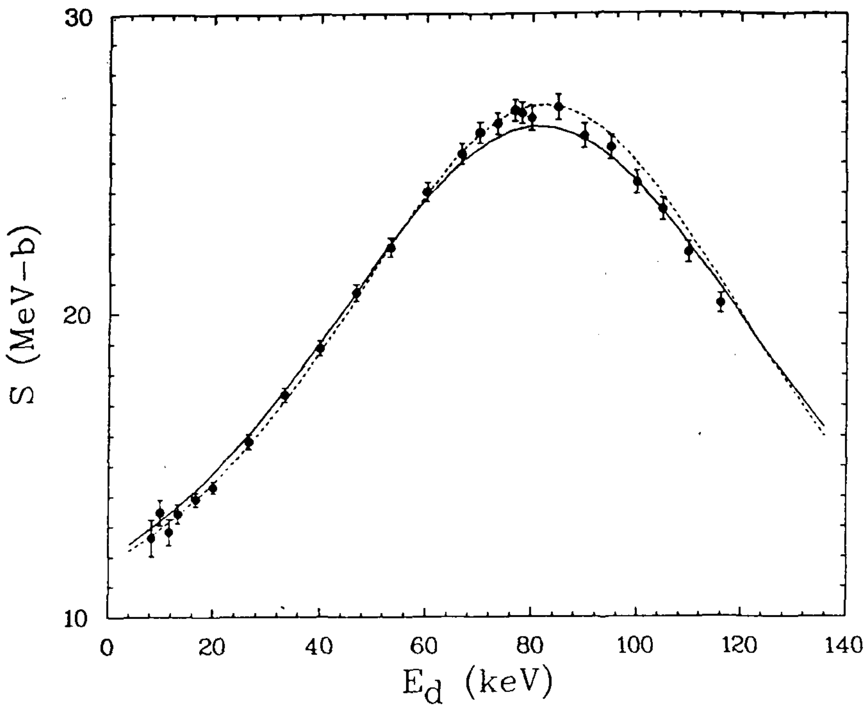

Fig. A-1 S Function vs deuteron bombarding energy E_d for the T(d,α)n reaction. The eight highest energy points show the new data, and the remaining points are those of our published work having been measured with the same apparatus as used in the new experiment. The dashed curve is from a two-level, two-channel R-matrix fit to a data base including the data shown and other data selected from the literature up to a deuteron energy of 250 keV. The solid curve is from a multilevel, multichannel R-matrix fit using data up to a deuteron bombarding energy of 8 MeV (G. M. Hale).

γ ray from the T(p,γ)^{4}He reaction at a proton energy of 100 keV in a BGO detector, and are considering how best to make a measurement of the absolute cross section for this capture reaction. Figure A-3 shows some of the results of the T(d,γ)^{5}Li work at Los Alamos. The low-energy branching ratio now appears to be settling in at about 5.5×10^{-5}, clearing up early discrepancies. Shown also is a data point from the ^{3}He(d,γ) experiment, also in agreement, as is expected for a mirror reaction.

3. Cross Sections For Nuclide Production by Spallation Neutrons [R. C. Reedy, D. R. Davidson, W. F. Sommer, Jr., and P. Englert‡]

A new target cell at the beam stop (target A-6) for the main beam at LAMPF was recently constructed and includes a number of ports for

‡ Univ. Cologne, Cologne, FRG

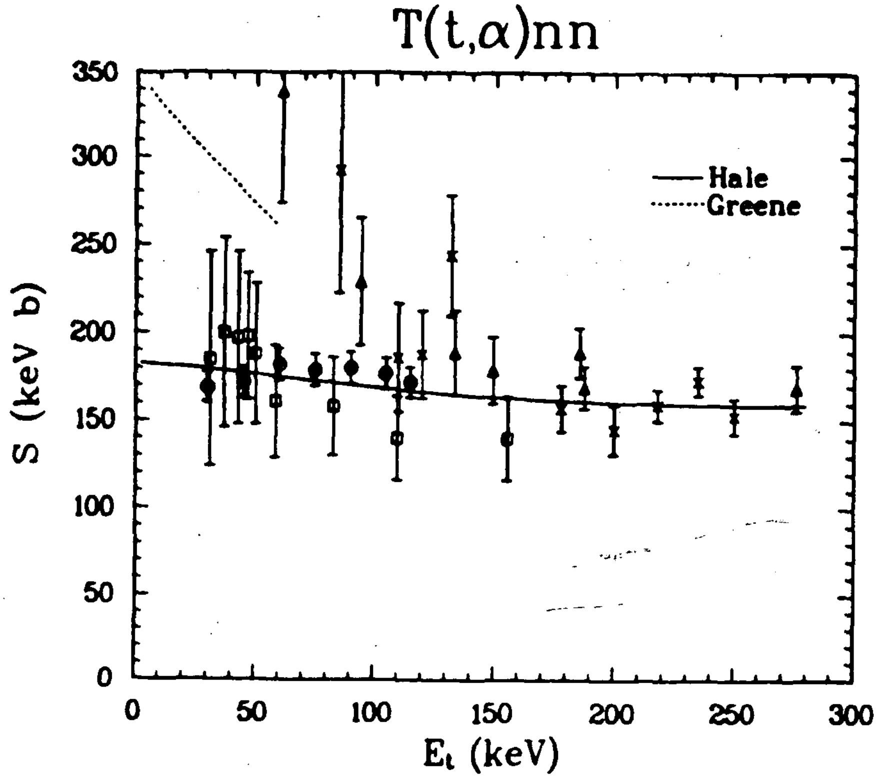

Fig. A-2 The S Function vs triton bombarding energy for the T(t,α)nn reaction. The solid circles are the preliminary LEFCS data shown with 5% errors. The solid curve is from an R-matrix analysis, and the dashed curve is from Greene's evaluation.

irradiations by protons and neutrons.[‡‡] An insert that can fit in any of the 1 neutron irradiation ports was build with four tubes that are 0.12, 0.18, 0.27, and 0.38 meters off beam center. Capsules with outer diameters of 10.2 mm can be pneumatically emplaced in any of these tubes using helium gas as the propellant and rapidly recovered at the top of the target cell. A series of targets were irradiated for periods of 3 to 48 hours in this insert to determine the proton and neutron fluxes. The proton fluxes were fairly low and dropped much faster than the neutron fluxes with distance from the beam. The cooling water results in a large intensity of thermalized neutrons. The fluxes and spectral shapes of the neutrons are being determined using reactions with known cross sections. Several irradiations were done to determine neutron-induced cross sections for a number of threshold reactions producing several radionuclides, including ^{26}Al, ^{14}C, and ^{10}Be from silicon and oxygen. These irradiations continue earlier work that showed that neutron-induced and proton-induced cross sections can be different for the same target-product pair.

‡‡ D. L. Grisham, J. E. Lambert, and W. F. Sommer, Jr., "Major Facility Overhauls at LAMPF," IEEE Trans. Nucl. Sci. NS-32, 3095-3097 (1985).

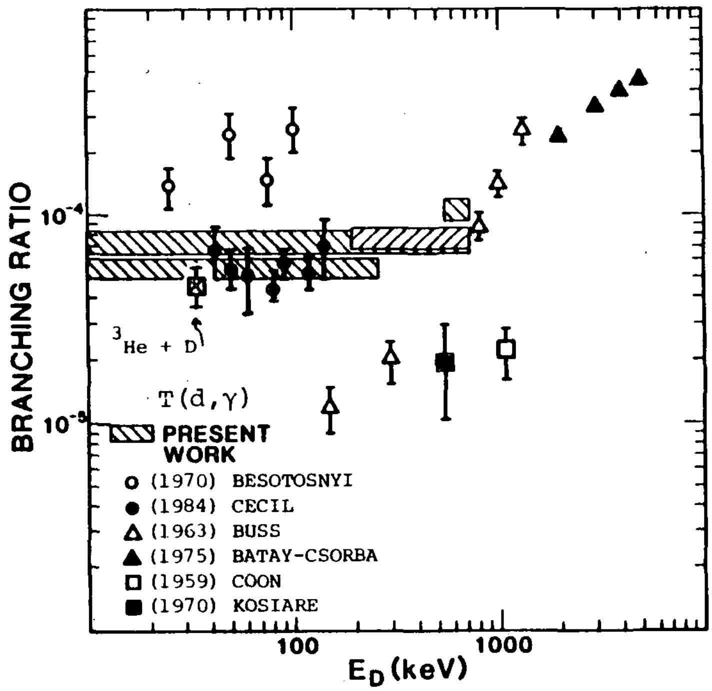

Fig. A-3 Comparison of our results for the T(d,γ)/T(d,n) branching ratio with other experiments. Below 3-400 keV the most recent experiments favor a value of 5.5×10^{-5}. Also shown is a point for the mirror reaction ^{3}He(d,γ)/^{3}He(d,p).

4. Measurement of the ^{7}Be(n,p)^{7}Li Cross Section from 0.03 eV to Approximately 300 eV [P. E. Koehler, C. D. Bowman, F. J. Steinkruger, C. D. Bowman, D. C. Moody, S. A. Wender, R. C. Haight, P. W. Lisowski, and W. L. Talbert]

Cross sections for protons emitted from the reactions ^{7}Be(n,p)^{7}Li and ^{7}Be(n,p)^{7}Li* (0.48 MeV) have been measured from 0.03 eV to $\gtrsim$ 300 eV. The measurements were made using a 95 ng ($\gtrsim$ 30 mCi) $^7BeF_2$ sample. In the field of eV neutron reaction spectroscopy this is the shortest half-life nucleus ever measured and the smallest sample used in such an experiment. Simultaneous measurement of the outgoing proton energy and incident neutron energy was made possible by using the "white" neutron source, driven by the newly-commissioned Proton Storage Ring (PSR), at the WNR Facility at LAMPF. All of the data were collected in about ten hours with the PSR running at about 25% of design intensity. The data are currently being analyzed. The preliminary ^{7}Be(n,p)^{7}Li cross section is shown in Fig. A-4. It is expected that this is the first in a series of measurements on short-lived targets. The high intensity and low duty cycle of the PSR along with our experimental techniques allow measurements on many unstable targets which are not possible anywhere else in the world.

$^{7}Be(n,p)^{7}Li$

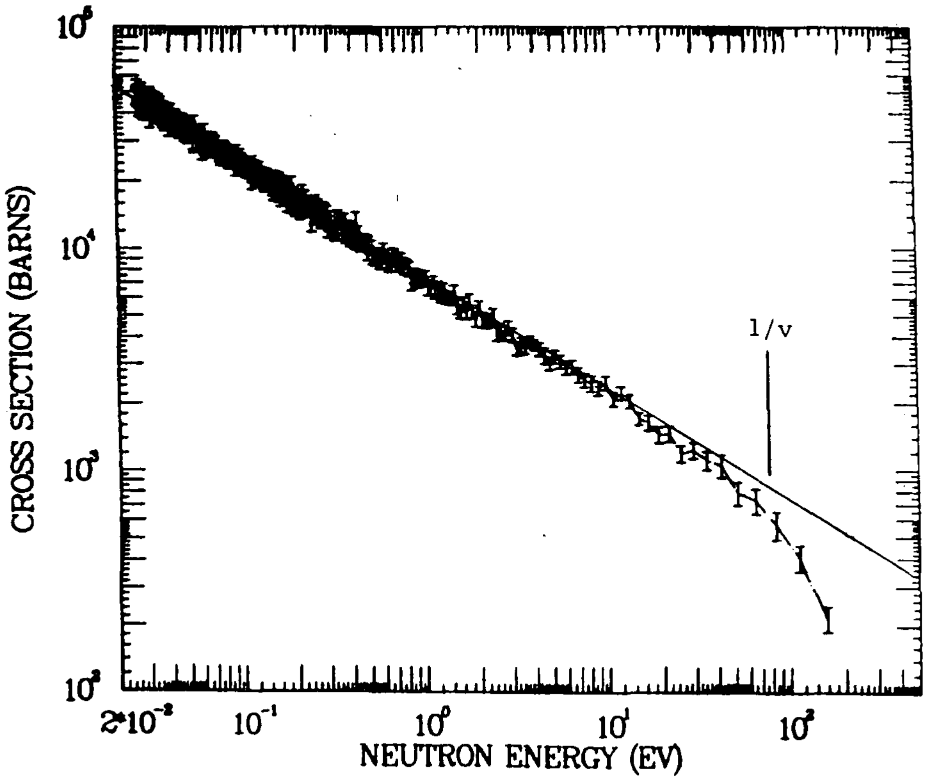

Fig. A-4 The preliminary $^{7}Be(n,p)^{7}Li$ total cross section from 0.03 eV 200 eV. The straight line labeled "1/v" shows the behavior expected if the cross section were strictly proportional to $1/\sqrt{E_n}$.

5. Gamma-Ray Production Cross-Sections for ^{165}Ho [S. A. Wender, P. E. Koehler, and D. Larson (Oak Ridge National Laboratory)]

We have started a series of gamma-ray spectral measurements on ^{165}Ho in order to resolve discrepancies which are on the order of factors of two among various calculations. We have measured gamma-ray pulse height spectra for incident neutron energies from 400 eV to 3 MeV using the Oak Ridge Electron Linear Accelerator (ORELA). The gamma-rays were detected with a 7.6 x 7.6-cm BGO detector mounted at 125° relative to the incident neutron beam. The measured gamma-ray energy range was from 0.5 MeV to 12 MeV. The data were binned into 19 neutron energy bins. Preliminary analysis of the 50 to 70 keV bin (see Fig. A-5) shows excellent agreement between the measured gamma-ray pulse height spectrum and the Los Alamos calculation.

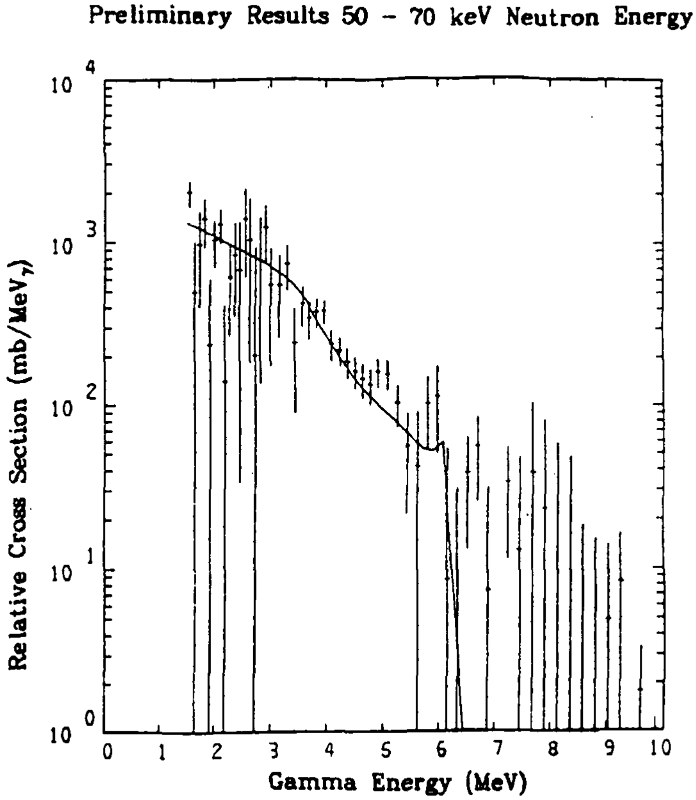

Fig. A-5 Preliminary results for the ^{165}Ho (n,xγ) experiment for 50-70 keV incident neutrons. The solid line shows the results of the Los Alamos calculation.

6. Cross Sections for (p,xn) Reactions [M. M. Meier, G. J. Russell, H. Robinson, R. Whitaker, G. L. Morgan, D. Holtkamp, W. Amian‡, and N. Paul‡]

Neutron yields from proton bombardment of elemental C, Al, Pb, and depleted U have been measured at bombarding energies of 318 and 800 MeV and laboratory angles of 7.5 and 30 degrees. Data were also obtained for Be, Ni, W, and Ta at 318 MeV. The data have been reduced to absolute double-differential cross sections and are in good agreement with intranuclear cascade evaporation calculations at 800 MeV but exceed calculation by as much as a factor of three at the lower energy. Typical data and calculations are shown in Fig. A-6.

‡ KFA-Jülich

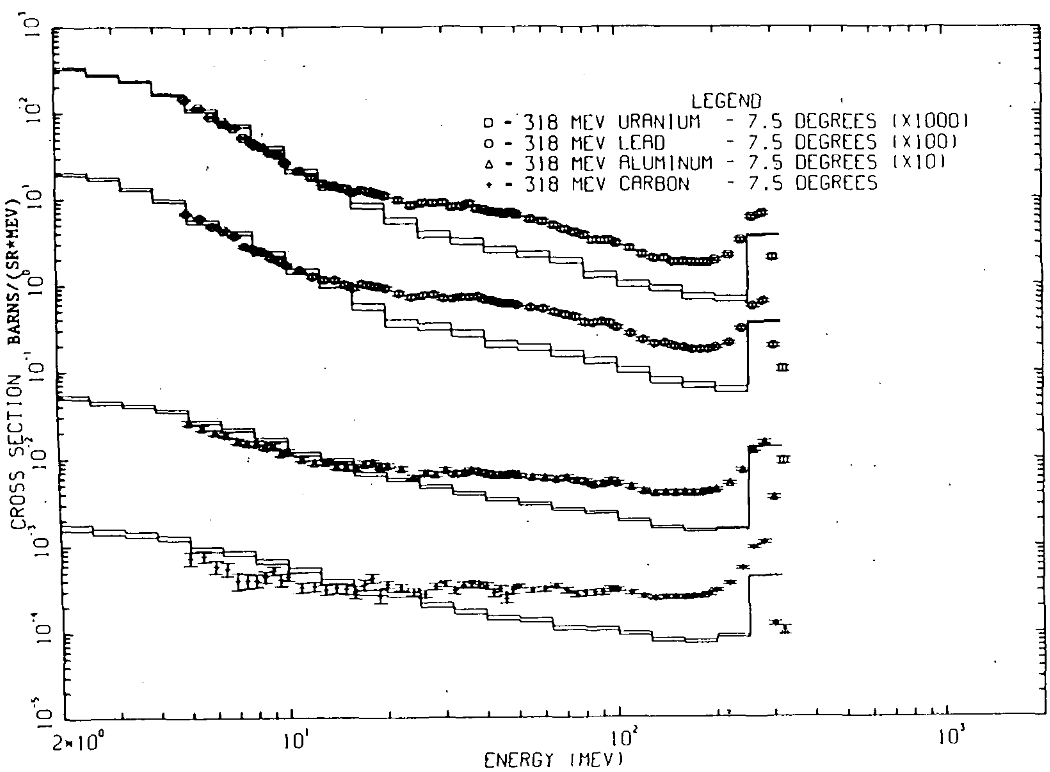

Fig. A-6 Double differential cross sections for carbon, aluminum, lead and depleted uranium at an angle of 7.5 degrees and bombarding energy of 318 MeV. The error bars include statistical error and uncertainty in attenuation, but not the uncertainty in the detector efficiency calibration. The solid curves show the 1σ uncertainty bounds of the HETC calculations.

7. Status of The WNR/PSR Facilities [P. W. Lisowski, C. D. Bowman, and S. A. Wender]

The Weapons Neutron Research Facility (WNR) has been operational since 1977 as a pulsed spallation neutron source at Los Alamos National Laboratory. At present the facility is being given significantly enhanced capabilities. The Proton Storage Ring (PSR), operational in 1985 with up to 35 microamperes of current on target, provided greatly improved intensity, time structure, and repetition rate for low energy neutron experiments. The PSR plus associated target is a powerful facility for condensed matter physics and is the centerpiece for the Los Alamos Neutron Scattering Center (LANSCE). The facility also offers exceptional capabilities for basic and applied neutron physics studies in the thermal to keV range. In addition, a target area is under construction for nuclear physics experiments which will take advantage of multiplexed operation and forward angle flight-paths to greatly enhance both the fast-neutron flux and beam availability.

The biological shield for the PSR has been upgraded to permit as much as 200 microamperes of 800-MeV proton beam, twice the PSR design goal of 100 microamperes, on target. The target-moderator and flight path geometry were optimized to use the PSR beam structure of 270 ns at 12 Hz to produce an intense thermal and epithermal source. The final design resulted in a split target-moderator-reflector (TMR) assembly located in the center of a 2-m high, 1-m diam. cylindrical void, and surrounded by a 4.2-m thick iron and laminated iron-concrete biological shield. The TMR geometry will eventually permit up to 17 neutron flight paths to operate simultaneously with six separately optimized moderators. The neutron flight paths view the moderators at 90^{o} to the incident proton beam, and the target is split so that experiments do not view the central neutron-producing target directly, thus reducing fast neutron background. Initial moderators include two conventional poisoned ambient water moderators, a 20^{o} K liquid H_2 cold moderator, and a high-resolution moderator decoupled at 3 eV which has been optimized for epithermal neutron experiments. For the ambient water moderators, the neutron spectrum is Maxwell-Boltzman at thermal, but proportional to 1/E at epithermal energies with an intensity of 3×10^{11}/E(eV) neutrons/(eV-sr-pulse) at 100 microamperes. In addition, the neutron pulse width is inversely proportional to velocity at epithermal energies so that time-of-flight experiments have constant energy resolution in that energy regime.

In order to provide a source of fast neutrons for nuclear physics experiments, a new white source is under construction. This facility will be shielded to permit as much as 25 microamperes of proton beam on target. In its design, present flexibility will be maintained by using an 8^{o} bending magnet to elevate the new white-source and its flight paths above those of an existing low-current target area; a high-resolution small-angle (p,n) experiment can be operated simultaneously with the white source; and the neutron flight paths for the new facility view the production target at forward angles, thus providing a source extending to nearly 500 MeV with greatly increased neutron intensity over that previously available above about 10 MeV. Target-4 has seven penetrations through the biological shield which view the production target at angles ranging from 15^{o} to 90^{o}. Construction started in late May of 1985 is on schedule for four flight paths to be implemented in time for experiments during the 1986 LAMPF Cycle. Those flight paths include a 250-m flight path for high resolution medium energy (p,n) reaction studies, a 15-m flight path at 30^{o} for fast-neutron capture and gamma-production experiments, a 67-m flight path at 15^{o} for (n,p) experiments, and a 30-m flight path at 60^{o} for fission and total cross section measurements.

The facility was operational with PSR beam during 1985 for both condensed matter and nuclear physics research as the most intense thermal and epithermal pulsed-neutron source in the world. By summer of 1986 the fast-neutron capability will be available with the addition of a multi-use white-neutron source for measurements in the 1-500 MeV range, and a 250-m flight path for (p,n) reaction studies.

B. NUCLEAR DATA EVALUATION

1. Low-Energy Transitions for Polarized d+d Reactions [G. Hale, H. Hofmann (Inst. für Theoret. Physik, Univ. Erlangen, W. Germany)]

The question of whether the d+d reactions can be suppressed at low energies by polarizing the deuterons spin-parallel, which is of great interest for advanced fusion concepts, centers on knowing the magnitudes of the $^5S_2$ transitions in the reactions. Liu, Zhang, and Shuy[1] claim, based on DWBA calculations, that they are small, resulting in high suppression. The R-matrix fits to the data[2] and resonating group calculations[3] that we have done independently give relatively large $^5S_2$ transitions, resulting in little suppression. We are continuing our efforts to understand the latter results in terms of the existing experimental data and improved resonating group calculations.

The Legendre polynomial expansion for the analyzing tensors of the d+d reactions in terms of transition matrix elements and angular momentum coupling coefficients (3j and 9j symbols) reveals that the second-rank tensors T_{2M} depend at low energies only on contributions from the $^5S_2$ (not $^1S_0$) and ^3P_J transitions, and that these contributions have opposite signs.[4] Thus, nonzero values of T_{2M} at low energies suggest the presence of $^5S_2$ transitions, and their signs are a strong indicator of whether the S- or P-wave transitions dominate. In Fig. B-1, which shows R-matrix calculations for $\frac{1}{2}(A_{xx}-A_{yy})\sim T_{22}$ both with (solid curve) and without (dashed curve) the $^5S_2$ transitions, one sees that the low-energy data of Ad'yasevich[5] require the presence of dominant $^5S_2$ transitions.

We are also repeating the earlier resonating group calculations[3] with more realistic (non-central) nucleon-nucleon forces and including D-state contributions from the bound deuterons. Preliminary results for the $^5S_2$ transitions show excellent agreement, both in magnitude and phase, with the $^5S_2$ transition elements from the R-matrix fit. Work continues on the other transitions ($^1S_0$, ^3P_J), important at low energies.

Thus, there is evidence in presently measured analyzing-power data and in realistic four-body calculations that the $^5S_2$ transitions of the d+d reaction are large at low energies, resulting in only slight suppression of the secondary neutron- and tritium-producing reaction occurring in a reactor fueled by polarized d and ^{3}He.

---

[1] K. F. Liu, J. S. Zhang, and G. W. Shuy, Phys. Rev. Lett. 55, 1649 (1985).

[2] G. M. Hale and D. C. Dodder, "A=4 Level Structure from an R-Matrix Analysis of the Four-Nucleon System," B. Zeitnitz, Ed., Proc. 10th Int. Conf. Few Body Problems in Physics, Karlsruhe, W. Germany, 1983, p. 207.

[3] H. M. Hofmann and D. Fick, Phys. Rev. Lett. 52, 2038 (1984).

[4] G. M. Hale, "Work on Polarized d+d Reactions Since the Madison Workshop," Los Alamos National Laboratory informal document LA-UR-2232 (1985).

[5] B. P. Ad'yasevich, V. G. Antonenko, and D. E. Fomenko, Sov. J. Nucl. Phys. 33, 313 (1981).

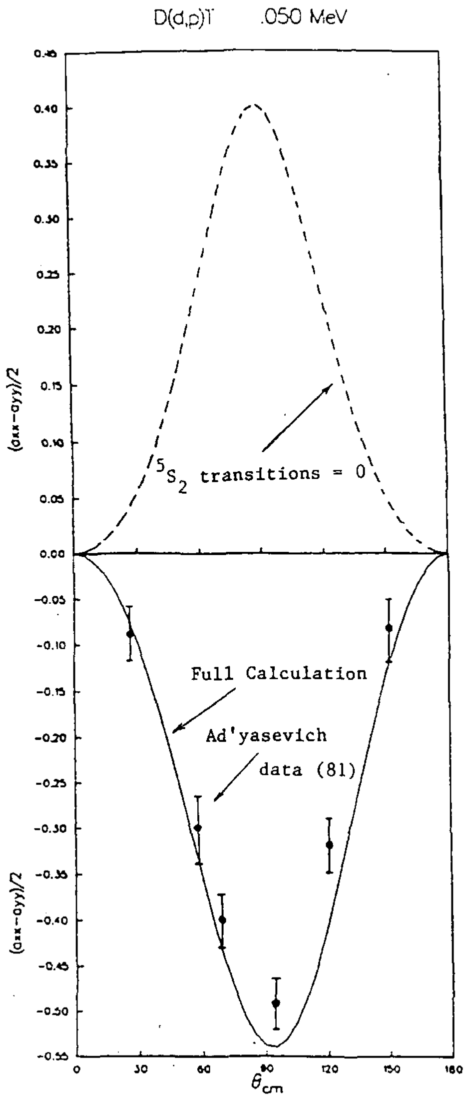

Fig. B-1. R-matrix calculations of the analyzing tensor $\frac{1}{2}(A_{xx}-A_{yy})$ for the D(d,p)T reaction at E_d = 50 keV, compared with data taken from contour plots in Ref. 5. The solid curve is the full calculation and the dashed curve is with the $^5S_2$ transition.

2. <u>R-Matrix Analysis of Reactions in the ^{5}He System</u> [G. Hale and D. Dodder (X-Division Consultant)]

Our R-matrix work on reactions in the ^{5}He system that began a number of years ago has been sustained by continuing interest in the d-t reaction as a fusion energy source, and by numerous experiments, particularly those made with polarized particles, that await interpretation in terms of the level structure of ^{5}He. We have obtained a solution for this problem in terms of R-matrix parameters that account for most of the known ^{5}He data at energies corresponding to E_x below 22 MeV.

The 3-channel analysis includes data for the reactions $^4He(n,n)^4He$, $T(d,n)^4He$, $T(d,d)T$, and $T(d,n)^4He^*$ at neutron energies up to 28 MeV and at deuteron energies up to ~ 8 MeV. The 2500-point data set is representative of every type of measurement that has been made for these reactions, and includes many measurements with vector- and tensor-polarized deuterons, in addition to the most recent and precise measurements of the d-t reaction cross section. The overall chi-square per degree of freedom for the fit is less than 2.5.

Using an elegant new numerical subroutine for calculating Coulomb functions in the complex plane, we have begun to explore the S-matrix pole structure for ^5He that results from our R-matrix parameters. Most of the levels, including the well-known $3/2^+$ resonance just above the d-t threshold, have poles on more than one unphysical sheet of the many-channel Riemann energy surface due to the multichannel nature of the system. We are exploring the consequences of this fact for alpha-particle sticking probability results in μ-catalyzed d-t fusion that recently have been attracting considerable attention.

3. Calculation and Data Library Production for Neutron- and Proton-Induced Reactions up to E=50 MeV (E. D. Arthur, P. G. Young, W. B. Wilson, R. J. LaBauve)

In order to extend several ENDF/B libraries to incident energies greater than 20 MeV, we have completed the first phase of theoretical calculations (Hauser-Feshbach, preequilibrium, DWBA, spherical and deformed optical model) required for such an effort. Theoretical calculations were made for neutron and proton-induced reactions on ^{27}Al, $^{54,56}Fe$, $^{58,60,62}Ni$, $^{63,65}Cu$, and $^{182,184}W$ over the energy range from a few MeV to 50 MeV. Total production cross sections and spectra were obtained for neutron, proton, and gamma-ray emission, while for lighter nuclei (^{27}Al-^{65}Cu) deuteron and alpha-particle emission data were calculated as well. Data libraries using new ENDF/B-VI File 6 formats have been completed for neutron and proton-induced reactions on ^{27}Al. Production cross sections and spectra were provided for n, p, d, α, and γ emission. Figure B-2 illustrates angle-integrated neutron and gamma-ray spectra calculated for 50 MeV n + ^{27}Al reactions.

The calculations for other nuclei described above are still being validated through comparison with numerous types of experimental data. As an example, Fig. B-3 illustrates the validity of our p + $^{63,65}Cu$ calculations, where comparisons are made with neutron spectra measured by Nakamura, et al.[1] for 52 MeV protons stopped in copper targets. Our results agree well with these data and lie well below spectra obtained from intranuclear cascade calculations.

---

[1] T. Nakamura, M. Fujii, and K. Shin, Nucl. Sci. Eng. 83, 444 (1983).

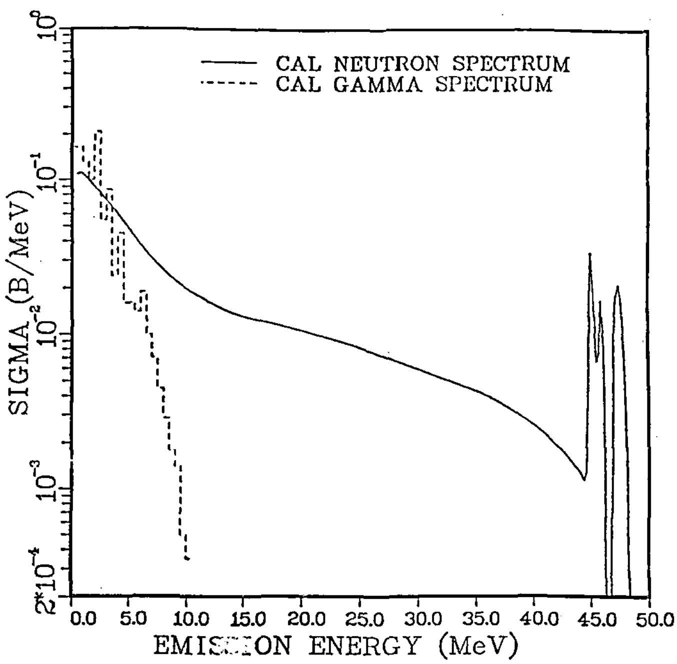

Fig. B-2. Calculated neutron (solid curve) and gamma-ray spectra (dashed histogram) from 50 MeV n + ^{27}Al reactions.

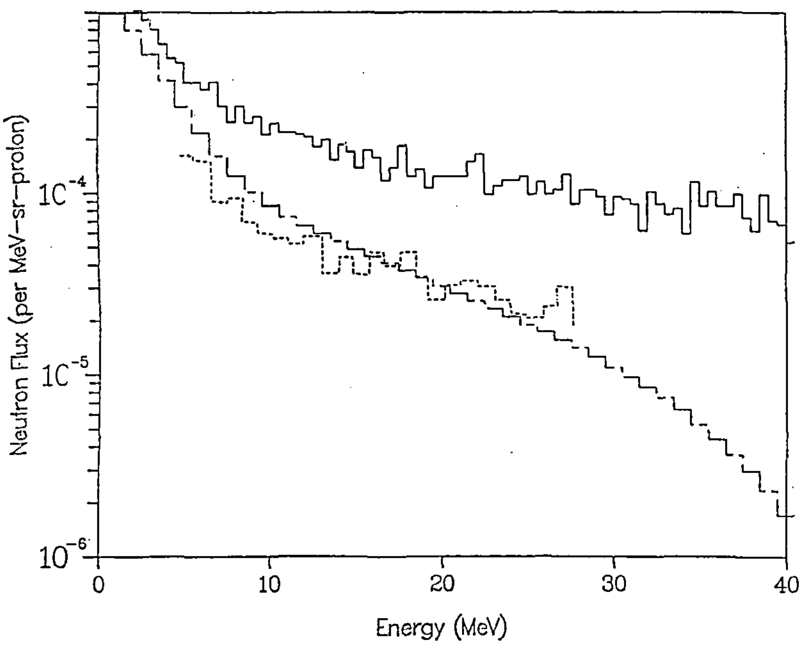

Fig. B-3. Comparison of calculated spectra for neutron emission at 15° with data for 52 MeV protons on a thick copper target. The dotted curve represents the Nakamura data; the chained curve our present calculations, while the solid curve illustrates results from intranuclear cascade calculations.

4. Determination of Neutron and Proton Optical Parameters Valid to 100 MeV (E. D. Arthur)

As part of our effort (described in the previous section) to produce higher energy data libraries, we have extended certain parameters determined for lower energy particle-induced reactions to incident energies as high as 100 MeV. In particular, optical model parameterizations have been developed that describe high energy neutron and proton data available for iron and tungsten isotopes.

In the case of the optical model describing n + ^{54,56}Fe reactions, the parameters determined in Ref. 1 were altered so as to better reproduce new nonelastic data[2] available at 40 MeV. Changes were also made in the parameterization of the volume term of the imaginary potential to reproduce available neutron total cross-section data up to 100 MeV. The changes made in this fashion allowed us to maintain good agreement with data below 50 MeV that was utilized in our previous determination[1] while reproducing higher energy data. This approach allowed us to reproduce a variety of data using standard Woods-Saxon forms for real and imaginary potentials rather than the complicated expressions utilized in Ref. 3 to fit similar data.

For neutron and proton reactions on tungsten isotopes, we utilized as starting values the deformed optical parameters of Ref. 4, and made changes in the volume term of the imaginary potential, as well as the energy dependence of the real potential, to produce agreement with higher energy neutron and proton data. No reliable higher energy total cross sections exist for tungsten so that ECIS[5] coupled-channel calculations were made for n + ^{165}Ho total cross sections based on the tungsten results. The agreement, as shown in Fig. B-4, is good. Additional comparisons were made using Lane consistent[6] forms of the potential to proton elastic and inelastic scattering data[7,8] available at energies of 16 and 55 MeV. Again, good agreement was obtained.

---

[1] E. D. Arthur and P. G. Young, "Evaluated Neutron Induced Cross Sections for ^{54,56}Fe to 40 MeV," Los Alamos National Laboratory report LA-8626-MS (ENDF 304) (December 1980).

[2] C. I. Zanelli, P. P. Urone, J. L. Romero, F. P. Brady, M. L. Johnson, G. A. Needam, J. L. Ullman, and D. L. Johnson, "Total Nonelastic Cross Section Measurements for Neutrons on C, O, Ca, and Fe at 40.3 and 50.4 MeV," Proc. Symp. on Neutron Cross Sections from 10-50 MeV," BNL-NCS-51245, Vol. I, p. 313 (1980).

[3] A. Prince, "Optical Model Calculations for the Chromium, Iron, and Nickel Isotopes in the Energy Range of 0.5 to 100 MeV," K. H. Böckhoff, Ed., Proc. Int. Conf. Nucl. Data for Sci. Technol., Antwerp, Belgium, Sept. 6-10, 1982 (D. Reidel Pub. Co., Boston), p. 574.

4 E. D. Arthur and C. A. Philis, "New Calculations of Neutron Induced Cross Sections on Tungsten Isotopes," in Los Alamos National Laboratory report LA-8630-PR, "Applied Nuclear Data Research and Development July 1-September 20, 1980" (December 1980), p. 20.

5 J. Raynal, "Optical Model and Coupled-Channel Calculations in Nuclear Physics," International Atomic Energy Agency report IAEA SMR-9/8 (1970).

6 A. M. Lane, Nucl. Phys. 35, 676 (1962).

7 T. Kruse, W. Maofske, H. Ogata, W. Savin, M. Slagowitz, M. Williams, P. Stoler, Nucl. Phys. A 169, 177 (1971).

8 H. Kamitsubo, H. Ohnuma, K. Ono, A. Uchida, M. Shinohara, M. Imaizumi, S. Kobayashi, and M. Sekiguchi, Phys. Lett. 9, 332 (1964).

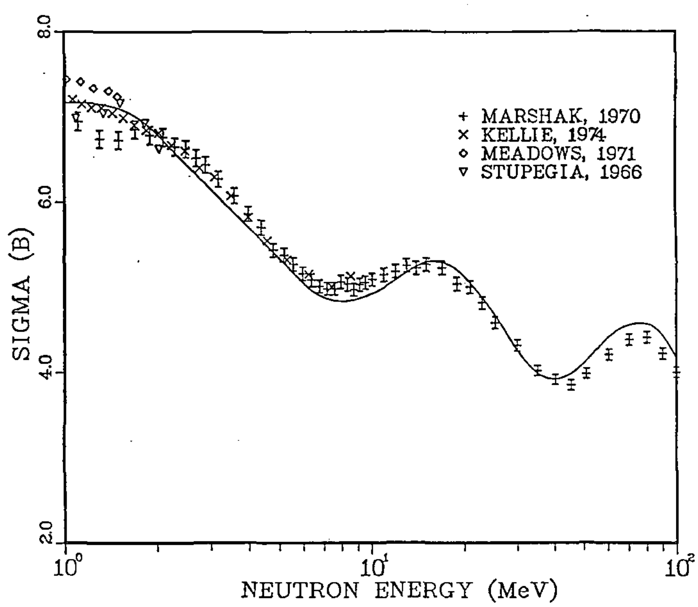

Fig. B-4. Coupled channel calculations of n + Ho total cross sections based on tungsten optical model parameters are compared with data.

5. Improvements to the GNASH Nuclear Model Code [E. D. Arthur, C. Kalbach-Walker (Duke University)]

A new version of the GNASH statistical preequilibrium nuclear model code[1] has been developed that incorporates improvements in the preequilibrium exciton model to include nuclear surface effects[2] important at higher projectile energies. At the same time, portions of the code were rewritten where the Hauser-Feshbach statistical model formalism was replaced with evaporation model expressions. While doing this, the detailed treatment of gamma-ray competition to particle emission was retained. Preliminary calculations made for gamma-ray production induced by 50-MeV protons on ^{184}W show little difference between gamma spectra obtained from this new version and results from GNASH versions that incorporate full angular momentum and parity effects. An expected exception occurs for gamma rays having energies less than 0.5-0.75 MeV where the new results are significantly lower than previously calculated.

The fast running speed of the new GNASH version allows greater numbers of reaction paths to be covered within one calculation. The code now allows the decay of 50 compound systems with emission of 5 radiation types (γ,n,p,d,α) from each each. To facilitate the setup of problems involving complecated reaction sequences, the user can now specify regions of ΔZ and ΔN over which cross sections are required. The code then automatically constructs reaction paths reached by emission of the above particle types.

---

[1] P. G. Young and E. D. Arthur, "GNASH: A Preequilibrium-Statistical Nuclear Model Code for Calculations of Cross Sections and Emission Spectra," Los Alamos Scientific Laboratory report LA-6947 (November 1977).

[2] C. Kalbach, Phys. Rev. C 32, 1157 (1985).

6. Sensitivity of n + ^{58}Ni Reaction Theory Calculations to Optical Model Potentials (P. G. Young)

To investigate the sensitivity of reaction theory calculations to optical model potentials in the structural region, a series of Hauser-Feshbach statistical theory calculations were performed for neutron-induced reactions on ^{58}Ni using different optical potentials.[1] A total of seven global and four local potentials were investigated. Standard Hauser-Feshbach statistical theory calculations (see following section) were carried out with all model parameters held fixed at default or systematic values except for the neutron transmission coefficients, which were obtained from the various optical potentials. The reactions studied include the (n,γ), (n,n'), (n,p), (n,α), (n,2n), and (n,np) cross sections from 0.01 to 20 MeV. Significant differences were found in cross sections for several reactions using the global potentials, whereas results from the local potentials were reasonably consistent. The greatest sensitivity was observed for the (n,2n) calculations.

---

[1] P. G. Young, "Global and Local Optical Model Parameterizations," Proc. OECD/NEANDC Specialists Meet. on Use of the Optical Model for Calculation of Neutron Cross Sections Below 20 MeV," Paris, Nov. 13-15, 1985, to be issued.

7. Deformed Optical Model and Reaction Theory Analyses of Rare Earth Nuclei (P. G. Young)

Deformed optical model neutron potentials have been obtained for the rare earth nuclei ^{151}Eu, ^{153}Eu, ^{154,158}Gd, ^{160}Gd, and ^{165}Ho for use in Hauser-Feshbach statistical-theory calculations. All nuclei were treated as rigid rotators, with the first three members of the ground-state rotational bands coupled in calculations with the ECIS78[1] coupled-channel code.

Because of the sparsity of experimental data, the analyses relied mainly on s- and p-wave neutron strengths and potential scattering radii for the isotopes, and total neutron cross sections for the natural elements. Parameter sets were obtained starting from the Nd-Sm potential of Shamu et al.[2] and from the Ho-Tm potential of Young et al.,[3] which utilize different geometries and forms for the imaginary surface potential.

The potentials that resulted from the analysis are given in Table B-1, and the deformation parameters are listed in Table B-2. The best Gd potential evolved from the Nd-Sm[2] starting parameters, whereas the Eu and Ho potentials were obtained using the Ho-Tm[3] initial values. The calculated neutron total cross section for natural gadolinium is compared to experimental data in Fig. B-5.

Hauser-Feshbach statistical theory calculations are being performed using neutron transmission coefficients from these analyses and the GNASH-COMNUC code systems.[4,5] The calculations include width fluctuation corrections and γ-ray strength functions from a measurement[6] on ^{169}Tm, normalized using $\langle\Gamma_{\gamma 0}\rangle$ and $\langle D_0\rangle$ determinations for the Eu, Gd, and Ho isotopes. A comparison of calculated (preliminary) and experimental cross sections for the ^{165}Ho(n,γ) reaction is given in Fig. B-6.

TABLE B-1. Neutron Deformed Optical Model Potentials.

Element	Potential* (MeV)		r_i, a_i (fm)
Eu	$V_R = 49.8 - 16\eta - 0.325E$		1.28, 0.63
	$W_D = 4.02 - 8\eta + 0.51E$	E<10	1.28, 0.48
	$W_D = 9.12 - 8\eta - 0.09\ (E-10)$	E$\geq$10	1.28, 0.48
	$W_V = -2.0 + 0.25E$		1.28, 0.63
	$V_{SO} = 6.0$		1.28, 0.63
Gd	$V_R = 49.8 - 18\eta - 0.22E$		1.245, 0.65
	$W_D = 4.02 - 9\eta + 1.1\sqrt{E}$	E<9	1.245, 0.50
	$W_D = 7.32 - 9\eta - 0.05\ (E-9)$	E$\geq$9	1.245, 0.50
	$W_V = -2.0 + 0.25E$		1.245, 0.65
	$V_{SO} = 8.5$		1.245, 0.65
Ho	$V_R = 49.8 - 16\eta - 0.325E$		1.26, 0.63
	$W_D = 5.02 - 8\eta + 0.51E$	E<6.5	1.26, 0.48
	$W_D = 8.34 - 8\eta - 0.092\ (E-6.5)$	E$\geq$6.5	1.26, 0.48
	$W_V = -1.8 + 0.2E$		1.26, 0.63
	$V_{SO} = 6.0$		1.26, 0.63

*$\eta = (N-Z)/A$

TABLE B-2. Deformation Parameters Used in Calculations.

	^{151}Eu	^{153}Eu	^{154}Gd	^{155}Gd	^{156}Gd	^{157}Gd	^{158}Gd	^{160}Gd	^{165}Ho
β_2	0.16	0.30	0.284	0.293	0.301	0.308	0.314	0.320	0.30
β_4	0	0	0.065	0.064	0.062	0.058	0.054	0.043	-0.02

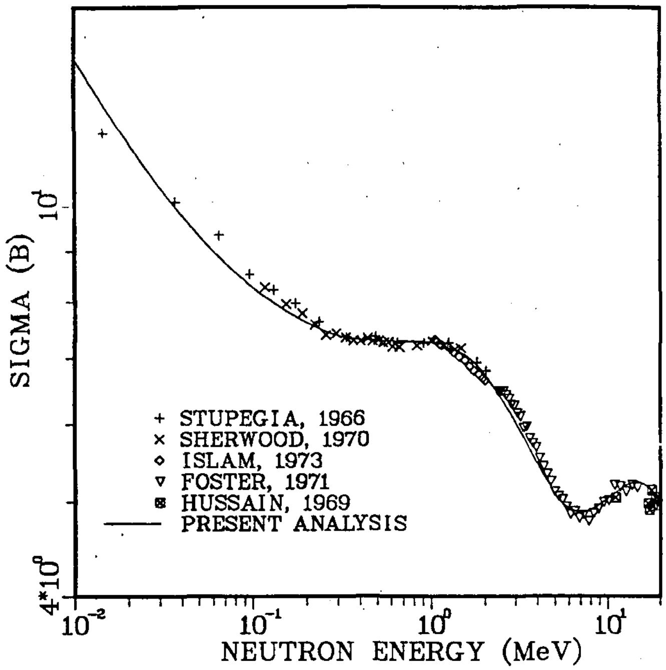

Fig. B-5. Measured and calculated total cross section of natural gadolinium for neutron energies between 0.01 and 20 MeV.

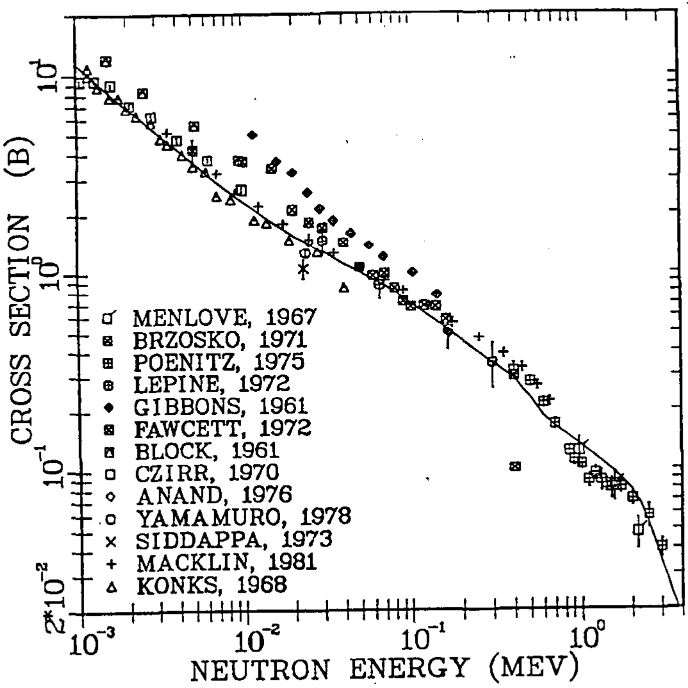

Fig. B-6. Comparison of experimental and calculated (solid curve) $^{165}Ho(n,\gamma)$ cross sections between 1 keV and 4 MeV.

[1] J. Raynal, "Optical Model and Coupled-Channel Calculations in Nuclear Physics," International Atomic Energy Agency report IAEA SMR-9/8 (1970).

[2] R. E. Shamu, E. M. Bernstein, J. J. Ramirez, and Ch. Lagrange, Phys. Rev. C 22, 1857 (1980).

[3] P. G. Young, E. D. Arthur, C. Philis, P. Nagel, M. Collin, "Analysis of n+ ^{165}Ho and ^{169}Tm Reactions," Proc. Nucl. Data for Sci. and Tech. Int. Conf., Antwerp, Belgium, Sept. 1982, p. 792.

[4] P. G. Young and E. D. Arthur, "GNASH: A Preequilibrium-Statistical Nuclear Model Code for Calculations of Cross Sections and Emission Spectra," Los Alamos Scientific Laboratory report LA-6947 (November 1977).

[5] C. L. Dunford, "A Unified Model for Analysis of Compound Nuclear Reactions," Atomics International report AI-AEC-12931 (1970).

[6] S. Joly, D. Drake, and L. Nilsson, Phys. Rev. C 20, 2027.

8. Prompt Fission Neutron Spectrum for the ^{252}Cf(sf) Standard Reaction (D. G. Madland, R. J. LaBauve, and J. Rayford Nix)

We have tested four representations of the ^{252}Cf(sf) prompt fission neutron spectrum against recent experimental measurements of the differential spectrum and threshold integral cross sections.[1] These representations are the Maxwellian spectrum, two versions of the Watt spectrum, the NBS spectrum, and the Los Alamos spectrum. Using least-squares adjustments to the differential measurements, we obtain the least well known parameters of the various representations. Our results are shown in Figs. B-7 and B-8 for parameter adjustment with respect to the Poenitz and Tamura experiment.[2] The Los Alamos spectrum gives the best overall agreement with experiment.

[1] D. G. Madland, R. J. LaBauve, and J. R. Nix, Proc. Int. Conf. on Nucl. Data for Basic and Applied Sci., Santa Fe, New Mexico, May 13-17, 1985 (to be published).

[2] W. P. Poenitz and T. Tamura, Proc. Conf. Nucl. Data for Sci. and Tech., Antwerp, Belgium, September 6-10, 1982, p. 465, D. Reidel, Dordrecht (1983).

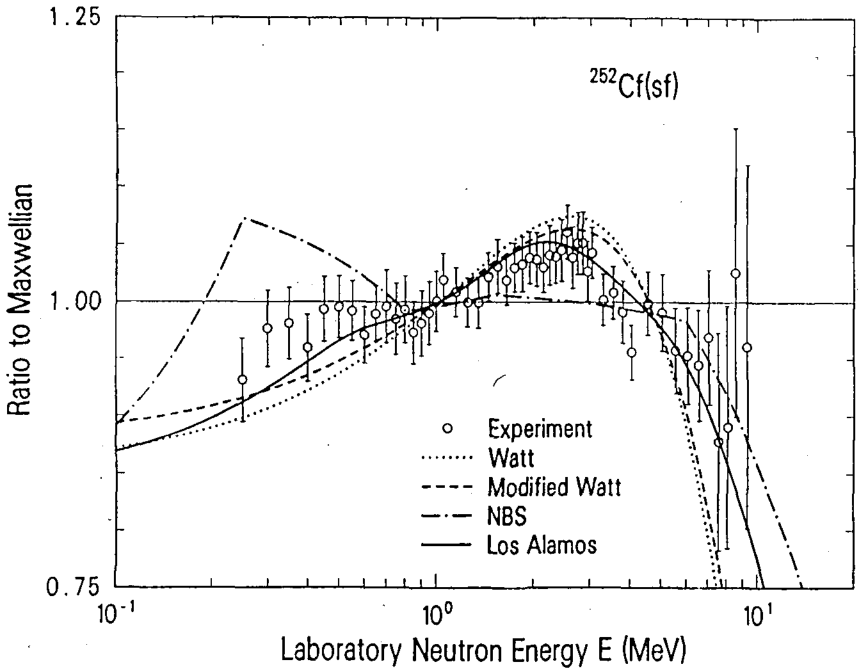

Fig. B-7. Differential spectrum comparisons for adjustments to the Poenitz and Tamura experiment (Ref. 2).

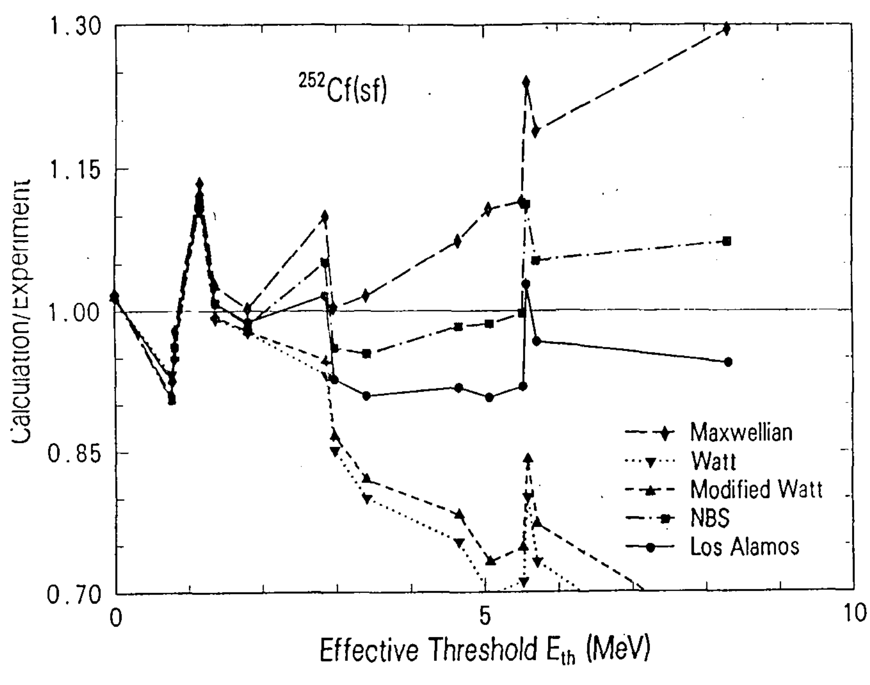

Fig. B-8. Integral cross-section comparisons for spectra adjusted to the Poentiz and Tamura experiment (Ref. 2.).

9. Delayed Neutron Spectra (T. R. England, M. C. Butler, R. J. La Bauve, E. D. Arthur, and W. B. Wilson)

In a cooperative effort with Hanford Engineering Development Laboratory (see their contribution), we now have emission probabilities for 270 precursors and corresponding neutron emission spectra. The data files include evaluations of measured probabilities (80 nuclides), spectra for 30 nuclides, and model estimates for the remainder. Of the 30 measured spectra, none extend above 3 MeV. These have been augmented at low (< 100 keV) and high (> 3 MeV) energies using the model code BETA.[1] Some shorter lived precursors have an energy emission exceeding 10 MeV. We also used the BETA code to calculate the unmeasured spectra for 80 nuclides. An additional 160 less important precursors have spectra based on an evaporation model in which the temperature was a simple modeling based on the measured spectra. These were included for completeness and to estimate their contribution at high energies. Their contribution to the total number of delayed neutrons is only 1-2%.

This effort is a continuation of earlier work for 110 precursors.[2-4] All data are used in a summation code to get aggregate, time-dependent spectra.

---

1 F. M. Mann, C. Dunn, and R. E. Schenter, Phys. Rev. C 25 (January 1982).

2 T. R. England, W. B. Wilson, R. E. Schenter, and F. M. Mann, Nucl. Sci. Eng. 62, 139-155 (October 1983).

3 F. M. Mann, M. Schreiber, R. E. Schenter, and T. R. England, Nucl. Sci. Eng. 87, 418-431 (August 1984).

4 T. R. England, M. C. Brady, W. B. Wilson, "Delayed Neutron Spectra and Intensities from Evaluated Precursor Data," Proc. Int. Conf. on Nucl. Data for Basic and Applied Sci., Santa Fe, New Mexico, May 13-17, 1985 (to be published).

UNIVERSITY OF LOWELL

A. NEUTRON SCATTERING CROSS SECTIONS IN THE ACTINIDES

(L.E. Beghian, G.H.R. Kegel, J.J. Egan, A. Mittler, G.C. Goswami, G.D. Brady, A. Aliyar and C.A. Horton)

During the past year we have published the results of our earlier (n,n) and (n,n'γ) studies on the states of ^{232}Th in the 700-to 1500-keV excitation energy range.[1,2] A portion of the results of a similar study on ^{238}U were presented at the International Conference on Nuclear Data for Basic and Applied Science in Sante Fe, NM last May[3], and a full detailed paper on our ^{238}U(n,n') work in collaboration with E.D. Arthur of Los Alamos National Laboratory has been accepted for publication in Nuclear Science and Engineering.[4]

Our ongoing neutron scattering studies during the past year have focused on four areas: (1) measurement of elastic and inelastic angular distributions for ^{232}Th, ^{235}U and ^{238}U at E_n = 185 keV; (2) a study of the gamma rays following neutron inelastic scattering in ^{235}U at incident energies below 500 keV; (3) preliminary measurements below 100 keV using an iron filter in the scattered neutron flight path; (4) inelastic scattering at 2.0 MeV $\leq E_n \leq$ 3.0 MeV for states of ^{232}Th and ^{238}U in the 600 - 1000 keV excitation energy range.

1. Angular Distribution Measurements at 185 keV for ^{232}Th, ^{235}U and ^{238}U

Last year we reported elastic and inelastic angular distribution measurements on ^{232}Th, ^{235}U and ^{238}U at 550 keV. We have extended these

---

[1] C.A. Ciarcia, G.P. Couchell, J.J. Egan, G.H.R. Kegel, S.Q. Li, A. Mittler, D.J. Pullen, W.A. Schier and J.Q. Shao, Nucl. Sci. Eng. 91, 428 (1985).

[2] J.H. Dave, J.J. Egan, G.P. Couchell, G.H.R. Kegel, A. Mittler, D.J. Pullen, W.A. Schier and E. Sheldon, Nucl. Sci. Eng. 91, 187 (1985).

[3] J.J. Egan, E.D. Arthur, G.H.R. Kegel, A. Mittler and J.Q. Shao, "A Comparison of Measured and Calculated Neutron Inelastic Scattering Cross Sections for Vibrational States from 680 to 1060 keV in ^{238}U", Proc. of the International Conference on Nuclear Data for Basic and Applied Science, Sante Fe, NM, May 1985. (To be published in Radiation Effects).

[4] J.Q. Shao, G.P. Couchell, J.J. Egan, G.H.R. Kegel, S.Q. Li, A. Mittler, D.J. Pullen, W.A. Schier and E.D. Arthur, Nucl. Sci. Eng. 1986 (in publication).

measurements down to 185 keV where we have obtained data on the ground and first excited states of ^{232}Th and ^{238}U. In addition we have measured the angular distribution of the composite ground and 13-keV state as well as that of the 46-, 52-keV doublet in ^{235}U. Figure A-1 shows a spectrum for ^{235}U taken at 125° and Figure A-2 shows the elastic cross section for ^{238}U compared to the values listed in ENDF/B-V.[5] These results were presented at the 1985 Fall Meeting of the Nuclear Physics Division of the American Physical Society at Asilomar in Pacific Grove, CA.[6]

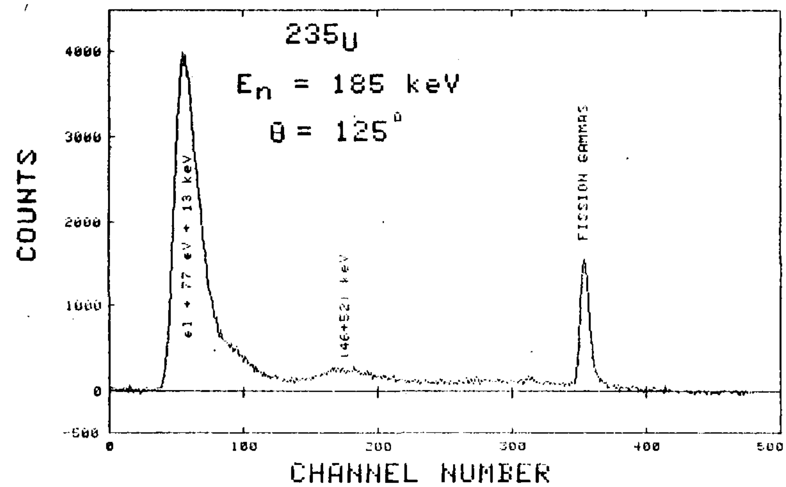

Fig. A-1. Background subtracted time-of-flight spectrum for 185-keV neutrons scattered from ^{235}U at 125°.

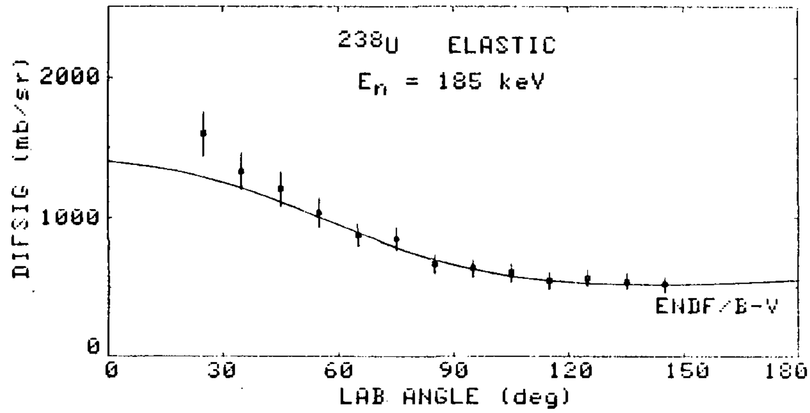

Fig. A-2. (a) Elastic angular distribution for ^{238}U at 185-keV.

---

[5] E.M. Pennington, A.B. Smith and W.P. Poenitz, Evaluated Nuclear Data File - B, Version V (ENDF/B-V) Mat. 1398, National Nuclear Data Center, Brookhaven National Laboratory, Upton, NY.

[6] J.J. Egan, G.H.R. Kegel, G.C. Goswami and A. Mittler, Bull. Am. Phys. Soc. 30, 1252 (1985).

2. Gamma Rays From Neutron Irradiated ^{235}U

The number of low lying excited states (E < 500 keV) in ^{235}U is far higher than in neighboring even-A nuclei; hence high resolution measurements have to be performed to obtain neutron scattering cross sections for individual levels. Neutron time-of-flight techniques provide adequate resolution for some composite "levels" but are unable to separate contributions from closely spaced doublets. It is expected that the $(n,n'\gamma)$ technique with its superior resolution will permit the determination of cross sections which supplement and clarify results from TOF measurements.

The gamma spectrometer used in this experiment incorporated a Ge(Li) detector with a resolution of 1.4 keV. After calibration we found it possible to measure gamma energies with an error not exceeding one channel, or about 140 eV. The spectrometer included both time and energy components, with the capability of accumulating data in two time regions, one of which is coincident with the primary neutron pulse to record prompt gamma emission and the other to observe gammas emitted at later times, e.g. gammas from the decay of fission products.

In addition to the usual detectors which we use for normalization, target making, and incident neutron fluence determination, we incorporated a fission neutron detector. This detector was operated with pulse shape discrimination to reject gamma signals. Neutron signals of 500 keV or less were also rejected by pulse height discrimination, thus the detector counted fission neutrons only, providing a relative measure of the number of fission events taking place during a run. Hence it could be used to account for the gamma-rays produced by fission neutrons.

Gamma-ray production cross sections for six inelastic scattering lines were corrected for fission neutron contributions, for finite scatterer size and for neutron multiple scattering. A description of the experiment and preliminary results were presented at the International Conference on Nuclear Data for Basic and Applied Science in Sante Fe.[7]

3. Cross Section Measurements Using an Iron Filter in the Scattered Neutron Flight Path

We have performed exploratory experiments with an iron filter with the aim of determining parameters needed for measuring the neutron scattering cross section of the second excited state of ^{235}U at 13 keV, for incident neutrons of 95 keV. We plan to place an iron filter in the scattered neutron

---

[7] G.H.R. Kegel, J.J. Egan, A. Mittler, G.D. Brady and J.Q. Shao, "Gamma Radiation from Neutron Irradiated U-235", Proc. of the International Conference on Nuclear Data for Basic and Applied Science, Sante Fe, NM May 1985 (to be published in Radiation Effects).

path (see e.g. Macklin et al.[8]) and to utilize the iron attenuation minimum near 82 keV.

Primary neutrons with an energy of 82 keV, scattered elastically, will pass through the iron filter and will reach the detector later than primary neutrons with an energy of 95 keV, scattered inelastically (E_{ex} = 13 keV), which also pass through the filter and reach the detector. The time separation Δt of the two neutron groups is equal to the neutron flight time difference over the primary flight path (target to scatterer) D; in our case

$$\Delta t \simeq 0.18 \frac{\mathrm{ns}}{\mathrm{cm}} \times D.$$

D should be as small as possible to obtain a strong neutron fluence incident upon the scatterer and it should be sufficiently large to produce a Δt which exceeds the detector-plus-accelerator time resolution.

At this writing our accelerator time resolution approaches 300 picoseconds (FWHM), much better than the detector resolution of about 2 ns for 82-keV neutrons. At present we are exploring several approaches to improve the detector time resolution.

4. ^{232}Th and ^{238}U Cross Sections for E > 2.0 MeV

We have begun preliminary measurements on states in the 600-to 1000-keV excitation energy range in ^{232}Th and ^{238}U at incident neutron energies above 2.0 MeV. This is a natural extension of the work reported in Refs. 1 and 4. For these measurements we use a 3-m flight path and carefully monitor the accelerator and Mobley buncher to maintain a beam pulse duration (FWHM for the gamma rays in the time-of-flight spectrum) of less than 400 ps. We have incorporated pulse shape discrimination into our spectrometer to reduce the gamma-ray background which becomes more significant as the incident energy increases.

B. DEVELOPMENT OF A "WHITE" NEUTRON SOURCE
(G.H.R. Kegel)

In several applications it is convenient to use a thick neutron target, either in pulsed or in a DC mode, to generate neutrons in a broad band of energies. At Lowell we have used an infinitely thick metallic lithium target for this purpose. A computer program[1] has been written to determine the neutron fluences and neutron energy spectra. A set of calculated isofluence lines is shown in Fig. B-1. Fig. B-2 shows a neutron energy spectrum.

---

[8]R.L. Macklin, R.R. Winters, N.W. Hill and J.A. Harvey Astro. J. 274, 408 (1983).

[1]G.H.R. Kegel, Computer Physics Communications 36, 321 (1985).

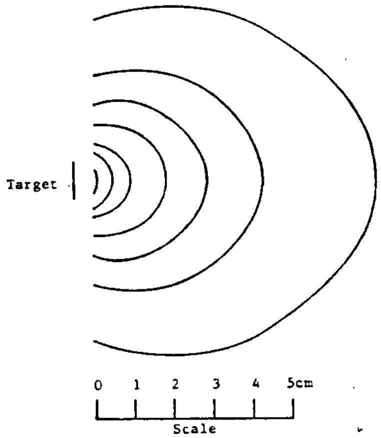

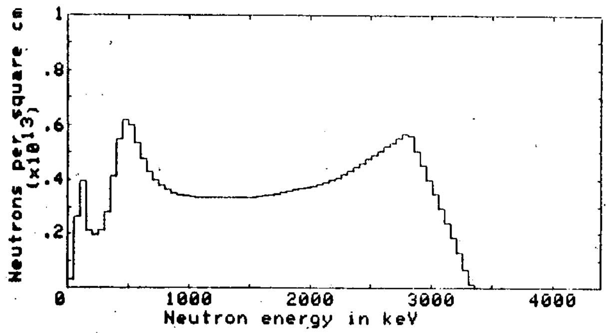

Fig. B-1. Isofluence lines for a 90-minute irradiation with a 20-μA, 5-MeV proton beam. The seven isofluence lines shown correspond to fluences of $2x10^{14}$, $1x10^{14}$, $5x10^{13}$, $2x10^{13}$, $1x10^{13}$, $5x10^{12}$ and $2x10^{12}$ neutrons per cm^2, respectively.

Fig. B-2. Neutron energy spectrum from $^7Li(p,n)^7Be$ reaction on an infinitely thick target.

C. LEVEL CROSS-SECTION CALCULATIONS FOR NEUTRON INELASTIC SCATTERING ON THE PRINCIPAL ACTINIDE NUCLEI
(E. Sheldon)

With the conclusion of the main body of computations of level total (angle-integrated) and differential cross sections for (n,n') scattering on the principal even-mass, fertile actinide nuclei, Th-232, U-238 and Pu-240, 242,244, in the statistical S-matrix (HRTW) and in the standard (CN+DI) formalisms, using the programs "NANCY", "CINDY" and "KARJUP", as described in the previous (1983 - 85) Reports to the DOE Nuclear Data Committee and in a series of three detailed review publications,[1-3] efforts are now underway

[1]E. Sheldon, Beghian, Ciarcia, Couchell, Dave, Egan, Goswami, Kegel, Li, Mittler, Pullen, Schier and Shao, J. Phys. G - Nucl. Phys. 1986 (in publication.

[2]E. Sheldon, Beghian, Chan, Chang, Couchell, Egan, Goswami, Kegel, Li, Mittler, Pullen, Schier, Shao and Wang, J. Phys. G - Nucl. Phys. 1986 (in publication).

[3]E. Sheldon and D.W.S. Chan, J. Phys. G - Nucl. Phys. 1986 (in publication).

to incorporate provision for fission channels preparatory to engaging in a similar batch of calculations for the principal odd-mass, fissile actinides currently under investigation by our experimental group, commencing with U-233,235.

Toward accomplishing this, a copy of the CN program "NRLY" assembled by Jacqueline Jary at Bruyeres-le-Chatel in FORTRAN-4 for an IBM system, containing provision for fission admixtures and other competition, has recently been generously made available to us by her and is in the process of being modified and recompiled for our CDC Cyber 170-825 system in a revised version, "JACQUI". As of this date, the new program has been successfully run partway with Th-232 test data, but has encountered core-memory difficulties which have to be obviated before total execution can be undertaken. When the final version is completed and all test runs and checks are carried through, we intend to assemble the requisite fission-barrier and other input parameters for the odd-mass, as well as the even-mass, actinides and perform the detailed computations of total and differential CN cross sections for the individual rotational and vibrational levels in order to derive level excitation functions and angular distributions over the incident neutron energy range of interest for comparison with previous data and ENDF/B-V evaluations. We also plan then to introduce the appropriate fission subroutines into our CN program "CINDY" and the HRTW program "NANCY", as well as extending the latter or provide differential cross sections for angular distribution analyses.

D. DELAYED-NEUTRON MEASUREMENTS

(G.P. Couchell, D.J. Pullen, W.A. Schier, L. Fisteag, M.H. Haghighi, Q. Sharfuddin and R.S. Tanczyn)

The extension of our delayed neutron (DN) study to Pu-239, which has a considerably lower delayed-neutron yield (ν_d) relative to U-235, required the introduction of pulse-shape discrimination (PSD) for gamma-ray suppression over the full neutron energy range. The previous inclusion of a PSD system to our Li-6 glass measurements gave us at least a factor of two improvement in the DN-to-background ratio. During the past year, we replaced our Pilot U plastic with Bicron BC 501 liquid scintillators, the latter having known PSD properties. The excellent performance of our system for neutron energies well below 0.5 MeV is especially interesting since we are not aware of any reported use of PSD in liquid scintillators for neutron time-of-flight (TOF) studies at neutron energies as low as 120 keV, where our neutron detection efficiency is still 60% of the maximum. Just as for our Pilot U measurements, it was found that considerably better energy resolution is achieved with BC 501 scintillators if each TOF spectrum is divided into two pulse-height ranges, viz, i) low amplitude (0.15 - 0.80 V) and ii) high amplitude (0.80 - 9.50 V), and the corresponding spectra accumulated separately in the multichannel analyzer. These are shown in Fig. C-1a and C-1b, respectively.

Recently we completed DN measurements with the Bicron scintillators on the thermal fission of Pu-239 for seven successive delay-time intervals between 0.17 and 29.0 s. The DN energy spectra extend from 0.13 - 3.0 MeV. We shall now extend the spectra down to 10 keV using Li-6 glass scintillators in our beta-neutron spectrometer.

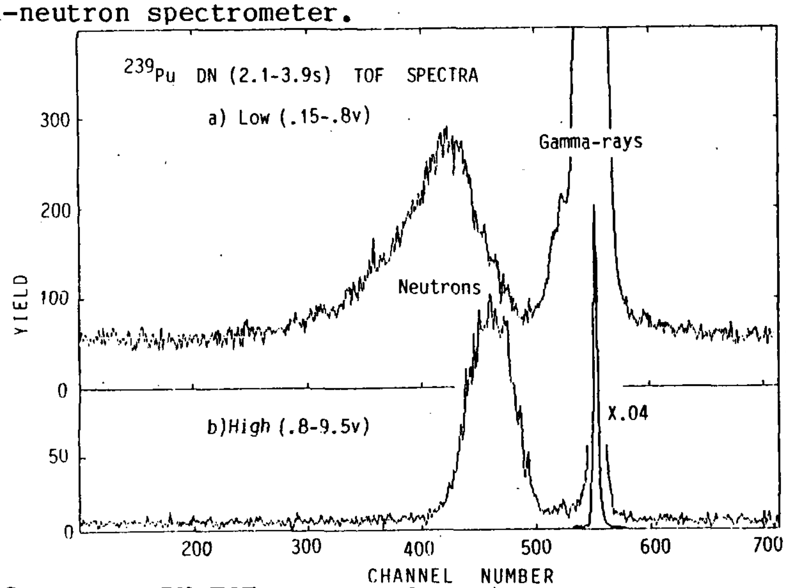

Fig. C-1. Composite DN TOF spectra from the thermal neutron fission of ^{239}Pu in the delay-time interval 2.1 - 3.9 s. PSD is applied to the four Bicron scintillators which are at a flight path of 50 cm.

During this past year we completed our search for a dependence of the composite DN spectra on the energy of the incident neutrons inducing fission in U-235. In seeking differences in spectral structure it is clearly desirable to perform the thermal and fast measurements successively for each delay time interval and under as nearly identical experimental conditions as possible. This requires that both sets of measurements be made using our 5.5 MV Van-de-Graaff accelerator and the ^{7}Li(p,n) reaction as a neutron source. To make thermal neutrons the dominant mode for inducing fission using the accelerator, the fission chamber and thick lithium target assembly are encased in a paraffin block, approximately 0.3 m^3 in volume. For the fast neutron measurements a nearly bare geometry is used, with the fission chamber wrapped in cadmium to shield against any residual thermal neutrons. The fast/thermal measurements were performed at all the delay-time intervals given Table C-1. The more recent measurements at the two shortest and the two longest time intervals incorporated the Bicron scintillators with PSD and were performed at a higher mean neutron energy (2 MeV) for the "fast" case. Analysis is underway and the results will soon be submitted for publication.

Our completed DN study for the thermal neutron fission of U-235 was submitted for publication in Nuclear Science and Engineering. Spectra were measured for eight successive time intervals between 0.17 and 85.5 s with equal weighting given each delay time. This time range covers 90% of the delayed neutrons emitted although our measurements actually encompass 78% due to small gaps between successive time intervals. Average neutron energies have been calculated for each spectrum and an equilibrium DN spectrum has also been constructed from the spectra. The average energies of our DN spectra were generally larger than those of ENDF/B-V[1] and Rudstam[2] but compared more favorably with recent He-3 spectrometer studies of Kratz and Gabelmann[3] (see Table C-1).

Table C-1. Average Delayed Neutron Energies of Composite Spectra

Delay Interval (s)	Present Study[a)] (keV)	Rudstam (keV)	ENDF/B-V (keV)	Kratz and Gabelmann (keV)[b)]
.17 - 0.37	473 (14)	407	422	
.41 - 0.85	482 (12)	413	423	
.79 - 1.25	506 (12)	422	423	
1.2 - 1.9	502 (12)	429	424	477
2.1 - 3.9	491 (13)	438	425	472
4.7 - 10.2	478 (14)	431	429	480
12.5 - 29.0	420 (12)	404	437	506
35.8 - 85.5	441 (17)	386	429	498
Equilibrium	470 (11)	418	425	

a) Listed uncertainties include the statistics of the DN yield together with uncertainties in the mean neutron flight time and path length.

b) Average energies for time intervals most nearly matching the present study.

An equilibrium DN spectrum (from a reactor operating at a steady power level) was calculated by two methods. If the full range of delay times is spanned in the composite DN spectra, an equilibrium DN spectrum can be constructed using the well-known DN fractions as a function of delay time (direct integration method). Alternatively, if one assumes the six-group representation is appropriate, spectra at every delay time interval are unnecessary since a mathematical solution exists for a set of six independent DN spectral measurements (matrix inversion method). The equilibrium spectra generated by both methods are in excellent agreement. Comparison of our equilibrium spectrum with those generated from ENDF/B-V and the Rudstam compilations is presented in Fig. C-2.

---

[1]Fission-Product Decay Library of the Evaluated Nuclear Data File (ENDF/B-V), National Nuclear Data Center at Brookhaven National Laboratory. Decay spectral files primarily evaluated at Idaho Nucl. Eng. Lab.; see R.L. Bunting and C.W. Reich, BNL-50847, Brookhaven National Laboratory (1977).

[2]G. Rudstam, Nucl. Sci. and Eng. 80, 238 (1982).

[3]K.L. Kratz and H. Gabelmann, in Proc. Int. Conf. Nucl. Data Basic and Applied Science, Sante Fe, May 1985, (in print).

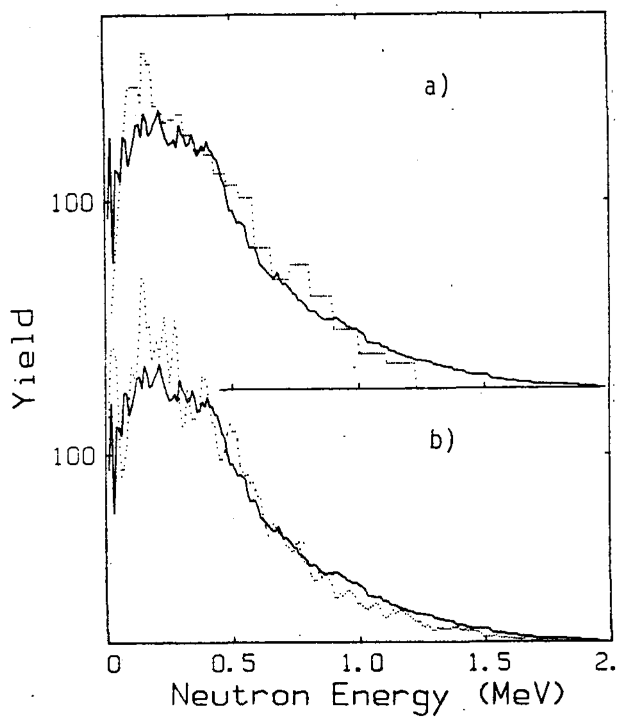

Fig. C-2. Our equilibrium DN spectra (solid) compared to a) ENDF/B-V and b) Rudstam.

During the upcoming year we will complete our DN studies for thermal-neutron induced fission of Pu-239 with the Li-6 glass measurements. We will also search for a dependence of Pu-239 DN spectra on the energy of the incident neutrons inducing fission.

In addition to these time-dependent studies, we propose also to measure the equilibrium delayed-neutron spectra for U-233,235,238 and Pu-239. With only minor modifications to our system, we shall in these measurements be able to span a time interval which includes approximately 95% of all delayed neutrons emitted following fission. Also, since these measurements involve only a single (0.1 - 130 s) time interval, we shall be able to examine their energy dependence in somewhat greater detail than for the time-dependent spectra, namely:

a) U-235 at thermal, 2-, 3- and 5-MeV mean incident neutron energy,
b) U-238 at 2- and 5-MeV mean incident energy,
c) Pu-239 and U-233 at thermal and 5-MeV mean incident energy.

We are also presently studying mathematical approaches to decompose our eight composite U-235 DN spectra into approximate six-group solutions. Although the analysis of this overdetermined problem is in its early stages, a least squares fitting approach which includes a weighted term comparing group spectra to test spectra appears promising. The purpose of the weighted term is to keep group spectra solutions positive everywhere. These test spectra will be allowed to change through an iterative procedure. The computer program will be interactive, provide graphical display of solutions and data spectra for comparison, and include optional spectrum smoothing.

Beyond 1986 our plans include the measurement of the composite DN spectra as a function of delay time from the neutron fission of U-233 and U-238. The incident neutron energy will again be varied as indicated in b) and c) above to search for an energy dependence in the DN spectra.

THE UNIVERSITY OF MICHIGAN
DEPARTMENT OF NUCLEAR ENGINEERING

A. INTRODUCTION

Nuclear data activities within the Department of Nuclear Engineering make use of two experimental laboratories. In conjunction with the Ford Nuclear Reactor, we have developed extensive facilities for the irradiation, handling, and calibration of photoneutron sources using gamma activities up to 30 Ci. A one-meter manganese bath is used to calibrate the sources. Experiments are carried out in an irradiation room completely lined with anhydrous boric acid for albedo reduction. In a separate facility, we have installed a 150 keV Cockroft-Walton neutron generator on a low mass platform within a heavily shielded large-volume laboratory. Extensive counting facilities have been developed in conjunction with both facilities.

B. MEASUREMENTS USING PHOTONEUTRON SOURCES
(S. Melton, E. Quang, G. Knoll)

1. Capture Cross Section of Th-232 at 265 and 964 keV

A series of measurements are nearing completion that have involved the radiochemical separation of induced Pa-233 activity from the large natural activity of the thorium target. Because of the very low activities induced in these experiments, we have developed a low background gamma counting facility to allow measurement of the separated activity with adequate statistical precision. The yield of the chemical separation process is quantified by using a Pa-232 tracer produced in a separate accelerator irradiation. An absolutely calibrated Np-237 source is used to determine the gamma counting efficiency.

2. Capture Cross Section of U-238 at 23, 265, and 964 keV

In an experiment modeled after our previous work on thorium[1] we are carrying out measurements using depleted uranium targets of several hundred gram mass in conjunction with three photoneutron sources. We have developed a radiochemical separation procedure involving a combination of solvent extraction and precipitation techniques that can isolate the induced Np-239 activity into a very small volume with good separation yield. In this case, Np-237 is used as a tracer to quantify the yield. Detection efficiency of the gamma counting systems are determined using a foil of Am-243 in which the Np-239 activity has grown to equilibrium. The activity of the reference foil is determined to by absolute alpha counting.

---

1. G. T. Baldwin and G. F. Knoll, Nucl. Sci. and Eng. 88, 2(1984).

C. MEASUREMENTS MADE WITH THE 14 MeV NEUTRON GENERATOR
(Y. Lai, K. Zasadny, G. Knoll)

1. Measurement of the $Cr(n,X)^{52}V$ Cross Section at 14.6 MeV

The total cross section for the $Cr(n,X)^{52}V$ reaction in elemental chromium at 14.6 MeV has been determined by the activation method. The $Cr(n,X)^{52}V$ activation at 14 MeV neutron energy includes four distinct threshold reactions, all of which lead to hydrogen production. Since the $^{52}Cr(n,p)$ reaction produces the dominant amount of ^{52}V activity, its cross section at 14 MeV is normally quoted in data files or original papers to represent the total element $Cr(n,X)^{52}V$ cross section.

Thin iron foils were chosen to be neutron fluence monitors. The cross section for the $^{56}Fe(n,p)$ reaction at 14.74-MeV neutron energy is quoted to 1% accuracy in a recent comprehensive evaluation.[2] We have assumed a value of 111.4 ± 1.0 mb for this reference value at 14.58 MeV.

A high-purity chromium sample sandwiched with two iron foils was simultaneously irradiated at a zero degree angle relative to the deuteron beam direction and at a distance of 5 cm from the DT neutron source. The subsequent chromium sample ^{52}V and iron foil ^{56}Mn activities were measured by a large volume intrinsic germanium detector and a $4\pi\beta$ flow proportional counter respectively. The efficiencies of both detectors were absolutely determined using standard ^{52}V and ^{56}Mn sources, with activities absolutely calibrated by a $4\pi\beta-\gamma$ coincidence counting system.

Because of the uncertainties introduced by the thickness of the tritium target, the neutron energy was determined experimentally at the time when the $Cr(n,X)^{52}V$ cross section was measured. The precise neutron energy was deduced by irradiating a fully-depleted silicon surface barrier detector at 0 and 96 degrees.[3] By observing the $^{28}Si(n,\alpha)$ reaction within the active volume of the detector, assuming a 14.00-MeV value for the neutron energy at 96 degrees and known Q-values for the α_0 and α_4 peaks, the shifted α_0 peak at zero degrees can then be used to determine the neutron energy at the time of the chromium sample irradiation. We obtain a value of $14.58 \pm .02$ MeV.

The induced ^{52}V activity within the chromium sample was impossible to measure absolutely using conventional techniques because of the short half life and low intensity of the induced activity. Our approach was to first generate high yield of ^{52}V using thin vanadium foil bombardment with thermal neutrons. The ^{52}V was absolutely determined by a 4 pi beta-gamma coincidence counting system. The absolute efficiency of the HPGe detector was then determined against this standard ^{52}V source.

2. T. Tyves and E. Axton, NBS Pub. 594, 980 (1980).

3. T. Ryves and K. Zieba, Nucl. Instru. and Meth., 167, 449 (1979).

Two consecutive measurements using independent target and reference foils gave results for the Cr(n,X)^{52}V cross section within 0.4% of each other. Their average value with estimated experimental uncertainty is 71.4 $\pm$ 1.7 mb. Principal contributions to the uncertainty arise from uncertainties in the reference (iron) cross section, detector efficiency, photopeak area determination, and dead time corrections. The result, together with previous measurements near 14 MeV, is shown in Fig. 1.

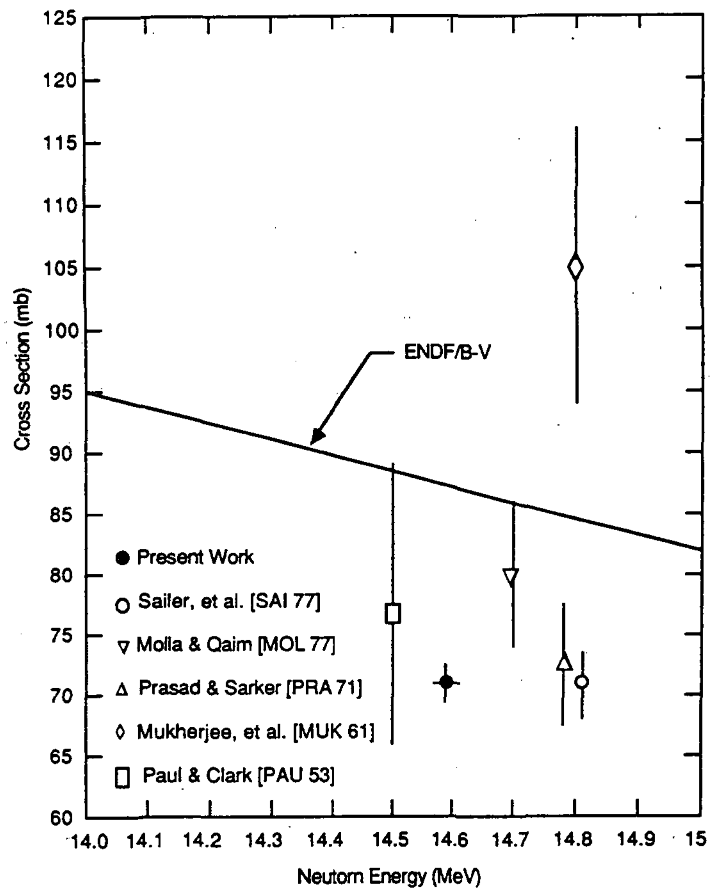

Figure 1. Comparison Data of the Cr(n,X)^{52}V Cross Section at the 14 MeV Neutron Region.

2. Measurements of the $^{65}Cu(n,2n)^{64}Cu$ and $^{64}Zn(n,p)^{64}Cu$ Cross Sections at 14.6 MeV

High purity targets of copper and zinc have been obtained in anticipation of a new series of measurements on these reactions. Since the product activity is the same in both reactions, we expect to be able to determine the ratio of these cross sections to a very high precision. Techniques to absolutely count the annihilation irradiation produced in the beta-plus decay of the product are being developed. We will inititally use iron foils as a flux monitor in this experiment, but hope to place the measurement on a more absolute basis using the proton recoil monitor described in the next section.

3. Absolute Measurement of the $^{56}Fe(n,p)^{56}Mn$ and $^{27}Al(n,alpha)^{24}Na$ Cross Sections at 14.6 MeV

Work is currently in progress to measure the iron and aluminum activation cross sections through the use of a proton recoil monitor of unique design. Because many of our previous measurements have been made relative to these two reference cross sections, this effort will provide an independent method to link our measurements to an absolute standard (the hydrogen scattering cross section). The design of the monitor employs time-of-flight techniques to effectively discriminate against contributions from scattered neutrons and other unwanted events.

The technique employed here is to replace the conventional radiator with a fast scintillating plastic. In this way, an interaction event in the radiator (start) is marked in time by the scintillation event. If the conventional detector is replaced by another fast scintillator (stop detector), and both are sufficiently separated spatially, the time between an event in the radiator (start) and subsequent particle leaking to the detector (stop) can be measured.

In addition to recoil carbon atoms from the radiator, other (n,α) and (n,p) reactions in surrounding materials may lead to events in both detectors, but they are easily identified by their relatively slow flight time compared to 14 MeV protons.

Testing of the first version of the monitor is now underway. Once its reliability and accuracy are proven, we will carry out activation measurements of the $^{56}Fe(n,p)^{56}Mn$ and $^{27}Al(n,alpha)^{24}Na$ cross sections near 14 MeV using the techniques similar to those of our previous 14 MeV measurments.

NATIONAL BUREAU OF STANDARDS

A. NUCLEAR DATA MEASUREMENTS

1. $^{235}U(n,f)$ Fission Cross Section Measurement from Thermal to 1 keV. (R. A. Schrack, A. D. Carlson, and R. G. Johnson)

Preliminary measurements have been made with a multiple-plate ionization chamber that combines a set of six ^{235}U foils and two ^{10}B foils. Measurements were made at the NBS electron Linac facility using the 8-and 20-meter flight paths. Black resonance filters of gold, cadmium, cobalt, rhodium, platinum, and manganese were used to obtain background measurements at a wide variety of energies. The "wrong energy" neutron background was found to be approximately one percent of the foreground counting rate at all energies measured for both the uranium and boron detectors. Tests were made of the effect of beam filtration, overlap neutrons, and source moderation. Data were taken at the two path lengths and comparisons were made with ^{6}Li and another boron ionization chamber of different design. It was found that the boron foils contained much less boron than the suppliers had indicated but that the thickness of the uranium foils were in agreement with the supplier's values.

The data obtained in the experiments were analyzed and integrals calculated for the energy ranges normally used in comparing ^{235}U fission cross sections. The source of the deviations from the ENDF/B-V values has been investigated to determine modifications in the experimental design. It has been found that a major source of error is the response functions of the detectors. To eliminate the wide response functions, the detectors have been redesigned to have no effective geometrical width. This will require more complex electronics and data acquisition programs. The chamber is being rebuilt and the data-taking system revised.

2. Measurement of Thickness of Boron Deposits for $^{235}U(n,f)$ Cross Section (R. A. Schrack and A. D. Carlson)

Interpretation of experimental data obtained with the multiple plate chamber designed for measurement of the ^{235}U fission cross section from thermal to 1 keV showed errors in the thickness of the boron or uranium deposits used in the chamber. Alpha particle counting and Rutherford back-scattering measurements of the uranium deposits were in good agreement with the supplier's values. Thus the error is in the boron deposits.

To check the boron foil thickness an experiment was carried out on the NBS Linac that simultaneously compared the absolute counting rates from the multiple-plate chamber, another boron chamber, and a ^{6}Li glass detector system. It was found that both boron ionization chamber systems had counting rates which indicated significantly less boron than had been stated by the supplier. As a check of the Linac measurements, another group at NBS measured the boron concentration of other samples of boron foils made at the same time as those used in the multiple plate chamber using prompt gamma ray activation analysis. The results of these measurements were in good agreement with the Linac measurements. The measurements of the four different foils yielded thicknesses which are approximately 40% less than that given by the suppliers in the United States and in Europe. The boron deposits are 76 mm in diameter on aluminum backings that are .05 mm thick. The production of these large diameter deposits required modification of the normal technique. However, smaller foils with deposits 12.5 mm in diameter were made in the European laboratory at the same time as the large foils. The small foils measured thickness is in agreement with the supplier°s values.

3. Computer Synthesis of $^{235}U(n,f)$ Cross Section Measurement
(R. A. Schrack)

A computer program was developed to examine the sensitivity of the $^{235}U(n,f)$ cross section measurement to various experimental conditions. The program uses the ENDF/B cross section files to create data as number of counts per experimental time bin for both the ^{235}U fission chamber and the ^{10}B ionization chamber. The code is limited in its use to neutron energies less than 82 eV. Above 82 eV the ENDF/B file of the ^{235}U fission cross section provides only an unresolved average cross section. The energy spectrum of the neutron flux was obtained from measurements at the NBS Linac. Using the synthesized data one can then observe the effect of modifying various parameters in the experiment or the data reduction.

When no errors are introduced into the synthesis-analysis loop, the ENDF/B cross sections are reproduced to one part in 100,000. The effect of overlap neutrons and other backgrounds, as well as the width of data taking bins, can be examined and optimum experimental conditions determined. The effect of data reduction techniques, sensitivity to flight path, and timing errors on the result can be determined. The end points of the energy ranges used as standard integrals for comparison of the ^{235}U fission cross section have been chosen arbitrarily (.1 to .5, .5 to 1., 1. to 10., etc). The proximity of resonances to those end points will cause the integrals derived from the data to vary for changes in the response function of the system and interpolation techniques used in the data reduction. It can be shown that this error can be reduced by as much as two orders of magnitude by using more sophisticated interpolation techniques.

4. Absolute Measurements of the $^{235}U(n,f)$ Cross Section for Neutron Energies from 0.3 to 3 MeV (A. D. Carlson, J. W. Behrens, R. G. Johnson, and G. F. Cooper*)

Measurements of the ^{235}U neutron fission cross section have been made at the NBS neutron time-of-flight facility. The neutron flux was measured at the 200 m end station with a Black Neutron Detector. The ^{235}U fission reaction rate was determined with a well-characterized fission chamber located on the same beam line at 69 m from the neutron target. Final corrections have been made to the data. The final data with extensive information on correlations and uncertainties have been made available for the ENDF/B-VI evaluation of the neutron cross section standards.

5. Measurements of the Ratio of the $^{10}B(n,\alpha)^7Li$ to $^6Li(n,t)^4He$ Cross Sections in the eV Energy Region (A. D. Carlson)

A previous measurement[1] of the $^{10}B(n,\alpha)^7Li$ to $^6Li(n,t)^4He$ cross section ratio was made in order to determine if the discrepancy between two sets of $^{235}U(n,f)$ cross section measurements [2,3] was a result of the standard cross sections used in measuring the neutron flux. The ratio measurements did not explain the discrepancy but showed an apparent difference of 1-2% below 20 eV compared with that obtained from ENDF/B-V cross sections. The present measurements were made in order to further study this effect.

The present experiment employs essentially the same equipment and setup as was used in the previous investigation. The $^{10}B(n,\alpha)^7Li(n,t)^4He$ rates were measured with a ^{10}B plated ionization chamber and a thin natural lithium glass detector located at the 20 m station of the NBS Neutron Time-of-Flight facility. Lower backgrounds were obtained in the present work through improvements in shielding and the use of a narrower pulse height window for the ^6Li detector. Additional Rh and Pt beam filters reduced the systematic error due to the interpolation of the background. The present measurements agree with the ENDF/B-V evaluations and indicate that the previous measurement was probably affected by systematic errors in the background subtraction.

---

* Student from Massachusetts Institute of Technology

1 J.B. Czirr and A.D. Carlson, Measurements of the $^{10}B/^6Li$ Cross Section Ratio Below 1 keV, in Proc. of the Int. Conf. on Nuclear Cross Sections for Technology, NBS Spec. Publ. 594, p. 84 (1980).

2 J.B. Czirr and G.W. Carlson, Nucl. Sci. Eng. 64, 892 (1977).

3 R. Gwin, Oak Ridge National Laboratory, (private communication) (1977).

6. Measurement of the $^{235}U(n,f)/^{10}B(n,\alpha)$ Cross Section Ratio in the Intermediate Energy Standard Neutron Field (ISNSF) (G. P. Lamaze, D. M. Gilliam, and J. A. Grundl)

The measurement of the $^{235}U(n,f)/^{10}B(n,\alpha)$ cross section ratio in the ISNF is planned for the first half of 1986. Thin (~10 μg/cm^2 and ~30 μg/cm^2) ^{10}B deposits on stainless steel backings have been obtained from CBNM, Geel, Belgium. Measurements of the ^{10}B density are underway using three different nondestructive techniques. At the conclusion of the measurement, a destructive assay of one of the deposits may also be made. The cross section ratio will be measured by placing ^{10}B and ^{235}U deposits back to back in an NBS double fission chamber. This has now been done with thermal neutrons both to test the method and as a means of determining the ^{10}B content. An overall experimental precision of better than 3% for the cross section ratio is expected.

7. Measurement of Absolute Fission Cross Sections for ^{252}Cf Spontaneous Fission Neutrons (I. G. Schröder, Li Linpei,** D. M. Gilliam, E. D. McGarry, and C. M. Eisenhauer)

A long series of measurements of the absolute fission cross sections of ^{235}U, ^{238}U, and ^{239}Pu for ^{252}Cf spontaneous fission neutrons has been completed and reported.[4] The absolute cross section for ^{235}U is the basis for all integral fission cross section measurements in NBS standard neutron fields and is recognized by the CSEWG subcommittee on standards as a basic normalization measurement for the ^{235}U fission cross section. The NBS results listed in Table A-1 contain two notable disagreements with ENDF/B-V. The result calculated from ENDF/B-V data relative to the experimental cross section (the C/E ratio) for ^{238}U is 0.945 ± .017 and for ^{239}Pu is 0.971 ± 0.013. Some unique features of the measurement are as follows:

** Present address: National Institute for Metrology, Beijing, Peoples Republic of China

[4] I.G. Schröder *et al.*, American Nuclear Society Winter Meeting, November 1985, Transactions, Vol. 50, p. 154.

- The ^{252}Cf source employed for the measurements has been calibrated repeatedly (5 times between 1979 and 1984) at the NBS Manganous Sulfate Bath Facility against the National Standard Ra-Be photoneutron source, NBS-1. The precision of the five measurements as determined by a least-squares fit to a 2.645-year half-life of ^{252}CF is ± 0.5 percent. The presently assigned neutron emission rate uncertainty of NBS-I is ± 0.85 percent leading to a total ^{252}Cf neutron source strength uncertainty of ± 1.1 percent.

- The measurement distance between fission chambers placed on opposite sides of the source (10 cm) was performed with a computer controlled digital cathetometer fitted with a piezoelectric sensor which operated to a precision of better than ± 0.003 cm.

- Monte Carlo and analytical calculations provided corrections for neutron scattering in the source capsule, in the fission chambers, its support structure, and in the fissionable deposit backings. Neutron return from the walls and floor of the NBS ^{252}Cf Irradiation Facility were investigated in a separate experiment and published separately.[5]

TABLE A-1. Experimental results.

Nucleus	Cross Sections or Ratio
^{235}U	1234 ± 17 mb
^{238}U	332 ± 5 mb
^{239}Pu	1844 ± 24 mb
$^{238}U/^{235}U$	0.269 ± 1.2%
$^{239}Pu/^{235}U$	1.500 ± 0.8%

8. International Intercomparison of Neutron Flux Measurement Capability at 500 keV (A. D. Carlson, R. G. Johnson, and O. A. Wasson)

A final report on the NBS participation in an international intercomparison of neutron flux measurement capability sponsored by the Consultative Committee for Ionizing Radiations (CCEMRI) at BIPM has been prepared and sent to AERE Harwell, the organizing laboratory. This intercomparison which uses a large ^{235}U fission ionization chamber allowed both linac and Van de Graaff neutron facilities to be used. The detector efficiencies measured at 500 keV at the linac and Van de Graaff facilities at NBS agree well within the 1.7 percent total error for each measurement. The final results of this intercomparison will not be available before 1987, when all participating laboratories have completed their measurements.

[5] Li Linpei, "Reflection of ^{252}Cf Fission Neutrons from a Concrete Floor," Radiation Protection Dosimetry, 5, 237 (1984).

B. DETECTORS AND FACILITIES FOR NUCLEAR DATA MEASUREMENTS

1. Development of a Standard 2.5 MeV Neutron Field (K. C. Duvall)

A 100 keV ion generator has recently been installed and tested. A beam current of 350 μA on target has been obtained, but an increase in beam current to 750 μA is expected by adjusting several fixed machine parameters. The D(d,n)^{3}He reaction will be utilized with the 100 kV deuteron beam to produce a stable 2.5 MeV neutron field. The time-correlated associated particle method will be used in a fixed setup for neutron flux determination and background elimination. Several standard neutron cross sections will be measured with this fixed setup. The measurement of the ^{235}U(n,f) cross section at 2.5 MeV is a high priority. The long term goal of this measurement program is to establish 2.5 MeV as an intermediate energy normalization point.

2. The Effect of Response Function Shape on Spectrum Unfolded Results (K. C. Duvall and K. Kudo†)

A radiation spectrum unfolding capability has been established on the NBS high-speed Central Computer. A matrix inversion unfolding code based on a version of FERD (developed at Oak Ridge National Laboratory) is being utilized. Several codes for generating response functions and simulated pulse height data have been developed. Some simulated problems have been carried out with different response function shapes for various radiation spectrums, matrix sizes, and smoothing parameters. The initial results indicate that the amplification of statistical errors in the pulse height data is affected by the shape of the response functions. Detectors utilized for radiation spectrum unfolding that have peaked response functions and a steeply decreasing efficiency with increasing energy appear to produce smaller uncertainty bands in the result. Further study will be aimed at correlating the magnitude of improvement in uncertainty with some shape parameters.

3. Continued Development of the Dual Thin Scintillator for Neutron Flux and Spectrum Measurement (K. C. Duvall, O. A. Wasson, and R. G. Johnson)

The characteristics of the Dual Thin Scintillator (DTS) continue to be investigated for possible improvement in neutron flux and spectrum measurement. The study is centered on the operation of the DTS detector in the sum-coincidence mode (previously referred to as the 1 + 2 coincidence), where a peaked response function is obtained for neutrons in the energy region of 1 to 15 MeV. The peaked pulse height response allows better peak channel definition and extrapolation to zero pulse height than obtained with typical thin plastic scintillators. The neutron flux determination with the DTS detector is comparable in accuracy to most proton recoil telescopes used in

† Electrotechnical Laboratory, Tsukuba, Japan

the same energy region. However, the DTS sensitivity to neutrons is a few orders of magnitude higher. Fast timing, a flat response with neutron energy, and possible improvements in neutron spectrum unfolding results are also useful aspects of the DTS response in the sum-coincidence mode.

4. Advances in the Use of ^{3}He in a Gas Scintillation Counter
(J. W. Behrens)

For several decades it has been suggested that the ^{3}He(n,p)T reaction should be utililzed for detecting neutrons over the entire range from thermal energies to MeV energies. In fact, this reaction has been suggested as a possible standard. The reaction has a Q value of 764 keV and is easily detected in both a gas proportional counter (gpc) and gas scintillation counter (gsc). The use of ^{3}He in gpcs is rather common today; however, its use in gscs is rare, in spite of the improved timing resolution available from the latter. A possible reason for this is the sensitivity of the uv photons to trace organic impurities in the gas. At the NBS, we have constructed a ^{3}He/Xe gsc which has been operating for over two years on its original high-purity gas fill without any continuous gas purification. This step marks a significant advance toward the possible standardization of the ^{3}He(n,p)T reaction.

Our gsc prototype has been studied at the NBS 10 MW Reactor, 3 MV Van de Graaff, and 120 MeV Linac over the past two years. The gas mixture of ^{3}He and xenon is contained in a right circular cylinder of length 250 mm and diameter 100 mm and is at a total pressure of 30 psia. Photomultiplier tubes are mounted onto the end windows consisting of pyrex glass coated on the inner surface with a 30 microgram/square cm coating of diphenylstilbene (dps). The gas mixture was varied from 5% Xe to a final 50% Xe composition. Light collection more than doubled as the composition was varied while holding the total pressure at 30 psia.

To improve the resolution of the gsc, our next gas cell will contain several changes. The new cell will have 60% of the inner surface areas dedicated to windows and the number of photomultipliers will be doubled. The cell will also be smaller, consisting of a cube with 150 mm sides. Four faces of the cube will contain window/pmt modules and the remaining two faces will be for beam entrance and exit. Wall effects will be reduced by using a collimated beam passing through a gas volume of uniform thickness.

Future measurements at the NBS might include absolute determination of the new ^{3}He(n,p)T cross section at 0.5 MeV using the NBS "Black Detector" at the 3 MV Van de Graaff facility and at 2.5 MeV using the associated particle technique at our new neutron facility. The shape of the cross section could be measured at our 120 MeV Linac using time-of-flight technique for the neutron energy range from thermal to 3 MeV. Improved gsc performance and accurate measurement of the ^{3}He(n,p)T cross section are crucial steps toward elevating this reaction to a viable standard level.

5. Utilizing the New NBS Computer to Calculate Detector Responses (J. W. Behrens)

Within the last year, the NBS has installed and made operational a CDC Cyber 855/205 computer. Efforts were made to convert our programs to it. Two Monte Carlo programs are now operating on the 855. One program calculates pulse-height responses for the DTS detector; whereas the other calculates responses for the NBS "Black" Detector. These codes run ~ 20 times faster on the Cyber 855 compared to the Harris/5 computer, used previously. A new code is presently under development to calculate the wall-effects and pulse-height response for the ^{3}He gas scintillation counter. Another code is under development to calculate fission cross sections from σ_{nf} systematics for a wide range of nuclides in the actinide range.

6. Neutron Detector Characterization (K. Kudo and A. Carlson)

Measurements have been made in the MeV energy region of the neutron response functions of a 2" diameter x 2" thick NE-213 detector at the NBS linac neutron time-of-flight facility. This detector has also been studied experimentally at PTB, Braunschweig, W. Germany and ETL, Ibaraki, Japan. These measurements should allow a determination of the consistency of results obtained under different experimental conditions and comparisons with calculated response functions. The present measurements were obtained in a two-parameter mode (pulse-height and time-of-flight). The neutron flux determined from the time-of-flight data will be compared with the result obtained from unfolding the pulse height data.

7. Conceptual Design of an Induction Linac for Neutron Research (R. G. Johnson)

A conceptual design of a linear induction accelerator for the neutron and high-LET radiation research programs at NBS has been completed. For the broadest applicability to these programs intense beams of electrons and light ions with energies of about 100 MeV are required. Consequently, the induction linac design features a final energy of 100 MeV, 250 A of electrons, and 2.5 A of protons. The pulse structure consists of pulse widths of up to 100 ns and repetition rates to 1000 Hz. The design relies heavily on the recent advances in induction linac technology especially that which has been developed at Lawrence Livermore National Laboratory. A report on the induction linac design was presented at the International Conference on Nuclear Data for Basic and Applied Science (May 13-17, 1985, Santa Fe, NM).

8. Data Acquisition System Development (R. G. Johnson)

The first computer system to replace one of our three Harris/5 systems was delivered in October 1985. This computer is a Charles River Data Systems UV 2403FT which is based on the Motorola 68000 microprocessor and the VME bus. The hardware for interfacing to CAMAC is on order. As a replacement this computer can be expected to provide approximately an order of magnitude improvement in most aspects of our data acquisition capabilities.

9. Detector Development for eV Scattering Spectrometers (R. G. Johnson)

A new detector system has been constructed for use in resonance detector spectrometers (RDS) which is intended for neutron scattering studies in the eV region. This detector system is based on the secondary emissions from the internal conversion of the primary γ rays following resonance neutron capture. A large area planar HPGe detector is used to detect X rays while conversion electrons are detected in a plastic scintillator. The scintillation detector consists of ten 5 cm x 5 cm thin (0.38 mm) plastic scintillators with nine 0.11-μm thick Au foils between each scintillator. Preliminary measurements have shown an improvement in the signal to background ratio of at least four when operating in a coincidence mode as opposed to a non-coincidence mode between the X-ray and electron detectors.

10. Neutron Driven Gamma-Ray Field (G. Lamaze, E. Boswell, D. Gilliam, D. Blackburn, and T. Williamson††)

A neutron driven gamma-ray field, similar to one in operation at SCK/CEN, Mol, Belgium, has been constructed to operate in the NBS Reactor thermal column cavity. The system consists of an extruded cadmium cylinder one mm thick and 55 mm diameter. In the thermal column cavity, the cadmium is exposed to a thermal neutron fluence rate of 3×10^{11} n/cm^{2}s. Since the cadmium is essentially black to thermal neutrons, a cadmium capture gamma ray fluence rate of about 2×10^{11} photons/cm^{2}s is produced at the center of the cylinder. This corresponds to a dose rate of close to a megarad/hr. The gamma ray field strength is determined by two methods: exposing gold foils on the cadmium surface, and by measuring the induced Cd-115 activity. These measurements provide an estimate of the neutron reaction rate in the cadmium from which a gamma ray source strength may be derived. The gamma-ray dose or fluence on the axis of the cylinder is obtained from a simple geometry calculation.

First application of the neutron driven gamma-ray field is a measurement of photofission rates in ^{238}U, ^{232}Th, and ^{237}Np and photon activation rates in indium. The photofission due to the background gamma fluence is presently estimated to be 7% of that from the cadmium source and fission from fast neutron leakage from the reactor to be 2% of the cadmium photofission rate.

††University of Virginia, Charlottesville, VA

C. NUCLEAR DATA COMPILATIONS

1. The Neutron Cross Section Standards Evaluations for ENDF/B-Vl (A. D. Carlson, W. P. Poenitz,* G. M. Hale,** and R. W. Peelle,***)

A paper on this work was given at the Santa Fe Conference on Nuclear Data for Basic and Applied Science. These evaluations are following a somewhat different process compared with that used for earlier versions of ENDF. The primary effort is concentrated on a simultaneous evaluation using a generalized least squares program, R-matrix evaluations and a procedure for combining the results of these evaluations. In the paper the evaluation procedure is outlined and preliminary simultaneous evaluation and R-matrix results are presented. Since the writing of this paper, a new procedure has been introduced for handling the thermal constants in the evaluation process. The new procedure uses the independent output quantities from a special evaluation of the thermal constants by Axton (CBNM) along with the associated correlation matrix as input to the generalized least squares analysis.

2. Critical Evaluation of X-Ray Cross Section Data in the Soft-X-Ray and Crystallographic Photon Energy Domains (J. H. Hubbell, E. B. Saloman, D. C. Creagh)

The NBS Photon and Charged Particle Data Center is now engaged in two low-energy data evaluation tasks, one examining available theoretical photoionization information, and the other examining measurement techniques and existing discrepancies in experimental results. In the first task, for photon energies 0.1 to 10 keV, Saloman[6] is numerically and graphically comparing several recent photoionization theoretical data sets with the Data Center cumulative file of measured x-ray attenuation coefficients abstracted from the literature. In the other task, focusing on photon energies 1 to 50 keV, initiated by the International Union of Crystallography in response to a suggestion from this Data Center (which now serves as task secretariat), new measurements are being stimulated in an attempt to resolve serious discrepancies in available measured attenuation coefficient data. Task chairman Creagh[7] (Australia) has fabricated and distributed well-characterized absorber samples, starting with silicon, copper, germanium, and pyrolytic graphite, to volunteer laboratories around the globe. Future tasks are a

---

* Argonne National Laboratory, Argonne-West, Idaho Falls, ID

** Los Alamos National Laboratory, Los Alamos, NM

*** Oak Ridge National Laboratory, Oak Ridge, TN

[6] E.B. Saloman, J.H. Hubbell, "Critical Analysis of Soft X-Ray Data," presented at the 3rd International Symposium on Radiation Physics, Ferrara, Italy, September 30-October 4, 1985.

[7] D.C. Creagh, J.H. Hubbell, "Problems Associated with the Measurement of X-Ray Attenuation Coefficients: Report on the IUCr X-Ray Attenuation Project, 1: Silicon," submitted to _Acta Cryst. A._

reevaluation of coherent scattering data[8] and an extension of energy-absorption coefficient tables[9] up to photon energy 100 MeV, including the effect of positron annihilation in flight in the computations.

3. Using Critically-Evaluated Data from the NBS Photon and Charged Particle Data Center (M. J. Berger)

A computer program to be run on personal computer (IBM PC or compatible) to calculate accurate photon cross sections for scattering, photo-absorption and pair production, as well as corresponding attenuation coefficients, in the energy region from 1 keV to 100 GeV has been developed. The program can be used to obtain these cross sections for a standard energy grid, or for any desired list of energies, for all elemental substances, for any compound, or for any mixture of elements and/or compounds. The program, when applied to compounds and mixtures, is based on the linear combination of data for elements, and allows production of a cross section table which includes the cross sections at and immediately below all absorption edges for all atomic constituents.

The program, written in FORTRAN 77, on an IBM PC XT, has also been tested on a Compaq PC, and will probably run on any IBM clone. The hardware requirements are modest; a 256-K memory and a 8087-coprocessor are sufficient. The computation time is typically a fraction of a minute for a cross section table (approximately 100 energies) for a given material. The required input data base is contained on a single 5-1/4" floppy disk, and a small part of another disk contains the program.

4. Photonuclear Data-Abstract Sheets (H. Gerstenberg and E. G. Fuller)

Thirteen volumes of the Photonuclear Data-Abstract Sheets,[10] including nuclei up through Thallium have been published. These abstract sheets cover most classes of experimental photonuclear data leading to information of the electromagnetic matrix element between the ground and excited states of a given nucleus. This fifteen volume work contains nearly 7200 abstract sheets and covers 89 chemical elements from hydrogen through americium. It represents a twenty-seven year history of the study of electromagnetic interactions.

---

[8] Hubbell, Veigele, Briggs, Brown, Cromer, Howerton, J. Phys. Chem. Ref. Data 4, 471 (1973); Erratum, 6,615.

[9] J.H. Hubbell, Int. J. Appl. Radiat. Isotopes, 33, 1269 (1982).

[10] E.G. Fuller and H. Gerstenberg, Photonuclear Data-Abstract Sheets, 1955-1982, NBSIR 83-2742 (1986)

UNIVERSITY OF NEW MEXICO

1. Standard Neutron Cross Sections in the 14 MeV Energy Region

J.C. Robertson, F. Ghanbari, D. Rutherford

Measurements have been completed of the $^{63}Cu(n,2n)^{62}$ and $^{65}Cu(n,2n)^{64}Cu$ cross sections. Separated isotope targets were irradiated with 14.8 MeV neutrons and the resulting ^{62}Cu and ^{64}Cu activities measured using both $4\pi\beta$-γ coincidence counting and by counting in coincidence the annihilation radiation produced following the β^+ decay of ^{62}Cu and ^{64}Cu. The variations in the neutron flux and the neutron energy were measured during each single irradiation. Good agreement was obtained for the cross section values using the two methods. However, the deviation in the $^{65}Cu(n,2n)^{64}Cu$ cross section measurements was significantly greater when the $4\pi\beta$-γ coincidence method was used than when the annihilation radiation were counted in the γ-γ coincidence system. Values of 549±11 mb and 968±20 mb were obtained using a value of 108.5 mb for the iron cross section. The reason for the discrepancy between the earlier measurements of Robertson et al (1973)[1] and Ryves et al (1978)[2] was traced to the large electron capture (43%) decay branch in the decay of ^{64}Cu and the resulting uncertainty of the efficiency of the β-counter for detecting the Auger electrons and X-rays. The values obtained for the $^{65}Cu(n,2n)^{64}Cu$ cross sections are in excellent agreement with the recent evaluation of Winkler and Ryves (1983)[3] and their measurement of this cross section. A paper entitled: "The $^{63}Cu(n,2n)^{62}Cu$ and $^{65}Cu(n,2n)^{64}Cu$ Cross Sections at 14.8 MeV" has been accepted for publication in the Annals of Nuclear Energy.

Measurements have been completed at 14.45, 14.73 and 14.80 MeV for the $^{19}F(n,2n)^{18}F$ and $^{14}N(n,2n)^{13}N$ cross sections. The agreement between the values obtained for the Fluorine cross sections and BNL325 is good but the agreement between the BNL325 values and the nitrogen cross section is not good. These results are being prepared for publication. Measurements have been completed on the $^{59}Co(n,2n)^{58}Co$ g, m state cross sections and the data is currently being analyzed.

We are currently measuring the $^{64}Zn(n,2n)^{63}Zn$, $^{64}Zn(n,p)^{64}Cu$ and $^{66}Zn(n,2n)^{65}Zn$ cross sections relative to the $^{63}Cu(n,2n)^{62}Cu$ and $^{65}Cu(n,2n)$ cross sections. Measurements are planned for the $^{58}Ni(n,2n)^{57}Ni$ and $^{92}Mo(n,2n)^{91}Mo$ cross sections.

---

[1] J.C. Robertson, B. Audric, P. Kolkowski, J. Nucl. Energy 27, 139, 1973
[2] T.B. Ryves, P. Kolkowski and K.J. Zieba, Metrologia 14, 127, 1978
[3] G. Winkler and T.B. Ryves, Ann Nucl. Energy 10, 601, 1983

2. The sulfur to hydrogen, manganese to hydrogen and boron to hydrogen therman neutron absorption cross section ratios

A. Arbildo, J.C. Robertson, T.B. Ryves*

A paper entitled: "The Sulfur to Hydrogen Thermal Neutron Absorption Cross Section Ratio," was prepared and has been accepted for publication in the Annals of Nuclear Energy. Based on a paper presented at the A.N.S. meeting in June 1983, a full co-variance - variance analysis was done of the data together with a thorough check of all computer programs and formulas used in the analysis. A value of 1.621±0.033 was obtained for the ratio. Taking the hydrogen 2200 ms^{-1} cross section as (332.55±0.69 mb) this ratio gives a value of (539±11 mb) for the 2200 ms^{-1} neutron cross section of sulfur. This supercedes the earlier provisional results of Arbildo and Robertson (1982). A similar re-analysis has been completed of the manganese to hydrogen and boron to hydrogen absorption cross section ratios. The value for the hydrogen to manganese ratio agrees well with the original measurement of Axton et al (1965)[4] at N.P.L. but does not agree with the values obtained by Smith et al (1980)[5] and Axton et al (1985)[6]. We feel that the well known $\bar{\nu}$ dilemma may just be an under estimation of errors in the manganese bath measurements of $\bar{\nu}$. A paper is in preparation and will be submitted to Annals of Nuclear Energy. The boron to hydrogen cross section ratio was found to be in excellent agreement with the recommended values of the individual cross sections. The effect of the co-variance - variance analysis was to slightly increase the estimated errors in the measurements. However, a programming error was found so that the earlier data of Arbildo and Robertson (presented at the ANS meeting, June 1984) is regarded as obsolete. Taking the hydrogen 2200 ms^{-1} cross section as 332.55±0.69 mb the measured ratios give values of (13.32±0.13 mb) and 770±6 mb) for the 2200 ms^{-1} cross sections of manganese and natural boron respectively.

3. Pulsed Neutron Activation Detector

M.S. Rowland and J.C. Robertson

The beryllium based pulsed neutron detector described by Rowland and Robertson (1984) has been successfully calibrated in the 14 MeV energy region. Theoretical predictions of the variation of the efficiency of this

* National Physical Laboratory, England

[4] E.J. Axton, P. Cross, J.C. Robertson, J. Nucl. Energy Parts A/B 19, 409, 1965

[5] J.R. Smith, S.D. Reeder and R.J. Gehrke, E.P.R.I.-N.P. 3436, 1984

[6] E.J. Axton, A. Bardell, S.J. Felgate and E.M.R. Long, Private Communication

detector with energy have been made using the M.C.N.P. Monte Carlo neutron transport code and the Tiger charged particle transport code. The use of the detector to measure the output from pulsed neutron sources and the total neutron output/burst from the Sandia National Laboratories, SPR III bare metal fast reactor, has been demonstrated. Incidental nuclear data obtained during this work, were the verification of the B-12, He-6 and Li-9 half lives. An estimate of the $^{12}C(n,p)^{12}B$ cross section yielded a value of 2 ± 1 mb in good agreement with the only previous measurement.

4. Publications

1. The $^{63}Cu(n,2n)^{62}Cu$ and $^{65}Cu(n,2n)^{64}Cu$ Cross Sections at 14.8 MeV. J.C. Robertson and F. Ghanbari. Int. Conference on Nuclear Data for Basic and Applied Science, Santa Fe, May 1985, JC10, p.49.
2. A Novel Neutron Detector for Measuring the Output of Pulsed Sources. M.S. Rowland and J.C. Robertson. Int. Conference on Nuclear Data for Basic and Applied Science, Santa Fe, May 1985, JA38, p.49.
3. The Sulfur to Hydrogen Thermal Neutron Absorption Cross Section Ratio. A. Arbildo, J.C. Robertson, T.B. Ryves. Accepted for publication in Annals of Nuclear Energy.
4. The $^{63}Cu(n,2n)^{62}Cu$ and $^{65}Cu(n,2n)^{64}Cu$ Cross Sections at 14.8 MeV. J.C. Robertson and F. Ghanbari. Accepted for publication in Annals of Nuclear Energy.

OAK RIDGE NATIONAL LABORATORY

A. CROSS SECTION MEASUREMENTS

1. Capture, Total and Reactions

a. $^{198,199,200,201,202,205}Hg(n,\gamma)$ Cross Sections and the Termination of s-Process Nucleosynthesis,[1] (H. Beer[2] and R. L. Macklin)

b. Nuclear Structure of Ca-49 Above 5 MeV and Astrophysics at 30 keV,[3] (R. F. Carlton,[4] J. A. Harvey, R. L. Macklin, C. H. Johnson, and Boris Castel[5])

The level structure of ^{49}Ca has been investigated above the neutron separation energy by measurements of the total and capture cross sections for neutron energies up to 10 MeV. Transmission data were obtained for two $^{48}CaCO_3$ samples enriched to 96% in ^{48}Ca and were analyzed in the R-matrix formalism up to 2 MeV. An upper limit of 0.07 x 10^{-4} was placed upon the s-wave strength function ($<\Gamma_n^o>/D$) and an optical model real potential was deduced from the low energy total cross section. Approximately 45% of the $2d_{5/2}$ single particle strength is observed in the region below 2 MeV neutron energy. Model configurations based on continuum shell model calculations which describe this strength and its distribution are presented. Combined low energy results are used to obtain the Maxwellian averaged capture cross section, and the result is discussed in relation to the nucleosynthesis of ^{49}Ca and the anomalous abundances observed in an inclusion of the Allende meteorite.

c. Resonance Structure of S-33 + n from Transmission Measurements,[3] (G. Coddens,[6] M. Salah,[7] J. A. Harvey, N. W. Hill, and N. M. Larson)

The total neutron cross section for ^{33}S has been determined for energies from 10 keV up to 2 MeV at the Oak Ridge Electron Linear Accelerator (ORELA) by a TOF transmission experiment. By combining these results with (n,α) data obtained at the Geel Electron Linear Accelerator (GELINA), resonance parameters (E_λ, J^π, and Γ_γ) have been determined up to 270 keV.

---

[1] Phys. Rev. C32, 738 (1985).
[2] Kernforschungszentrum Karlsruhe, Institut fur Kernphysik III, D-7500 Karlsruhe, Federal Republic of Germany.
[3] Submitted to Nuclear Physics.
[4] Middle Tennessee State University, Murfreesboro, Tennessee 37132
[5] Queen's University, Kingston, Ontario, Canada K71 3N6
[6] Commisariat a L'Energie Atomique, Laboratoire Leon Brillouin, France.
[7] Graduate student from Minia University, Egypt.

Neutron strength functions for s- and p-wave resonances were derived. The p-wave strength function is much larger than for other nuclides in this mass region (^{30}Si, ^{32}S, and ^{34}S). This is discussed in the framework of the spherical model.

d. Study of Radionuclides Created by $^{nat}Ni(\gamma,xn\ yp)$ Reactions for Bremsstrahlung Photons Produced by 140-MeV Electrons,[1] (J. K. Dickens)

Twelve radionuclides from ^{48}V to ^{57}Ni produced by photon interactions with a sample of elemental Ni have been studied to obtain relative yields of these reaction products. Precision half lives were determined for ^{56}Ni and ^{57}Ni. For ^{56}Ni, $T_{1/2} = 35.54 \pm 0.05$ hr, in agreement with the 1982 measurement of Grutter but $\sim$0.5 hr shorter than earlier measurements. Relative yields of the 127-keV, 1758-keV, and 1919-keV gamma rays following decay of ^{57}Ni were determined with respect to the 1338-keV gamma ray of that decay and the results agree better with measurements of Grutter and of Gatrousis et al. than they do with the Lederer et al. evaluation.

e. Half Life of ^{57}Ni,[2] (J. K. Dickens)

The half life of ^{57}Ni has been measured by Ge(Li) gamma-ray spectroscopy. The ^{57}Ni radioisotope was created by bremsstrahlung impinging on a sample of elemental Ni. Time change of the activity of the 1377.6-keV gamma ray following decay of ^{57}Ni was analyzed to obtain a half life of 35.54 ± 0.05 hr for ^{57}Ni.

f. The Test of Fermi Gas Model Predictions of Level Density in Xe-137,[3] (B. Fogelberg,[4] J. A. Harvey, M. Mizumoto,[5] and S. Raman)

We have studied the unbound levels of ^{137}Xe via neutron resonance reactions and β decay of ^{137}I. High-resolution neutron transmission data revealed a total of 35 resonances below a neutron energy of 500 keV. At least 27 of the resonances are p-wave resonances. The near absence of s-wave resonances in this energy region resulted in an extremely low value for the s-wave neutron strength function. The current γ-ray data complement earlier studies of γ rays and delayed neutrons following the β decay of ^{137}I. By combining all data, we have obtained a detailed picture of the level density in ^{137}Xe for a wide range of angular moments. With the exception of

---

[1]ORNL/TM-9764 (1986).
[2]Accepted by Journal of Radioanalytical and Nuclear Chemistry, Letters.
[3]Phys. Rev. C31, 2041 (1985).
[4]The Studsvik Science Research Laboratory, S-611 82 Nyko, Sweden.
[5]Japan Atomic Energy Research Institute, Tokai-muri, Naka-gun, Ibaraki-ken, Japan.

$1/2^+$ and $1/2^-$ levels, the overall agreement is good between the current data and predictions of the Fermi gas model.

g. Single-Particle $2d_{5/2}$ Strength in the $^{48}Ca + n$ Reaction,[1] (J. A. Harvey, C. H. Johnson, R. F. Carlton,[2] and B. Castel[3])

The neutron total cross section of $^{48}Ca + n$ has been measured up to 10 MeV and analyzed up to 4 MeV using the R-matrix formalism to obtain resonance parameters and potential scattering phase shifts. Very little s-wave neutron strength was observed, and the small cross section (0.5 ± 0.2 b) observed for low-energy neutrons (<150 keV) can be described by a real Woods-Saxon potential with $V_o = 47.3 \pm 0.7$ MeV, $r_o = 1.21$ fm, and a = 0.66 fm. Three strong $d_{5/2}$ resonances amounting to 45% of the single-particle width were found in the 0.8- to 2.0-MeV energy region. These results compare well with cross-section predictions from two microscopic calculations. The $p_{1/2}$, $p_{3/2}$, and $d_{3/2}$ resonance strengths are very weak (<< than the $d_{5/2}$ strength).

h. High Resolution Structural Material (n,xγ) Production Cross Sections For E_n from 0.2 to 40 MeV,[4] (D. C. Larson)

i. Resonance Neutron Capture by Manganese Below 2.5 keV,[5] (R. L. Macklin)

j. Neutron Capture by P-31,[6] (R. L. Macklin and S. F. Mughabghab[7])

Resonance parameters for $^{31}P + n$ were determined, largely from (n,γ) cross-section data measured by time of flight at the Oak Ridge Electron Linear Accelerator facility. The energy range investigated extended from 2.6 keV to 500 keV, with the lowest energy resonance found at 26.75 keV. The 30-keV stellar reaction rate is dominated by this resonance, giving 1.74 ± 0.09 mb for a temperature kT = 30 keV. The thermal capture data are examined within the framework of the direct reaction mechanism.

k. Neutron Capture Measurements on Radioactive Zr-93,[8] (R. L. Macklin)

---

[1] Phys. Rev. C32, 1114 (1985).
[2] Middle Tennessee State University, Murfreesboro, Tennessee 37132.
[3] Queen's University, Kingston, Ontario, Canada K71 3N6.
[4] Radiation Effects 92, 71 (1986).
[5] Nucl. Sci. Eng. 89, 362 (1985).
[6] Phys. Rev. C32, 379 (1985).
[7] Brookhaven National Laboratory, Upton, NY.
[8] Astrophysics and Space Science 115, 71 (1985).

l. A Self-Calibrated Neutron-Capture Measurement of the 1.15-keV Resonance of Iron.[1] (R. L. Macklin)

A measurement with thick and thin iron samples showed that $\Gamma_n\Gamma_\gamma/\Gamma$ = (54.9 $\pm$ 0.6) meV and Γ_n = (60.7 $\pm$ 0.7) meV for the 1.15-keV iron resonance.

m. Neutron Transmission Measurement and Resonance Analysis of Zr-93 from 60 to 6000 eV,[1] (R. L. Macklin, J. A. Harvey, and N. W. Hill)

Neutron transmission through a zirconium oxide sample containing the radioactive ^{93}Zr isotope was measured by pulse neutron time of flight. R-matrix parameters for some of the resonances up to 6-keV neutron energy were determined. The first resonance, for example, was found at (110.43 $\pm$ 0.01) eV with partial widths Γ_n = (348 $\pm$ 21) meV and quantum numbers $J^\pi = 2^+$.

n. Summary Talk Covering Application-Oriented Sessions,[2] (R. W. Peelle)

Conference contributions are reviewed relative to the applications of neutron cross sections to technology. The field of neutron cross section research is described as well balanced with respect to the various categories of research ranging from basic science to engineering, and the detailed data being obtained are matched to the needs and capabilities of the technology. "Victories" have been won in the last several years in the areas of nonfuel actinide cross sections, fusion charged particle reactions, the Li-7 breakup reaction, the number of neutrons emitted per fission, short-term decay heat from fission products, the shape of the fission neutron spectrum, and neutron scattering differential cross sections. Several research approaches and shifts of research concentration are welcomed as indicating favorable trends. Challenges for the future are identified in the areas of kerma data for neutron energies above 10 MeV, helium production from neutrons reacting with boron-10, the acquisition of fully satisfactory data for the resonance and thermal regions of fuel nuclides, and satisfying tightened accuracy targets for the most important cross sections. It is concluded that while the normal accuracy needs of various applications are being met, neutron cross-section scientists throughout the world need to focus attention on meeting the most important and demanding challenges.

---

[1]Submitted to Nuclear Science and Engineering.
[2]International Conference on Nuclear Data for Basic and Applied Science, Santa Fe, New Mexico, May 13-17, 1985.

o. Thermal Neutron Capture Gamma Rays from Sulfur Isotopes: Experiment and Theory,[1] (S. Raman, R. F. Carlton,[2] J. C. Wells,[3] E. T. Jurney,[4] and J. E. Lynn[5])

We have carried out a systematic investigation of γ rays after thermal neutron capture by all stable sulfur isotopes (^{32}S, ^{33}S, ^{34}S, and ^{36}S). The measurements were made at the internal target facility at the Los Alamos Omega West Reactor. We detected a larger number of γ rays: $\sim$100 in ^{33}S, $\sim$270 in ^{34}S, $\sim$60 in ^{35}S, and $\sim$15 in ^{37}S. Before developing detailed level schemes, we culled and then consolidated the existing information on energies, and J^{π} values for levels of these nuclides. Based on the current data, we have constructed detailed decay schemes, which imply that there are significant populations of 26 excited states in ^{33}S, 70 states in ^{34}S, 20 states in ^{35}S, and 7 states in ^{37}S. By checking the intensity balance for these levels and by comparing the total intensity of primary transitions with the total intensity of secondary γ rays feeding the ground state, we have demonstrated the relative completeness of these decay schemes. For strongly populated levels, the branching ratios based on the current measurements are generally better than those available from previous measurements. In all four cases, a few primary electric dipole (E1) transitions account for a large fraction of the capture cross section for that particular nuclide. To understand and explain these transitions, we have recapitulated and further developed the theory of potential capture. Toward this end, we reviewed the theory relating off-resonance neutron capture to the optical-model capture. We studied a range of model-dependent effects (nature and magnitude of imaginary potential, surface diffuseness, etc.) on the potential capture cross sections, and we have shown how experimental data may be analyzed using the expression for channel capture suitably modified by a factor that takes into account the model-dependent effects. The calculations of cross sections for most of the primary transitions in the sulfur isotopes are in good agreement with the data. Some discrepancies for weaker transitions can be explained well by an interfering compound-nucleus contribution to capture. This contribution is of the magnitude expected from statistical surveys of resonance capture data. Estimates of the cross section due to the valence-capture mechanism in s-wave resonances show that this cross section should dominate the more complicated compound-nucleus contributions.

p. Accurate Determination of the Parameters of the 292.4-eV Resonance of Zr-91 and the 301.3-eV Resonance of Zr-96,[6] (M. M. Salah,[7] J. A. Harvey, N. W. Hill, A. Z. Hussein,[7] and F. G. Perey)

---

[1]Phys. Rev. C32, 18-69 (1985).
[2]Middle Tennessee State University, Murfreesboro, Tennessee 37132.
[3]Tennessee Technological University, Cookeville, Tennessee 38501.
[4]Los Alamos National Laboratory, Los Alamos, New Mexico 87545.
[5]Atomic Energy Research Establishment, Harwell, England.
[6]International Conference on Nuclear Data for Basic and Applied Science, Santa Fe, New Mexico, May 13-17, 1985.
[7]Visiting scientists from Egypt.

q. Capture in the 1.15-keV Iron Resonance,[1] (L. W. Weston and J. H. Todd)

r. Maxwellian-Averaged Neutron-Capture Cross Sections for Te-99 and Mo-96,98,[2] (R. R. Winters[3] and R. L. Macklin)

This paper presents the Maxwellian-averaged neutron capture cross sections for ^{99}Tc and ^{95,96,97,98}Mo. An extensive temperature range (5-100 keV) is included to encompass the model calculations for ongoing s-process nucleosynthesis in red giant stars where technetium has been observed. At T = 30 keV, the most often chosen temperature for the s-process, we find (782 + 39) mb for ^{99}Tc, (292 $\pm$ 2) mb for ^{95}Mo, (112 $\pm$ 6) mb for ^{96}Mo, (339 $\pm$ 2) mb for ^{97}Mo, and (99 $\pm$ 5) mb for ^{98}Mo. These results are used to estimate the duration of the third dredge-up phase for two thermally pulsing asymptotic giant branch stars for which the technetium to molybdenum abundances have been measured.

s. The ^{189}Os(n,γ) Cross Section and Implications for the Duration of Stellar Nucleosynthesis,[2] (R. R. Winters,[3] R. L. Macklin, and R. L. Hershberger[4])

This paper reports the results of a measurement of the ^{189}Os(n,γ) cross sections over the energy ranges 200 to 500 eV and 2.6 to 500 keV. We report resonance parameters for the lower energy region and these results yield an observed s-wave mean level spacing D_0 = (3.4 $\pm$ 0.2) eV, a neutron strength function S_0 = (2.9 $\pm$ 0.5) x 10^{-4} and an average total radiation width $\langle\Gamma_\gamma\rangle$ = (83 $\pm$ 5) meV. The averaged cross sections over the upper energy range provide constraints on the optical model potential and giant dipole resonance model used to represent the cross section. For astrophysical applications we report the 30-keV Maxwellian averaged cross section $\langle\sigma_\gamma\rangle$ = (1168 $\pm$ 47) mb and use the ^{187}Re beta decay to estimate the duration of stellar nucleosynthesis as (11.0 $\pm$ 2.5) Gyr.

t. A Spherical Optical Model Potential for the Re/Os Stellar Nucleosynthesis Chronometer from s-Wave Neutrons on ^{186,187,188}Os,[5] (R. R. Winters,[3] R. F. Carlton,[6] J. A. Harvey, and N. W. Hill)

This paper reports resonance parameters and spherical optical model potentials obtained from the analyses of neutron transmission measurements for ^{186,188}Os over the incident neutron energy range 27 to 1000 eV and

[1]International Conference on Nuclear Data for Basic and Applied Science, Santa Fe, New Mexico, May 13-17, 1985.
[2]In preparation.
[3]Department of Physics, Denison University, Granville, Ohio 43023.
[4]University of Kentucky, Lexington, Kentucky.
[5]Submitted to Physical Review C.
[6]Middle Tennessee State University, Murfreesboro, Tennessee 37132.

for ^{187}Os over the range 27 to 140 eV. Multilevel R-matrix analyses of 77 s-wave resonances yielded sets of resonance parameters (E_λ,Γ_n) and the associated external (background) R-functions. The statistical properties of the resonance parameters, mean-level spacings, and strength functions are reported. The external R-functions and strength functions were used to determine spherical optical model potential (OMP) well depths, which in the case of ^{187}Os we find to be strongly dependent on the spin of the compound nucleus. These optical model well depths can be used to estimate the capture cross section of the first excited state in $^{187}Os + n$. Since this state is highly populated at stellar temperatures, the ratio of excited to ground-state capture cross sections is an important parameter in using the s-process model of stellar nucleosynthesis to determine what fraction of the abundance of ^{187}Os should be ascribed to the radiogenic decay of ^{187}Re. That fraction determines, in part, the estimate of the duration Δ of stellar nucleosynthesis to be derived from ^{187}Re beta decay. A determination of Δ for the Re/Os chronometer based on our data leads to an age of the universe of $(17 \pm 3) \times 10^9$ y.

2. Actinides

a. Fission-Product Yield Data from the US/UK Joint Experiment in the Dounreay Prototype Fast Reactor,[1] (J. K. Dickens and S. Raman)

The United States and the United Kingdom have been engaged in a joint research program in which samples of fissile and fertile actinides are irradiated in the Dounreay Prototype Fast Reactor in Scotland. The purposes of the program are to study the materials behavior and nuclear physics characteristics of selected actinide elements and/or isotopes. Samples of the actinides were incorporated in fuel pins inserted in the core. For the fission-yield measurements of this report, the samples were milligram quantities of actinide oxides of ^{248}Cm, ^{246}Cm, ^{244}Cm, ^{243}Cm, ^{243}Am, ^{241}Am, ^{244}Pu, ^{241}Pu, ^{240}Pu, ^{239}Pu, ^{238}Pu, ^{238}U, ^{236}U, ^{235}U, ^{234}U, ^{233}U, ^{231}Pa, ^{232}Th, and ^{230}Th encapsulated in vanadium holders. The samples were in core for about 14 months and were exposed to a total fluence of approximately 2.7×10^{22} fast neutrons.

Following irradiation the samples were prepared for further study using high-resolution gamma- and x-ray detectors. One series of measurements was made approximately nine months following the end of the irradiation, and a second series of measurements was made approximately six months later. Gamma rays and x-rays were observed (and quantitatively measured) corresponding to decay of several long-lived fission products, namely ^{91}Y, ^{95}Zr, ^{95}Nb, ^{103}Ru, ^{106}Rh (following decay of ^{106}Ru), ^{110m}Ag, ^{125}Sb, ^{134}Cs, ^{137}Cs, ^{141}Ce, ^{144}Ce, and ^{144}Pr, and ^{155}Eu. The gamma-ray yield data were analyzed to obtain fission-product yields. However, because of uncertainties

[1]ORNL-6266 (in preparation).

associated with various parameters of the experiment (e.g. initial sample compositions, effective fission cross sections, etc.), it was found that all of the experimental data could not be reported on an absolute basis. Instead, the yield data for the fission product ^{137}Cs were designated as monitor data for the yield data of the other fission products.

In addition to the fission-product yield data, the spectral measurements provided information on amounts of heavy elements in the samples. These results provided information on the initial sample composition as well as on actinides created during the irradiation.

The experimental relative-yield fission-product data were manipulated to provide data to compare with presently existing evaluated data. The comparisons are generally favorable and the exceptions are discussed.

b. Measurements of the Energy Dependence of Prompt Neutron Emission from U-233, U-235, Pu-239, and Pu-241 for E_n = 0.005 to 10 eV Relative to Emission from Spontaneous Fission of Cf-252,[1] (R. Gwin, R. R. Spencer, and R. W. Ingle)

c. Measurements of the Energy Dependence of Prompt Neutron Emissions from ^{233}U, ^{235}U, and ^{239}Pu for E_n = 0.0005 to 10 MeV Relative to Emission from Spontaneous Fission of ^{252}Cf,[2] (R. Gwin, R. R. Spencer, and R. W. Ingle)

A series of experiments was performed to measure the dependence on the incident neutron energy of the average number of prompt neutrons emitted per fission from ^{233}U, ^{235}U, and ^{239}Pu relative to the average number of prompt neutrons emitted in spontaneous fission of ^{252}Cf. The incident neutron-energy range was 0.0005 to 10 MeV. A white neutron source was generated by the Oak Ridge Electron Linear Accelerator, and the energies of the neutrons incident on the fissile samples were determined by time-of-flight techniques. In each experiment the samples, including the ^{252}Cf standard, were contained in a fission chamber surrounded by a large volume (0.91 m^3) of liquid scintillator loaded with gadolinium. The fission chamber detected the fission events, and the scintillator detected the accompanying prompt neutrons. The resulting data were analyzed to yield: $R_p(E) = \bar{\nu}_p(E)(\text{fissile})/\bar{\nu}_p(^{252}Cf)$. For ^{235}U and ^{239}Pu our results overlap, within the experimental uncertainty, the results of the evaluation of Manero and Konshin (1972), and in the case of ^{235}U our data show the same general structure apparent in the evaluation up to 0.5 MeV. Our $R_p(E)$ for ^{233}U does not show the structure near 0.2 MeV obtained by Manero and Konshin.

d. Neutron Total Cross Section of Pu-240 Below 6 eV and the Parameters of the 1.0-eV Resonance,[1] (R. R. Spencer, J. A. Harvey, N. W. Hill, and L. W. Weston)

---

[1] International Conference on Nuclear Data for Basic and Applied Science, Santa Fe, New Mexico, May 13-17, 1985.
[2] Submitted to Nuclear Science and Engineering.

e. Resolved Resonance Parameters for 238-U from 1 to 10 keV,[1] (D. K. Olsen)

Neutron widths for 676 resonances from 0.9 to 10.0 keV are reported from a consistent least-squares simultaneous-sample shape analysis of the Oak Ridge Electron Linear Accelerator (ORELA) 150-m four-sample ^{238}U transmission data. The neutron widths from 0.9 to 6.0 keV from this improved analysis are meant to supersede previously published values. These resonances give an s-wave strength function of about 0.94×10^{-4} from 0 to 10 keV.

f. Neutron Capture Cross Section of Americium-243,[2] (L. W. Weston and J. H. Todd)

The neutron capture cross section of ^{243}Am was measured from 258 eV to 92 keV. The relative capture cross sections were normalized to 74.8 b at 0.0253 eV from ENDF/B-V. Agreement with the one previous measurement in the keV neutron energy range is reasonably good ($\sim$8%). These results are needed for calculating the buildup of higher actinides in operating reactors.

3. Experimental Techniques

a. Calculations Pertaining to the Design of a Prebuncher for a 150-MeV Electron Linear Accelerator. III. Comparisons with Experimental Data,[3] (R. G. Alsmiller, Jr., F. S. Alsmiller, and T. A. Lewis)

b. An NE-213-Scintillator-Based Neutron Detection System for Diagnostic Measurements of Energy Spectra for Neutrons Having Energies $\geq$0.8 MeV Created During Plasma Operations at the Princeton Tokamak Fusion Test Reactor,[4] (J. K. Dickens, N. W. Hill, F. S. Hou,[5] J. W. McConnell, R. R. Spencer, F. Y. Tsang[6])

A system for making diagnostic measurements of the energy spectra of $\geq$0.8-MeV neutrons produced during plasma operations of the Princeton Tokamak Fusion Test Reactor (TFTR) has been fabricated and tested and is presently in operation in the TFTR Test Cell Basement. The system consists

---

[1]Submitted to Nucl. Sci. Eng.
[2]Nucl. Sci. Eng. 91, 444 (1985).
[3]Particle Accelerators 17, 215-226 (1985).
[4]ORNL/TM-9561 (August 1985).
[5]Princeton Plasma Physics Laboratory, Princeton University, Princeton, New Jersey.
[6]Idaho National Engineering Laboratory, Idaho Falls, Idaho.

of two separate detectors, each made up of cells containing liquid NE-213 scintillator attached permanently to RCA-8850 photomultiplier tubes. Pulses obtained from each photomultiplier system are amplified and electronically analyzed to identify and separate those pulses due to neutron-induced events in the detector from those due to photon-induced events in the detector. Signals from each detector are routed to two separate Analog-to-Digital Converters, and the resulting digitized information, representing (1) the raw neutron-spectrum data and (2) the raw photon-spectrum data, are transmitted to the CICADA data-acquisition computer system of the TFTR. Software programs have been installed on the CICADA system to analyze the raw data to provide moderate-resolution recreations of the energy spectrum of the neutron and photon fluences incident on the detector during the operation of the TFTR. A complete description of, as well as the operation of, the hardware and software is given in this report.

c. Majority-Logic NE-110 Detector for keV Neutrons;[1] (N. W. Hill, J. A. Harvey, D. J. Horen, G. L. Morgan,[2] and R. R. Winters[3])

B. DATA ANALYSIS

1. Theoretical

a. Pairing Correction of Particle-Hole State Densities for Two Kinds of Fermions,[4] (C. Y. Fu)

b. Simplified Spin Cutoff Factors for Particle-Hole Level Densities in Precompound Nuclear Reaction Theory,[5] (C. Y. Fu)

A logical first step toward incorporating a precompound nuclear reaction theory in the Hauser-Feshbach formalism, widely used for compound reaction cross-section calculations, is to develop unified level density formulas needed for the two parts of the calculation. In the present paper, an advanced formulation of the spin cutoff factors for particle-hole level densities, based on the uniform pairing model, is simplified. This simplified formula, explicitly dependent on the excitation energy and the exciton number, is easy to use for the precompound part of the calculation and is shown to be consistent with the formula used for the Hauser-Feshbach part of the calculation. Differences between the present approach and a previous one are analyzed.

---

[1]Nuclear Science NS-32, 367 (1985).
[2]Los Alamos National Laboratory, Los Alamos, New Mexico 87545.
[3]Department of Physics, Denison University, Granville, Ohio 43023.
[4]International Conference on Nuclear Data for Basic and Applied Science, Santa Fe, New Mexico, May 13-17, 1985.
[5]Submitted to Nuclear Science and Engineering.

c. ℓJ-Dependence of the Real Optical Potential Near Neutron Threshold,[1] (D. J. Horen, C. H. Johnson, and A. D. MacKellar[2])

The unique features of low-energy neutron scattering have been used to observe an ℓJ-dependence of the depth of the real volume optical potential near threshold for $^{208}Pb + n$. At E = 0.5 MeV the s- and d-wave potentials are ∿3 MeV deeper than those for the p-waves.

d. Energy Average of the Scattering Matrix in Picket-Fence Models,[3] (C. H. Johnson, C. Mahaux,[4] and R. R. Winters[5])

The optical-model potential at low energy is defined by the requirement that it yields a suitably defined energy average of the scattering function. It is argued that the quantities which appear in the expression for this energy average derived by Lane and Thomas in the framework of R-matrix theory can be identified with those which appear in a convenient parametrization of the fine structure cross section. The accuracy of this identification is illustrated with the help of various picket-fence models. We discuss the independence of the results with respect to the size of the energy domain covered by the experimental data and to the nature of the R-matrix boundary parameters. Also we discuss terms that can be included if one wishes to discuss fluctuations about a smooth average.

e. Optical Models in the Resolved Resonance Region,[6] (C. H. Johnson)

Using modern time-of-flight facilities the resolved resonance region can be extended upward to about 1 MeV for nuclei with $A < 60$ and for heavier nuclei near closed shells. A careful measurement both on and off resonances followed by an R-matrix analysis yields partial wave scattering functions which are easily energy averaged for comparison to those from an optical model. A comparison of average scattering functions of opposite parities can provide information on surface effects because the wave functions for different parities are out of phase at the surface. Thus, a unique supplement is made to the information that can be obtained from other types of measurements for both the bound region and higher energies.

f. Uncertainty Propagation from Raw Data to Final Results,[7] (N. M. Larson)

---

[1] Physics Letters, 161B(4,5,6), (1985).
[2] University of Kentucky, Lexington, KY 40506
[3] Physical Review C32, 359 (1985).
[4] Institut de Physique, Universite de Liege, 4000 Liege, Belgium.
[5] Denison University, Granville, Ohio 43023.
[6] Invited paper to be published in proceedings of Specialists Meeting on the Use of the Optical Model for the Calculation of Cross Sections Below 20 MeV, Paris, November 1985.
[7] International Conference on Nuclear Data for Basic and Applied Science, Santa Fe, New Mexico, May 13-17, 1985.

g. Analysis of Neutron Data in the Resonance Region Via the Computer Code SAMMY,[1] (N. M. Larson)

h. Updated Users' Guide for SAMMY: Multilevel R-Matrix Fits to Neutron Data Using Bayes' Equations,[2] (N. M. Larson)

In August of 1984 the users' guide for version P of the multilevel multichannel R-matrix code SAMMY was published. Recently, major changes within SAMMY have led to the creation of version O, which is documented in this report. Among these changes are: (1) an alternative matrix-manipulation method for use in certain special cases; (2) division of theoretical cross-section generation and broadening operations into separate segments of the code; (3) an option to use the multilevel Breit-Wigner approximation to generate theoretical cross sections; (4) new input options; (5) renaming all temporary files as SAM??.DAT; (6) more sophisticated use of temporary files to maximize the number of data points that may be analyzed in a single run; and (7) significant internal restructuring of the code in preparation for changes described here and for planned future changes.

i. Optical Model for Low-Energy Neutrons on ^{60}Ni,[3] (R. R. Winters,[4] C. H. Johnson, and A. D. MacKellar[5])

A previously published s-wave scattering function for 1-450 keV neutrons on ^{60}Ni is averaged for comparison to the scattering from an optical model potential. The scattering length R' is found to be 5.5 $\pm$ 0.03 fm at 225 keV. Averaging of the scattering function (both by integration with a normalized weight function and by use of an analytical approximation) produces shape elastic and compound nucleus cross sections which are then fitted by adjustment of the real and imaginary well depths in both spherical and vibrational optical models with a Woods-Saxon real well (r_o = 1.21 fm, α_o = 0.66 fm) and a surface derivative imaginary well (r_D = 1.21 fm, α_D = 0.48 fm). The fitted depths are V_o = 48 MeV and W_D = 29 MeV for the spherical potentials, and V_o = 50 MeV and W_D = 24 MeV for the vibrational potentials. Uncertainties are $\pm$5 MeV. From an upper limit on the p-wave strength function the W_D for p waves is found to be 1.5 MeV for the vibrational model. Thus, the imaginary potential is ℓ dependent for the assumed geometry. For s waves the vibrational model gives a good fit also with W_D = 1.5 MeV and V_o = 54.4 MeV; however, with that V_o the 2p states are bound too deeply in ^{61}Ni and the 3s size resonance is predicted at too low a mass.

[1]Proc. International Conference on Nuclear Data for Basic and Applied Science, Santa Fe, New Mexico, May 13-17, 1985.
[2]ORNL/TM-9179/R1 (April 1985).
[3]Physical Review C32, 384 (1985).
[4]Denison University, Granville, Ohio 43023.
[5]University of Kentucky, Lexington, Kentucky 40506.

2. ENDF/B Related Work

a. R-Matrix Analysis of the Pu-239 Cross Sections up to 600 eV,[1] (H. Derrien,[2] G. de Saussure, R. B. Perez, N. M. Larson, and Roger L. Macklin)

The ENDF/B-V representation of the ^{239}Pu neutron cross sections in the resonance region is unsatisfactory: the single-level formalism is used, necessitating a structured file-3 contribution. Furthermore, M. Salvatores, R. N. Hwang, and others have stressed the need to extend the resolved resonance region above the present ENDF/B limit of 300 eV for the calculation of Doppler effect and self-shielded group cross sections. The purpose of our work is to improve the representation of the Pu-239 cross sections by using a multilevel formalism (which avoids the need for the file-3 contributions) and by extending the resolved resonance range from 300 eV up to 600 eV. The present resonance analysis is based on the Reich-Moore multilevel formalism and was performed with the Bayesian code SAMMY. The resonance parameters published in 1974 by Derrien were used as prior information. More than 200 levels and 1000 resonance parameters are included in the analysis. The present resonance analysis improves upon the ENDF/B-V description of the Pu-239 cross sections by using a multilevel formalism, which avoids the use of the awkward structured file 3, and by extending the resolved resonance description to 600 eV. Furthermore, the parameters obtained in this work describe accurately and consistently the experimental data, hence providing a firm basis for reactor design calculations.

b. Impact of 57-Fe on Neutron Penetration in Thick Sodium-Iron Shields,[3] (C. Y. Fu and D. T. Ingersoll)

The latest release of the VITAMIN-E multigroup cross-section library contains two different versions of neutron cross sections for natural iron, one based on ENDF/B-V MOD-1 and the other on MOD-3. The difference between the two versions is that ENDF/B-V MOD-3 is the first ENDF/B iron cross-section set to include inelastic level excitation functions for ^{57}Fe. Even though natural iron contains only 2.1% ^{57}Fe, as opposed to 91.8% ^{56}Fe, ^{57}Fe inelastic scattering cross sections have been found to affect significantly the results for thick sodium-iron geometries. On the basis of this analysis, the following conclusions can be drawn: (1) In neutron penetration calculations through thick steel regions, ^{57}Fe can be ten times more important than is indicated by its isotopic abundance in natural iron. (2) The 14.4-keV inelastic level of ^{57}Fe is sufficiently important that it may be worthwhile to perform a measurement of this cross section to validate the ENDF/B-V MOD-3 value, which was obtained from nuclear model calculations. (3) Shielding analyses done with iron cross sections predating ENDF/B-V MOD-3 should be reviewed and may need to be revised.

---

[1] To be presented at the American Nuclear Society Meeting, Reno, Nevada, June 15, 1986.
[2] CEA, Cadarache, France.
[3] Trans. Am. Nucl. Soc. 50, 470 (1985).

c. R-Matrix Analysis of the Pu-239 Neutron Cross Sections,[1] (G. de Saussure, R. B. Perez, and Roger L. Macklin)

d. Calculated Neutron-Induced Cross Sections for $^{63,65}Cu$, $^{58,60}Ni$, and ^{52}Cr from 1 to 20 MeV and Comparisons with Experiments,[1] (D. M. Hetrick, C. Y. Fu, and D. C. Larson)

e. Ni-58 + n Transmission Capture and Differential Elastic Scattering Data Analysis in the Resonance Region,[1] (C. M. Perey, F. G. Perey, J. A. Harvey, N. W. Hill, and R. L. Macklin)

f. Status of the Parameters of the 1.15-keV Resonance of Fe-56,[1] (F. G. Perey)

g. Multilevel Analysis of the Low Energy ^{239}Pu Cross Sections,[2] (R. B. Perez, G. de Saussure, N. M. Larson, and Roger Macklin)

Several sets of ^{239}Pu neutron cross-section data have been analyzed with the R-matrix Bayesian program SAMMY. The cross sections computed with the multilevel parameters are consistent with recent fission and transmission measurements, as well as with older capture and alpha measurements. The Reich-Moore type R-matrix resonance parameters were converted into equivalent Adler-Adler type parameters using the computer program POLLA.

---

[1]Proceedings of the International Conference on Nuclear Data for Basic and Applied Science, Santa Fe, New Mexico, May 13-17, 1985.
[2]Accepted by Nuclear Science and Engineering.

OHIO UNIVERSITY

A. MEASUREMENTS

1. Neutron Elastic and Inelastic Differential Cross Sections from ^{10}B.* (E. Sadowski, D. Resler, H. Knox and R. Lane)

Differential cross sections for $^{10}B(n,n)^{10}B$ and $^{10}B(n,n')^{10}B^*$ (0.718, 1.740, 2.154, 3.587) have been obtained for incident neutron energies between 5.0 MeV $\leq E_n \leq$ 5.75 MeV in 0.25 MeV steps. At each energy measurements were made at eleven angles between 18° and 160°. The scattering sample used in these measurements was 99.6% isotopically pure ^{10}B. The data have been corrected for sample attenuation, dead time and air scattering. Multiple scattering corrections are presently underway.

2. Partial Kerma Factors for Neutron Interactions with ^{12}C at $20 \leq E_n \leq 65$ MeV.** (R.W. Finlay, Ali S. Meigooni***, J.S. Petler† and J.P. Delaroche††)

New measurements of elastic and inelastic scattering of 20-26 MeV neutrons from ^{12}C have been carried out and analyzed in terms of a deformed optical model potential. Results of these analyses have been compared with other recent differential and total neutron scattering measurements and with proton scattering data in order to develop a consistent representation of the energy dependence of the n-^{12}C interaction over a broad energy range. Applications of the data and the model to problems in neutron dosimetry have been investigated.

3. Nucleon-Induced Excitation of Collective Bands in ^{12}C.** (Ali S. Meigooni***, R.W. Finlay, J.S. Petler† and J.P. Delaroche††)

Detailed differential elastic and inelastic neutron scattering data for ^{12}C at E_n = 20-26 MeV were obtained and analyzed in terms of a deformed optical potential and rotation-vibration interaction in a coupled-channel formalism. All well-established states in ^{12}C up to 15 MeV excitation energy are observed in the experiment. Additional neutron scattering, total and reaction cross section data for $20 < E_n < 100$ MeV are incorporated into

---

* Work supported by U.S. Department of Energy.

** Work supported by the National Cancer Institute.

*** Present address: University Hospital and Clinic, Minneapolis, MN 55455

† Present address: British Petroleum Research Center, Middlesenc, Great Britain

†† Present address: Center d'Etudes de Bruyéres-le-Chatel, B.P. No. 12, 91680 Bruyéres-le-Chatel, France

the analysis to determine more precisely the energy dependence of the deformed potential well parameters. A newly developed formalism for the treatment of radius, diffuseness and potential depth oscillations of a nucleus with a deformed equilibrium shape is compared with both (p,p') and (n,n') data. The resulting model provides an improved description of earlier (p,p') data and confirms K^{π} assignments for some excited bands in ^{12}C.

4. Structure of ^{19}O from Measurement and R-Matrix Analysis of $\sigma(\theta)$ for $^{18}O(n,n)^{18}O$ and $^{18}O(n,n')^{18}O^*$ (1.98 MeV).* (P.E. Koehler**, H.D. Knox, D.A. Resler, R.O. Lane and G.F. Auchampaugh**)

Differential cross sections for neutrons elastically scattered from ^{18}O and inelastically scattered to the first excited state of $^{18}O^*$ (1.98 MeV) have been measured at forty-two incident energies for $5.0 < E_n < 7.5$ MeV corresponding to excitation energies in ^{19}O of 8.7 to 11.1 MeV. The cross sections were measured at eleven laboratory angles per energy from 20° to 160° and show considerable resonance structure. These new elastic and inelastic 1.98 MeV level data have been analyzed together with previously published cross sections for $0 < E_n < 2.5$ MeV using a multilevel-multichannel R-matrix program to determine J, π, E_λ and $\gamma_{\lambda c}$ for states in ^{19}O. The new assignments are compared to previous work where possible. Several previous assignments for resonances in the $0 < E_n < 2.5$ MeV region were verified, and disagreements over the J^{π} assignments for several levels in this region have been resolved. A total of fourteen new J^{π} assignments were made in the $5 < E_n < 7.5$ MeV region. An attempt was made to identify T = 3/2 analog states in ^{19}F for the newly assigned levels in ^{19}O. On the basis of spin, parity, excitation energy and a comparison of reduced neutron widths in ^{19}O with reduced proton widths in ^{19}F, six previously-identified T = 3/2 analogs were verified and eight new T = 3/2 analogs were tentatively assigned.

5. Identification of New Excited Levels in ^{28}Si Through the $^{27}Al(d,n)^{28}Si$ Reaction.* (H. Satyanarayana, M. Ahmad†, C.E. Brient, P.M. Egun, S.L. Graham, S.M. Grimes and S.K. Saraf)

Neutron spectra from the $^{27}Al(d,n)^{28}Si$ reaction have been measured with an energy resolution of better than 10 keV. Bombarding energies ranged from 2.5 to 8 MeV, permitting various regions of excitation in ^{28}Si to be populated with 1 to 3 MeV outgoing neutrons. Levels corresponding to contaminants could be identified by the energy shift with angle. We have identified four new levels below 13 MeV and 22 new levels above 13.4 MeV. The (d,n) reaction at low bombarding energies appears to be nonselective;

---

* Work supported by U.S. Department of Energy.
** Present address: Los Alamos National Laboratory, Los Alamos, NM 87545
† Present address: TRIUMF, Vancouver, B.C., Canada V6T 2A3

we observe every previously known level as well as the new ones, with the only exception being those which are unresolved ($E_1 - E_2 \lesssim 8$ keV) from neighboring levels. We are not able to deduce the spins and parities of these levels from the present data.

6. Nucleon Scattering from ^{34}S and the Relative Sign of Neutron and Proton Transition Matrix Elements for the ($0 \to 2^+_2$) Transition.* (R. Alarcon**, J. Rapaport, R.T. Kouzes***, W.H. Moore*** and B.A. Brown†)

Data obtained by scattering 29.8 MeV protons and 21.7 MeV neutrons from ^{34}S are used in a consistent analysis to obtain values and relative signs for proton (M_p) and neutron (M_n) multipole matrix elements for E2 transitions to the first three 2^+ states in ^{34}S. The data for the 0^+ (g.s.) $\to 2^+_2$ (3.30 MeV) transition are consistent only with the assumption of the same relative sign of M_p and M_n.

7. Cross Sections and Spectra for (n,xp) and (n,xα) Reactions on ^{58}Ni ^{60}Ni at Energies of 9.4 and 11 MeV.†† (S.L. Graham, M. Ahmad†††, S.M. Grimes, H. Satyanarayana and S.K. Saraf)

Cross sections and spectra for (n,xp) and (n,xα) reactions on ^{58}Ni and ^{60}Ni at energies of 9.4 and 11 MeV and for ^{58}Ni at 8 MeV have been measured. This energy range spans the threshold for the (n,n'p) reaction. Based on a comparison of Hauser-Feshbach calculations with the measured spectra, this reaction provides a large fraction of the proton spectrum at 11 MeV for ^{58}Ni. Both (n,xp) and (n,xα) processes appear to be due largely to compound nuclear processes. Comparison of the measurements obtained here and those previously published at 15 MeV with calculations allows us to infer information about the nuclear level densities. Cross sections for (n,d) reactions are sufficiently small that only upper limits can be derived from them.

8. Direct Neutron Scattering from ^{182}W and ^{184}W*. (J.R.M. Annand‡ and R.W. Finlay)

Differential elastic and inelastic neutron scattering cross sections for ^{182}W and ^{184}W have been measured at incident energies 4.87 and 6.00 MeV. Cross sections for the first (0^+, 2^+, 4^+, 6^+), second (0^+, 2^+), and some higher excitations are presented. Angular distributions exhibit

---

* Work supported in part by the National Science Foundation.
** Present address: University of Illinois, Champaign, IL 61820
*** Present address: Princeton University, Princeton, New Jersey 08547
† Present address: Michigan State University, East Lansing, MI 48824
†† Work supported by U.S. Department of Energy.
††† Present address: TRIUMF, Vancouver, B.C., Canada V6T 2A3
‡ Present address: University of Glasgow, Glasgow, Scotland G75 0QU

direct reaction characteristics, suggesting that compound cross sections for these states are small. This is supported by statistical-model calculations. Coupled-channel calculations of cross sections are made using a phenomenological deformed optical potential. Quadrupole and hexadecapole deformations have been searched to optimize fits. The necessary of introducing a β_6 deformation is investigated. Electric multipole transition matrix elements, used in the coupled-channel analysis, are obtained from the rotation-vibration model and the dynamic-deformation theory.

9. Anomalous Behavior of the n+^{208}Pb Potential Near the Fermi Energy.*
(R.W. Finlay, J.R.M. Annand**, J.S. Petler*** and F.S. Dietrich†)

New measurements of elastic neutron scattering from ^{208}Pb and ^{209}Bi at E_n < 7 MeV have revealed the detailed shape of the Fermi surface anomaly in the nucleon-nucleus potential in an energy region inaccessible by proton scattering. The resulting energy dependence of the real potential strongly supports recent dispersion-theory corrections to the Hartree-Fock mean field.

10. A Low-Energy Optical-Model Analysis of ^{208}Pb and ^{209}Bi.*
(J.R.M. Annand**, R.W. Finlay and F.S. Dietrich†)

New measurements of differential elastic and inelastic neutron scattering cross sections for ^{208}Pb and ^{209}Bi at energies 4-7 MeV were obtained. Elastic scattering data have sufficient accuracy to reveal clearly differences between cross sections in these neighboring nuclei. Phenomenological and microscopic, spherical, optical-model analyses are performed with compound elastic scattering accounted for using the statistical model. The methods of Moldauer, Tepel et al. and Hofmann et al. for calculating the latter are compared. The improvement to the low-energy phenomenological description resulting from inclusion of a surface-peaked real component to the potential was examined. A possible connection between the observed energy dependence of the real potential and the anomalous behavior of the nucleon reduced mass near the Fermi energy is discussed. Microscopic calculations of the optical potential are made using the methods of Brieva and Rook and Jeukenne et al. Inelastic scattering cross sections for the $7/2^-$ and $13/2^+$ single-particle states of ^{209}Bi and the first two excited states of ^{208}Pb, the 3^- and 5^- collective states, are presented. Direct inelastic scattering from these states is calculated using the DWBA or coupled-channel formalism. Compound inelastic scattering is calculated using the statistical model.

---

* Work supported in part by the National Science Foundation.

** Present address: University of Glasgow, Glasgow, Scotland G75 0QU

*** Present address: British Petroleum Research Center, Middlesenc, Great Britain

† Present address: Lawrence Livermore National Laboratory, Livermore, Ca 94550

11. Total Charged-Particle Emission Cross Sections for 9.4 and 11 MeV Neutron Bombardment of Type 316 Stainless Steel.* (Munir Ahmad**, S.L. Graham, S.M. Grimes, H. Satyanarayana, S.K. Saraf and S. Stricklin***)

Total cross sections for the emission of protons and alpha particles have been measured at 9.4 and 11 MeV neutrons incident on a 4.11 mg/cm^2 thick Type 316 stainless steel target. A newly developed charged-particle time-of-flight spectrometer was used to obtain (n,xp) and (n,xα) cross section data. The measured gas production cross sections have been compared with the values predicted on the basis of measured or calculated cross sections of the constituent materials.

B. MODEL CALCULATIONS AND ANALYSIS

1. Use of Shell Model Calculations in R-Matrix Studies of Neutron-Induced Reactions.* (H.D. Knox, D. Resler and R.O. Lane)

R-matrix analyses of neutron-induced reactions for many of the lightest p-shell nuclei are difficult due to a lack of distinct resonance structure in the reaction cross sections. Initial values for the required R-matrix parameters, E_λ and $\gamma_{\lambda c}$ for states in the compound system, can be obtained from shell model calculations. In the present work, the results of recent shell model calculations (1) for the lithium isotopes have been used in R-matrix analyses of ^{6}Li+n and ^{7}Li+n reactions for $E_n < 8$ MeV. Consequences of the shell model predictions for the level structure of ^{7}Li and ^{8}Li on the ^{6}Li+n and ^{7}Li+n reaction mechanisms and cross sections are being studied. Applications of this type of study to a broader group of nuclei will be investigated.

2. The Ohio University Shell Model Code CRUNCHER.* (D.A. Resler, S.M. Grimes and R.O. Lane)

The prediction of cross sections by the use of shell model calculations in conjunction with the R-matrix has proven to be very successful (2). To facilitate this type of study the Ohio University Shell Model Code CRUNCHER (3) is now operational on an in-house dedicated HP 1000 A 900

---

* Work supported by U.S. Department of Energy.
** Present address: TRIUMF, Vancouver, B.C., Canada V6T 2A3
*** Summer intern from Mansfield State University, Mansfield, PA 16933.
(1) D. Resler, H.D. Knox, R.O. Lane and S.M. Grimes, Bull. Am. Phys. Soc. 29, 1036 (1984).
(2) H.D. Knox, Conf. Nuclear Cross Sections for Basic and Applied Science, Santa Fe, 1985.
(3) D.A. Resler, S.M. Grimes and R.O. Lane, BAPS 28, 971 (1983).

computer system. Recent modifications of the code allow for greater flexibility in its use. The present limitations of the code will be discussed. Also the current status of our calculations for the p-shell nuclei will be reported.

3. Gamow-Teller Matrix Elements for the $^{11}B(p,n)^{11}C$ Reaction at $E_p \approx 26$ MeV. (S.M. Grimes, J.D. Anderson**, J.C. Davis**, R.H. Howell**, C. Wong**, A.W. Carpenter***, J.A. Carr*** and F. Petrovich***)

New data are presented for the $^{11}B(p,n)^{11}C$ reaction taken at 1 MeV intervals for proton bombarding energies in the E_p = 16-26 MeV range. In the experiment, final states in ^{11}C up to $E_x \simeq 10$ MeV were clearly identified and differential cross sections were extracted for the first four levels in ^{11}C. The E_p = 26 MeV data are examined in microscopic distorted-wave approximation calculations using the wave function of Cohen and Kurath to describe the states in ^{11}B and ^{11}C and using the G matrix interaction of Bertsch et al. for the effective nucleon-nucleon interaction. Gamow-Teller matrix elements for transitions to excited states in ^{11}C are extracted on the basis of these calculations, thus extending the information on Gamow-Teller matrix elements in the mass 11 system beyond the ground state matrix element known from β decay. Throughout, the results are contrasted with existing information from electromagnetic studies of ^{11}B. It is concluded that the Cohen-Kurath model places too much Gamow-Teller strength in the low lying states of the mass 11 systems and not enough strength at higher excitation energies. In addition, this model underestimates the net contribution to M1 matrix elements from the isoscalar spin and current and isovector current parts of the M1 operator.

4. Microscopic Optical Model Analysis of Nucleon Scattering from Light Nuclei.† (J.S. Petler††, M.S. Islam, R.W. Finlay and F.S. Dietrich**)

Differential cross sections for neutron elastic scattering from ^{12}C, ^{14}N, ^{16}O and ^{27}Al have been measured in the energy range 18-26 MeV. These data, together with previously published neutron and proton data for these nuclei and for ^{12}C in the energy region 20 to 65 MeV, have been analyzed in terms of two microscopic optical potentials. The spherical

---

** Present address: Lawrence Livermore National Laboratory, Livermore, CA 94550

*** Present address: Department of Physics, Florida State University, Tallahassee, FL 32306

† Work supported in part by the National Cancer Institute, DHHS, and by the National Science Foundation.

†† Present address: British Petroleum Research Center, Middlesenc, Great Britain

potential derived from the work of Jeukenne, Lejeune and Mahaux provides a consistent representation of the differential data, provided the imaginary central potential is renormalized. Predictions from the interaction of Brieva and Rook give less satisfactory agreement. In particular, there is a significant overprediction of the forward angle data below $\sim$ 25 MeV and an underprediction above $\sim$ 35 MeV.

5. Single-Particle Effects in Precompound Reactions: Influences of the $f_{7/2}$ Shell Closure. (M. Blann*, S.M. Grimes, L.F. Hansen*, T.T. Komoto*, B.A. Pohl*, W. Scobel**, M. Trabandt** and C. Wong*)

We present angle integrated spectra for the (p,n) reaction with 25 MeV protons on targets of $^{50,52,53}_{24}Cr$ and on $^{58}_{26}Fe$, $^{59}_{27}Co$, $^{60}_{28}Ni$ and $^{63}_{29}Cu$. These spectra are compared with two-quasiparticle state densities for proton-particle--neutron-hole configurations calculated using Nilsson-model single-particle energies. The influence of shell structure of the precompound spectra, previously shown for the $g_{9/2}$ neutron shell closure, is shown here for the $f_{7/2}$ neutron and proton shells. Semiquantitative agreement is shown between experimental results and calculated two-quasiparticle densities. The parameter space of pairing energy, deformation and oscillator stiffness is explored. Precompound spectra near shell closure are in better agreement with particle state densities from Nilsson-model considerations than with results from more commonly used equidistant spacing models.

6. Comparison of Lanczos Methods and Moment Methods in Calculating Nuclear Level Densities. (B. Strohmaier***, S.M. Grimes and S.D. Bloom*)

Special distribution methods have been used to make nuclear level-density calculations with full inclusion of two-body forces. The demands on computer time are large, however, and the information obtained in the very lowest energy region is not as extensive as would be desirable. We present calculations of the level density of ^{20}Ne obtained with an alternative, but closely related, procedure based on the Lanczos algorithm. In addition, we discuss the possibility of accelerating the calculation of the moments for conventional spectral distribution calculations. Very encouraging results for both the Lanczos technique and the revised moment algorithm are obtained; some remaining problems are examined.

---

* Present address: Lawrence Livermore National Laboratory, Livermore, CA 94550

** Present address: Universität Hamburg, D-2000 Hamburg, Federal Republic of Germany

*** Present address: Institut für Radiumforschung und Kernphysik Boltzmanngasse 3, Austria

PACIFIC NORTHWEST LABORATORY

A. DELAYED NEUTRON STUDIES (Reeder, Warner, Edmiston*, Gill**, Piotrowski**)

The TRISTAN on-line mass separator facility at Brookhaven National Laboratory is being used to measure half-lives and delayed neutron emission probabilities (P_n) of fission-product delayed-neutron precursors. Because delayed neutron emission can be detected with high sensitivity in the presence of large intensities of beta and gamma radiations, we also use neutron counting to search for new isotopes among the very neutron-rich fission products.[1]

Mass separated beams of fission products from TRISTAN were deposited on an aluminized Mylar tape in the center of a high efficiency neutron counter. Beta particles at the deposition point were counted with a totally depleted surface barrier Si detector. The experiments consisted of simultaneous multiscaler measurements of growth and decay curves for the beta counting rate, neutron counting rate, beta-neutron coincidence rate, and accidental coincidence rate. The coincidence rate was measured by a simple overlap coincidence module where the beta pulse input was stretched to 40 μs by a gate and delay generator to allow for the neutron residence time in the polyethylene moderated neutron counter. The beta singles, neutron singles, and coincidence growth and decay curves were analyzed by the least square fitting program MASH to give the saturation counting rate of each component in the sample. Half-lives were varied by an iterative procedure to find the best fits. The coincidence counting rate is particularly useful because the P_n can be determined independently of the beta counting efficiency.[1]

The half-lives and P_n values are presented in Table A-1. The P_n values are normalized to the P_n value of ^{98}Rb of 13.6 ± 0.9%. We have assumed equal neutron counting efficiencies for all precursors. The uncertainties on the P_n values include all the statistical uncertainties plus a systematic uncertainty of 10% or 20% depending on the configuration of the neutron counter. These systematic uncertainties are due to the neutron energy dependence of the counter and to our lack of knowledge of the neutron energy spectrum of these precursors. The

---

* Bluffton College, Bluffton, OH

** Brookhaven National Laboratory, Upton, NY

1 P.L. Reeder, R.A. Warner, R.M. Liebsch, R.L. Gill, and A. Piotrowski, Phys. Rev. C 31, 1029(1985).

Table A-1. Half-lives and delayed neutron emission probabilities

Precursor	Half-life (s)	P_n (%) [a]	P_n (%) (Mann) [b]
75 Cu	1.3 ± 0.1	3.5 ± 0.6	
79 Ga	2.85 ± 0.01	0.055 ± 0.012	0.10 ± 0.01
80 Ga	1.69 ± 0.01	0.69 ± 0.16	0.86 ± 0.08
81 Ga	1.218 ± 0.004	11.7 ± 1.2	12.2 ± 1.2
82 Ga	0.609 ± 0.003	20.9 ± 2.2	21.9 ± 2.6
83 Ga	0.308 ± 0.004	62.8 ± 6.3	44. ± 8.
95 Rb	0.377 ± 0.001	9.0 ± 1.1	8.59 ± 0.60
97 Rb	0.169 ± 0.001	26.1 ± 5.4	26.9 ± 1.9
98 Rb	0.106 ± 0.001	13.6 ± 0.9 [c]	13.4 ± 0.9
99 Rb	0.059 ± 0.001	20.7 ± 2.3	13.1 ± 1.8
100 Rb	0.059 ± 0.010	5.0 ± 1.0	
97 Sr	0.429 ± 0.005	<0.05	0.006 ± 0.003
98 Sr	0.653 ± 0.002	0.23 ± 0.05	0.32 ± 0.13
99 Sr	0.269 ± 0.001	0.093 ± 0.012	0.33 ± 0.13
100 Sr	0.201 ± 0.001	0.75 ± 0.08	
101 Sr	0.115 ± 0.001	2.49 ± 0.25	
102 Sr	0.069 ± 0.015	4.8 ± 2.3	
97 Y(m)	1.18 ± 0.04	<0.08	0.11 ± 0.04
97 Y(g)	3.76 ± 0.02	0.054 ± 0.012	0.059 ± 0.008
98 Y	0.548 ± 0.001	0.23 ± 0.05	0.23 ± 0.05
99 Y	1.470 ± 0.007	1.09 ± 0.11	2.6 ± 2.2
100 Y	0.735 ± 0.004	0.85 ± 0.09	
101 Y	0.431 ± 0.007	2.07 ± 0.21	
102 Y	0.44 ± 0.06	6.0 ± 1.7	
127 In(m)	3.70 ± 0.04	0.54 ± 0.11	0.70 ± 0.08
128 In	0.800 ± 0.001	0.030 ± 0.007	0.060 ± 0.015
129 In(m)	1.18 ± 0.03	2.52 ± 0.52	3.0 ± 0.5
129 In(g)	0.61 ± 0.01	0.13 ± 0.03	0.26 ± 0.05
130 In(m)	0.532 ± 0.006	1.72 ± 0.18	4.4 ± 1.6
130 In(g)	0.278 ± 0.007	0.91 ± 0.10	1.43 ± 0.11
131 In	0.278 ± 0.003	1.70 ± 0.18	1.76 ± 0.25
132 In	0.204 ± 0.006	6.8 ± 1.4	4.3 ± 0.9
147 Cs	0.229 ± 0.001	26.4 ± 2.9	26.4 ± 3.7
148 Cs	0.146 ± 0.003	25.1 ± 2.5	
147 Ba	0.892 ± 0.001	0.021 ± 0.018	0.031 ± 0.22
148 Ba	0.653 ± 0.002	0.057 ± 0.020	0.055 ± 0.013
149 Ba	0.356 ± 0.008	0.58 ± 0.08	
147 La	4.02 ± 0.01	0.041 ± 0.017	0.033 ± 0.008
148 La	1.38 ± 0.02	0.143 ± 0.015	0.13 ± 0.02
149 La	1.10 ± 0.03	1.07 ± 0.13	

[a] This work [b] Recommended values from Ref. 2 [c] Used for determination of neutron counting efficiency

table also shows recommended P_n values from a recent compilation.[2] Previously unknown P_n values have been measured for 11 precursors. Preliminary reports of this work have been presented.[3] [4]

B. INDEPENDENT ISOMER YIELD RATIO FOR ^{90}Rb AND ^{138}Cs (Reeder, Warner, Willmes*, and Ford**)

At the SOLAR on-line mass spectrometer facility which we operate at Washington State University, we have measured the isomer yield ratios of ^{90}Rb and ^{138}Cs for fission of ^{235}U with thermal neutrons. The mass spectrometer was tuned to the desired mass number. Fissions were induced by a burst of neutrons from the TRIGA reactor. Fission product ions were collected for a time interval short compared to the decay half-life of the parent nuclide. For ^{90}Rb, the decay of the two isomers was followed by beta counting. The isomeric components were resolved from the decay curves and the ratio of saturation activities was plotted versus the ion collection time. This procedure allowed the yield ratio to be extrapolated to zero ion collection time in order to eliminate the contribution from the parent decay. The experimental isomer yield ratio for $^{90}Rb^m(3^-)/^{90}Rb^g(0^-)$ was 8.7 ± 1.0. A statistical model was used to convert the isomer yield ratio to the average angular momentum J value of 4.5 which is consistent with average J values determined for several other fission products.[5] This work has been published.[6]

We have also obtained beta decay curves for ^{138}Cs isomers with the same technique. In this case the branching fraction for the isomeric transition is quite large ($\approx$0.75). The analysis of the beta decay curves is heavily dependent on the branching fraction. We have therefore used gamma multi-spectrum scaling techniques to measure this branching fraction. The gamma counting technique can also give the isomer yield ratio. These data are currently being analyzed. The statistical model calculation has already been performed so that once the isomer yield ratio is known we can determine the average angular momentum for ^{138}Cs in thermal neutron fission of ^{235}U.

---

* University of Idaho, Moscow, ID

** Los Alamos National Laboratory, Los Alamos, NM

2 F.M. Mann, M. Schreiber, R.E. Schenter, and T.R. England, Nucl. Sci. Eng. 87, 418(1984).

3 R.A. Warner and P.L. Reeder, Int. Conf. Nuclear Data for Basic and Applied Science, Santa Fe, NM, May 13-17, 1985. PNL-SA-12858.

4 P.L. Reeder, R.A. Warner, M.D. Emiston, R.L. Gill, and A. Piotrowski, Symposium on Recent Advances in the Study of Nuclei Off the Line of Stability, Am. Chem. Soc. National Meeting, Chicago, IL, Sept. 8-13, 1985. PNL-SA-13117.

5 G.P. Ford, K. Wolfsberg, and B.R. Erdal, Phys. Rev. C 30, 195(1984).

6 P.L. Reeder, R.A. Warner, G.P. Ford, and H. Willmes, Phys. Rev. C 32, 1327(1985).

UNIVERSITY OF PENNSYLVANIA

A = 13 - 15

This review has been published as Nuclear Physics A449 (1986) pp. 1-186.

A = 16, A = 17

Preprints of A = 16 and A = 17 have been sent out to 120 colleagues as PPP 4-85 (October 1985) and PPP 1-86 (February 1986). We plan to submit A = 16-17 to Nuclear Physics in July 1986 and to begin at that time the review of A = 18-20.

F. Ajzenberg-Selove and G. C. Marshall

RENSSELAER POLYTECHNIC INSTITUTE

A. NUCLEAR DATA

1. "Neutron-Induced Fission Cross-Section Measurements of ^{244}Cm, ^{246}Cm and ^{247}Cm", H. T. Maguire, Jr.*, C. R. S. Stopa**, R. C. Block, D. R. Harris, R. E. Slovacek (KAPL), J. R. T. Dabbs (ORNL), R. J. Dougan (LLL), R. W. Hoff (LLL) and R. W. Lougheed (LLL).

This research is completed and is now published in Nuclear Science and Engineering, 89, 293-304 (1985).

2. "Measurement of the Fission Cross-Section of ^{238}Pu", B. Alam, R. C. Block, R. E. Slovacek (KAPL), R. W. Hoff (LLL) and R. W. Lougheed (LLL).

A new fission chamber was prepared which utilized electroformed hemispherical electrodes and for which the electrode-to-electrode capacitance was minimized by removing most of the non-hemispherical material from the basic hat-shaped electrodes. This chamber is designed for ^{242}Cm fission cross-section measurements at the RINS system, utilizing essentially the same technique employed for the already completed ^{244}Cm, ^{246}Cm and ^{248}Cm measurements. Three pairs of electrodes have been prepared and they contain respectively a mixture of 3.5 μg of ^{238}Pu (99.995%) plus 2.3 pg ^{252}Cf, a mixture of 6.4 μg of ^{235}U plus 2.86 pg of ^{252}Cf, and 0.96 ng of ^{252}Cf.

Measurements have been carried out at RINS and the fission cross-section has been determined for ^{238}Pu from a few tenths of an eV into the tens of keV region. A preliminary cross-section is shown in Fig. A-1 where the cross-section has been normalized to the ENDF-B/V cross-section at the 9.6 and 18.3 eV resonances. It is observed that the resonances at energies 2.98 eV, 9.6 eV and 18.3 eV have been resolved while clusters of resonances are seen near 80, 120, 200 and 300 eV. The broad peaks observed near 500, 3000 and 6500 eV are such that the RINS resolution averages over so many levels that individually strong resonances contribute little to the observed structure. We interpret this structure as strongly suggestive of the existence of intermediate structure.

A better normalization factor will be determined at a later date from the present experimentally determined ^{235}U fission data and the resolution-broadened ^{235}U ENDF-B/V library data so as to obtain a better measured fission cross-section of ^{238}Pu.

---

*H. T. Maguire, Jr. is now at Westinghouse Nuclear Center, Monroeville, PA.

**C. R. S. Stopa is with the Centro Tecnico Aeroespacial, Instituto de Estudos Avancados, Caixa Postal 6044, 12200 - Sao Jose dos Campos, Brasil.

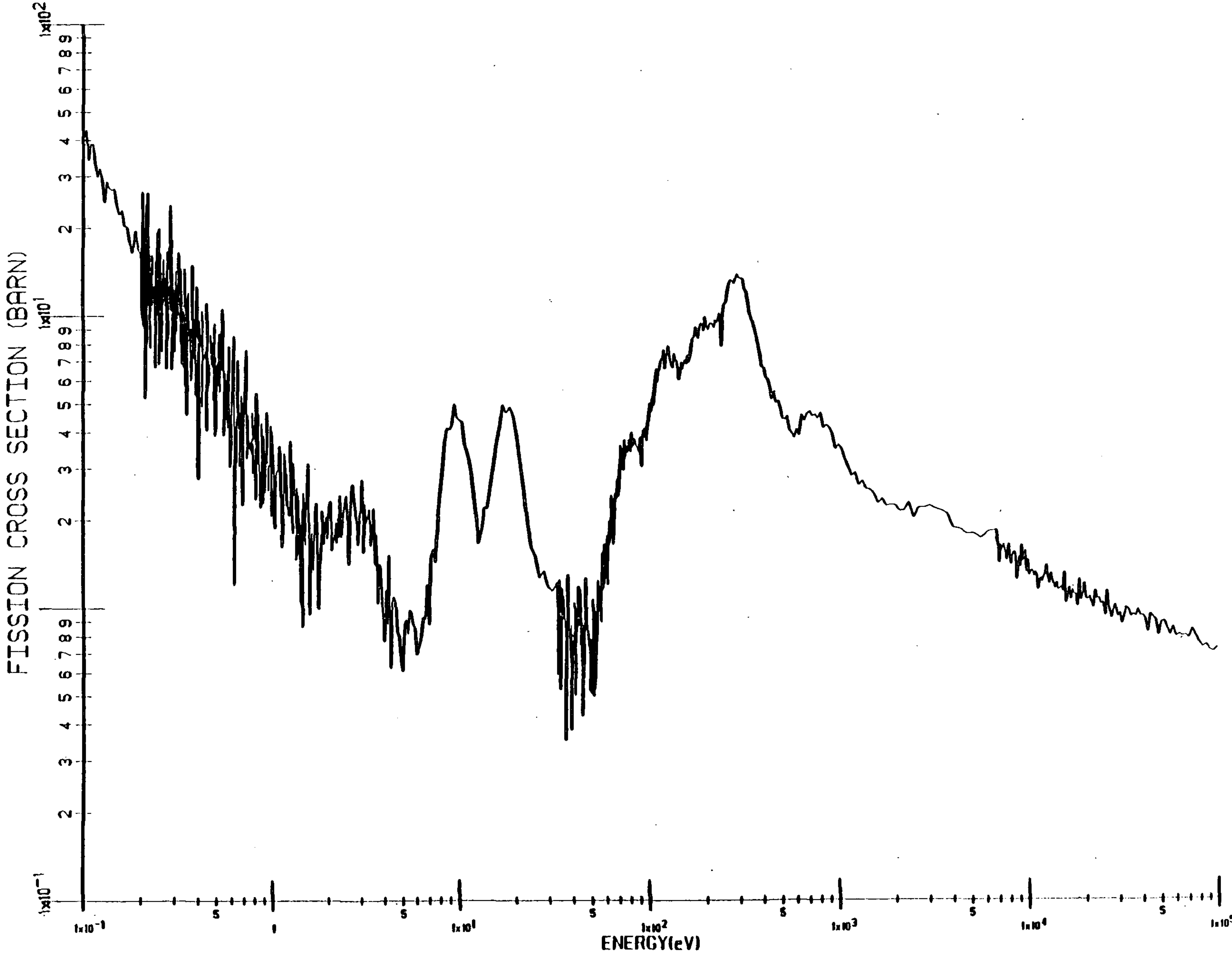

Fig. A-1: Fission cross-section versus neutron energy for the ^{238}PU isotope.

A. NEUTRON PHYSICS

1. Helium Generation Cross Sections for Fusion Applications
(D. W. Kneff, B. M. Oliver, R. P. Skowronski, and Harry Farrar IV)

Neutron-induced helium generation is a major consideration in the development of materials for reactor environments. Rockwell International is engaged in two programs to measure total helium generation cross sections for fusion reactor applications. The measurement of the cross sections of a large range of separated isotopes and their associated pure elements for fast (8-15 MeV) monoenergetic neutrons is sponsored by the Department of Energy's Office of Basic Energy Sciences (OBES). Cross section measurements for other fusion-related materials in fast-neutron environments, and for all fusion-related materials in other neutron fields used for fusion reactor materials testing, are sponsored by the Office of Fusion Energy (OFE).

Recent work has concentrated on the measurement of helium generation in pure elements irradiated in mixed-spectrum (comparable fast and thermal neutron flux) reactor environments under OFE sponsorship. In this work, performed jointly with Argonne National Laboratory (ANL), samples of selected pure elements are irradiated in the neutron spectrum of interest. The amount of helium generated in each sample is subsequently measured by high-sensitivity gas mass spectrometry, with typical measurement uncertainties of ~1-3%. The neutron fluence and energy distributions are unfolded using a comprehensive set of radiometric neutron dosimeters. Helium predictions based on this spectral unfolding and ENDF/B-V helium generation cross sections are then compared directly with the spectrum-integrated helium measurements. The results are important for the interpretation of fusion materials experiments in mixed-spectrum fission reactors.

Total helium generation for the elements Ni, Fe, Cu, and Ti has been measured in several different reactor environments. The results show that helium production in reactor-irradiated nickel can be predicted accurately (within ±10%) using evaluated cross sections and the measured neutron spectra. Iron also generally agrees within about 10% with predictions, while an ~240% overprediction for Ti indicates a large discrepancy with the ENDF files for that element.

The copper measurements[1] show that helium production in copper by thermal neutrons increases nonlinearly at high fluences ($\gtrsim 10^{22}$ neutrons/cm^2) due to a previously unrecognized three-stage reaction mechanism, which proceeds from ^{65}Cu through ^{64}Cu and ^{64}Zn to ^{65}Zn(n,α). Cross sections have been deduced for three thermal-neutron reactions that allow calculation of the

[1]Kneff, Greenwood, Oliver, and Skowronski, "Helium Production in Copper by a Thermal Three-Stage Reaction," Proc. Int. Conf. Nuclear Data for Basic and Applied Science, Santa Fe, NM, May 1985, Radiat. Eff. (to be published).

total ^{4}He production in copper for high-fluence irradiations in the mixed-spectrum High Flux Isotopes Reactor (HFIR). These cross sections, which include effects of a 7% HFIR epithermal flux, are: $^{64}Cu(n,\gamma)^{65}Cu$, 270 ± 170 b; ^{65}Zn(n,absorption), 66 ± 8 b; and $^{65}Zn(n,\alpha)^{62}Ni$, 4.7 ± 0.5 b. These measurements also show that the ENDF files underpredict helium production in HFIR-irradiated copper by fast neutrons by 24%.

Future work will include the analysis of other fusion-related materials irradiated in mixed-spectrum reactors and comparisons with ENDF/B-V predictions. Helium production measurements with fusion-energy neutrons will include new high-energy irradiations to expand our now extensive helium production cross section data base.[2,3] These measurements will involve the use of the Rockwell-developed constant-temperature sample furnace.

---

[2] Kneff, Oliver, Farrar, and Greenwood, "Helium Production in Pure Elements, Isotopes, and Alloy Steels by 14.8-MeV Neutrons," Nucl. Sci. Eng. (in press).

[3] Kneff, Oliver, Goldberg, and Haight, "Helium Production Cross Sections for 15-MeV Neutrons on ^{6}Li and ^{7}Li," Nucl. Sci. Eng. (submitted for publication).

TRIANGLE UNIVERSITIES NUCLEAR LABORATORY

A. NEUTRON CROSS SECTIONS

1. Overview (C. R. Gould, G. Honoré, C. R. Howell, K. Murphy, H. Pfutzner, R. Pedroni, M. L. Roberts, L. W. Seagondollar, W. Tornow, R. L. Walter, R. C. Byrd,* P. P. Guss,** J. P. Delaroche+)

For a number of years the neutron time-of-flight facility at TUNL has been used to explore differential cross sections $\sigma(\Theta)$ for a wide range of nuclei primarily for the energy range between 8 to 17 MeV. Two heavily shielded detectors at flight paths of 4m and 6m are the core of the system which has allowed an efficient accumulation of data for nearly thirty isotopes ranging from ^{6}Li to ^{208}Pb.

The major portion of the data is elastic scattering, although in cases where the inelastic groups are well-separated from the elastic and other inelastic groups, inelastic differential cross sections have been obtained as well. Many of the nuclei selected for study at TUNL have importance in the design of fusion energy devices.

Complementing the measurements of the conventional cross section $\sigma(\Theta)$ is a large effort to measure the scattering probability when the incident beam is polarized, that is, to determine the observable called the analyzing power $A_y(\Theta)$. This set of measurements utilizes the polarization transfer reaction $^{2}H(\vec{d},\vec{n})^{3}He$ and focusses on the 8 to 17 MeV neutron energy range. Because of the relatively high accuracy of the data and the nature of the research in terms of the systematic investigation as a function of energy and atomic weight, the results of this study have provided a unique data base for testing nuclear model calculations and for investigating details of the spin-sensitive terms of the nucleon-nucleus interaction.

The model developments have proceeded along four main avenues: 1) Spherical optical models to parametrize the energy dependence of the neutron-nucleus interaction for describing elastic neutron scattering for individual nuclei, 2) Lane models (i.e., isospin consistent models) to describe (n,n), (p,n) and energy range with a unique potential, 3) Deformed optical potentials which describe details of both elastic and inelastic neutron scattering (and in some cases proton scattering) in terms of specific nuclear structure aspects, and 4) Global spherical optical model

---

* Present address: Indiana University Cyclotron Facility, Bloomington, Ind.

** Present address: Dept. of Physics, The College of William and Mary, Williamsburg, Va.

\+ Permanent address: Centre d'Etudes de Bruyeres-le-Chatel, France representations that are capable of describing neutron and proton elastic scattering from a broad range of nuclei, such as the 1p-shell nuclei. These systematic model calculations are extremely useful tools in data evaluation.

The emphasis in this report is on experiments and analyses of cross sections although the separation from Section B, where polarization experiments are emphasized, is quite arbitrary since there is often considerable overlap in the analyses. For a detailed review of the progress of the measurements and analyses of the analyzing power studies, the reader is referred to the Annual Report of our lab, TUNL XXIV, Section B. Excerpts from the overview from Section B are reproduced below.

2. Facility Modifications

No major facility change for neutron time-of-flight cross-section measurements has been initiated this past year. However, some tests for improving the timing resolution to the 1-nanosecond range have been performed with the buncher. These tests stimulated beam optics calculations which indicated how two electrostatic triplets can be positioned prior to the bunching to give considerably improved timing. In addition, tests were performed which indicated that raising the voltage of the ion-source from the present 50 kV to 100 kV will also narrow the pulse width considerably. However, before this change can be successfully incorporated, the buncher tubes will be modified in order to handle the higher velocity particles.

3. Studies of $\sigma(\Theta)$ in the 1p Shell

a. ^{9}Be and ^{14}N Neutron Cross Sections (with J. H. Davé,* J. A. Templon,** and S. Singkarat***)

Measurements of $\sigma(\Theta)$ for $^{14}N(n,n)$ at 11, 14 and 17 MeV have been accepted for publication in Nucl. Sci. and Engineering. Excerpts of the abstract follow:

"Neutron scattering cross sections have been measured for ^{14}N and ^{9}Be at incident neutron energies 11, 14 and 17 MeV using time-of-flight methods. Angular distributions for ^{14}N and ^{9}Be elastic scattering and ^{9}Be inelastic scattering to the 2.429 MeV excited state were obtained between 20° and 160° in 5° increments. Legendre polynomial coefficients deduced by fitting the experimental data are tabulated. The results of a spherical optical model analysis for the ^{14}N data are reported. Coulomb correction terms are obtained from a comparison of neutron and proton elastic scattering data for ^{14}N."

b. ^{12}C Neutron Scattering Cross Sections (with A. Naqvi[+])

Following discussions with H. Klein of PTB (Braunschweig) and M. Drosg (LANL and Vienna) at the Santa Fe Nuclear Data Conference, we have remeasured the 10-year old data of Hogue et al. of TUNL. The question to be addressed is the true accuracy to which one can determine $\sigma(\Theta)$ for elastic scattering and inelastic scattering to the first excited state of ^{12}C. Measurements have been made at PTB with great care and corrections to the yields for multiple scattering, attenuation and geometric effects have been cautiously estimated and applied. It is intended that these PTB measurements are to serve as an international standard. Discrepancies larger than the reported error bars exist between the PTB data and the earlier TUNL data, as well as between results obtained at Bruyeres-le-Chatel, also about 10 years ago. Since this first time-of-flight (TOF) measurement at TUNL, a number of important modifications have been added to the TOF system, to the computer code EFFIGY for handling of multiple scattering, and to the detector efficiency determination. Our new data, obtained at 11 and 14 MeV, were measured with a statistical accuracy of better than 1%. Data in 10° steps were recorded with each detector over the entire range from 30° to 160° in order to reduce the possibility of introducing spurious errors and to compare measurements at the same lab with different detectors. Presently, the spectra are being analyzed off-line.

4. Studies in the 1p Shell Involving Both $\sigma(\Theta)$ and $A_y(\Theta)$

a. Analysis of $^{9}Be(n,n)$, $^{10}B(n,n)$ and $^{11}B(n,n)$

An analysis which focussed on the details of the spherical optical potential (SOM) description of $^{9}Be(n,n)$ scattering from 9 to 17 MeV was reported in Nucl. Phys. A427 (1984) 36. A fairly good representation of $\sigma(\Theta)$ and $A_y(\Theta)$ was obtained, and strong evidence for a moderately large imaginary term of the spin-orbit potential was uncovered; the magnitude and sign of this term was unexpected. Coupled-channel calculations, also reported in the paper, did not diminish the need for this term. A Lane model description of the nucleon + ^{9}Be interaction is reported in Sec. B5, TUNL XXIV. Differential cross sections were obtained at 15 and 17 MeV for ^{10}B and ^{11}B and have been incorporated into Lane model analyses for the boron isotopes. The results are discussed in Sec. B6, TUNL XXIV.

---

* Present address: Naval Research Laboratory, Washington, D.C.

** Present address: Physics Dept., Indiana University, Bloomington, Indiana

*** Present address: Physics Dept., Chiang Mai University, Thailand

\+ Permanent address: Dept. of Physics, University of Petroleum and Minerals, Dhahran, Saudi Arabia

b. Scattering of Neutrons from $^6Li(n,n)$ (with H. Hofmann of University of Erlangen-Nürnberg, FRG)

A paper on the analysis of the $\sigma(\Theta)$ and $A_y(\Theta)$ data for $^6Li(n,n)$ has been submitted to the International Polarization Symposium at Osaka. We have also recently measured $\sigma(\Theta)$ and $A_y(\Theta)$ for $^6Li(p,p)$ from 5 to 17 MeV for inclusion into the nucleon + ^6Li analysis, but these data have not been handled off-line yet. The Osaka contribution contained extended microscopic multi-channel resonating group calculations which included the T=1 excited states of ^6Li and ^6He + p structures in addition to the ^4He + ^3H, ^6Li + n, and ^5He + d structures.

c. Phase Shift Analysis for $^{12}C(n,n_0)$ from 9 to 12 MeV

A paper on the extension of the phase-shift-analysis upwards into the 9 to 12 MeV region has been published in Jour. Phys. G: Nucl. Phys. 11 (1985) 379. The abstract follows:

> "The excitation energy, spin and parity of levels in ^{13}C have been determined for excitation energies between 13 and 16 MeV via a phase-shift analysis of the measured total cross section, elastic differential cross section and analyzing power for n + ^{12}C in the neutron energy range from 8.9 to 12.0 MeV. New analysing power measurements are reported for this energy range. The present and previous experimental data are well described by the phase shifts obtained. The non-elastic cross section for n + ^{12}C predicted from the phase shifts is in good agreement with the ENDF/B-V evaluation. The need for further experimental data is pointed out."

An extension of this work to 17 MeV, as discussed in Sec. B4 of TUNL XXIV, is also underway.

5. Elastic and Inelastic Neutron Scattering from ^{27}Al at 11, 14 and 17 MeV (with J. Davé and S. Whisnant)

A publication on $\sigma(\Theta)$ for elastic scattering and inelastic scattering to three low-lying groups for 11, 14 and 17 MeV neutrons has appeared in Phys. Rev. 30, 1435 (1984). A complementary project to study the spin-orbit and symmetry terms of the spherical optical model is described in Sec. B8 of TUNL XXIV.

6. Cross Sections and Analyzing Powers for ^{28}Si and ^{32}S

As described in the last progress report, $\sigma(\Theta)$ and $A_y(\Theta)$ for neutron scattering to the ground state and first excited state of ^{28}Si and ^{32}S have been measured between 8 and 17 MeV. The data have been combined with other data available up to 40 MeV and have been described in the spherical and deformed optical model formalism. The combination of the (n,n) with previously published (p,p) data permitted a thorough study of the Coulomb correction terms. An example of the coupled channel description of the cross section data for n + ^{28}Si is shown in Fig. A6-1. Since the completion of this analysis, tabulations of some more published (p,p) data have been obtained. After the model predictions are checked against these new data, the analyses will be published.

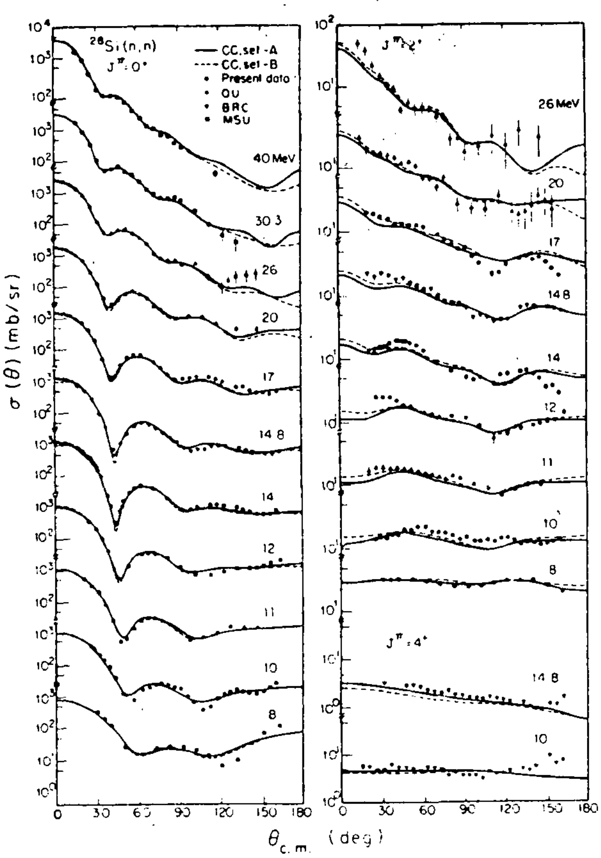

Fig. A6-1. The $\sigma(\theta)$ for elastic and inelastic neutron scattering from ^{28}Si. The curves through the data are the results of CC calculations.

7. Elastic and Inelastic Neutron Scattering from ^{40}Ca up to 80 MeV

Differential cross sections $\sigma(\theta)$ and analyzing powers $A_y(\theta)$ for neutron scattering to the ground and first 3^- excited states of the double-closed-shell nucleus ^{40}Ca have been measured in the energy range from 11 to 17 MeV. These measurements have been combined with other neutron $\sigma(\theta)$ data from Ohio University and from M.S.U., previous TUNL $A_y(\theta)$ data, and total cross section measurements to form a large set of scattering and reaction data for incident energies up to 80 MeV. The data have been described in the framework of coupled-channel formalism. A report of the work pertaining to σ_T was given at the Burr Oak, Ohio conference on Neutron-Nucleus Collisions. For a second analysis, the above data, were combined with $\sigma(\theta)$ and $A_y(\theta)$ measurements available for (p,p) and (p,p') scattering in this energy range. Figure A7-1 shows comparisons of the available $\sigma(\theta)$ and $A_y(\theta)$ for neutron elastic scattering data

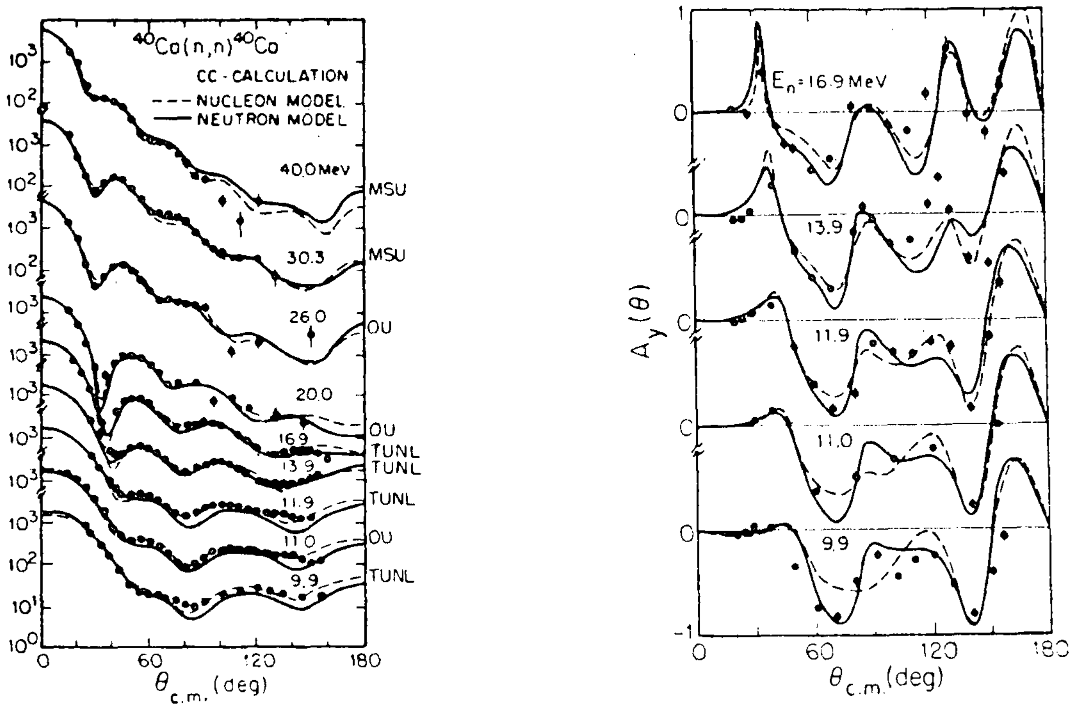

Fig. A7-1. Neutron elastic scattering from ^{40}Ca. The solid curve is from a parametrization based solely on neutron data, the dashed curve is a calculation from a model based on both neutron and proton data.

to curves representing the two families of coupled-channel calculations. The solid curves are from the parametrization based exclusively on neutron data, and the dashed curve is from the broader nucleon representation, suitable for both projectiles.

These highly-constrained analyses have led to a precise determination of geometries, energy dependencies and deformation parameters for the nucleon + ^{40}Ca interaction. The combined analysis of neutron and proton data has allowed us to map the behavior of the Coulomb correction term ΔU_C ($\Delta U_C = \Delta V_C + i\Delta W_C$) to the real central and surface absorptive potentials. We have used unconventional analytic representations for the energy dependencies of the surface and volume absorptive strengths W_d and W_v. That is, unlike the usual linear energy variations ascribed to these strengths, we have chosen to represent them with more realistic functions, for instance, a W_v that does not increase without bound with increasing incident energy.

The energy dependencies also incorporate the information that the absorptive potential behaves like $(E-\varepsilon_F)^2$ near the Fermi energy ε_F, as predicted by the Fermi gas model. Another outcome of the present work is that one can compare directly the vibrational amplitudes determined from the (n,n') and (p,p') scattering analyses; the results indicate that core polarization may not be as important in double-closed-shell nuclei as in those with single-closed shells. Preliminary presentations of this work were given at the APS meeting in Crystal City and at the International Conference on Nuclear Data at Santa Fe, and at the Sixth International Polarization Conference in Osaka.

8. Elastic and Inelastic Scattering from ^{54}Fe and ^{58}Ni

A new CC analysis for ^{58}Ni is proceeding. This analysis is an extension of the work of Guss[1] and incorporates the new TUNL 17 MeV $\sigma(\Theta)$ and $A_y(\Theta)$ elastic and inelastic (to the first 2^+ excited state) scattering data into the ^{58}Ni data base of Guss. Also included in the analysis are new $A_y(\Theta)$ data for inelastic scattering to the first 2^+ excited state of ^{58}Ni at 10 and 14 MeV. The inelastic $A_y(\Theta)$ data are being used to study the relationship between the spin-orbit and central potential deformation lengths. Preliminary results from this analysis and the new 10, 14 and 17 MeV inelastic A_y data were presented at the Crystal City spring APS meeting. Presently, the analysis is proceeding along similar lines to the analysis for ^{40}Ca with the surface absorption term W_d having a $(E - \varepsilon_F)^2$ dependence (E is the neutron energy and ε_F is the Fermi energy). The volume absorption term W_v has an energy dependence of the form $A/(1. + \exp((B - E)/C)$ (a Woods-Saxon type shape with A, B and C being numerical parameters). Figure A8-1 shows the Ni σ_T data of Larson with

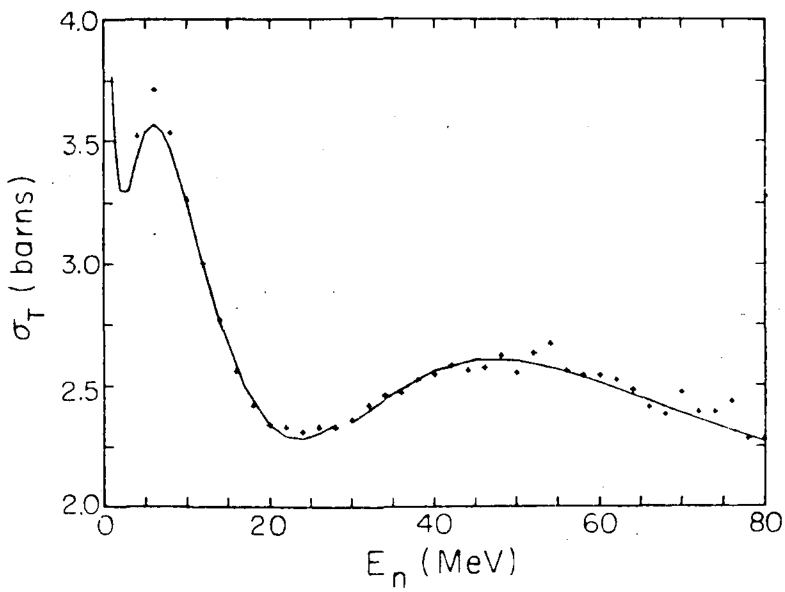

Fig. A8-1. Comparison of the present CC calculations for nickel to the σ_T data of Larson. The break in the curve between 28 and 30 MeV is due to switching from non-relativistic to relativistic kinematics in the calcu[illegible]ns above 30 MeV.

the current CC prediction. The ^{58}Ni σ_T data of Budtz-Jorgensen, together with the Larson data, will be used to explore the energy dependence for the real potential V_r for energies between 1 and 8 MeV -- looking specifically for the types of effects which have been seen by Finlay for Pb and Bi. A CC analysis for ^{54}Fe is proceeding in the same manner as that for ^{58}Ni.

9. Elastic Scattering Cross Section for ^{89}Y and ^{93}Nb

Measurements of $\sigma(\Theta)$ for elastic scattering of neutrons at energies of 7.9, 9.9, 11.9, 13.9, and 16.9 MeV from ^{89}Y have been prepared in final form. A systematic, energy-dependent spherical optical model (SOM) parametrization of elastic scattering from this nucleus has now been completed. Fig. A9-1 shows the differential cross section data and the $A_y(\Theta)$ data compared to these SOM calculations at each energy. The data have also been incorporated in the global SOM study of many nuclei discussed in Section A12.

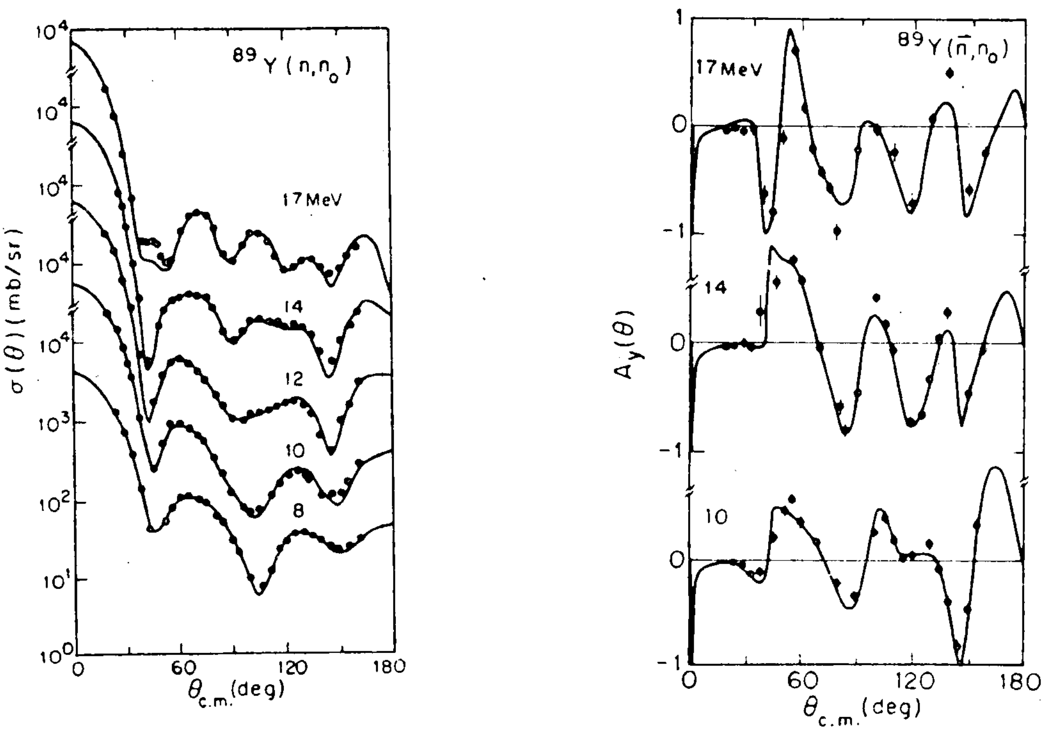

Fig. A9-1. Neutron scattering from ^{89}Y. The $\sigma(\Theta)$ and $A_y(\Theta)$ data are all from TUNL. The spherical optical model calculations are made with systematic energy dependencies of the potential.

The data for ^{93}Nb have been rechecked, as there seemed to be a 10% normalization problem when these data (and those for ^{89}Y) were incorporated into the global optical model analysis of Section A12. The check established the validity of the earlier data stripping and the multiple-scattering corrections. Our small-angle scattering data for

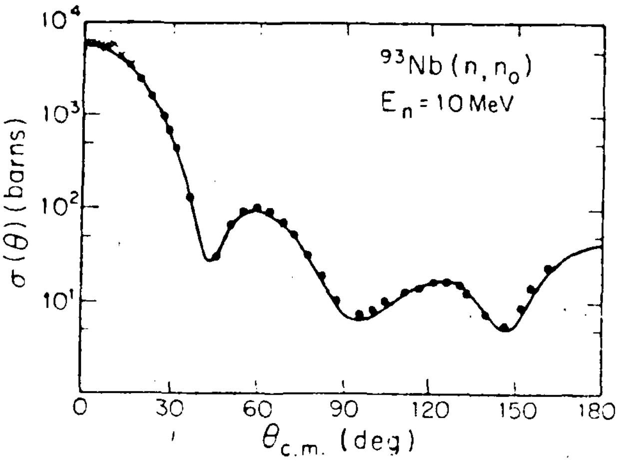

Fig. A9-2. The $\sigma(\Theta)$ data for elastic neutron scattering from ^{93}Nb at 10 MeV. The data obtained during the small-angle experiment are represented by crosses. The remaining data were acquired during a normal time-of-flight measurement. The curve is a SOM calculation using a preliminary set of energy-dependent parameters.

$2^o < \Theta < 16^o$ have been finalized and are shown in Fig. A9-2 along with our earlier larger-angle $\sigma(\Theta)$ measurements. The data will be employed, along with our $\sigma(\Theta)$ data at 8,10, 12, 14 and 17 MeV and with our A_y at 10 and 14 MeV, to develop a spherical optical model for this region of the periodic table and for comparison to the specialized ^{89}Y model. The curve shown in Fig. A9-2 is from calculations from a preliminary energy-dependent SOM for Nb.

10. <u>Scattering Cross Sections for ^{116,117}Sn and ^{208}Pb</u>

The $\sigma(\Theta)$ measurements from 8-17 MeV for ^{120}Sn and 8-14 for ^{116}Sn have been included in an SOM and a coupled-channel analysis as described in TUNL XXIII. After minor modifications to the potential in the 50-80 MeV region, a paper will be submitted for publication. This work should be completed and submitted in a few weeks. The analysis of the ^{208}Pb $\sigma(\Theta)$ from 8-17 MeV is undergoing an additional stage which will incorporate the recent high accuracy data from Ohio University at 20-24 MeV and the σ_T data of ORELA up to 80 MeV.

11. Optical Model Representation of σ_T up to 80 MeV (with D. Larson, D. M. Hetrick and J. A. Harvey)

A paper was submitted to the Burr Oak Neutron-Nucleus Conference titled "Energy Dependence of the Local Optical Potential for Neutron-Nucleus Scattering" which reviews our coupled-channel calculations for neutron scattering from ^{120}Sn, ^{58}Ni, ^{40}Ca and ^{28}Si. The main emphasis was to stress the importance of the total cross section σ_T for constraining the energy dependence of the volume and surface absorption terms of the optical potentials. The data employed are from unpublished ORELA work of the above collaborators.

12. Global Optical Model for Neutron Scattering

A global optical model for neutron scattering for $A > 53$ and $10 \text{ MeV} < E < 80$ MeV has been under development at TUNL for a couple of years. The status was reported at the Santa Fe Nuclear Data Conference in an invited contribution. Many of the $\sigma(\theta)$ and $A_y(\theta)$ data obtained at TUNL in the last six years were included in the analysis, along with σ_T data from ORELA up to 80 MeV. Also included is $\sigma(\theta)$ and $A_y(\theta)$ data from about six other labs. The description is satisfying. One unusual feature is the desire for the positive W_{SO} term at the lower energies. Some more tuning of the parameters will be conducted in the future.

B. NEUTRON POLARIZATION STUDIES

1. Overview

Polarization measurements in neutron-induced reactions or (p,n) reactions aid in our understanding of the fundamental nucleon-nucleon interaction, few-body forces and the nucleon-nucleus potential. The group at TUNL has been focussing on all these topics during the past year. The $^2H(\vec{d},\vec{n})$ polarization transfer reaction is used as the source of polarized neutrons for the scattering studies. The pulsing system at the Lamb Shift polarized ion source permits delivery of 80% of the normal d.c. beam at the target to be compressed into 2 ns bursts at a 4 MHz rate. Two large shielded detectors in the time-of-flight area are used to perform spectral analysis of the neutrons scattered from various samples.

A large percentage of the beam time has been spent developing the techniques for observing A_y for the breakup of deuterons by polarized neutrons. The method utilizes a deuterated scintillator as a target and six side detectors, three on each side of the incident neutron beam axis. Various coincidences between events in several combinations of the side detectors and the recoiling protons in the deuterated scatterer permit identification of several types of 3-body processes. Source reaction permit identification of events induced by the "monoenergetic" 12-MeV neutrons produced in the source reaction. As a byproduct, the analyzing power $A_y(\theta)$ for $^2H(n,n)^2H$ elastic scattering is obtained to high accuracy.

These experiments, which involve the most complex electronic techniques ever used at TUNL, are now delivering their first statistically significant data.

Light nuclei in the range from ^{6}Li to ^{11}B are being studied with incident polarized neutron and proton beams, and ^{14}N and ^{16}O have been studied with polarized neutron beams. The elastic scattering data are analyzed with either the ordinary spherical optical model or with an isospin-consistent Lane optical model, when (p,n) data are available. In the intermediate mass region, studies of the nucleus ^{40}Ca have been given a large share of the time. The effect of introducing Mahaux and Ngo's energy-dispersion relationship was investigated, along with the effect of coupling to giant resonances. As previously reported, nucleon scattering from ^{28}Si and ^{32}S has also been studied in spherical and deformed optical model formalisms.

For heavier nuclei the spherical optical model for ^{89}Y has been completed. The data set for ^{93}Nb has been increased by the inclusion of the small angle $\sigma(\theta)$ data at forward angles at 10 MeV and the spherical model for this nucleus will be explored further. The analysis of the ^{110}Sn and ^{120}Sn has been completed, both spherical and deformed. The ^{208}Pb $A_y(\theta)$ and $\sigma(\theta)$ data reported in previous TUNL publications has been included in a global analysis, but no further progress on the spherical model specific to nucleon scattering from ^{208}Pb has been accomplished. Lastly, all the $A_y(\theta)$ data obtained at TUNL for neutron scattering for $A \geq 54$ have been included in a global spherical optical model search that concentrated mainly on neutron data, but which took account of recent data and analyses for proton scattering at 80 MeV.